

ALMA MATER STUDIORUM – UNIVERSITÀ DI BOLOGNA

DOTTORATO DI RICERCA IN

**Scienze Chimiche**

Ciclo XXVIII

Settore Concorsuale di afferenza: 03/C2 - Chimica Industriale

Settore Scientifico disciplinare: CHIM/04 – Chimica Industriale

**SYNTHESIS AND CHARACTERIZATION OF**  
**NEW POLYMERS FOR INDUSTRIAL**  
**APPLICATIONS**

*Presentata da: **Dott. Francesco Paolo Di Nicola***

Coordinatore Dottorato: **Prof. Aldo Roda**

Relatore: **Prof. Massimiliano Lanzi**

Esame finale 2016



*“Misurate ciò che è misurabile e  
rendete misurabile ciò che non lo è.”*

Galileo Galilei

*“Il problema non è tanto vedere  
ciò che nessuno ha ancora visto,  
quanto pensare ciò che nessuno ha  
mai pensato su qualcosa che tutti vedono.”*

Erwin Schrödinger



# **TABLE OF CONTENTS**

<b><u>LIST OF FIGURES .....</u></b>	<b><u>VI</u></b>
<b><u>LIST OF SCHEMES .....</u></b>	<b><u>X</u></b>
<b><u>LIST OF TABLES .....</u></b>	<b><u>XI</u></b>
<b><u>PART 1: POLYTHIOPHENES .....</u></b>	<b><u>1</u></b>
<b><u>CHAPTER 1: INTRODUCTION.....</u></b>	<b><u>3</u></b>
1.1 <b>PII-CONJUGATED POLYMERS .....</b>	<b>3</b>
1.2 <b>ELECTRONIC STRUCTURE OF CONJUGATED POLYMERS .....</b>	<b>5</b>
1.2.1 <b>SYSTEMS WITH DEGENERATE GROUND STATE .....</b>	<b>7</b>
1.2.2 <b>SYSTEMS WITH NON-DEGENERATE GROUND STATE .....</b>	<b>9</b>
1.3 <b>CHARACTERIZATION OF CONDUCTIVE POLYMERS .....</b>	<b>10</b>
1.4 <b>APPLICATION OF CONJUGATED POLYMERS IN THEIR ELECTROCONDUCTIVE DOPED STATE.....</b>	<b>11</b>
1.4.1 <b>CONDUCTOR DEVICES.....</b>	<b>11</b>
1.4.2 <b>RADAR APPLICATION .....</b>	<b>11</b>
1.4.3 <b>CORROSION PROTECTION.....</b>	<b>12</b>
1.4.4 <b>BATTERIES.....</b>	<b>12</b>
1.4.5 <b>CATALYSTS .....</b>	<b>13</b>
1.4.6 <b>ELECTROCHROMIC CELLS .....</b>	<b>13</b>
1.4.7 <b>SENSORS .....</b>	<b>14</b>
1.4.7 <b>CONTROLLED RELEASE APPLICATION .....</b>	<b>14</b>
1.5 <b>APPLICATION OF CONJUGATED POLYMERS IN THEIR NEUTRAL SEMI-CONDUCTIVE STATE .....</b>	<b>15</b>
1.5.1 <b>POLYMERIC LIGHT EMITTING DIODES (PLEDs).....</b>	<b>15</b>
1.5.2 <b>PHOTOVOLTAIC CELLS.....</b>	<b>17</b>
1.5.3 <b>FIELD EFFECT TRANSISTORS (FET) .....</b>	<b>17</b>
<b><u>REFERENCES FOR CHAPTER 1 .....</u></b>	<b><u>19</u></b>
<b><u>CHAPTER 2: POLYTHIOPHENE AND ITS DERIVATIVES .....</u></b>	<b><u>21</u></b>
2.1 <b>POLYTHIOPHENE.....</b>	<b>21</b>

2.1.1 ELECTROCHEMICAL SYNTHESIS .....	21
2.1.2 CHEMICAL SYNTHESIS .....	23
<b>2.2 3-ALKYL FUNCTIONALIZED POLYTHIOPHENES.....</b>	<b>24</b>
<b>2.3 PATs SYNTHESSES .....</b>	<b>25</b>
2.3.1 ELECTROCHEMICAL POLYMERIZATION .....	25
2.3.2 CROSS-COUPLING POLYMERIZATION WITH METALS AS CATALYSTS .....	25
2.3.3 OXIDATIVE POLYMERIZATION.....	26
<b>2.4 REGIOREGULAR PATs SYNTHESIS .....</b>	<b>28</b>
2.4.1 RIEKE-CHEN POLYMERIZATION.....	29
2.4.2 STILLE COUPLING POLYMERIZATION .....	29
2.4.3 HECK COUPLING POLYMERIZATION.....	30
2.4.4 SUZUKI COUPLING POLYMERIZATION .....	30
2.4.5 MCCULLOUGH POLYMERIZATION.....	31
<b>2.5 PATs CHARACTERIZATION .....</b>	<b>32</b>
2.5.1 NUCLEAR MAGNETIC RESONANCE (NMR) SPECTROSCOPY .....	32
2.5.2 INFRARED SPECTROSCOPY .....	33
2.5.3 UV-VIS ABSORPTION SPECTROSCOPY .....	34
<b>2.6 OPTICAL PROPERTIES OF PATs .....</b>	<b>34</b>
<b>2.7 B-FUNCTIONALIZED POLYTHIOPHENES .....</b>	<b>36</b>
2.7.1 POST-POLYMERIZATION FUNCTIONALIZATION .....	37
<b><u>REFERENCES FOR CHAPTER 2 .....</u></b>	<b><u>37</u></b>

## **CHAPTER 3: CONJUGATED POLYMERS FOR THE OBTAINMENT OF CONDUCTIVE PATTERNS THROUGH LASER TRACING.....**

<b>3.1 INTRODUCTION .....</b>	<b>39</b>
<b>3.2 EXPERIMENTAL .....</b>	<b>42</b>
<b>3.3 MONOMER SYNTHESIS.....</b>	<b>43</b>
3.3.1 SYNTHESIS OF 3-(BUTHYLTHIO)THIOPHENE (TSBu) .....	43
3.3.2 SYNTHESIS OF 2,5-DIBROMO-3-BUTHYLTHIOTHIOPHENE (2,5BTSBu) .....	43
<b>3.4 POLYMER SYNTHESIS .....</b>	<b>43</b>
3.4.1 SYNTHESIS OF POLY[(3-METHYLTHIO)THIOPHENE] (PSMe) .....	44
3.4.2 SYNTHESIS OF POLY[(3-BUTHYLTHIO)THIOPHENE] PSBu – OXIDATIVE POLYMERIZATION .....	44
3.4.3 SYNTHESIS OF POLY[(3-BUTHYLTHIO)THIOPHENE] PSBu – GRIM PROCEDURE.....	44
<b>3.5 RESULTS AND DISCUSSION .....</b>	<b>45</b>

3.6 CONCLUSION .....	65
<b><u>REFERENCES FOR CHAPTER 3 .....</u></b>	<b><u>66</u></b>
<b><u>CHAPTER 4: USE OF POLY(3-METHYLTHIO)THIOPHENE BLENDS FOR DIRECT LASER TRACING AND BULK HETEROJUNCTION SOLAR CELLS.....</u></b>	<b><u>73</u></b>
4.1. INTRODUCTION .....	73
4.2. EXPERIMENTAL .....	75
4.2.1. SYNTHESIS AND POLYMERIZATION.....	75
4.2.2 SYNTHESIS OF THE MONOMER 2,5-DIBROMO-3-METHYLTHIOTHIOPHENE (2,5-BTSM <sub>e</sub> ) .....	75
4.2.3 SYNTHESIS OF THE REGIOREGULAR POLY(3-METHYLTHIO)THIOPHENE (PTSM <sub>e</sub> ) .....	76
4.2.4 PREPARATION OF THE PTSM <sub>e</sub> -P3HT BLEND (PB).....	76
4.3 MEASUREMENTS.....	76
4.3.1 ITO/PEDOT/PB:PCBM/AL SOLAR CELL ASSEMBLY .....	77
4.4. RESULTS AND DISCUSSION .....	78
4.5 CONCLUSIONS.....	91
<b><u>REFERENCES FOR CHAPTER 4 .....</u></b>	<b><u>92</u></b>
<b><u>CHAPTER 5: SOLVENTLESS DEPOSITION OF OLIGO- AND POLYTHIOPHENES FOR BHJ SOLAR CELLS .....</u></b>	<b><u>95</u></b>
5.1. INTRODUCTION .....	95
5.2. EXPERIMENTAL .....	96
5.3. RESULTS AND DISCUSSION .....	98
5.4. CONCLUSIONS.....	110
<b><u>REFERENCES FOR CHAPTER 5 .....</u></b>	<b><u>111</u></b>
<b><u>CHAPTER 6: A REGIOREGULAR POLYTHIOPHENE-FULLERENE FOR POLYMERIC SOLAR CELLS.....</u></b>	<b><u>115</u></b>
6.1 INTRODUCTION .....	115
6.2 EXPERIMENTAL .....	117
6.2.1 MATERIALS .....	117
6.2.2 MEASUREMENTS.....	117

<b>6.3 SYNTHESSES OF MONOMERS .....</b>	<b>118</b>
6.3.1 SYNTHESIS OF THE MODEL COMPOUND 1-FULLERENYLHEXANE (HEXF).....	118
6.3.2 SYNTHESIS OF 3-(6-FULLERENYLHEXYL)THIOPHENE (T6F) .....	120
<b>6.4 SYNTHESSES OF POLYMERS .....</b>	<b>121</b>
6.4.1 SYNTHESIS OF POLY[3-HEXYLTHIOPHENE-CO-3-(6-BROMOHEXYL)THIOPHENE] (COP1) .....	121
6.4.2 SYNTHESIS OF POLY[3-HEXYLTHIOPHENE-CO-3-(6-FULLERENYLHEXYL)THIOPHENE] (COP2) .....	122
<b>6.5 RESULTS AND DISCUSSION .....</b>	<b>123</b>
<b>6.6 CONCLUSIONS.....</b>	<b>134</b>
 <b>REFERENCES FOR CHAPTER 6 .....</b>	 <b>135</b>
 <b>PART 2: FKM.....</b>	 <b>141</b>
 <b>CHAPTER 1: INTRODUCTION.....</b>	 <b>145</b>
 1.1 INTRODUCTION ON FLUOROPOLYMERS .....	145
1.2 PVDF.....	146
1.3 COPOLYMER BASED ON VDF .....	146
1.4 OVERVIEW .....	148
1.4.1 DIFFERENT CROSSLINKING AGENTS.....	148
1.4.2 COMPOUNDING .....	149
1.4.3 PRESS-CURE AND POST-CURE STEPS FOR CROSSLINKING .....	150
<b>1.5 CROSSLINKING OF VDF-BASED FLUOROELASTOMERS.....</b>	<b>152</b>
1.5.1 CROSSLINKING WITH AMINES AND DIAMINES.....	152
1.5.2 DEHYDROFLUORURATION OF THE FLUOROPOLYMER .....	152
<b>1.6 CROSSLINKING WITH BISPHENOLS.....</b>	<b>160</b>
1.6.1 CROSSLINKING MECHANISM.....	160
1.6.2 <sup>19</sup> F NMR STUDY .....	161
1.6.3 OSCILLATING DISC RHEOMETER (ODR) RESPONSE .....	163
1.6.4 LIMITATIONS OF THE BISPHENOL-CURED FLUOROELASTOMERS.....	165
<b>1.7 CROSSLINKING WITH PEROXIDES .....</b>	<b>165</b>
1.7.1 REACTION CONDITIONS .....	166
1.7.2 IMPORTANCE OF THE COAGENT.....	169
1.7.3 INFLUENCE OF THE NATURE AND THE AMOUNT OF THE PEROXIDE .....	171
1.7.4 MECHANISM OF CROSSLINKING.....	175
<b>1.8 COMPARISON OF PHYSICAL AND MECHANICAL PROPERTIES.....</b>	<b>177</b>



<b>1.9 APPLICATIONS .....</b>	<b>183</b>
<b><u>REFERENCES FOR CHAPTER 1 .....</u></b>	<b><u>185</u></b>
<b><u>CHAPTER 2: BISPHENOL-BASED CURING SYSTEMS.....</u></b>	<b><u>193</u></b>
<b>2.1 INTRODUCTION .....</b>	<b>193</b>
<b>2.2 EXPERIMENTAL .....</b>	<b>194</b>
2.2.1 TYPICAL PREPARATION OF THE CROSSLINKING SYSTEM .....	194
2.2.2 PREPARATION OF THE RUBBER COMPOUNDS.....	194
2.2.3 INSTRUMENTS USED.....	194
<b>2.3 <sup>1</sup>H-NMR ANALYSIS .....</b>	<b>195</b>
<b>2.4 ODR ANALYSIS .....</b>	<b>198</b>
<b>2.5 STRESS-STRAIN CURVES.....</b>	<b>200</b>
<b>2.6 CONCLUSIONS.....</b>	<b>201</b>
<b><u>CHAPTER 3: DEHYDROFLUORURATION OF VDF/HFP COPOLYMER .....</u></b>	<b><u>202</u></b>
<b>3.1 INTRODUCTION .....</b>	<b>202</b>
<b>3.2 EXPERIMENTAL .....</b>	<b>202</b>
3.2.1 INSTRUMENTS .....	202
3.2.2 BIPHASIC DEHYDROFLUORURATION REACTION .....	202
3.2.3 HOMOGENEOUS PHASE DEHYDROFLUORURATION .....	203
3.2.4 PHOTOCROSSLINK SAMPLES PREPARATION.....	204
3.2.5 COMPOUND PREPARATION FOR THERMAL CROSSLINKING.....	204
<b>3.3 RESULTS AND DISCUSSION .....</b>	<b>204</b>
3.3.1 <sup>19</sup> F-NMR.....	207
3.3.2 FT-IR ANALYSIS.....	212
3.3.3 PHOTOCROSSLINKING .....	213
3.3.4 THERMAL CROSSLINKING.....	216
<b>3.4 CONCLUSIONS.....</b>	<b>218</b>

# LIST OF FIGURES

Figure 1. Winners of the Nobel Prize in Chemistry in 2000. _____	3
Figure 2. Isomeric structures of Polyacetylene. _____	4
Figure 3. Structure of some conjugated polymers. _____	5
Figure 4. Schematization of valence and conduction bands model. _____	6
Figure 5. Conductivity comparison between conjugated polymers and some conventional materials _____	6
Figure 6. Structure and energy diagram for the two phases of PA. _____	8
Figure 7 A neutral soliton separates phases A and B. _____	8
Figure 8. Energy levels diagram for a) neutral, b) positive and c) negative soliton. _____	8
Figure 9. a) Aromatic and chinoid forms of polythiophene and b) energy diagram of the two configurations. _____	9
Figure 10. Soliton-antisoliton couple of polythiophene. _____	9
Figure 11. a) Positive charged and b) negative charged polarons with their energy diagrams. _____	10
Figure 12. Bipolarons with a) positive and b) negative charge with their corresponding energy levels for polythiophene. _____	10
Figure 13. Ion-selective transport by an electroactive bi-layer. _____	15
Figure 14. Schematic structure of a single layer PLED. _____	16
Figure 15. Diagram for single-layer PLED bands. _____	16
Figure 16. Schematic structure of a FET. _____	18
Figure 17. Mechanism of thiophene electropolymerization. _____	22
Figure 18. Possible triads in PATs. _____	25
Figure 19. Proposed mechanism of oxidative polymerization. _____	27
Figure 20. Aromatic region of <sup>1</sup> H-NMR spectrum of poly(3-hexylthiophene). _____	33
Figure 21. Equilibrium between A and B forms. _____	35
Figure 22. Absorption spectra for P3HT in CHCl <sub>3</sub> /CH <sub>3</sub> OH mixtures at different molar ratios of CH <sub>3</sub> OH: a) 0.00; b) 0.28; c) 0.39; d) 0.50; e) 0.66; f) 0.80; g) 0.98. _____	36
Figure 23. <sup>1</sup> H-NMR spectrum of PATAC-Me. _____	46
Figure 24. FT-IR spectra of PATAC-Me before (left) and after (right) laser treatment. _____	46
Figure 25. Detail of the FT-IR spectra of PATAC-Me before (a) and after (b) laser exposure. _____	47
Figure 26. Raman spectra of PATAC-Me before (left) and after (right) laser exposure. _____	47
Figure 27. UV-Vis spectra of PATAC-Me films. _____	48
Figure 28. Solvatochromism of PATAC-Me. _____	49
Figure 29. Optical microscope image of a partially traced film of PATAC-Me. _____	50
Figure 30. SEM micrograph of a PATAC-Me film after laser tracing. _____	51
Figure 31. EDS topographic microanalysis of the film reported in Fig. 30. Left: Carbon, right: sulfur. _____	51
Figure 32. <sup>1</sup> H-NMR spectrum of PSMe. _____	53
Figure 33. FT-IR spectrum of PSMe. _____	53
Figure 34. UV-Vis spectra of PSMe in solution and in film. _____	54
Figure 35. Adopted atoms numbering for NMR analysis. _____	57
Figure 36. <sup>1</sup> H-NMR of PSBu prepared using the McCullough procedure. _____	58

Figure 37. $^{13}\text{C}$ -NMR of PSBu prepared using the McCullough procedure. _____	58
Figure 38. Solvatochromism of PSBu in DMPU/MeOH (top) and THF/MeOH (bottom) at increasing methanol molar fractions. _____	59
Figure 39. UV-Vis spectrum of PSBu in film. _____	60
Figure 40. Optical microscope images of traced PSBu films. Top left: 50 $\times$ , right: 400 $\times$ . Bottom: 3D elaboration, 50 $\times$ . _____	61
Figure 41. SEM image of a traced PSBu film (left). EDS microanalysis relative to sulfur on the same film (right). _____	62
Figure 42. FT-IR spectrum of a PSBu film. a) untraced b) traced. _____	62
Figure 43. DSC thermograms of PATAC-Me (left) and PSBu (right). _____	63
Figure 44. TGA thermograms of PATAC-Me (left) and PSBu (right). _____	64
Figure 45. FT-IR spectrum of PB in film cast on Ge disk from $\text{CHCl}_3$ solution. The C-SMe stretching band is evidenced by an asterisk. _____	80
Figure 46. $^1\text{H}$ -NMR spectrum of PB in $\text{CDCl}_3$ . $\text{CHCl}_3$ peak is indicated by an asterisk. _____	80
Figure 47. UV-Vis spectra of polymers in film cast from $\text{CHCl}_3$ solutions. _____	81
Figure 48. Optical microscope image of a traced PB sample ( $\times 50$ ). The film was cast from the polymer solution in $\text{CHCl}_3$ . _____	82
Figure 49. 3D image of PB traces on the polymer film cast from $\text{CHCl}_3$ solution. _____	83
Figure 50. SEM micrograph of a PB film after laser tracing. The polymer film was cast from PB solution in $\text{CHCl}_3$ . _____	83
Figure 51 FT-IR spectrum (expansion) of a PB film on Ge disk from $\text{CHCl}_3$ solution before and after the laser tracing procedure. The C-SMe stretching band is evidenced by an asterisk. _____	84
Figure 52. SEM micrograph of a pre-annealed PB film, cast from $\text{CHCl}_3$ solution, after laser tracing. _____	85
Figure 53. EDS topographic microanalysis of PB film reported in Figure 8. Left: Carbon; Right: Sulfur. _____	85
Figure 54. J-V characteristic curves for the prepared solar cells under AM 1.5 irradiation with an intensity of 1 sun ( $100 \text{ mW}/\text{cm}^2$ ) from a calibrated solar simulator. _____	86
Figure 55. Cyclic voltammograms of the polymer films on Pt recorded in 0.1 M $\text{Bu}_4\text{NPF}_6$ acetonitrile solution at a scan rate of $50 \text{ mV s}^{-1}$ . _____	87
Figure 56. Band diagram with HOMO/LUMO levels of the ED polymers and EA PCBM in relation to the work functions of ITO and Al electrodes. _____	88
Figure 57. AFM images of the examined blends (tapping mode, scale in nm; top: height modulated images; bottom: phase modulated images). The blends were obtained by casting the polymer/PCBM solutions in $\text{CHCl}_3$ on ITO glasses. _____	90
Figure 58. TGA thermogram of P3HT and OCT under nitrogen. _____	99
Figure 59. $^1\text{H}$ -NMR spectrum of P3HT. Up: evaporated polymer redissolved in $\text{CDCl}_3$ . Down: the same polymer before vacuum evaporation, dissolved in $\text{CDCl}_3$ . _____	100
Figure 60. $^1\text{H}$ -NMR spectrum of OCT. Up: evaporated oligomer redissolved in $\text{CDCl}_3$ . Down: the same oligomer before vacuum evaporation, dissolved in $\text{CDCl}_3$ . _____	102
Figure 61. IR spectrum of evaporated (up) and pristine (down) OCT. _____	104
Figure 62. UV-Vis spectra of pristine and evaporated OCT (film on quartz). _____	105
Figure 63. X-Ray diffractograms of OCT films obtained by casting (left) and VTE (right). _____	106
Figure 64. Cyclic voltammogram of an OCT film obtained by VTE (1st scan). _____	106
Figure 65. J/V curves under AM 1.5 illumination of the prepared cells. _____	108
Figure 66. AFM images of OCT/ $\text{C}_{60}$ (left) and P3HT/ $\text{C}_{60}$ (right) evaporated blends. _____	109
Figure 67. $^1\text{H}$ NMR spectrum of COP2 in ODCB- $d_4$ . _____	126
Figure 68. IR spectra of T6F, COP1 and COP2. _____	127
Figure 69. UV-Vis spectrum of COP2 and P3HT/PCBM blend in film _____	129
Figure 70. DSC curve of COP2. _____	130

Figure 71. TGA graphs of COP2 under nitrogen and in air. _____	130
Figure 72. Current density-voltage for tested cells under AM 1.5 one sun illumination. _____	131
Figure 73. IPCE curves of the prepared OPV solar cells. _____	132
Figure 74. AFM images of a P3HT/PCBM blend (left) and of a COP2 film (right). _____	133
Figure 75. Amount of elimination of HF from primary, secondary and tertiary amines cured Viton A. _____	153
Figure 76. Infrared spectra of an uncured poly(VDF-co-HFP) copolymer before (A) and after (B) heating at 300°C for 20 min in air. _____	153
Figure 77. <sup>19</sup> F-NMR spectra of a poly(VDF-co-HFP) copolymer before (top) and after (bottom) treatment with hydroxyl base (2,5-trifluorobenzotrifluoride internal standard). Changes in peak intensities are indicated. _____	156
Figure 78. Effect of MgO on the mechanical properties of a formula comprising Viton A cured with dithiol. _____	158
Figure 79. Evolution of the yield of fluoride atom of VDF-based fluoropolymer heated at 200°C versus time and amount of MgO (acid acceptor) _____	158
Figure 80. Comparison of the efficiency of acid acceptors: a) metal oxide at 275°C, b) hydroxide acceptors at 275°C and c) carbonate acceptors at 275°C. _____	159
Figure 81. Crosslinking mechanism with bisphenol. _____	161
Figure 82. <sup>19</sup> F-NMR spectra of a poly(VDF-co-HFP) copolymer treated with DBU in a solution of DMAC (top) and the gel which results from this reaction in the presence of BAF (bottom). _____	162
Figure 83. <sup>19</sup> F-NMR spectra of a poly(VDF-co-HFP) copolymer treated with DBU and BAF in as solution of DMAC (top) and the same sample after several purifications (bottom). _____	163
Figure 84. Cure response by ODR at 177°C of a VDF-based polymer cured with BAF. _____	164
Figure 85. Evolution of the ODR units (crosslink density) at 177°C: (O) with variation of BAF concentration (in phr), in the presence of BTTPCl and (Δ) with BTTPCl concentration in the absence of BAF. _____	165
Figure 86. Evolution of the gel fraction as a function of peroxide dose (phr) for a peroxide-cured poly(TFE-alt-P) copolymer (a) without any coagent; (b) with 3 phr of TAIC; (c) with 2.4 phr of divinylbenzene; (d) with 3 phr of TAC. _____	170
Figure 87. Interactions between peroxide and coagent, in the evolution of initial cure state (Nm) of a poly(VDF-co-HFP) copolymer, measured by ODR at 177°C for 30 min. _____	171
Figure 88. Rheometer curve of the compounds containing different peroxides. _____	175
Figure 89. Crosslinking density of cured gum stocks versus post cure time at 204°C, under nitrogen: (A) diamine cured system; (B) peroxide cured system and (C) bisphenol cured. _____	178
Figure 90. Dependence of elongation at break versus aging time of a poly(VDF-co-HFP) copolymer crosslinked with piperazine carbamate and trimethyl diamine carbamate (curve A) and cured with Bisphenol AF (curve B). _____	181
Figure 91. Dependence of tensile strength versus ageing time of the same sample than Fig. 90. _____	181
Figure 92. Bisphenol AF and BTTPCl curing system. _____	193
Figure 93. Different salts used in the curing systems. _____	194
Figure 94. <sup>1</sup> H-NMR spectrum of bisphenol AF. _____	195
Figure 95. <sup>1</sup> H-NMR spectra of benzyltriphenylphosphonium chloride (top) and crosslinking system 1 (bottom). _____	195
Figure 96. <sup>1</sup> H-NMR spectra of tetrabutylphosphonium bromide (top) and crosslinking system 2 (bottom). _____	196
Figure 97. <sup>1</sup> H-NMR spectra of butyltriphenylphosphonium bromide (top) and crosslinking system 3 (bottom). _____	197
Figure 98. <sup>1</sup> H-NMR spectra of tetrabutylphosphonium hexafluorophosphate (top) and crosslinking system 4 (bottom). _____	198
Figure 99. ODR curves for the four examined crosslinking systems. _____	199
Figure 100. Stress-strain curves for the four crosslinking systems in exam. _____	200

Figure 101. Schematic structure of VDF/HFP copolymer. _____	204
Figure 102. Typical product for the biphasic dehydrofluoruration. _____	205
Figure 103. Typical product for homogeneous phase dehydrofluoruration. _____	206
Figure 104. Typical $^{19}\text{F}$ -NMR spectrum (up) and expansion (down) of a FKM copolymer. _____	207
Figure 105. $\text{CF}_3$ and $\text{CF}_2$ region expansion of a typical spectrum of dehydrofluorinated polymer. _____	209
Figure 106. Percentage of double bonds formed as a function of reaction time. _____	212
Figure 107. FT-IR spectra of the pristine (left) and treated (right) polymer in exam. _____	212
Figure 108. FT-IR spectra relative to sample 1 (up) and sample 2 (down) under UV radiation at different times _____	214
Figure 109. Bands ratio as a function of crosslinking time. _____	214
Figure 110. UV-Vis spectra in film relative to sample 1 (up) and sample 2 (down) at different times after UV exposure. _____	215
Figure 111. FT-IR spectra of a sample exposed to sunlight at different times. _____	216
Figure 112. ODR curve for a peroxide-curable compound. _____	217

## LIST OF SCHEMES

<i>Scheme 1. PT synthesis according to a) Yamamoto and b) Lin and Dudek.....</i>	<i>23</i>
<i>Scheme 2. Dehalogenative polycondensation. ....</i>	<i>23</i>
<i>Scheme 3. PT synthesis according to a) Wudl, b) Yamamoto and c) Sugimoto.....</i>	<i>24</i>
<i>Scheme 4. Cross-coupling polymerization with metals as catalysts. ....</i>	<i>26</i>
<i>Scheme 5. Oxidative polymerization with FeCl<sub>3</sub>.....</i>	<i>27</i>
<i>Scheme 6. Synthesis of a HH-TT regioregular PAT starting from a) HH dimer and b) TT dimer. ....</i>	<i>28</i>
<i>Scheme 7. Rieke-Chen polymerization.....</i>	<i>29</i>
<i>Scheme 8. Stille coupling polymerization.....</i>	<i>30</i>
<i>Scheme 9. Heck coupling polymerization. ....</i>	<i>30</i>
<i>Scheme 10. Suzuki coupling polymerization. ....</i>	<i>31</i>
<i>Scheme 11. McCullough polymerization. ....</i>	<i>32</i>
<i>Scheme 12. McCullough new polymer synthesis.....</i>	<i>32</i>
<i>Scheme 13. Synthesis of the monomer TSBu. ....</i>	<i>55</i>
<i>Scheme 14. Synthesis of the polymer PSBu by using the GRIM reaction. ....</i>	<i>55</i>
<i>Scheme 15. Synthesis of the monomer 2,5-BTSM<sub>e</sub> and polymer PTSM<sub>e</sub>. ....</i>	<i>75</i>
<i>Scheme 16. Structure of 3,3''',4''',3''''''-tetra(6-methoxyhexyl)-2,2':5',2'': 5'',2''':5'',2''': 5''',2''':5''',2''': 5''''',2''''''-octithiophene (OCT). ....</i>	<i>96</i>
<i>Scheme 17. Synthesis route for the preparation of HexF.....</i>	<i>119</i>
<i>Scheme 18. Synthesis route for the preparation of T6F.....</i>	<i>120</i>
<i>Scheme 19. Synthesis of copolymer COP2 .....</i>	<i>122</i>
<i>Scheme 20. Diels-Alder reaction during post-curing forms aromatic ring with loss of HF. ....</i>	<i>154</i>
<i>Scheme 21. Dehydrofluorination mechanism of poly(VDF-co-HFP) copolymer in the presence of base.....</i>	<i>157</i>
<i>Scheme 22. Crosslinking mechanism with peroxide. ....</i>	<i>176</i>
<i>Scheme 23. Biphasic dehydrofluoruration reaction. ....</i>	<i>205</i>
<i>Scheme 24. Homogeneous phase dehydrofluoruration reaction. ....</i>	<i>206</i>
<i>Scheme 25. Possible mechanisms for FKM dehydrofluoruration.....</i>	<i>210</i>

## LIST OF TABLES

Table 1. Overview of reported polymer thin film applications using R2R techniques.....	41
Table 2. FT-IR absorption bands ( $\text{cm}^{-1}$ ) and relative assignments for TSBu, 2,5-BTSBu and PSBu samples.....	56
Table 3. $^1\text{H}$ - and $^{13}\text{C}$ -NMR signals (ppm) and relative assignments for TSBu, 2,5-BTSBu and PSBu samples.....	57
Table 4. Electrical conductivity ( $\sigma$ ) of PATAC-Me and PSBu at different temperatures.....	65
Table 5. Photovoltaic parameters for the devices obtained using the two different photoactive blends.....	87
Table 6. Optical and electrochemical properties of the films cast from $\text{CHCl}_3$ solutions.....	88
Table 7. IR absorption bands and relative assignments for evaporated OCT.....	103
Table 8. Photovoltaic properties of the assembled solar cells.....	108
Table 9. Copolymers characteristics.....	125
Table 10. IR absorption bands (in $\text{cm}^{-1}$ ) and respective assignments for the synthesized materials.....	128
Table 11. Photovoltaic parameters for the devices obtained using the two different photoactive polymers.....	132
Table 12. List of ABBREVIATIONS and SYMBOLS.....	144
Table 13. Monomer reactivity ratios for the radical copolymerization of VDF (A) with other fluoroalkenes (B) (and vinyl acetate and ethylene) .....	147
Table 14. Improvement of mechanical properties of bisphenol, and peroxide-cured poly(VDF-ter-HFP-ter-TFE) terpolymer with post cure step. .....	149
Table 15. Compression set resistance measured at $204^\circ\text{C}$ for 70h, of a peroxide cured VDF/HFP/TFE terpolymer.....	151
Table 16. Soluble fraction in acetone of a poly(VDF-co-HFP) copolymer heated in air at $250^\circ\text{C}$ .....	154
Table 17. Influence of the coagent on the gel fraction and the compression set resistance of a peroxide-cured poly(VDF-co-HFP) copolymer ( $M_n=100000$ g/ mol).....	169
Table 18. Crosslinking of two peroxides onto poly(VDF-co-HFP) copolymer and the influence of their cure temperature on ODR values.....	172
Table 19. Half-life and gel fraction values of poly(TFE-co-P) copolymers ( $M_n=100000$ g/ mol) cured with acyl-, alkyl- or hydroperoxides.....	173
Table 20. Composition of different Viton GF compounds cured with peroxide.....	174
Table 21. Composition of vulcanizates I and II.....	178
Table 22. Mechanical properties of vulcanizates I (diamine cure) and II (peroxide cure) after press cure at $150^\circ\text{C}$ for 30min and post cure from $120^\circ\text{C}$ to $200^\circ\text{C}$ at heating rate of $25^\circ\text{C}/\text{h}$ then heat at $200^\circ\text{C}$ for 24h.....	179
Table 23. Mechanical and chemical properties of a peroxide-cured poly(TFE-alt-P) elastomer and a diamine-cured poly(VDF-ter-HFP-ter- TFE) elastomer.....	180
Table 24. Mechanical properties for press cure and post cure VDF/HFP copolymer cured with BAF or peroxide.....	182
Table 25. ODR values for the four examined crosslinking systems.....	199
Table 26. Modulus and elongation at break for the four examined crosslinking systems.....	201
Table 27. Conditions of biphasic dehydrofluoruration.....	203
Table 28. Conditions of homogeneous phase dehydrofluoruration.....	203
Table 29. $^{19}\text{F}$ -NMR signals attribution for a typical VDF/HFP copolymer.....	208
Table 30. Summary of the values obtained.....	211
Table 31. Attribution of FT-IR bands for a dehydrofluorinated product.....	213
Table 32. ODR data for a peroxide-curable compound.....	217









## **PART 1: POLYTHIOPHENES**



## CHAPTER 1: INTRODUCTION

### *1.1 $\pi$ -CONJUGATED POLYMERS*

Conjugated polymers (ICPs) are organic polymers that conduct electricity. Such compounds may have metallic conductivity or can be semiconductors. Conductive polymers are generally not thermoplastics, i.e., they are not thermoformable, but, like insulating polymers, they are organic materials. They can offer high electrical conductivity but do not show similar mechanical properties to other commercially available polymers. The electrical properties can be fine-tuned using the methods of organic synthesis or by advanced dispersion techniques.

Conjugated polymers in their semiconducting or less conductive forms are widely used in the organic electronic field for applications such as light-emitting diodes [1], thin film field effect transistors [2], and bulk heterojunction solar cells (BHJ).

$\pi$ -conjugated polymers are of relatively recent interest when, back in 1977, professors Alan J. Heeger, Alan G. MacDiarmid and Hideki Shirakawa found that polyacetylene, properly treated, showed conductivity comparable to a metal; this discovery was awarded with the Nobel Prize in Chemistry in 2000 (Fig. 1).



A. J. Heeger



A. G. MacDiarmid



H. Shirakawa

*Figure 1. Winners of the Nobel Prize in Chemistry in 2000.*

Polyacetylene (PA), with its two structural isomers, is the simplest conjugated organic polymer (Fig. 2).

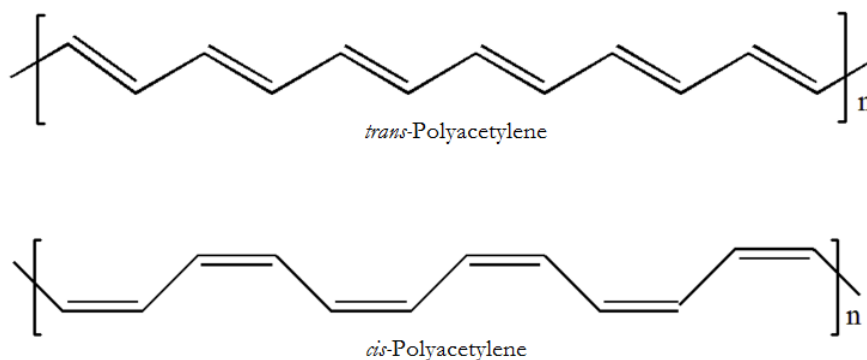


Figure 2. Isomeric structures of Polyacetylene.

PA was synthesized as a conjugated polymer with high molecular weight, high crystallinity and regular structure in 1958 when Natta et al. [3] polymerized acetylene in hexane using  $\text{Al}(\text{Et})_3/\text{Ti}(\text{OPr})_4$  as initiator. For long time PA was considered of poor interest due to the impossibility of obtaining a processable polymer regardless of the method of polymerization: in fact, it could be only obtained as a black powder, infusible, insoluble and air-unstable. Only at the beginning of '70s a renewed interest on this kind of material was raised by the studies made by Shirakawa et al. [4-7] that prepared flexible and high quality films both of the auburn *cis*-isomer and of the silver *trans*-isomer, in presence of ZieglerNatta catalyst and they also developed different techniques for controlling the ratio between the two isomers in the final product [6-7].

However, both product showed poor conductivity, i.e. to  $10^{-8}$ - $10^{-7}$  S/m for *cis*-PA and  $10^3$ - $10^2$  S/m for *trans*-PA. Shirakawa noticed that IR spectra of PA film exposed to bromine or chlorine vapors, showed a significant decrease of transmittance, that increased back after the complete alogenation of the polymer, a fact that suggested unusual electronic properties of this product. The collaboration with Heeger and MacDiarmid was crucial for the studies that worthed the Nobel Prize in Chemistry in 2000: until 1977 they studied the electronic properties of PA exposed to iodine and bromine vapors [8] and treated with arsenic pentafluoride [9], measuring conductivity values ranging from  $10^3$  to  $10^{11}$  S/m, which are typical values of metals.

Increasing the conductivity of this material up to 18 orders of magnitude, depending on the treatment used, allows to control its electronic properties from insulating material to semiconductor, till metal. These discoveries and the consequently studies on the mechanisms of this behavior, led to the development of the so-called “synthetic metals”, named “Intrinsecally Conductive Polymers” (ICPs). The opportunity to combine processability, lightness, versatility, reliability of polymeric materials with the properties of conductive and semi-conductive materials, which are crucial for modern electronic and optical fields, led, from the 80s, to an intense study of conductive polymers; the main are (Fig. 3): polyparaphenylene (PPP), polyparaphenylenesulfide (PPS), polyparaphenylenevinylene (PPV),

polyaniline (PANI), polypyrrole (PPy), polythiophene (PT), polyisothianafene (PITN) and polyethylenedioxythiophene (PEDOT).

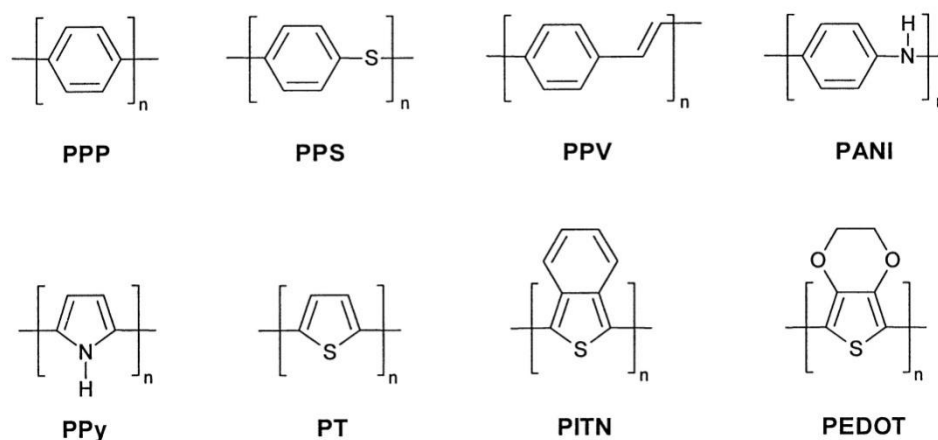


Figure 3. Structure of some conjugated polymers.

Polyacetylene is the polymer which shows higher conductivity, but its high sensitivity to air and moisture make it not suitable for practical uses although it's still studied as the archetype of this class of polymers.

Other products are more air stable both in neutral and electro-conductive forms. They show lower conductivity, usually around  $10^4$  S/m, which is however sufficient for many practical applications.

Nowadays, the studies are mainly focused on the analysis of the structures and electronic properties of these polymers, on the development of synthetic routes which can lead to a better control on their properties, on the synthesis of functional polymers where polymeric backbone properties are associated with lateral groups in the side chains and on their technological applications. These polymers can be used from antistatic covers and energy storage systems to sophisticated electronic devices such as transistors, organic light emitting diodes (OLEDs), solid state lasers and modified selective electrodes and sensors.

## 1.2 ELECTRONIC STRUCTURE OF CONJUGATED POLYMERS

In common polymers, the electronic structure of the atomic chain forming the backbone of the macromolecule, consists exclusively of  $\sigma$ -type bonds. The high energy gap,  $E_{\text{gap}}(\sigma)$ , between bond and anti-bond levels, makes these materials electrically insulating and, generally, they don't absorb visible radiation. For example, in polyethylene the  $E_{\text{gap}}(\sigma)$  is about 8 eV.

Instead, conjugated polymers consist of a continuous network of close double bonds. The PA backbone is composed of  $sp^2$  hybridized carbon atoms, each of them forming three  $\sigma$  bonds, while the  $p_z$  orbital is overlapped with the nearest other  $p_z$  orbital, leading to a the  $\pi$ -type double bond.

This kind of structure causes the formation of  $p$  states delocalized throughout the whole polymeric chain that create two bands, called “valence” and “conduction” bands as for metals, when the number of conjugated double bonds increases (Fig. 4) [10].

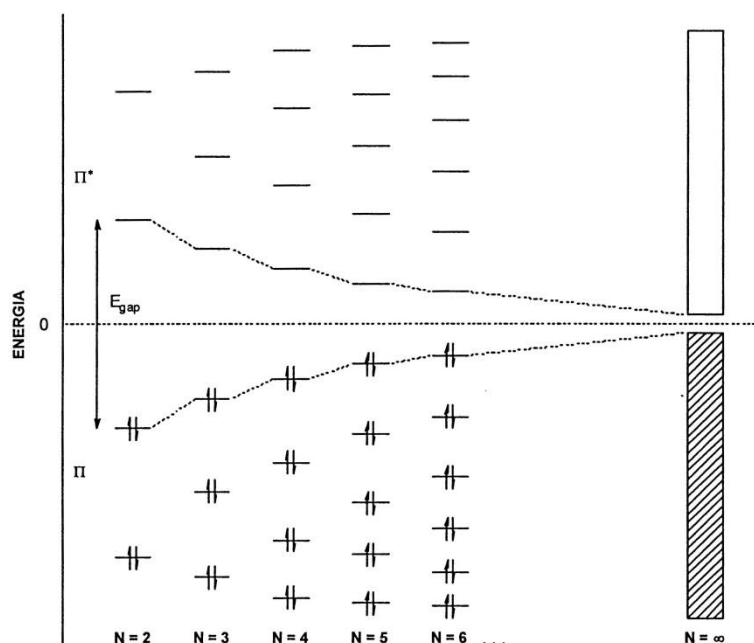


Figure 4. Schematization of valence and conduction bands model.

The energy gap between  $\pi$ -bonding and  $\pi^*$ -antibonding levels,  $E_{\text{gap}}(\pi)$ , tends asymptotically to a limit value which is lower than  $E_{\text{gap}}(\sigma)$ , explaining the absorption of lower energy photons in the region of visible light. The small value of  $E_{\text{gap}}(\pi)$  ( $\sim 1\text{-}4$  eV) is responsible for the semiconducting characteristics of conjugated polymers (Fig. 5).

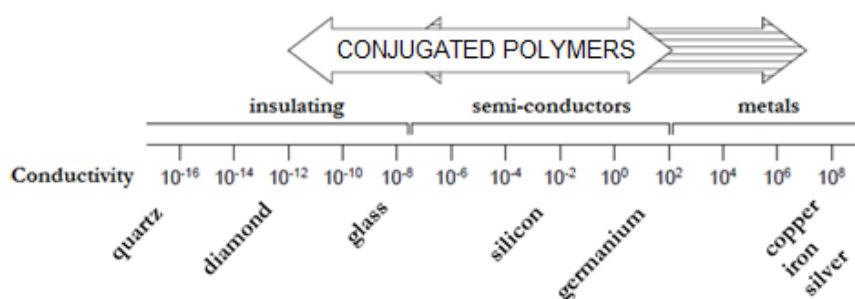


Figure 5. Conductivity comparison between conjugated polymers and some conventional materials



The polymeric chains can be easily oxidized or reduced, generally by means of charge transfer with dopant molecules. This process leads to the formation of charged species with sufficient mobility to obtain high conductivity values.

In traditional semiconducting materials, the atom coordination through covalent bond leads to the formation of a rigid three dimensional structure in which the excited electronic states are constituted by excess or lack of electrons.

Instead, in ICPs, that have mono dimensional structure, the excited states are connected with backbone distortions. Two classes of polymer can be distinguished: the ones that have *solitonic* degenerate excited state with ground state and non-degenerate *polaronic* and *bipolaronic* excited state, as described in the following paragraphs.

### 1.2.1 Systems with degenerate ground state

Polyacetylene (CH)<sub>x</sub> in its *trans* form, which is the most thermodynamically stable, is the model for this class of polymers. Charge carriers, generated from the doping process, lead to a charge transfer from the polymer towards an electron acceptor (A), where the macromolecular chain acts as a polycation in presence of A<sup>-</sup> species. Similarly, with an electron donor (D), the polymer acts as a polyanion in presence of D<sup>+</sup> species. Chemical compensation has been demonstrated, showing that the doping process is reversible and can also be made with an electrochemical process.

In *trans*-(CH)<sub>s</sub>, if bonds length were equal, the repeating unit would be a CH group and the polymer would behave as an almost mono dimensional metal with a band half full of electrons. However, this system is unstable among the dimerization distortion, known as *Peierls distortion*, where the movement of the contiguous CH groups towards each other determines the alternating formation of shorter (partially double) and longer (partially single) bonds, lowering the system energy. Single and double bonds can be interchanged for symmetry, without energy variations. Therefore, two state at the lowest energy, A and B, possessing two different bonding structures, can exist. The transition from one form to another is described by the dimerization parameter, as follows:

$$u = d_{C=C} - d_{C-C}$$

where  $d_{C=C}$  e  $d_{C-C}$  indicate the bond lengths for double and single bond respectively. The energy of the two states is function of the dimerization parameter (Fig. 6).

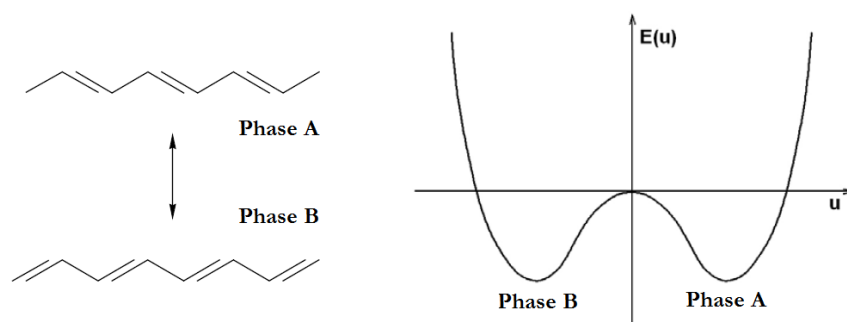


Figure 6. Structure and energy diagram for the two phases of PA.

This degeneration in two levels leads to the existence of non-linear topological excitations (bonds alternation border domain or *soliton*) which seems responsible of many of the properties of PA. The *soliton* proposed for this polymer [11] is a “defect” in the electronic system: a border point that links phase A with phase B having different bond alternation (Fig. 7).

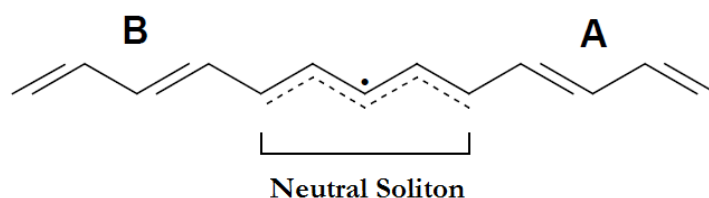


Figure 7 A neutral soliton separates phases A and B.

The existence of the soliton leads to the formation of a new energy level, called Fermi's level, that is collocated exactly in the middle of the gap between valence and conducting bands (Fig. 8a). The doping with electron-acceptors determines the formation of positive charged soliton (non-occupied state, Fig. 8b) while doping with electron-donors is obtained a negative charged soliton (double occupied state, Fig. 8c).

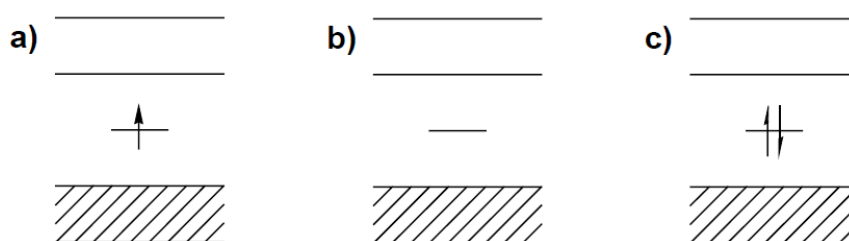


Figure 8. Energy levels diagram for a) neutral, b) positive and c) negative soliton.

From the chemical point of view, neutral solitons are equivalent to a radical with no charge and spin of  $1/2$ . Charged solitons, instead, don't have spin and can move across the polyconjugated backbone by means of a potential difference generating the conductivity.

Finally, it should be noted that during the doping process, a couple of defects, in the form of soliton-antisoliton, is always formed. The separation energies of this couple have been studied by J. L. Bredas *et al.* [12]. The results show that, at low levels of doping, charges released in the macromolecular chain determine the formation of *polaronic* type charge carriers and not only of charged solitons. With the increase of doping, the *polarons* evolve, leading to the formation of charged solitons.

### 1.2.2 Systems with non-degenerate ground state

As PA, all ICPs have two resonance structures: aromatic and chinoid (e.g. polythiophene, Fig. 9a). However, these two forms are not isoenergetic, because the chinoid form has higher energy and consequently determines the presence of a non-degenerate ground state (Fig. 9b).

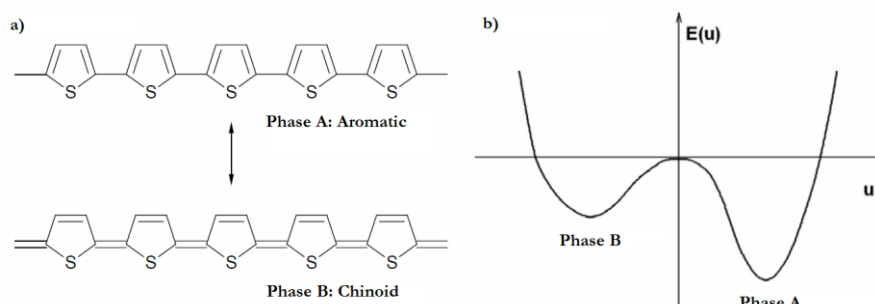


Figure 9. a) Aromatic and chinoid forms of polythiophene and b) energy diagram of the two configurations.

In these polymers, the existence of a single state located in the middle of the energy gap between  $\pi$  and  $\pi^*$  bands is not possible. The formed defects are always constituted by a couple soliton-antisoliton and they appear to be “confined”. This confinement is due to the presence, caused by the formation of the soliton-antisoliton couple, of some rings in the chinoid form and therefore in higher energy state (Fig. 10). Therefore, a compromise must be created between the energy separation of the defects and the extent of relaxation of the lattice induced by them.

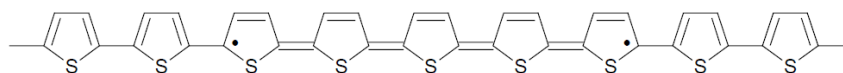


Figure 10. Soliton-antisoliton couple of polythiophene.

When an electron is removed from the polymeric system or added through doping, a unit called *polaron* is formed, which introduces one state of bonding and one antibonding state in the energy gap. Polarons can be positively or negatively charged and have spin equal to  $\frac{1}{2}$  (e.g. for PT, Fig. 11)

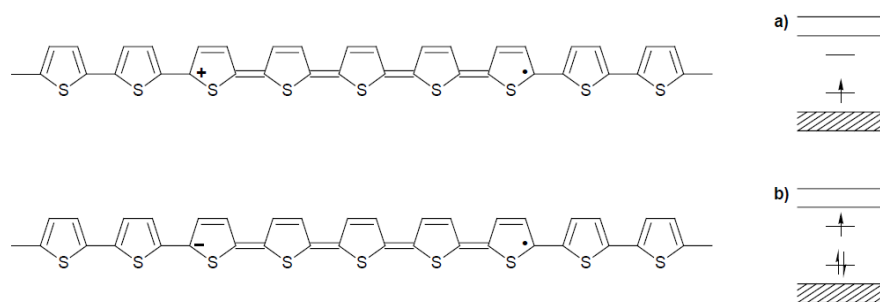


Figure 11. a) Positive charged and b) negative charged polarons with their energy diagrams.

From the electronic levels point of view, we are in a similar situation to that of *trans*-PA with low level of doping. But, differently from *trans*-PA, in other ICPs the formation of *bipolarons* (dianions or dications with zero spin) is observed (Fig. 12).

Although the formation of a bipolaron implies a higher deformation of the lattice, it's energetically more favored than the formation of two polarons [13]. The high deformation, derived from the presence of the bipolaron, determines a further increase of the anti-bonding level above the valence band (Fig. 12), making the ionization processes easier.

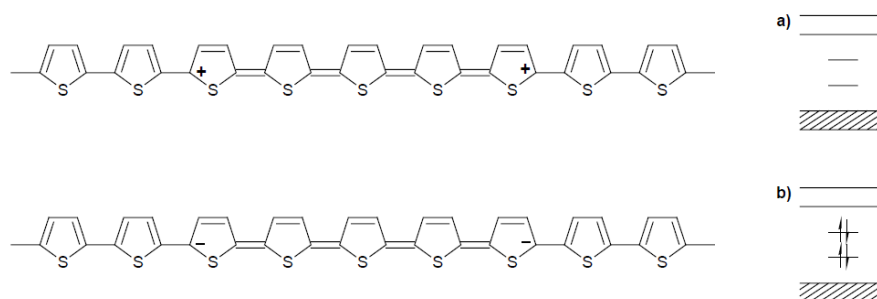


Figure 12. Bipolarons with a) positive and b) negative charge with their corresponding energy levels for polythiophene.

Charges of the bipolarons are very confined and they are localized for PT, PPy and PPP, on an average of five rings.

With the increase of the doping level, several new levels emerge from the  $\pi$  band and form a new band with high energy. The conductivity of ICPs could come from the motion of several bipolaronic entities across the macromolecule.

### 1.3 CHARACTERIZATION OF CONDUCTIVE POLYMERS

As for many others polymers, ICPs can be characterized through different analysis techniques [14], such as:

- cyclic voltammetry, which allows to know redox processes;
- optical characterization, for electrochromic application;
- nuclear magnetic resonance for structural analysis and orientation of the chains;
- gel permeation chromatography, for the molecular weight analysis;
- Raman and FT-IR analysis, for the identification of the vibrational motions;
- differential scanning calorimetry and thermogravimetric analysis for the identification of glass transition, melting and decomposition temperature;
- electroluminescence measurements for the possible use in PLEDs;
- X-ray diffraction for determining the crystal structure.

## ***1.4 APPLICATION OF CONJUGATED POLYMERS IN THEIR ELECTROCONDUCTIVE DOPED STATE***

In these kind of applications, ICPs can be used in substitution of metals for their better properties, for the easier processing or for problems connected with toxicity or environmental pollution. It is possible to use directly these products for their conductivity or exploit the variation of physical properties of the material when the doping process occurs [15, 16].

### ***1.4.1 Conductor devices***

The most obvious application of ICPs is their use as conductors, combining high conductivity with the excellent mechanical properties and high lightness of plastic materials.

In the modern technology, a remarkable request for transparent conductors exists. Due to their high molar extinction coefficient, conjugated polymers are transparent only as thin films, but blends with insulating polymers allow to obtain a good optical transparency without a significant decrease of conductivity. The easy processing of polymeric materials allows to obtain antistatic covering and homogeneous fibers also in blends with other polymers.

### ***1.4.2 Radar application***

Radar detecting consists in determining the position, direction and speed of an object from the analysis of the signal obtained by reflection of a magnetic radiation which invests the object itself. The coverage with a doped conductive polymer lead to the absorption of more than 50% of the incident

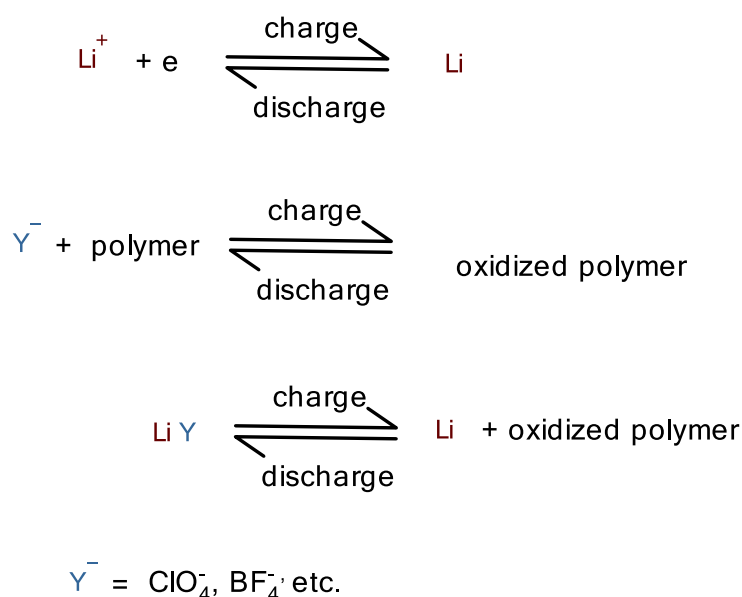
radiation and the reflected part has such characteristic that the object is not distinguishable anymore, making it completely invisible at radar controls. This property generates a remarkable interest, especially in the military field, for the production of shield systems.

### *1.4.3 Corrosion protection*

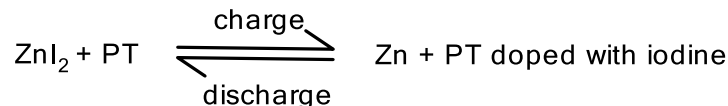
The current corrosion protection systems, especially in the marine field, use sacrificial metal electrodes which oxidize in place of the substrate determining a high environmental impact due to toxic metals release. Also coating with epoxy resins is widespread, but not very durable because a little break immediately exposes the substrate to oxidation. Coatings with conducting polymers having oxidation potential lower than the substrate, in addition to act as physical coverage, can be easily oxidized instead of the substrate even in case of cracks. Moreover, conjugated polymers, in the doped state, are completely insoluble, so the coating continues to resist eliminating the problem of environmental spread. Alternatively, conductive polymers with higher oxidation potential than the substrate can be used too. In this case, the polymer reacts with the material to be protected determining the passivation of the exposed surface.

### *1.4.4 Batteries*

The field of accumulators of electricity [17] is one of the first in which ICPs have demonstrated a high commercial impact. In batteries, a cathode and an anode are present which are respectively reduced and oxidized in a reversible manner thanks to the presence of a support electrolyte that separates the two electrodes and acts as ions source for the redox reaction balancing. ICPs can be employed as cathodes offering ease of manufacture, processability and low weight. Lithium-polymeric batteries are interesting; the reactions that take place are:



Similarly, charge/discharge reaction take place when a  $\text{ZnI}_2$  solution is electrolyzed using Zn and polythiophene (PT) as negative and positive electrodes:



### 1.4.5 Catalysts

The doped surface of an ICP constitutes a hybrid material that can be seen as a heterogeneous catalyst supported on a polymeric matrix which can be used in many industrial processes such as the conversion of alcohols or olefin oxidation. The dispersion of the catalytic specie using the doping process and the chemical bond that is formed with the carrier prevent the release of the catalyst itself. Moreover, the possibility of easily varying the doping level allows to efficiently modulate the catalytic activity of the system.

### 1.4.6 Electrochromic cells

ICPs show different optical properties both in the neutral and in the doped state. Doping can be made electrochemically determining the so-called *electrochromic effect*. Electrochromic windows are based on this principle. Generally, one electrode of conducting polymer, a proper transparent electrolyte and a

counter-electrode are sandwiched together. The application of a difference of potential between the two electrodes induces the doping of the polymer and, consequently, a variation of its color.

### 1.4.7 Sensors

Conjugated polymers offer the possibility to combine the interaction with an analyte with an observable response since this process usually determines a variation in the polyconjugated backbone conformation resulting in a change of its optical or electrochemical properties. It derives the possibility of using ICPs as sensors [18] where polymer structures provide a higher sensitivity than molecular ones.

ICPs based sensors exploit different schemes. Conductimetric sensors record a variation of the polymer conductivity, in the neutral or doped state, using a pair of electrodes. Instead, potentiometric sensors measure the variation of the potential of the system and only require the immobilization of the polymer onto an electrode. Optical sensors, such as colorimetric or fluorescence also exist.

Unmodified ICPs are non-selectively sensible to pH and to many analytes as organic vapors, oxygen, nitrogen oxides, amines, hydrazines, moisture, various ions and cytochrome C. The functionalization with polyalkylether chains, crown ethers and azo crown ethers allows to obtain specific selectivity for cations; with pyridine-based ligands, metals can be detected; chiral substituent exhibits enantioselectivity towards chiral dopant ions; metalcyanide, metaporphyrin and calixarene give high ionchromic response. Furthermore, simple acid-base interaction can be exploited for the determination of cations or anions or for the development of biological sensors for the recognition of proteins, DNA or RNA sequences and enzymes.

### 1.4.7 Controlled release application

Inorganic or biological ions can be selectively released by polymeric systems through the application of a controlled potential. A simple device and its working schemes are reported (Fig. 13). A conducting polymer **A**, with an oxidation potential  $E_{Aox}$ , is electrodeposited on a substrate with a mobile counter-ion  $X^-$ . A second polymer **B**, with an oxidation potential  $E_{Box}$  higher than **A**, is electrodeposited on the **A** film using non-mobile counter-ion  $Y^-$ . The system results then exposed, from the **B** side, to the electrolyte solution. During the complete reduction (Fig. 13a)  $X^-$  ion leaves the device and, as  $Y^-$  is fixed, the charge balance is achieved only by from the input of a cation  $M^+$  from the external solution of the electrolyte. The selective oxidation of **A** calls back  $X^-$  again in the internal layer (Fig. 13b) while with the oxidation of **B**,  $M^+$  is freed once again (Fig. 13c).



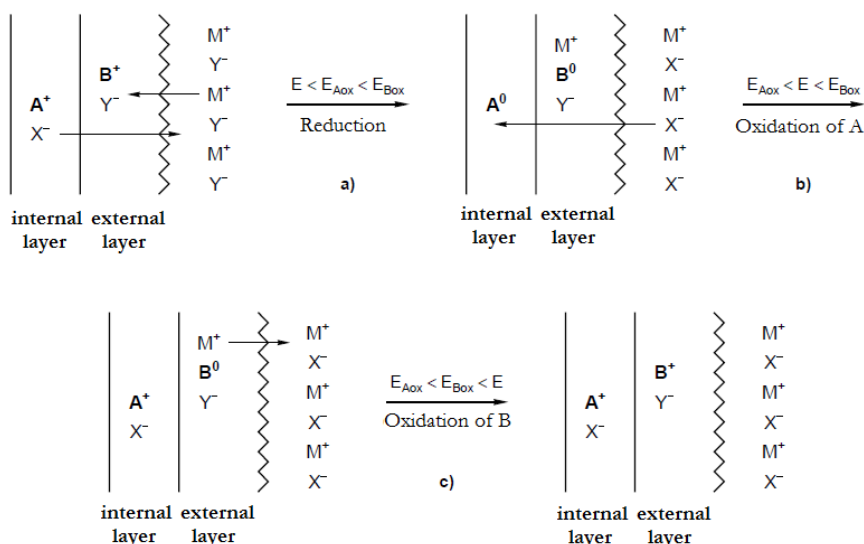


Figure 13. Ion-selective transport by an electroactive bi-layer.

Ions transport as a function of the potential is an interesting system of drugs dosage in biological systems. Cycling the potential with  $E < E_{Aox} < E_{Box}$  it is possible to distribute anions and receive cations, while in the return cycle, with  $E_{Aox} < E < E_{Box}$  only anions are released or only cation if  $E_{Aox} < E_{Box} < E$ .

## 1.5 APPLICATION OF CONJUGATED POLYMERS IN THEIR NEUTRAL SEMI-CONDUCTIVE STATE

Non-doped conjugated polymers are semi-conductors whose energy gap is depending not only by the chemical constitution of the backbone, but also by the nature of the substituent bonded to the main chain. Consequently, ICPs properties can be widely modified by means of an appropriate functionalization [19,20].

### 1.5.1 Polymeric Light Emitting Diodes (PLEDs)

The studies made by Friend *et al.* [21] on the PP electroluminescence have opened a new field for the application of ICPs in technologies exploiting this phenomenon. Electroluminescence can be easily defined as the generation of light induced by electric excitation.

In its simplest type, a PLED consists in a single layer of electroluminescent polymer sandwiched between two electrodes, one of them transparent to the light produced during electroluminescence effect (Fig. 14). This electrode is usually the anode (which injects electronic vacancy or “holes”) and it's constituted of a layer of indium/tin oxide (ITO). The cathode, which generates electrons, must be composed of a easily oxidizable material such as Ca, Mg or Al.

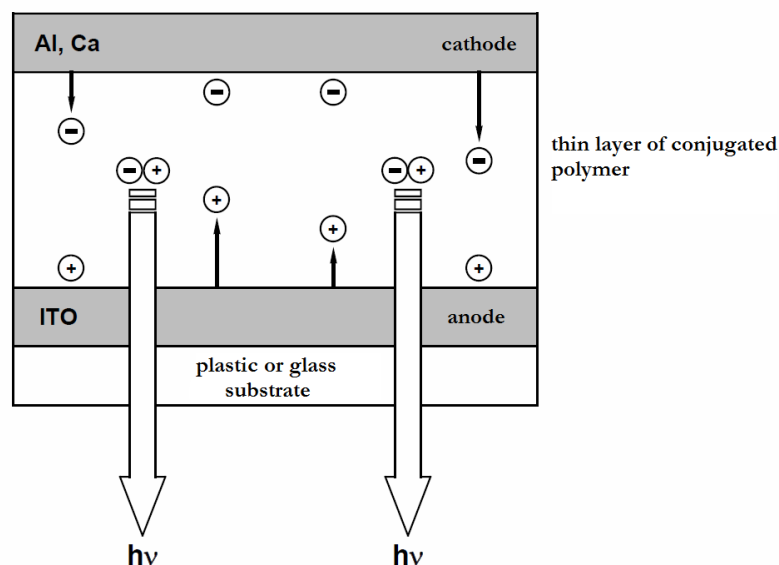


Figure 14. Schematic structure of a single layer PLED.

Up to a determined threshold voltage, current doesn't flow; beyond this value, current increases rapidly with increasing of applied voltage. Opposite charge carriers, holes and electrons, are injected in the conjugated polymer layer respectively from the anode and the cathode. Vacancies are generated in the highest occupied molecular orbital (HOMO) of the  $\pi$  valence band, while electrons are injected in the lowest unoccupied molecular orbital (LUMO) of the  $\pi^*$  conduction band (Fig. 15). In both electrodes a potential threshold that must be overcome in order to insert charges in the polymer clearly exist. The process can lead to the formation of excited states of singlet or triplet of which only the first one decays with a radiative process with light emission.

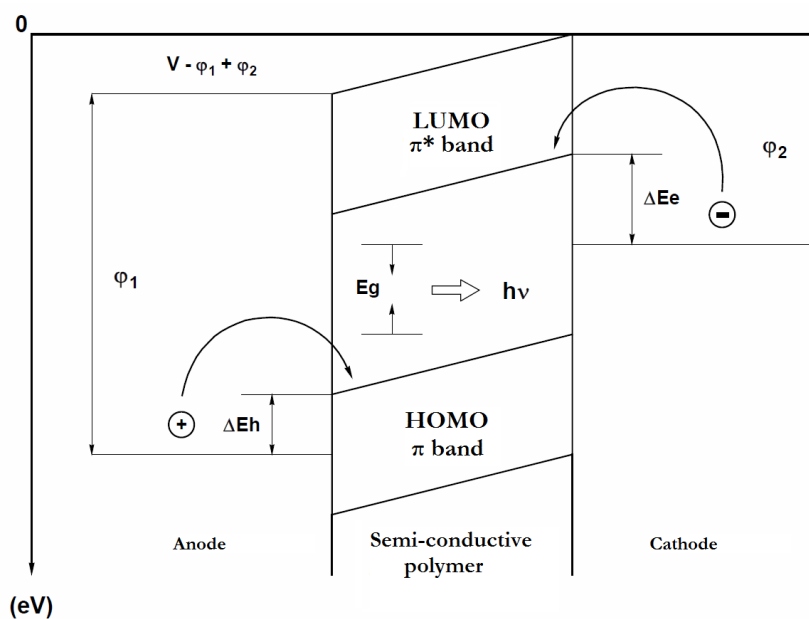


Figure 15. Diagram for single-layer PLED bands.

In conjugated polymers, positive charges have higher mobility so electroluminescence mainly develops near the cathode. In this area, unfortunately, the probability of nonradiative charges recombination is higher with consequently decrease of device efficiency. To overcome to this disadvantage a bi-layer system can be used; in this system, an electrons carrier layer is inserted, between the cathode and the polymer.

The frequency of emitted light is nearly equal to the difference between the potentials of oxidation and reduction of the polymer and, since it is possible to synthesize a wide range of polymeric structures, multicolor display can be obtained.

### ***1.5.2 Photovoltaic cells***

Photovoltaic cells allow the transformation of light radiation into electric energy and can be then considered as the opposite of a PLED. Unfortunately, the photo-induced charge generation, needed for the working of the device, has an extremely low efficiency because the ICPs are electron-donors if subject to photoexcitation. If an electron-acceptor molecule is available in the close area, charge separation occurs due to photo induced electronic transfer. In this case in the conjugated backbone a configuration of stable charge storage is formed: a highly mobile and delocalized positive polaron. Fullerene molecules are highly effective as electron-acceptors. It is then possible to imagine a bilayer photovoltaic cell where a layer of fullerene is inserted between the polymer and the cathode, improving considerably the photovoltaic efficiency and the photo induced current.

### ***1.5.3 Field effect transistors (FET)***

FET are electronic devices that are crucial in modern electronics, because they are present, for example, in the computers chips. A FET is formed by one semi conductive layer on which are deposited two electrodes: the one is a dispenser of electrons (source) and the other retrieves charge (drain). They are separated from each other and from a third electrode (gate) by a dielectric layer (Fig. 16)

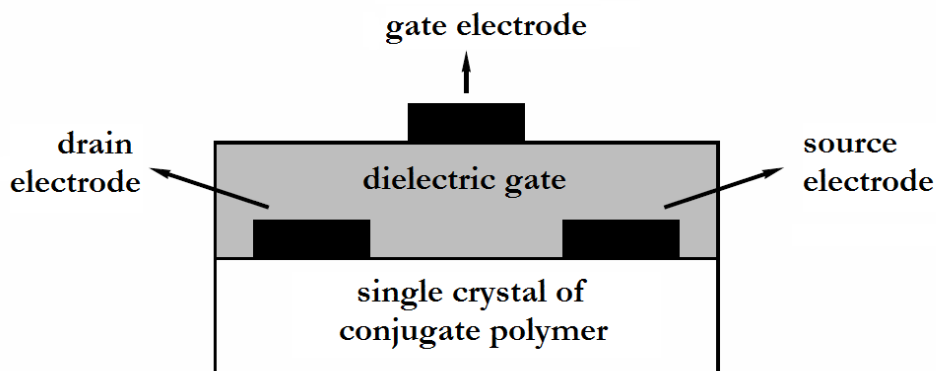


Figure 16. Schematic structure of a FET.

If no voltage between source and drain is applied, the device is in its insulating form (OFF). FET becomes conductive (ON) when a voltage is applied between source and drain electrodes through the organic semiconductor. The third electrode, the gate, allows, through small voltage variations, to control the concentration of generated charges in the polymer with a principle similar to old thermoionic valves.

## REFERENCES FOR CHAPTER 1

- [1] Gunes S, Neugebauer H, Sariciftci NS (2007) Chem Rev 107:1324
- [2] Murphy AR, Frechet JMJ (2007) Chem Rev 107:1066
- [3] G. Natta, G. Mazzanti, P. Corradini, Atti Accad. Naz. Lincei Rend. Cl. Sci. Fis., Mat. Natur. 25 (1958) 3
- [4] H. Shirakawa, S. Ikeda, Polymer J. **2** (1971) 231
- [5] H. Shirakawa, T. Ito, S. Ikeda, Polymer J. **4** (1973) 460
- [6] T. Ito, H. Shirakawa, S. Ikeda, J. Polymer Sci., Part A-1, Polymer Chem. **12** (1973) 11
- [7] T. Ito, H. Shirakawa, S. Ikeda, J. Polymer Sci., Part A-1, Polymer Chem. **13** (1975) 1943
- [8] H. Shirakawa, E. J. Louis, A. G. McDiarmid, C. K. Chiang, A. J. Heeger, J. Chem. Soc. Chem. Commun. (1977) 578
- [9] C. K. Chiang, C. R. Fincher, Y. W. Park, A. J. Heeger, H. Shirakawa, E. J. Louis, S. C. Gau, A. G. McDiarmid, Phys. Rev. Letters 39 (1977) 1098
- [10] G. Zerbi, La Chimica e l'Industria 73 (1991) 355
- [11] W. P. Su, J. R. Schrieffer, A. J. Heeger, Phys. Rev. Letters 42 (1979) 1698
- [12] J. L. Bredas, R. R. Chance, R. Silbey, Phys. Rev. Part A 26 (1982) 5843
- [13] J. L. Bredas, R. R. Chance, R. Silbey, Phys. Rev. Part A 26 (1982) 5843
- [14] J. D. Stenger-Smith, Prog. Polym. Sci. 23 (1998) 57
- [15] J. D. Stenger-Smith, Prog. Polym. Sci. 23 (1998) 57
- [16] A. Pron, P. Rannou, Prog. Polym. Sci. 27 (2002) 135
- [17] D. Cumar, R. C. Sharma, Eur. Polym. J. 34 (1996) 1053
- [18] D. T. McQuade, A. E. Pullen, T. M. Swager, Chem. Rev. 100 (2000) 2537
- [19] J. D. Stenger-Smith, Prog. Polym. Sci. 23 (1998) 57
- [20] A. Pron, P. Rannou, Prog. Polym. Sci. 27 (2002) 135
- [21] J. H. Burroughes, D. D. C. Bradley, R. H. Friend, A. R. Brown, R. N. Marks, K. MacKay, P. L. Burn, A. B. Holmes, Nature 347 (1990) 539



## CHAPTER 2: POLYTHIOPHENE AND ITS DERIVATIVES

Between the conducting polymers, polythiophene (PT) is very interesting and studied thanks to its high air and moisture stability both in the neutral and the doped states. Moreover, the relative ease to functionalize the heterocycle ring allows to synthesize a wide range of derivatives, employable in different fields.

### ***2.1 POLYTHIOPHENE***

PT is much studied for its high conductivity (10-100 S/cm) and its high stability [1] (until 350°C in air and up to 900°C under inert atmosphere in the neutral state) which derives from the high redox potential ( $E^0 = 0.70$  V). Its completely insolubility even at low molecular weights, due to  $\pi$ -stacking interactions, limits the processability and consequently industrial applications. In the following paragraphs, the main preparation methods of PT will be indicated since they can be applied also to its soluble derivatives. These preparations aim to the obtainment of a polymer in which the thiophenic rings are bonded exclusively by the  $\alpha$  positions because  $\beta$ -linkages lead to the decrease of electronic delocalization and consequently of every property derived from there.

The two main techniques for PT synthesis and its derivatives are electrochemical and chemical polymerizations.

#### ***2.1.1 Electrochemical synthesis***

Polythiophene can be synthesized by both cathodic and anodic polymerization [2]. In the first case the electroreduction of (2-bromo-5-thienyl)triphenyl nickel bromide in acetonitrile is used. The main disadvantage is that the polymer formed is in the neutral state leading to the quick passivation of the electrode resulting in low thickness of the film that does not exceed 100 nm. This method is the only possible when anodic corrosion susceptible electrodes are used.

The anodic electropolymerization, a more convenient and widely used method, doesn't require a catalyst and allows to obtain an already doped polymeric film directly on the electrode. The thickness of this film is easy tunable and it is possible to characterize *in situ* the process of growth of the polymer through electrochemical and/or spectroelectrochemical techniques.

The process begins with the formation of charged species on the surface of the anode by monomer oxidation. The required stoichiometry is two moles of electron for each mole of monomer and a slight excess of charge used for the doping of the polymer. The first step consists in the oxidation of the monomer to radical-cation. As the electronic transfer reaction is quicker than the monomer diffusion in the solution, a high radical concentration is maintained near the electrode. The second step involves the coupling of two radicals for the formation of a dihydro dimer dicathionic which evolves at dimer with the loss of two protons and rearomatization that constitutes the driving force of the process (Fig. 17). Due to the applied potential, the dimer, which is easier oxidizable than the monomer, is converted to radical-cation. The coupling between a radical-cation and one monomer and the subsequently rearomatization leads to the formation of the trimer that starts again the cycle until the oligomer becomes insoluble and precipitates onto the surface of the electrode. However, some of the steps are still not completely clear and are currently subject to different interpretations.

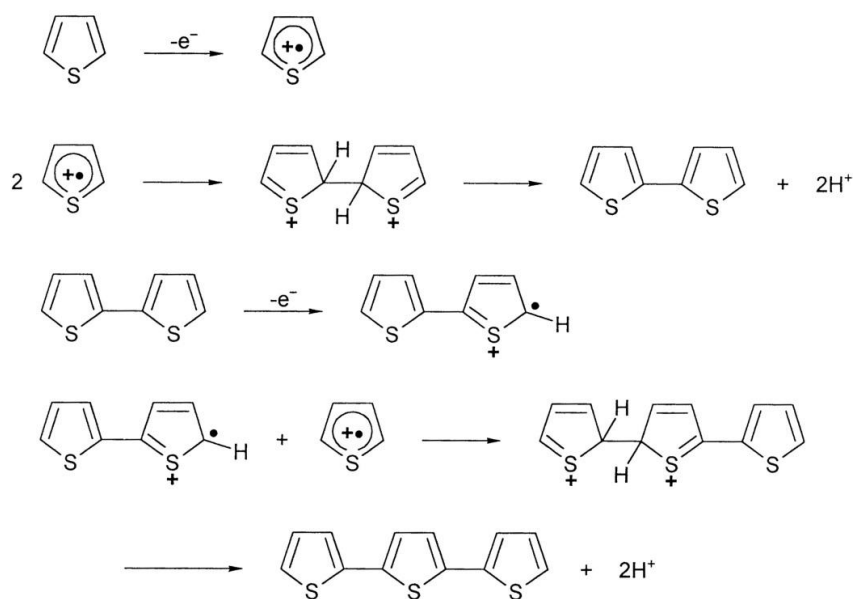


Figure 17. Mechanism of thiophene electropolymerization.

Polymerization conditions greatly affect the structure and the properties of the obtained PT. It's crucial the usage of anhydrous, aprotic, poorly nucleophile, with high dielectric constant and potential stable ( $\sim 1.4$ - $2.3$  V/SCE) solvents, such as acetonitrile, benzonitrile, nitrobenzene and propylene carbonate. Low temperatures allow the preparation of PT with higher average conjugation length, because the formation of  $\alpha$ - $\beta$  bonds chain defects is minimized. The anode must be constituted of a noble metal (platinum or gold) or of ITO covered glass so that the polymer can settle permanently on it. The deposition can be both potentiometric and galvanostatic, taking care not to use a too high potential since it can lead to polymer degradation.

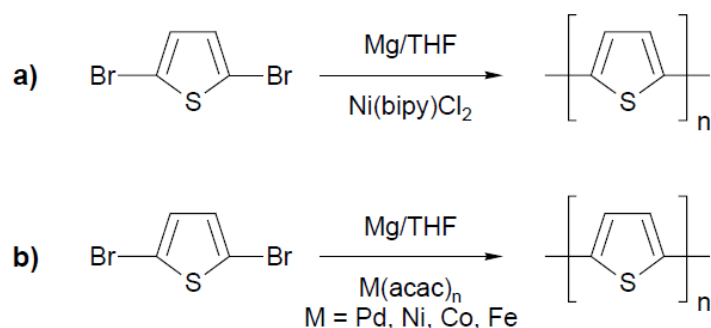


### 2.1.2 Chemical synthesis

The first chemical syntheses [3] of PT were reported in 1980 from two research groups, both based on the polycondensation of 2,5-dibromothiophene with transition metals as catalysts.

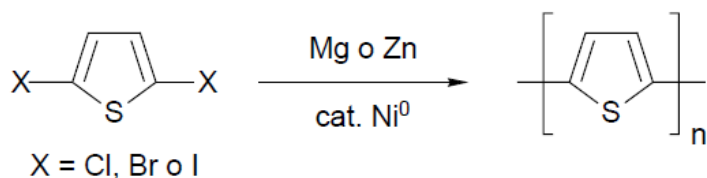
The Yamamoto procedure (Sch. 1a) involves the reaction of 2,5-dibromothiophene with Mg for the formation of the corresponding Grignard reagent in the 2 and 5 positions and its subsequent homocoupling catalyzed by nickel(bipyridine)dichloride.

Lin and Dudek used a similar procedure (Sch. 1b) using instead  $\text{Pd}(\text{acac})_2$  (acac = acetylacetonate) or  $\text{Ni}(\text{acac})_2$  or  $\text{Co}(\text{acac})_2$  or  $\text{Fe}(\text{acac})_2$ .



Scheme 1. PT synthesis according to a) Yamamoto and b) Lin and Dudek

2,5-dihalo thiophenes can be polymerized by dehalogenative polycondensation with  $\text{Ni}^0$  based catalysts (Sch. 2)

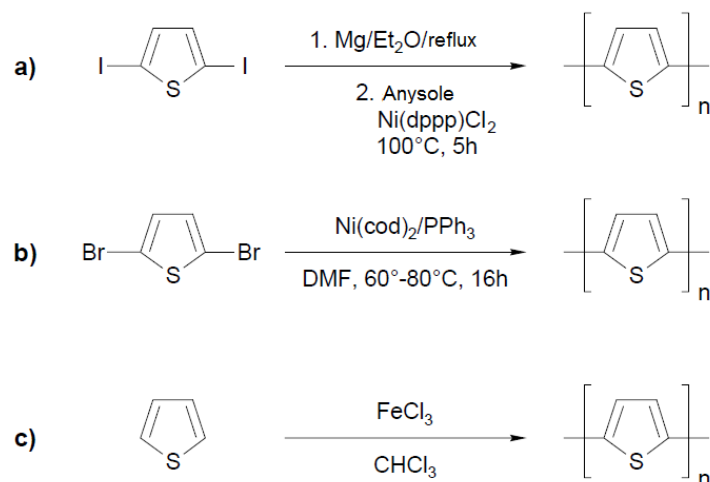


Scheme 2. Dehalogenative polycondensation.

Wudl and his collaborators prepared the iodomagnesiumiodothiophene starting from the 2,5-diiodothiophene in diethylether and, by the  $\text{Ni}(\text{dppp})\text{Cl}_2$  (dppp = 1,3-diphenylphosphinopropane) catalyzed homocoupling in hot anisole, obtained the corresponding polymer (Sch. 3a).

A new procedure from Yamamoto (Sch. 3b) lead to a quantitative yield in PT from 2,5-dibromothiophene,  $\text{Ni}(\text{cod})_2$  (cod = cyclooctadiene) and triphenylphosphine in hot N,N-dimethylformamide (DMF).

Sugimoto, instead, proposed the oxidative polymerization that allows to obtain PT by direct oxidation of thiophene with ferric trichloride (Sch. 3c).



Scheme 3. PT synthesis according to a) Wudl, b) Yamamoto and c) Sugimoto.

## 2.2 3-ALKYL FUNCTIONALIZED POLYTHIOPHENES

The insertion of alkyl chains in the 3 position of the thiophenic ring, allows to reduce the intrinsically insolubility of PT in a very effective way, since poly[(3-alkyl)thiophene]s (PATs) thus obtained possess good solubility in common organic solvents, such as CHCl<sub>3</sub>, CH<sub>2</sub>Cl<sub>2</sub>, THF, xylene, toluene, anisole, nitrobenzene, benzonitrile and nitropropane, even at high molecular weights. This kind of functionalization slightly lowers the conductivity of the polymers, without affecting their practical use. The first chemical synthesis of PATs, a polycondensation with organometallic derivatives, is reported by Elsenbaumer *et al.* [4] and puts in evidence that a good solubility can be obtained with an oligomethylenic chain with at least four carbon atoms. PATs preserve the high stability of PT together with an excellent filmability allowing the preparation of homogenous and self-standing polymeric films.

By introducing a substituent in the 3 position of thiophene, the repeating unity becomes asymmetrical and the 2 and 5 positions are no longer equivalent. This results in the possibility to obtain different regioisomers where the thiophenic unities can be concatenated headtail (HT, 2-5' bond), headhead (HH, 2-2' bond) and tailtail (TT, 5-5' bond), leading to the possibility of four triads linkages (Fig. 18).

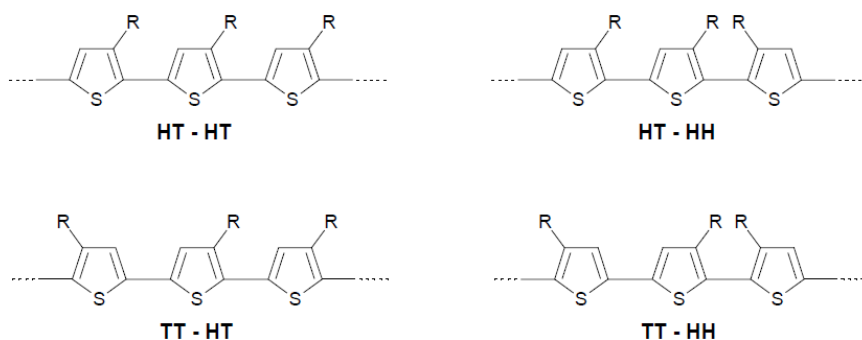


Figure 18. Possible triads in PATs.

## 2.3 PATs SYNTHESSES

Generally, with common syntheses techniques PATs with different concatenation are obtained, but regioregular systems can be prepared through opportune synthetic strategies.

### 2.3.1 Electrochemical polymerization

The electropolymerization of 3-alkylthiophene [5] is obtained in condition similar to those described for thiophene. Obviously the electrochemical behavior of the monomer must be preventively studied through cyclic voltammetry, with very low monomer concentration to avoid polymerization, in order to determine the optimal potential value to be used in the polymer synthesis.

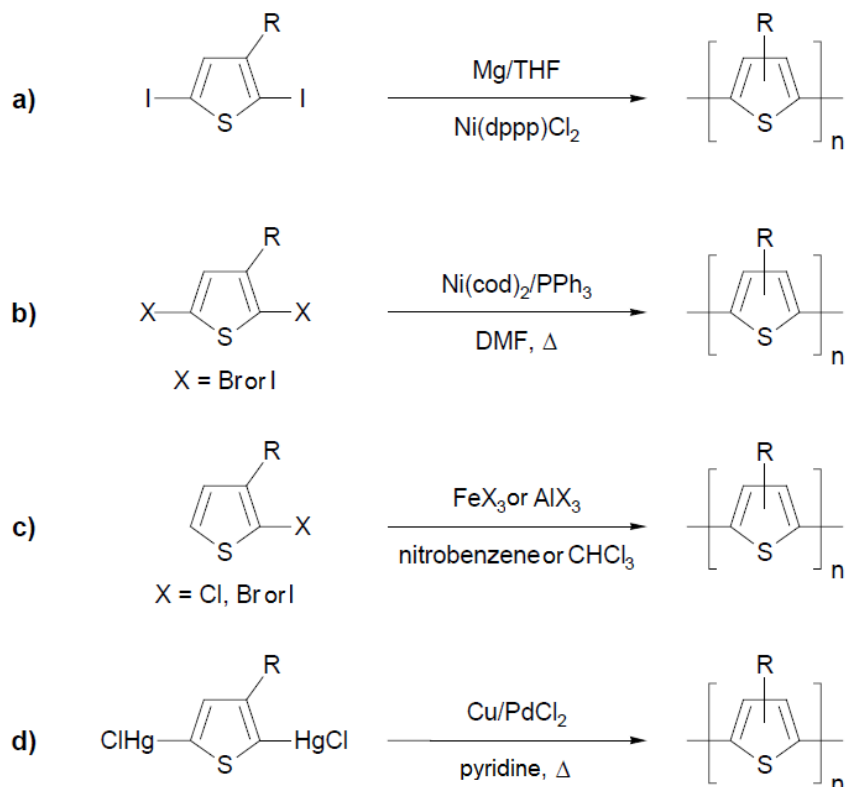
### 2.3.2 Cross-coupling polymerization with metals as catalysts

In the first synthesis of this class [6], a 2,5-diiodo-3-alkylthiophene (Sch. 4a) is treated with one equivalent of Mg in THF producing a mixture of Grignard reactivities. Then a catalytic amount of Ni(dppp)Cl<sub>2</sub> is added and, by Halogen-Grignard coupling, a polymer consisting of only 2-5 linkage, which has random regioselectivity is formed

PATs can be synthesized from 2,5-diiodo-3-alkylthiophenes, through coupling with nickel (0) (Sch. 4b) in similar condition to those used for PT preparation. The only difference consists in the reaction times that are higher for PATs, for which the use of the more reactive diiodothiophenes is preferable instead of dibromo derivatives. The polymerization mainly occurs by 5-5' coupling so the obtained product has high rate of HH-TT linkage. This is probably due to the oxidative addition of Ni in the 5 position of the monomer, which is the less sterically hindered.

Another technique provides the polymerization by dehydrohalogenation of 2-halogen-3-alkylthiophene with metal halide such as  $\text{AlCl}_3$  or  $\text{FeCl}_3$  (Sch. 4c) which leads to products with very low metal impurities, high molecular weights and regiorandom concatenations.

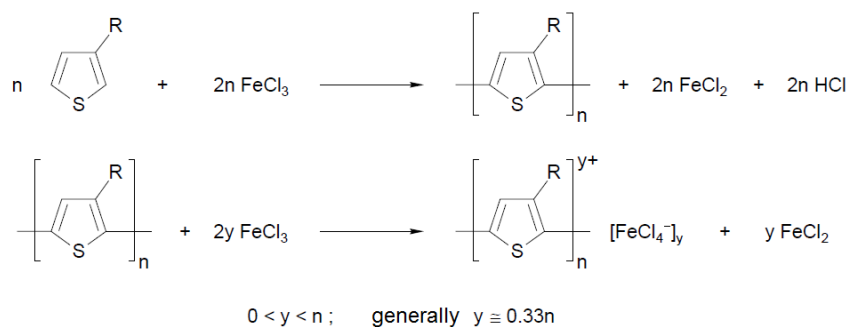
Finally, the method proposed by Curtis *et al.* uses the polymerization of 2,5-bis(chloromercury)-3-alkylthiophenes using copper powder and catalytic amount of  $\text{PdCl}_2$  in pyridine (Sch. 4d). Also in this case, the method isn't regiospecific and leads to regiorandom polymers.



Scheme 4. Cross-coupling polymerization with metals as catalysts.

### 2.3.3 Oxidative polymerization

With this technique [7] PATs can be obtained by reacting 3-alkylthiophenes with  $\text{FeCl}_3$ , which acts both as polymerizing agent and as dopant for the polymer (Sch. 5).

Scheme 5. Oxidative polymerization with  $\text{FeCl}_3$ .

The used reaction medium is a solvent in which the oxidant is insoluble, such as  $\text{CHCl}_3$  or  $\text{CCl}_4$ , in order to keep the coordination vacancies active, that makes it a Lewis acid. In fact, in solution it is transformed in  $\text{Fe}_2\text{Cl}_6$  dimer without free orbitals. Ferric chloride is used in a fourfold molar excess respect of the monomer to be polymerized because it is consumed also to form  $\text{HFeCl}_4$  when it reacts with  $\text{HCl}$  that is evolved during the reaction. A vigorous flow of inert gas is kept in order to avoid oxygen presence which can interfere with the polymerization mechanism and, at the same time, to remove the  $\text{HCl}$  evolved.

The proposed mechanism of the reaction (Fig. 19) begins with the formation of the thiophenic radical-cation which evolves to 5-thienylradical (more stable by 1.456 kJ/mol than 2-thienylradical). The coupling with another thiophenic monomer molecule in the position with higher electronic density (2 position, which has 0.0122 ue atomic charge higher than the 5 position) and its subsequently rearomatization, by loss of a proton and further oxidation, leads to the formation of a dimer. The latter is oxidized again and the cycle starts again allowing the growth of the macromolecule.

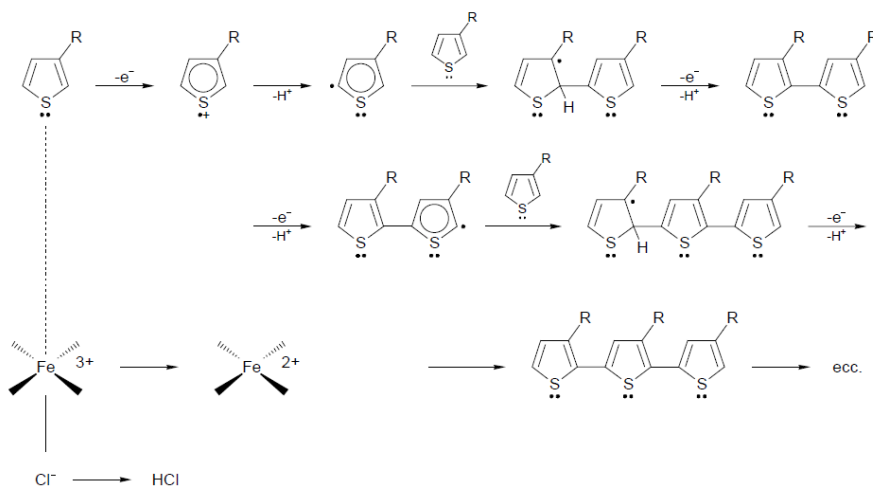


Figure 19. Proposed mechanism of oxidative polymerization.

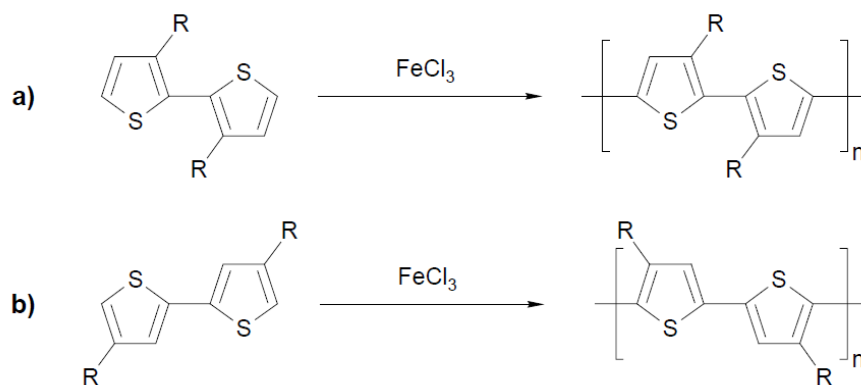
Thanks to the weak inductive effect of the alkyl substituent in the 3 position of the heterocycle, the synthesis process results regioselective, leading to a polymer with HT concatenation of about 75%.

This technique, when compared to those previously described, is particularly easy and convenient because it ensures good yield and high molecular weights in a short period of time (generally 1 hour) working at room temperature and using cheap and non-toxic reagent such as the ferric trichloride; furthermore, the obtained polymer is in its electroconductive form.

Recent developments of this technique [8,9] include the *in situ* precipitation of  $\text{FeCl}_3$  through the addition of a saturated solution of the oxidizer agent in  $\text{CH}_3\text{NO}_2$  to  $\text{CCl}_4$  where the salt is not soluble. The ferric trichloride precipitates in a finely dispersed, high reactive form that allows the synthesis of polymer with lower molecular weight completely avoiding the formation of insoluble products.

## 2.4 REGIOREGULAR PATS SYNTHESIS

Regarding 3-functionalized polythiophenes, two kinds of regular concatenation can be defined: HH-TT and HT. A product belonging to the first class of polymer can be easily obtained by oxidative polymerization both of a HH dimer, that is a 3,3'-dialkyl-2,2'-bithiophene, and of a TT dimer, that is a 4,4'-dialkyl-2,2'-bithiophene (Sch. 6).



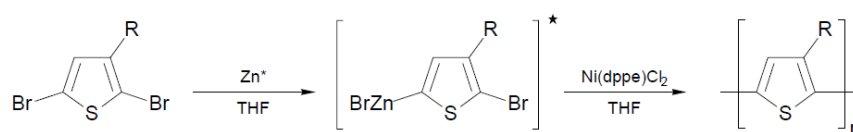
Scheme 6. Synthesis of a HH-TT regioregular PAT starting from a) HH dimer and b) TT dimer.

The syntheses of HT polymers are generally more difficult, but more studied and used because this kind of configuration ensures higher mean conjugation lengths and, consequently, better electronic properties. Heterocyclic rings, in fact, prefer a *trans*-coplanar orientation which can be obtained with almost only HT concatenations, for which torsional angles of only  $7^\circ$ - $8^\circ$  between the rings have been calculated [10]. HH bonds, instead, show a deviation from coplanarity of about  $40^\circ$ , a too high value for the correct orbitals overlapping, leading to a structure with low conjugation length throughout the

backbone. PATs with high HT linkages content are generally synthesized starting from alkylthiophene monomers where the 2 and 5 positions are functionalized with different groups that can react through coupling reactions.

### 2.4.1 Rieke-Chen polymerization

Rieke zinc ( $\text{Zn}^*$ ) reacts with 2,5-dibromo-3-alkylthiophenes to obtain 5-(bromozinc)-2-bromo derivatives (Sch. 7) without the formation of bis-metallation product [11]. The intermediate can be polymerized with  $\text{Ni}(\text{dppe})\text{Cl}_2$  in refluxing THF for 4 h, obtaining a PAT with 98.5% of HT linkage.



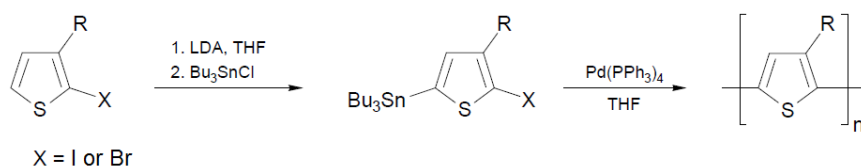
Scheme 7. Rieke-Chen polymerization.

The rate of regioregularity is strongly influenced by the kind of both metal and ligand used, since with  $\text{Pd}(\text{PPh}_3)$  a regiorandom polymer is obtained while with  $\text{Ni}(\text{PPh}_3)$  or  $\text{Pd}(\text{dppe})\text{Cl}_2$  are observed respectively 65% and 70% of HT linkage.

The method is quite versatile because, thus reactive, the organozinc compounds can be employed also in the presence of  $\alpha$ ,  $\beta$  unsaturated ketones, carbonyl groups, nitriles and compounds with acid chlorides.

### 2.4.2 Stille coupling polymerization

Iraqi *et al.* [12] and Lère-Porte *et al.* [13] employed this kind of coupling for the synthesis of regioregular PATs using, respectively, 2-iodo and 2-bromo-3-alkylthiophenes (Sch. 8). The halogenated monomer in the 2 position get selectively lithiated in the 5 position with lithiumdiisopropylamide (LDA) at  $-40^\circ\text{C}$ . The obtained product is directly converted to tributylstannyl derivative by reaction with  $\text{Bu}_3\text{SnCl}$  at  $-40^\circ\text{C}$ . The latter intermediate is stable and can be purified with the most common preparation techniques before its polycondensation with  $\text{Pd}(\text{PPh}_3)$ , leading to the desired polymer with a regioregularity never less than 96% of HT linkage.



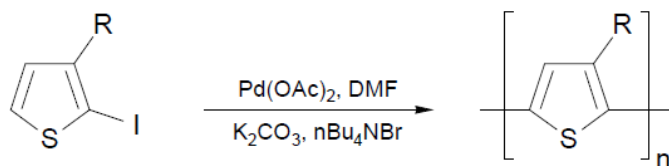
*Scheme 8. Stille coupling polymerization.*

Higher yield can be achieved by heating and only with long reaction time that, from the 18 hours for iodo-derivatives, it can take up to 72 hours when 2-bromo-3-alkylthiophene are employed. The nature of the solvent influences only the weight features of the product. In THF, for example, only short oligomers are obtained while with more polar solvents a considerable increase of the molecular weight is observed.

It is important to underline that one of the advantage of this procedure is the possibility to synthesize a stable organometallic intermediate that can be easily purified from the impurities, bad concatenations in the final polymer to be avoided; this procedure is also scarcely reactive towards many functional groups.

### 2.4.3 Heck coupling polymerization

Sevignon *et al.* [14] recently developed a method involving 2-iodo-3-alkylthiophenes. The monomer reacts with a catalytic amount of  $\text{Pd}(\text{OAc})_2$ , equimolar tetrabutylammonium bromide and an excess of  $\text{K}_2\text{CO}_3$  in DMF at  $80^\circ\text{C}$  (Sch. 9), allowing to obtain with high yields regioregular oligomers constituted by a mean of 15 repeating units.



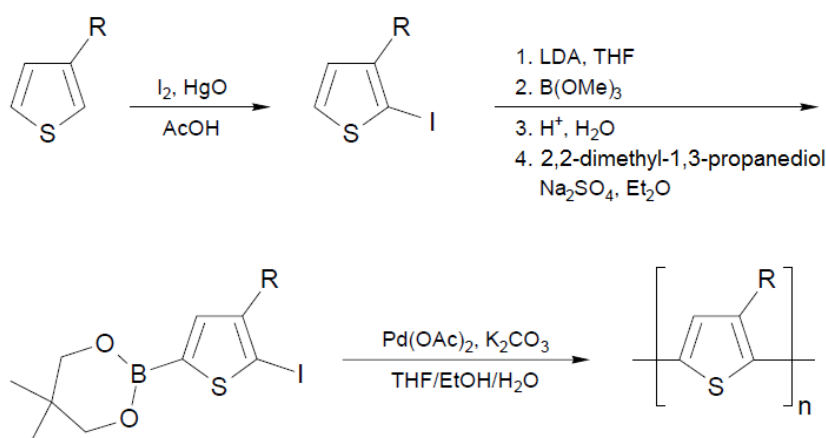
*Scheme 9. Heck coupling polymerization.*

The same procedure, applied to 2-bromo-3-alkylthiophenes, leads to similar results with the advantage of employing a simpler synthesizable monomer starting from less toxic and expensive reagents.

### 2.4.4 Suzuki coupling polymerization



Also in this case, a 2-iodo-3-alkylthiophene is employed; the latter is easily obtained by the corresponding 3-alkylthiophene with powdered iodine and yellow mercury oxide in acetic acid at room temperature [15] (Sch. 10). The following step involves the lithiation in the 5 position of the intermediate obtained, with LDA at  $-40^{\circ}\text{C}$  and subsequently quenching with trimethylborate. The boron ether, which is hydrolyzed *in situ* to form boronic acid, is directly converted in a stable ester when it reacts with an equivalent of 2,2-dimethyl-1,3-propanediol. The obtained boronate is stable and can be purified with common techniques. Its next polymerization, catalyzed by  $\text{Pd}(\text{OAc})_2$  and heated at reflux for 16 hours in a mixture of THF, water and ethanol, leads to the desired polymer with a good yield, high molecular weights and with 9697% of HT concatenations.

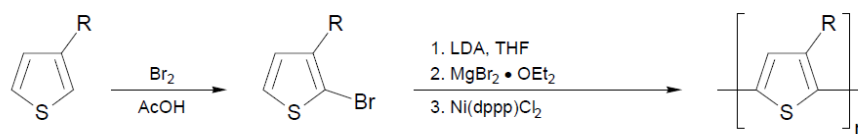


Scheme 10. Suzuki coupling polymerization.

As for the Stille coupling, the possibility to obtain a stable organometallic intermediate, easy to purify and compatible with many functional groups, constitutes a great advantage.

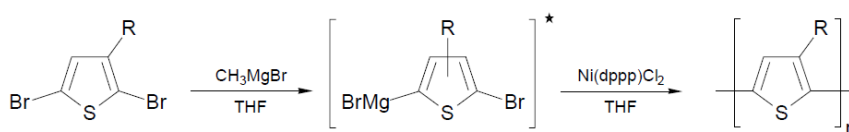
#### 2.4.5 McCullough polymerization

This kind of polymerization [16] is based on the use of the Kumada cross-coupling catalyzed by  $\text{Ni}(\text{dppp})\text{Cl}_2$ . A 3-alkylthiophene is brominated in the 2 position with bromine in acetic acid. Then the lithiation in the 5 position takes place, using LDA at  $-40^{\circ}\text{C}$ , and the subsequent formation of 2-bromo-3-alkyl-5-bromomagnesium thiophene by reaction with ether  $\text{MgBr}_2$  at  $-60^{\circ}\text{C}$ . The reaction mixture is warmed to  $-5^{\circ}\text{C}$  and then, the catalyst is added and the mixtures is allowed to react at room temperature for 18 hours (Sch. 11). In this way polymers having at least 98% of HT concatenation, are obtained with good yields.



Scheme 11. McCullough polymerization.

The described procedure is particularly time-consuming and laborious and requires to work with high purity products and cryogenic temperatures. McCullough himself recently proposed an alternative procedure [17] very simple, quick and cheap. Practically, it deals with a 2,5-dibromo-3-alkylthiophene, easy to synthesize and purify, with an equivalent of  $\text{CH}_3\text{MgBr}$  in refluxing THF (Sch. 12). In this way, by Grignard reactive metathesis, a mixture of isomers is obtained with a predominance of the isomer metalated in 5 position. Despite the non-complete regioselectivity, the addition of  $\text{Ni(dppp)Cl}_2$  in catalytic amount allows to obtain the desired polymer only after 2 hours of reflux, with yield of about 70% and 99% of regioregularity.



Scheme 12. McCullough new polymer synthesis.

## 2.5 PATs CHARACTERIZATION

PATs, and more generally, PT derivatives are characterized by all of the most common polymeric analysis techniques. Studies for the determination of particular properties can be associated to the latters, linked to a specific use of these materials, such as the measure of conductivity, of electroluminescence or solar cells efficiency.

Nuclear magnetic resonance, infrared spectroscopy and UV-Vis absorption play a crucial role in the structural study of these materials and provide many and useful information that can be easily achievable in modern research laboratory.

### 2.5.1 Nuclear magnetic resonance (NMR) spectroscopy

The analysis of  $^1\text{H}$  and  $^{13}\text{C}$  NMR of PATs allows to determine, in addition to the structure, the regiochemistry of the backbone.

As for  $^1\text{H}$ -NMR, the presence of four signals in the aromatic region attributable to the  $\beta$  hydrogens belonging to the four possible triads, can be observed. In poly(3-hexylthiophene) (P3HT), the expansion of the aromatic region is reported as an example (Fig. 20), the signals at 6.98, 7.00, 7.03 and 7.05 ppm are attributable to the HT-HT, TT-HT, HT-HH and TT-HH configurations respectively [18].

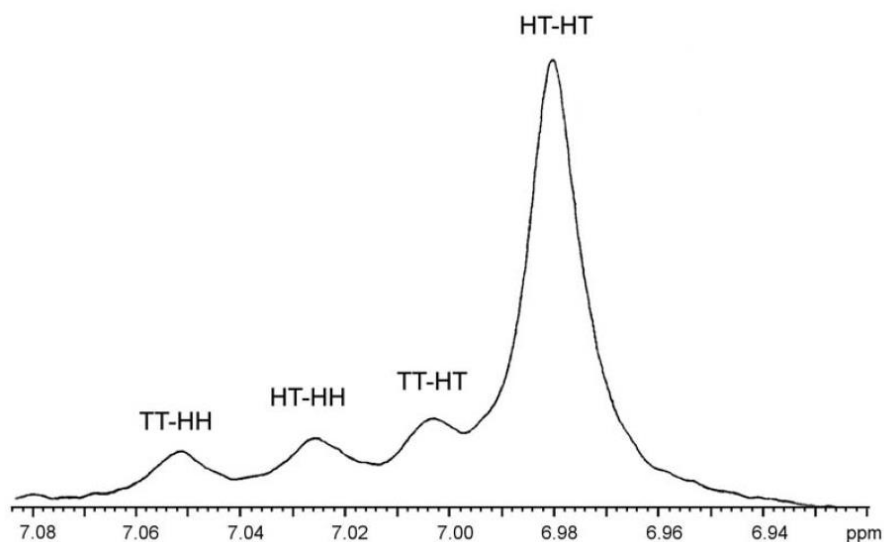


Figure 20. Aromatic region of  $^1\text{H}$ -NMR spectrum of poly(3-hexylthiophene).

Also the signal of methylenic protons bonded to the  $\alpha$  carbon of the heterocycle is affected by the kind of concatenation and it originates two signals, at 2.79 and 2.56 ppm for P3HT, the former is attributable to HT dyads while the other one to HH/TT dyads. Calculating the ratio between the relative integrals of the two peaks, it is possible to determine, in a very easy way, the percentage of backbone regioregularity.

The  $^{13}\text{C}$ -NMR analysis allows to record in the aromatic region, sixteen different signals, more or less intense, attributable, in groups of four, to the thiophenic carbons belonging to rings that are linked in the different four triads.

### 2.5.2 Infrared spectroscopy

The stretching of the C-H bond (weak intensity) which involves the  $\beta$  hydrogen of the thiophenic ring and its out-of-plane bending (high intensity) together with symmetric and antisymmetric stretching (medium intensity) of the C=C double bond constitute the characteristic bands of the macromolecular backbone. In the case of P3HT the frequencies of these signals are about  $3055\text{ cm}^{-1}$  ( $\nu_{\text{C-H}}$ ),  $825\text{ cm}^{-1}$  ( $\gamma_{\text{CH}}$ ),  $1510\text{ cm}^{-1}$  ( $\nu_{\text{anti}}$ ),  $1460\text{ cm}^{-1}$  ( $\nu_{\text{sim}}$ ). The frequency of out-of-plane bending of the C-H bond is affected by the kind of backbone configuration and it slightly shifts toward lower energies for system with high

regioregularity while the ratio ( $I_s/I_a$ ) between the intensity of the two bands attributable to symmetric and antisymmetric stretching of the thiophenic C=C allows to evaluate the conjugation length that increases as  $I_s/I_a$  lowers [19].

### 2.5.3 UV-Vis absorption spectroscopy

PATs UV-Vis spectra in solution show a maximum of absorption, with a high molar extinction coefficient, that is collocated at about 440 nm and corresponds to the  $\pi$ - $\pi^*$  electronic transition of the polyconjugated backbone. The wavelength of the maximum absorption ( $\lambda_{\max}$ ) is connected with the conjugation length of the polymeric chain and is influenced by the regioregularity of the system, by the nature of the solvent or mixture of solvents employed for the analysis and by the temperature.

The spectra of the polymer in film state are generally characterized by a red shift of the  $\lambda_{\max}$ , indicating the presence of a higher conformational order when compared to the solution, and a spectral structuration with the clear evidence of three or four vibronic quantum.

## 2.6 OPTICAL PROPERTIES OF PATs

The word “chromism” means the modification of the UV-Vis spectral behavior of a product as a function of the variation of the chemical-physical boundary conditions. This behavior, in the case of PATs and other PT derivatives, comes from the conformational mutation of the backbone, that influences the mean conjugation length and consequently the entity of the energetic gap between HOMO and LUMO, which is involved in the electronic transitions observable by visible light. A completely reversible alteration in the system is made, from a configuration with high degree of disorder with lower mean conjugation length, named *A form*, to a more ordered configuration and with higher mean conjugation, named *B form* [20] (Fig. 21).

The *A form*, whose electronic delocalization is limited to 5-6 thiophenic rings, evolves according to a mainly interchain mechanism that involves two segments whose interactions determine, with a second order kinetic, an almost double mean conjugation length for the *B form* [21,22].

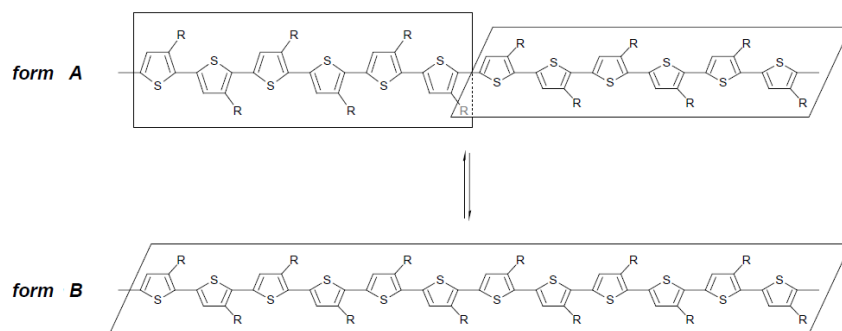


Figure 21. Equilibrium between *A* and *B* forms.

This behavior can be induced by a variation of temperature (thermochromism), pressure (piezochromism) or by mean of solvent (solvatochromism). In the first two cases, the increase of temperature or the decrease of pressure determine a freer rotation around C-C bonds that link the thiophenic rings with consequently increase of conformational disorder which leads, by the UV-Vis spectrum point of view, to a prominent isochromic shift of maximum wavelength absorption.

Solvatochromism is observed when a non-solvent is added to a solution of a polymer. The latter progressively removes the solvent molecules from the polymeric chain that is allowed to assume a more coplanar conformation with a consequent bathochromic shift of  $\lambda_{\max}$ .

UV-Vis spectra of P3HT in chloroform/methanol mixtures are reported as an example (Fig. 22). By increasing of the molar fraction of methanol, a prominent  $\lambda_{\max}$  red-shift is observed together with always more structured spectral profiles that derive from the high conformational order of the system. Four vibronic transitions are clearly identifiable including the pure electronic ( $E_{0-0}$ ), at about 600 nm, that shows an absorption value directly proportional to the concentration of the *B form* in solution. An isosbestic point is also observed, confirming the presence of only two species, *A form* and *B form*, in equilibrium between them.

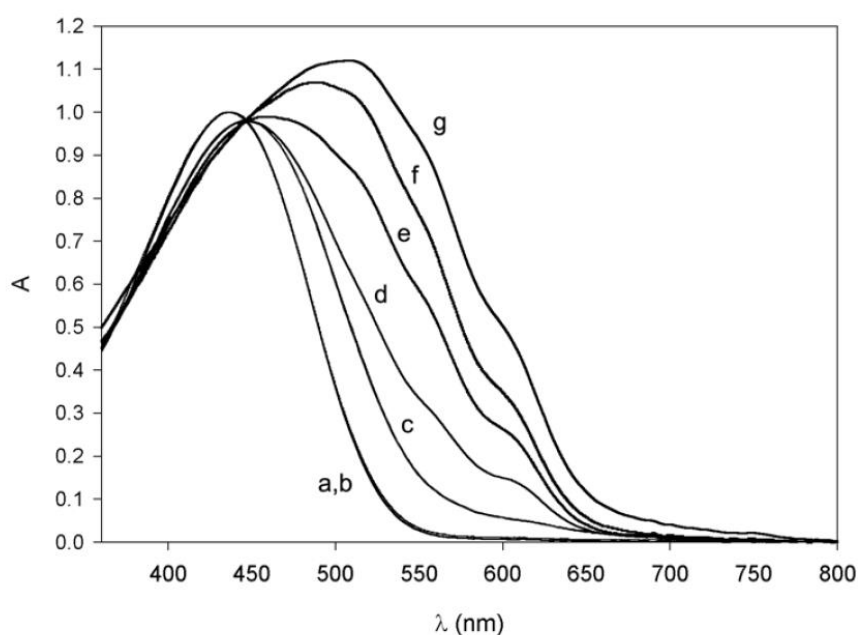


Figure 22. Absorption spectra for P3HT in  $\text{CHCl}_3/\text{CH}_3\text{OH}$  mixtures at different molar ratios of  $\text{CH}_3\text{OH}$ : a) 0.00; b) 0.28; c) 0.39; d) 0.50; e) 0.66; f) 0.80; g) 0.98.

The entity of the chromic effects is linked to the structural factors specific of the analyzed polymer: the high percentage of regioregularity or the presence of groups in the side chains able to stabilize coplanar conformation, effectively contribute to the increase of the planarization of the backbone. The described phenomena, not only allow for an accurate study of the electronic structure of conjugated polymers, but also are the base of the study of their possible application in the field of chromic sensors based on the principle of chemical recognition.

## 2.7 $\beta$ -FUNCTIONALIZED POLYTHIOPHENES

The great versatility of the thiophenic ring made PATs only the starting point for the preparation of polythiophenes variously substituted in the  $\beta$  or  $\beta$ - $\beta'$  positions. In fact, it is possible to synthesize, in an easy way, monomers bearing alkyl chains  $\omega$ -functionalized for example with hydroxyl or sulfonic groups, acids, amines, amino acids, or halides. Furthermore, also chiral substituents, aromatics rings, ester groups, ethers or thioethers, oxaethylenic chains, crown ethers, calixarenes, or porphyrins have been included. The synthesis and the study of a great variety of products reported in the literature and nowadays subject to study, derives from the need to prepare a specific derivative for a specific use. Thanks to the  $\beta$ -functionalization, it is possible to modulate and improve the properties of the polyconjugated backbone so that the system has a specific characteristic that is particularly suitable for a specific application.

The synthesis of such derivatives can be made, in the major of the cases, by direct polymerization of an appropriate monomer, using similar procedures to those described for PATs. But sometimes it is possible to incur in a poorly reactive monomer that leads to a low yield for the desired product. In other cases, instead, some functional groups cannot be used because their reactivity towards one or more reactive involved in the polymerization is too low. These problems can be effectively removed with the development of a new synthetic route, named *post-polymerization functionalization*.

### 2.7.1 Post-polymerization functionalization

The post-polymerization functionalization (PPF) consists in the preparation of a reactive polymeric precursor that is subsequently converted in the derivative of interest. The precursor polymer has to be synthesized with high yield and high molecular weights through direct polymerization of an appropriate monomer and must be soluble in the solvents that will be used in the next functionalization step. The choice of the reactive group is crucial: it must be quantitatively converted to the desired substituent in order to avoid the formation of only partially substituted macromolecules, that would unavoidably lead to copolymers. The functionalization of a polymeric precursor requires longer reaction time that are “compensated” by the easier and quicker purification that in most cases consists in just a fractionation.

Finally, since the macromolecular chain is preformed, all the polymers which derives from the same precursor will have the same kind of concatenations and the same mean polymerization degree: consequently, it will be easier to compare the properties just according to the present functional group.

## REFERENCES FOR CHAPTER 2

- [1] J. L. Bredas, B. Themans, J. Am. Phys. Soc. 29 (1984) 6761
- [2] J. Roncali, Chem. Rew. 92 (1992) 711
- [3] R. D. McCullough, Adv. Mater. 10 (1998) 93
- [4] G. G. Miller, R. L. Elsenbaumer, J. Chem. Soc. Chem. Commun. 17 (1986) 1346
- [5] J. Roncali, Chem. Rew. 92 (1992) 711
- [6] G. G. Miller, R. L. Elsenbaumer, J. Chem. Soc. Chem. Commun. 17 (1986) 1346
- [7] V. M. Niemi, P. Knuuttila, J. E. Osterholm, J. Korvola, Polymer 33 (1992) 1559

- [8] P. Costa Bizzarri, M. Lanzi, L. Paganin, C. Della Casa, F. Bertinelli, M. Casalboni, F. Sarcinelli, A. Quatela, *Macromol. Chem. Phys.* 204 (2003) 1982
- [9] P. Costa Bizzarri, M. Lanzi, L. Paganin, D. Caretti, F. Parenti, *Polymer* 45 (2004) 8629
- [10] R. D. McCullough, R. D. Lowe, M. Jayaraman, D. L. Anderson, *J. Org. Chem.* 58 (1993) 904
- [11] J. P. Lère-Porte, J. J. E. Moreau, C. Torrealles, *Eur. J. Org. Chem.* 2001 1249
- [12] A. Iraqui, G. W. Barcher, *J. Mater. Chem.* 8 (1998) 25
- [13] J. P. Lère-Porte, J. J. E. Moreau, C. Torrealles, *Eur. J. Org. Chem.* 2001 1249
- [14] M. Sevignon, J. Papillon, E. Schulz, M. Lemaire, *Tetrahedron Letters* 40 (1999) 5873
- [15] S. Guillerez, G. Bidan, *Synth. Met.* 93 (1998) 123
- [16] R. D. McCullough, R. D. Lowe, M. Jayaraman, D. L. Anderson, *J. Org. Chem.* 58 (1993) 904
- [17] R. D. Lowe, S. M. Khersonsky, R. D. McCullough, *Adv. Mater.* 11 (1999) 250
- [18] G. Barbarella, A. Bongini, M. Zambianchi, *Macromolecules* 27 (1994) 3039
- [19] Y. Furukawa, M. Akimodo, I. Harada, *Synth. Met.* 18 (1987) 151
- [20] F. Bertinelli, P. Costa Bizzarri, C. Della Casa, M. Lanzi, *Synth. Met.* 122 (2001) 267
- [21] F. Bertinelli, P. Costa Bizzarri, C. Della Casa, M. Lanzi, *Spectrochimica Acta* 58 (2002) 583
- [22] F. Bertinelli, C. Della Casa, *Polymer* 37 (1996) 5469



## CHAPTER 3: CONJUGATED POLYMERS FOR THE OBTAINMENT OF CONDUCTIVE PATTERNS THROUGH LASER TRACING

### *3.1 INTRODUCTION*

Conjugated polymers (ICPs) in their semi-conducting or less conductive forms are widely used in the organic electronic field for applications such as light-emitting diodes [1], thin-film field effect transistors [2], and bulk heterojunction solar cells [3]. Moreover, the lithographic patterning of conductive polymer films has been successfully applied to various conjugated polymers by means of different approaches such as photochemical-induced doping [4], photochemical polymerization [5] and reactive ion etching [6]. In all cases, the crucial step for obtaining acceptable results was the choosing of both the conjugated polymer and the right source of irradiation, generally Xe-lamps, Ar ion lasers and KrF excimer lasers [7]. The conversion of polymers by laser irradiation from their non-conductive form to the conductive one has been reported for different conjugated and non-conjugated polymers such as poly(bis-alkylthioacetylene)s (PATACs) [8], polyimides (PIs) [9], and polyvinylchloride (PVC) [10]. Among the latter, disubstituted polyacetylenes are very promising materials for potential applications at the industrial and commercial level. Indeed, they are soluble in some solvents and can be prepared as thin and homogeneous films with a good thermal and environmental stability [11]. PATACs can be easily filmed from their concentrated solutions on several surfaces like glass, Si, Ge, ceramics, and metals by means of simple techniques such as spin-coating, doctor-blading or drop-casting.

The most studied PATAC is poly(bis-methylthioacetylene) (PATAC-Me); it can be easily synthesized with good yields starting from dimethylthioacetylene with a Ni(II) catalyst in tetrahydrofuran [12]. The low temperature polymerization of acetylene leads to the prevalence of the cis isomer which converts to the thermodynamically more stable trans isomer at high temperatures. This is also true for polyacetylenes bringing thioalkylic substituents when the side chain is not a sterically demanding group. Poly(terbuthylthioacetylene), for example, [13] leads to the predominance of the trans-isomer already during the polymerization step [14].

Disubstituted polyacetylenes with thioalkylic groups are sensitive to visible and UV-radiation; when their thin films are exposed to a laser light of suitable wavelength and intensity they can be easily

and rapidly converted from the insulating to the conductive form, keeping a high electrical conductivity for long times also in presence of oxygen, moisture or aggressive atmosphere.

Today, many techniques are employed to cast active polymer layers (films) onto stiff or flexible substrates with the aim to cover large areas with low cost and high speed. The generated patterned polymeric structures can be the active components of organic field-effect transistors (OFETs) [15], organic light emitting diodes (OLEDs) [16] and organic photovoltaics (OPVs) [17] exploiting, in turn, the polymer semiconducting [18] or conducting properties (when nanoscaled composites are formed [19]), their transparency [20] or light-absorbing properties [21] and their thermal stability [22] or reactivity [23]. The most studied technique is called roll-to roll (R2R) or reel to reel coating [24] which is compatible with many deposition systems, an important feature considering that each system has its strengths and weaknesses and can present some applicative restrictions.

The continuous deposition techniques which are compatible with R2R coating are: gravure printing, flexographic printing, rotary screen printing, knife/slot die coating, inkjet printing and spray coating.

A very exhaustive and recent review exploring in detail all of these systems is reported in Ref. [25]. A concise overview of polymer thin film devices obtained using R2R techniques is reported in Table 1 [26,27,28,29,30,31,32,33,34,35,36,37,38,39,40,41,42].

Table 1. Overview of reported polymer thin film applications using R2R techniques.

Processing method	Applications	Comments
Gravure printing	Active layers for OPV [26,27], OTFT [28], PLED [29]	High speed (up to 15 m/s) Different substrates (PC, PET, glass) Less expensive Requires a pre-patterned printing form
Flexographic printing	Loudspeakers [30]	Works well on paper Expensive Requires a pre-patterned printing form
Screen printing (flat bed) Rotary screen printing (RSP)	Silver electrodes for OPV [31]	High speed (RSP) Simple and less expensive Requires a pre-patterned mesh Stepwise process (flat bed)
Knife coating Slot die coating	OPV (all layers) [32], PLED [33], EC [34]	High speed (up to 200 m/min) Less expensive Wide applicability (premetered coating system)
Inkjet printing	OPV [35,36], PLED [37]	High resolution High speed (up to 75 m/min) No premanufactured printing form required Expensive
Spray coating	Active layers and electrodes for OPV [38,39], photodiodes [40], EC [41]	Simple and less expensive Not very uniform coating
Light-induced thermocleavage	Active layers for OPV [42]	Simple and effective High speed Quite expensive Requires a prepatterned mask for the photonic sintering system and a suitable polymer
Laser-induced thermocleavage	Potential applications: OPV, TFT, PLED	High speed Inexpensive Simple and effective No premanufactured printing form required Requires a suitable functional polymer

This work mainly aims to find the best operating conditions for the laser-patterning of PATAC-Me films by means of commercial, lightweight, quite inexpensive diode lasers operating at low optical powers (lower than 1W), with the aim of bringing these techniques one step forward toward the industrialization of the process. Prepared samples have been deeply characterized by using FT-IR, UV-Vis spectroscopy, optical microscopy, and SEM/EDS probe for in situ elemental analysis. Moreover, an attempt has been made to substitute PATAC-Me with a thiophenic polymer bearing a thioalkylic side chain. The properties and the applicability of the polythiophene derivative have been evaluated, showing that the latter is an easier obtainable polymer with better characteristics in terms of solubility, filmability and optical transparency as compared to the acetylenic polymer.

### 3.2 EXPERIMENTAL

$^1\text{H}$ - and  $^{13}\text{C}$ -NMR were recorded on a Varian Mercury Plus spectrometer (400 MHz) using TMS as a reference. FT-IR spectra of the monomers (pure liquids) and polymers (films) were carried out on Ge disks using a Perkin Elmer Spectrum One spectrophotometer. Raman spectra were recorded using polymer films on glass slides and a Renishaw RM 1000 instrument with an excitation wavelength of 785 nm. Molecular weights were determined by gel permeation chromatography (GPC) using polystyrene standards and THF as an eluent on a HPLC Lab Flow 2000 apparatus equipped with a PL Gel MXL column and a Linear Instrument UV-Vis detector model UVIS-200 working at 263 nm. Elemental analyses were performed by Redox Laboratory, Monza, Italy. UV-Vis spectra were recorded using a Perkin Elmer Lambda 19 spectrophotometer. Polymer solutions on Hellma Suprasil quartz cuvettes were prepared using spectroquality solvents stored under molecular sieves, with a polymer concentration of about  $7 \times 10^{-5} \text{ mol} \times \text{l}^{-1}$ , while films on quartz slides were cast from either chlorobenzene (PATAC-Me) or THF (PSBu) solutions ( $\text{ca. } 10^{-3} \text{ mol} \times \text{l}^{-1}$ ).

Thermal analyses were performed on a TA Instruments DSC 2920 in a nitrogen atmosphere and on a TGA 2050 in air at a heating rate of  $10^\circ\text{C}/\text{min}$ . Electrical measurements were performed in air at room temperature using a Keithley 2101 electrometer (traced films) and an Alpha Lab teraohmmeter (pristine films). The reported values were the means of some measurements performed on different parts of the same sample as well as on different samples. In all cases the differences did not exceed 2-3% of the final value. Electrical conductivity of the laser-traced samples was also examined in the  $20\text{-}180^\circ\text{C}$  range by means of a hot-plate controlled by a Pt100 thermocouple. The laser sources were a Wicked Lasers Spyder III Arctic class 4 diode laser, operating at 445 nm and a Wicked Lasers Spyder III Krypton, class 4 diode laser, operating at 532 nm, both with a nominal power of 750 mW. The effective power of laser beams on the polymer surface was measured with a Coherent FieldMax II laser power meter.

Samples were mounted on a computer-controlled positioning system (Thorlabs L490MZ) and moved on a plane perpendicular to the focused laser beam using two Thorlabs MTS TDC001 controllers. SEM analyses were performed on a Carl Zeiss EVO MA10 SEM apparatus, equipped with an EDS microanalysis probe. Optical 2D and 3D microscopy was performed using a Hirox KH-7700 Digital Microscope.

### ***3.3 MONOMER SYNTHESIS***

#### ***3.3.1 Synthesis of 3-(buthylthio)thiophene (TSBu)***

10.01 g (61.2 mmol) of 3-bromothiophene in 56 ml of anhydrous diethyl ether were stirred at -78°C under Ar atmosphere and added dropwise with 40 ml of a 1.6 M butyllithium solution in n-hexane. The mixture was stirred at -78°C for 30 min, added with 2.06 g (64.2 mmol) of sulfur and stirred for 40 min at the same temperature. After heating to 0°C, 16.77 g (0.122 mol) of bromobutane were added and the mixture was stirred overnight at room temperature. 50 ml of aqueous 1M HCl were then added to the reaction mixture and the organic phase washed with both a saturated solution of NaHCO<sub>3</sub> (3×150 ml) and distilled water to neutrality, dried over MgSO<sub>4</sub>, and concentrated. The crude product was purified by column chromatography (silica gel, n-pentane/n-heptane 1:1) to give 4.13 g (24.0 mmol) of pure TSBu (40% yield).

#### ***3.2.2 Synthesis of 2,5-dibromo-3-buthylthiophene (2,5BTsBu)***

A solution of 1.22 g of N-bromosuccinimide (NBS, 6.88 mmol) in 7 ml of N,N-dimethylformamide (DMF) was added dropwise to a solution of 1.18 g (6.80 mmol) of TSBu in 7 ml of DMF. After stirring for 6h at room temperature, 1.59 g (8.95 mmol) of NBS in 9 ml of DMF were added dropwise and the reaction mixture was stirred for 24 h at room temperature. The mixture was then poured into 450 ml of distilled water and extracted with n-pentane (3×150 ml). The collected organic phases were washed with 2×300 ml of a 5% KHCO<sub>3</sub> solution, then with water to neutrality, dried with MgSO<sub>4</sub> and concentrated. The crude 2,5BTsBu was purified by chromatography (silica gel, n-heptane) giving 1.59 g of pure 2,5BTsBu (70% yield).

### ***3.4 POLYMER SYNTHESIS***

Elemental analysis: [C<sub>4</sub>H<sub>6</sub>S<sub>2</sub>]<sub>n</sub> Calcd: 40.64 C%; 5.12 H%; 54.24 S%. Found: 41.22 C%; 4.98 H%; 53.80 S%.

### 3.4.1 Synthesis of Poly[(3-methylthio)thiophene] (PSMe)

1.6 ml of an aqueous solution of  $\text{FeCl}_3$  ( $7.5 \times 10^{-3}$  M) was added dropwise to a solution of 0.622 g (2.31 mmol) of sodium dodecylsulfate (SDS) and 3-methylthiophene (TSM, 0.200g, 1.54 mmol) in 10 ml of distilled water and 3 ml of  $\text{H}_2\text{O}_2$  (35% vol). The mixture was stirred for 6 h at  $50^\circ\text{C}$  under Ar atmosphere and filtered on a Teflon septum ( $0.45 \mu\text{m}$  pore size). The recovered polymer was diluted with 100 ml of distilled water and poured into a dialysis membrane (100 nm average pore size) which was immersed in a beaker and washed continuously with a gentle flow of distilled water. After two weeks the polymer solution was concentrated, giving 0.100 g (51% yield) of PSMe.

### 3.4.2 Synthesis of Poly[(3-buthylthio)thiophene] PSBu – Oxidative polymerization

A solution of 0.200 g (1.16 mmol) of TSBu in 12 ml of  $\text{CHCl}_3$  was added in 20 min to a suspension of 0.753 g (4.64 mmol) of  $\text{FeCl}_3$  in 10 ml of  $\text{CHCl}_3$ . After stirring for 40 min at  $20^\circ\text{C}$  under a gentle flux of Argon, 20 ml of freshly distilled THF were added to the reaction mixture. The resulting mixture was then poured into 150 ml of a 5% HCl solution in methanol and filtered on a Teflon septum ( $0.20 \mu\text{m}$  pore size). The recovered polymer was washed several times with methanol and dried, giving 0.311 g of PSBu (40% yield).

$^1\text{H-NMR}$  ( $\text{CDCl}_3$ , 400 MHz, ppm)  $\delta$ : 7.40 (s, 1H); 7.37 (s, 1H); 7.20 (s, 1H); 2.82 (t, 2H); 1.60 (m, 2H); 1.43 (m, 2H); 0.93 (t, 3H).

$^{13}\text{C-NMR}$  ( $\text{CDCl}_3$ , 400 MHz, ppm)  $\delta$ : 134.0, 132.3, 112.8, 110.9, 35.0, 31.5, 21.8, 13.6.

FT-IR (Ge disk,  $\text{cm}^{-1}$ ) 3101, 3057, 2956, 2927, 2869, 1521, 1463, 1377, 837, 746, 716.

### 3.4.3 Synthesis of Poly[(3-buthylthio)thiophene] PSBu – GRIM procedure

2.10 ml (2.10 mmol) of a 1M solution of methylmagnesium bromide in di-n-buthylether was added to a solution of 0.688 g (2.08 mmol) of 2,5BT'SBu in 12 ml of anhydrous THF. The reaction mixture was refluxed for 1h under stirring and under a gentle flux of Argon. 11.85 mg (0.022 mmol) of [1,3-bis(diphenylphosphino)propane]nickel(II) chloride ( $\text{Ni}(\text{dppp})\text{Cl}_2$ ) were then added and the mixture was refluxed again for 2 h. The mixture, cooled down to room temperature, was filtered on a Teflon septum ( $0.45 \mu\text{m}$  pore size). The recovered polymer was washed several times with methanol and dried, giving 0.200 g of regioregular PSBu (57% yield).

Elemental analysis:  $[\text{C}_8\text{H}_{10}\text{S}_2]_n$  Calcd: 56.42 C%; 5.92 H%; 37.66 S%. Found: 57.03 C%; 5.55 H%; 37.42 S%.

### 3.5 RESULTS AND DISCUSSION

PATAC-Me and PATAC-Et (poly(bis-ethylthioacetylene) films require only a laser exposure to become electrically conducting materials, without the need of doping or other treatment. In fact, if they are irradiated with an excimer laser (351 nm) or argon ion laser (488 nm), they can change their electrical conductivity by 16 orders of magnitude (from  $10^{-14}$  to  $10^2 \text{ S}\times\text{cm}^{-1}$ ) if the radiation is correctly focused on the film surface and of the suitable intensity [43]. In fact, on the one hand a too-intense laser radiation can lead to polymer pyrolysis (graphitization process), with the consequent formation of non-conductive carbon residues, while, on the other hand, if the radiation intensity is too low (or the tracing speed too high) no conversion toward the more conductive form is observed. The right conversion conditions reported in literature for the use of an  $\text{Ar}^+$  laser are well described: 200 mW of power and 13 mm/sec of scan speed for PATAC-Et, leading to a specific electrical conductivity ( $\sigma$ ) of  $2 \text{ S}\times\text{cm}^{-1}$ , while for PATAC-Me it is possible to reach  $4 \text{ S}\times\text{cm}^{-1}$  by using 300 mW and 15 mm/sec [44]. During the laser exposure, the color and morphology of PATAC dramatically change, passing from the yellowish-brown of the untreated sample to the blue-black of the laser exposed films, also exhibiting an irregular and porous surface probably determined by the emission of gaseous reaction products. The conversion of PATAC samples starts with the generation of free radicals whose concentration reaches its peak and then remains almost constant [45]. This process can be considered a photopyrolysis of the polymer, leading to the formation of unsaturated structures with an extended  $\pi$ -system mainly made of  $\text{sp}_2$  hybridized carbon atoms partly linked with sulfur. The outflow of gaseous products during the conversion process (mainly sulfides and mercaptanes) and the insolubility of the final treated polymer suggest that the laser is able to both split-off thioalkylic side chains and determine a partial inter- or intra-chain cross-linking. This process can reduce the conformational mobility of the backbone, making the polymer more prone to assuming planar conformations with a more extended conjugation, thus leading to enhanced charge mobility and better electrical conductivity.

In view of the foregoing, the first examined polymer was the PATAC-Me, bought from Aldrich Chemical Co. This sample had a  $M_n$  of  $4000 \text{ g}\times\text{mol}^{-1}$ , a polydispersity index of 1.15 and a  $\text{DP}_n$  of about 34 repeating units. Its  $^1\text{H-NMR}$  in  $\text{CDCl}_3$  is shown in Figure 23.

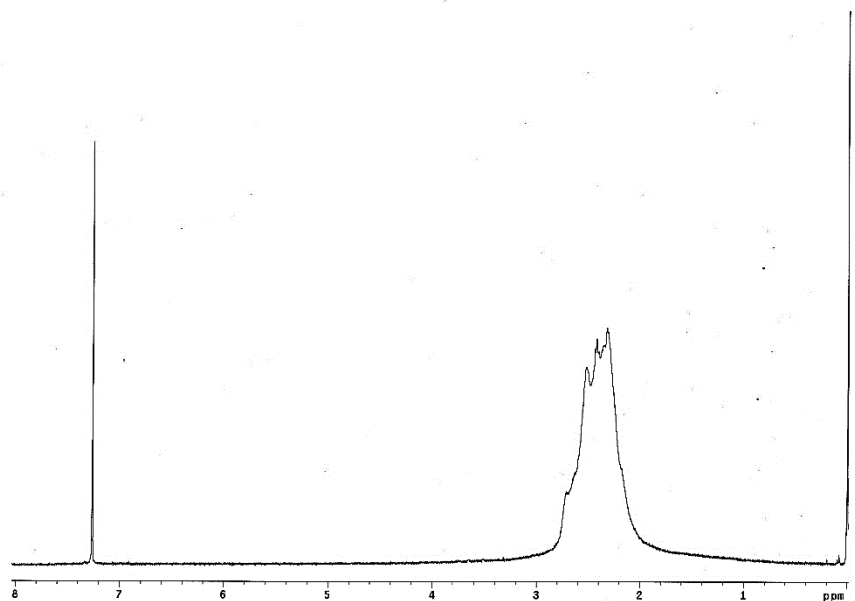


Figure 23.  $^1\text{H}$ -NMR spectrum of PATAC-Me.

The presence of only one peak, fairly broad and centered at 2.50 ppm, is clearly evident.

This signal is ascribable to the thiomethylic protons, while its broadness is due to the presence of different proton chemical surroundings since commercial PATAC-Me is a mixture of stereoisomers. The elemental analysis of the polymer was in good agreement with the expected structure. In Figure 24 the FT-IR spectrum of PATAC-Me in film cast from chloroform on Ge disk is shown before and after the laser tracing with blue laser ( $\lambda = 445$  nm).

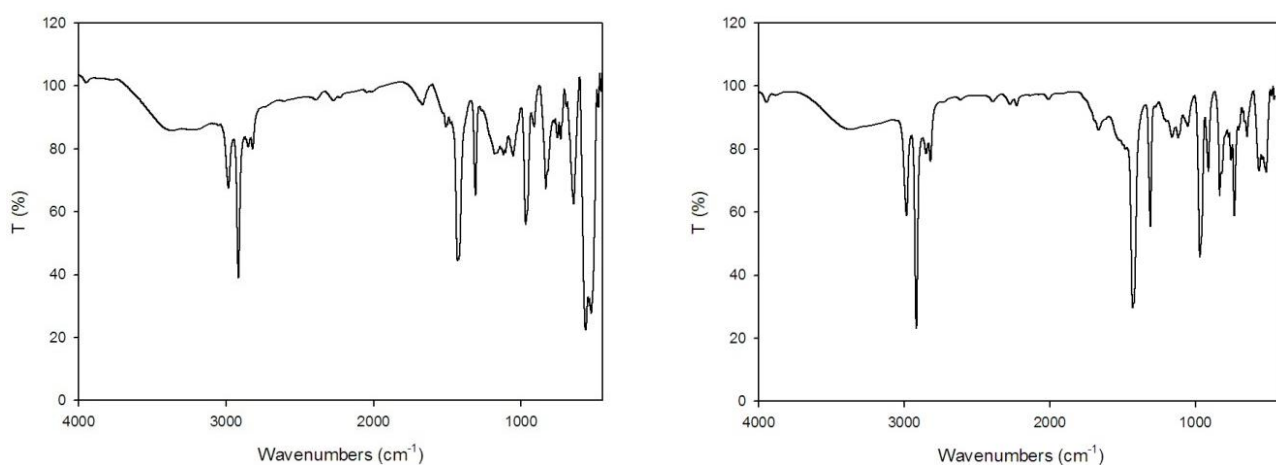


Figure 24. FT-IR spectra of PATAC-Me before (left) and after (right) laser treatment.



In the spectrum of the pristine polymer, the signals ascribable to its chemical structure were clearly evident:

- 2984, 2916  $\text{cm}^{-1}$ :  $\text{CH}_3$  antisymmetric and symmetric stretching;
- 1664  $\text{cm}^{-1}$ :  $\text{C}=\text{C}$  stretching;
- 1430  $\text{cm}^{-1}$ :  $\text{CH}_3$  antisymmetric deformation;
- 1308  $\text{cm}^{-1}$ :  $\text{CH}_3$  symmetric deformation;
- 645  $\text{cm}^{-1}$ :  $\text{S}-\text{CH}_3$  symmetric stretching.

The evolution in the intensity of the latter signal, which can range from 715 to 620  $\text{cm}^{-1}$ [46], could be evidence of the effectiveness of the laser treatment. In fact, its transmittance sensibly increased after the exposure to the coherent light (Figure 25).

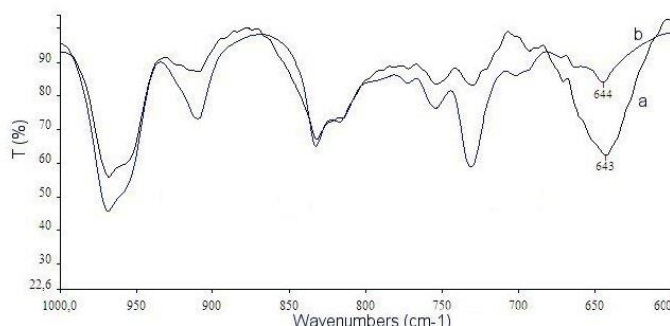


Figure 25. Detail of the FT-IR spectra of PATAC-Me before (a) and after (b) laser exposure.

Figure 26 shows the Raman spectra of unconverted and converted PATAC-Me films.

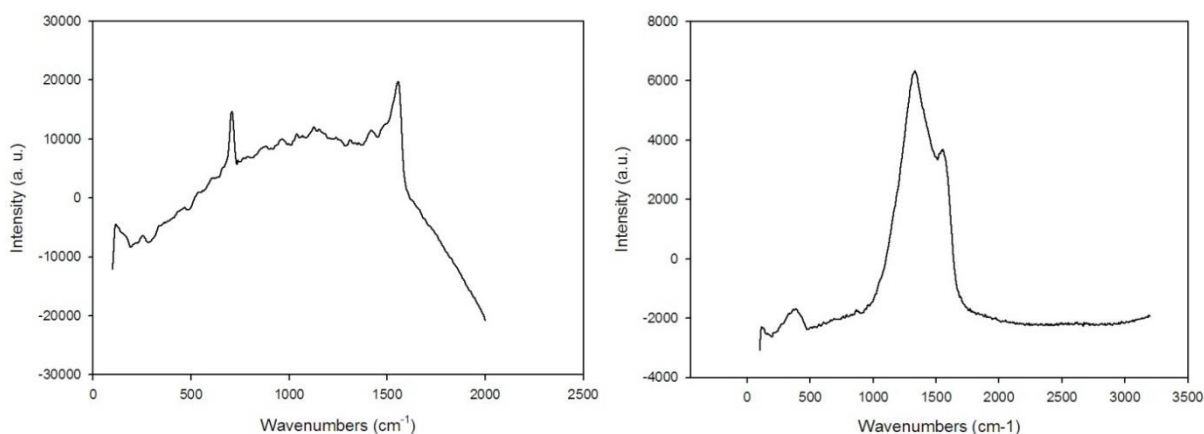


Figure 26. Raman spectra of PATAC-Me before (left) and after (right) laser exposure.

Before laser exposure, the film spectrum showed a non-linear baseline and a high level of noise; this was due to the high reflective surface of the pristine polymer, giving a lot of scattering of the red

laser radiation (785 nm) used to record the spectrum. In any case, two peaks could be found at 1554 and 708  $\text{cm}^{-1}$ ; the first signal was ascribable to the in-phase vibration of the C=C double bonds, since polyenes usually show an intense absorption in the 1600-1500  $\text{cm}^{-1}$  range, whose intensity may also be related to their extension of conjugation [47], while the signal around 700  $\text{cm}^{-1}$  could be related to the C-S stretching of the -SMe groups. After laser exposure, the latter signal could not be found, while the peak around 1300  $\text{cm}^{-1}$  could be ascribed to the in-phase vibration of the C-C bonds in polymeric chains.

The UV-Vis spectra of PATAC-Me in film on quartz slides are shown in Figure 27.

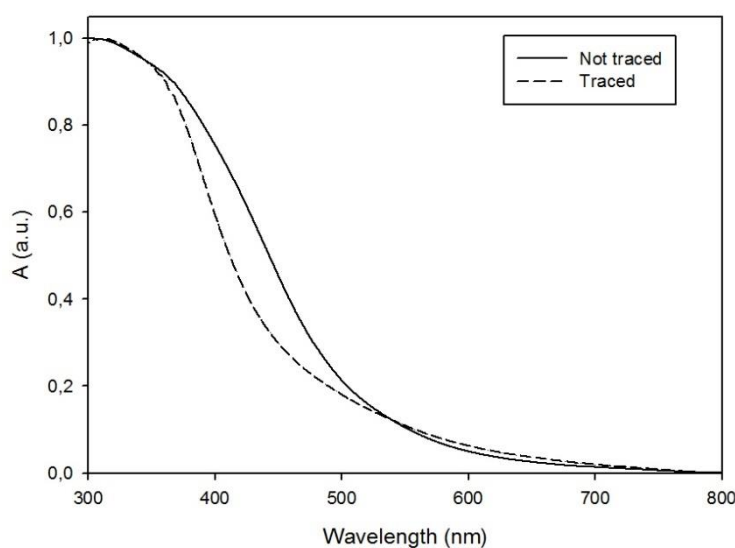


Figure 27. UV-Vis spectra of PATAC-Me films.

The polymer exhibited a non-structured profile, with a maximum absorption wavelength at 315 nm. The film was homogeneous and devoid of macroscopic aggregates and was obtained by dissolving PATAC-Me in chlorobenzene. The absence of any evident peak at the lower energies evidenced that this polymer had a high energy gap ( $E_g$ ), probably determined by its reduced conjugation length, as a consequence of the steric hindrance due to the presence both of the thiomethylic substituent on each C atom of the backbone, and of the non-stereoregularity of the sample. The spectral behavior changed after laser conversion since the inhomogeneous broadening of the spectrum decreased slightly while the absorption at the lower energies slightly increased.

The solvatochromism of PATAC-Me was examined in  $\text{CHCl}_3$  (solvent)/ $\text{CH}_3\text{OH}$  (non-solvent) mixtures. In Figure 28 the spectra of the polymer in pure chloroform (methanol molar fraction: 0.00) and at the higher non-solvent molar fraction (methanol molar fraction: 0.99) are shown. A further increase in the non-solvent concentration inevitably caused the precipitation of the polymer.

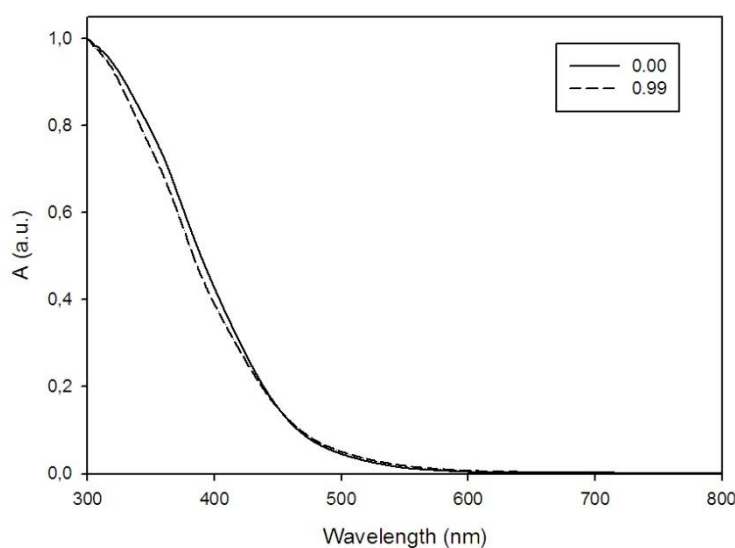


Figure 28. Solvatochromism of PATAC-Me.

PATAC-Me was completely insensitive to the non-solvent additions, since the presence of the thiomethylic substituents strongly reduced the rotational mobility of the polymeric backbone even when the polymer was almost completely devoid of the solvent molecules. Unfortunately the solvatochromic behavior of the laser-converted PATAC-Me had not been examined since the exposed polymer is insoluble in common organic solvents.

PATAC-Me was then dissolved in chlorobenzene (5 mg in 2 ml) and the solution, sonicated for 30 min, was deposited by doctor blading on 10×2.5 cm glass slides. Samples were heated at 80°C for 4h and cooled down to room temperature. The conversion was made by means of Wicked Laser portable diode lasers, Artic (blue light, 1 W of peak power,  $\lambda_{\text{max}}$  445 nm) and Krypton (green light, 1 W of peak power,  $\lambda_{\text{max}}$  532 nm). The effective power of the laser radiation on the polymer surface was measured using a Coherent power meter while the laser beam was well focused at a lens-sample distance of 3.7 cm. The exposure of the polymer was performed line-by-line using a Thor Labs computer-controlled positioning system which allowed for both an accurate control of the samples' position and their speed during irradiation. Samples were moved on the x-y plane from left to right using different scan speeds, by tracing a series of parallel 10-cm-long traces. The system was set so that the laser irradiated the same trace only once. The polymer film thickness, measured by means of a Burleigh Vista AFM used as a profilometer, ranged from 1 to 10  $\mu\text{m}$  and was influenced both by the adopted deposition technique (doctor blade, spin coating or drop casting, the latter giving thicker films) and by the possibility to make multiple depositions.

Under the same operating conditions (laser power, scan speed, and sample thickness), the Artic (blue) laser was more effective for the PATAC-Me conversion than the Krypton (green) one, being able to make the traces visible also from the opposite side of the sample. This fact is probably ascribable to the higher absorbance of PATAC-Me at 445 nm than at 532 nm.

The best sample conversion was obtained using the Artic laser at a scan speed of  $5 \text{ cm} \times \text{s}^{-1}$  with an effective power of 600 mW. Figure 29 shows an image of a partially traced PATAC-Me film (optical microscope, magnification:  $50\times$ ).



*Figure 29. Optical microscope image of a partially traced film of PATAC-Me.*

In the lower part of the image, traces are clearly visible. The polymer morphology notably changed after the conversion, passing from a smooth surface, even if crossed by some cracks ascribable to the glassy nature of the film, to a rough, dull, and less homogeneous surface. Traces had a worm-like appearance and a porous structure, probably caused by the outflow of gaseous reaction products. Laser-converted paths had an average width of  $50 \text{ }\mu\text{m}$  and a mean depth of  $3 \text{ }\mu\text{m}$ . The laser-induced conversion of PATAC-Me using the blue laser was undoubtedly effective, since the pristine polymer conductivity was around  $10^{-14} \text{ S} \times \text{cm}^{-1}$  and, after exposure, the value increased greatly, up to  $80 \text{ S} \times \text{cm}^{-1}$ .

Figure 30 shows the SEM micrograph of a traced sample of PATAC-Me. Paths are clearly evident on the left side of the image.

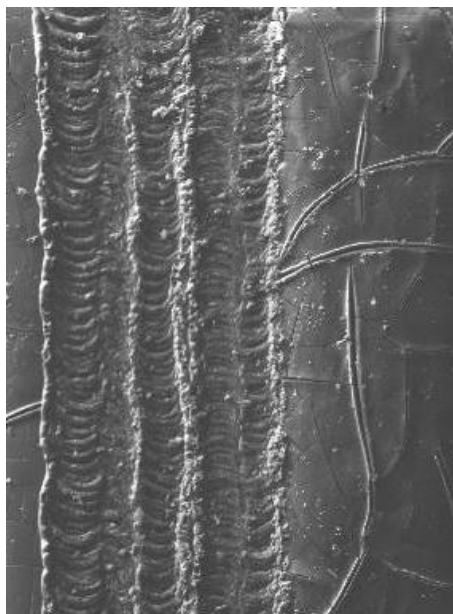


Figure 30. SEM micrograph of a PATAC-Me film after laser tracing.

Figure 31 shows the topographic microanalysis of the latter sample in relation to the C and S elements recorded using an Energy-dispersive spectrometer (EDS) probe.

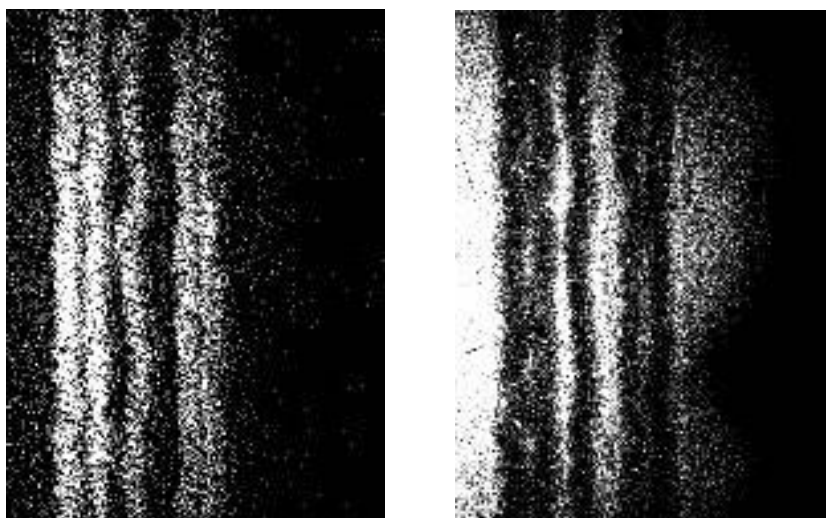


Figure 31. EDS topographic microanalysis of the film reported in Fig. 30. Left: Carbon, right: sulfur.

Since the concentration of the element is proportional to the intensity of white, it is evident that in the converted pathways there was a higher amount of C and a lower amount of S than in the unexposed ones. In fact, C and S concentrations passed from 41 and 54% of the unexposed area to 75 and 20% of the laser treated portions, respectively, thus confirming the partial loss of side chains.

Even if PATAC-Me is a good candidate for electric and electronic applications, its non-complete solubility in common organic solvents is undoubtedly a great drawback. Concentrated solutions of this polymer can only be obtained in chlorinated or aromatic high-boiling solvents, such as chlorobenzene or

o-dichlorobenzene. Films prepared from these solvents are usually quite homogeneous even though they sometimes appear spotted, dotted or with some cracks. Moreover, PATAC-Me solutions cannot be cast on transparent polymeric layers, such as PET, PMMA, or cellulose acetate, since the solvent corrodes the substrate and, in any case, the resulting film would be too fragile for a permanent adhesion to flexible and bendable surfaces.

The synthesis of a new polymer which, at the same time, has a conjugated backbone and photo-cleavable side chains while being capable of giving homogeneous and elastic films, could be a first attempt at circumventing these problems. Poly[(3-methylthio)thiophene] (PSMe) seemed to be a good substitute for PATAC-Me since it belongs to the ICP class and bears thioalkylic substituents. 3(methylthio)thiophene- was purchased from Atlantic Chemical Co. and subjected to an oxidative polymerization procedure in water, using  $\text{H}_2\text{O}_2$  and  $\text{FeCl}_3$  as oxidizing agents and sodium dodecylsulfate as a surfactant [48]. This method should be particularly effective in molecular weight control, generally leading to low molecular weight polythiophenic fractions that are soluble in a wide range of organic solvents; it appeared particularly suitable for synthesizing PSMe, since short side chains usually lead to little-soluble polyalkylthiophenes [49].

The polymerization reaction proceeded with an initial dark-brown color and the subsequent formation of a black oil, without any trace of precipitate. A first attempt to recover the polymer by multiple extractions of the reaction products with halogenated solvents did not give satisfying results, since the surfactant was found in both organic and aqueous phases. The polymer purification was then performed by means of a dialysis membrane (100 nm pore size), which allowed the recovery of the polymer without any trace of SDS and  $\text{FeCl}_3$  being detected. Contrary to expectations, PSMe was only partially soluble in organic solvents, leading to inhomogeneous and brittle films. Since its molecular weight was not particularly high, as evidenced by the  $^1\text{H}$ -NMR spectrum shown in Figure 32, where the chain-end signals are clearly evident, its low solubility might be ascribed to the too-short substituent inserted in the 3-position of the aromatic ring.



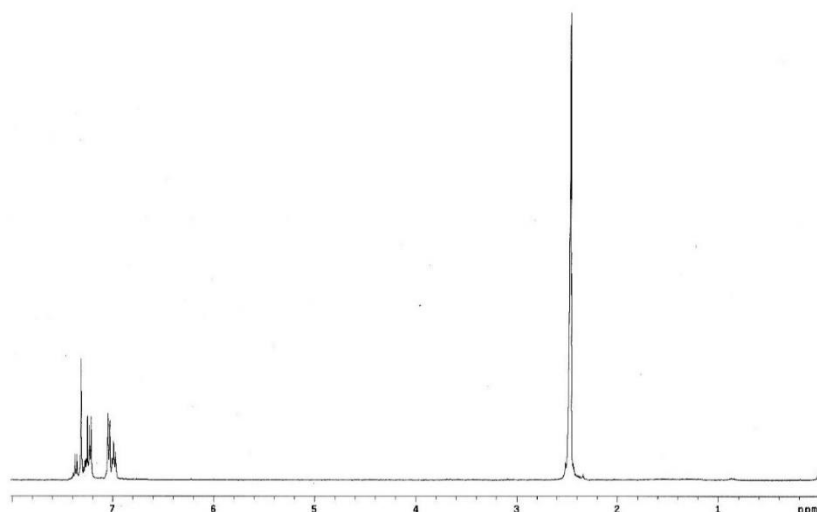


Figure 32. <sup>1</sup>H-NMR spectrum of PSMc.

The NMR spectrum shows only one signal in the aliphatic region ( $-\text{SCH}_3$  at 2.65 ppm) while the aromatic region is more complex, showing three signals ascribable to the protons of the ending thiophenes (H4 at 6.97 ppm, H2 at 7.03 ppm and H5 at 7.37 ppm [50]) and one signal at 7.25 ppm, belonging to the  $\beta$ -proton of the central thiophene units of polymeric chains. The FT-IR analysis of PSMc was performed on a thin film cast on a Ge disk (Figure 33).

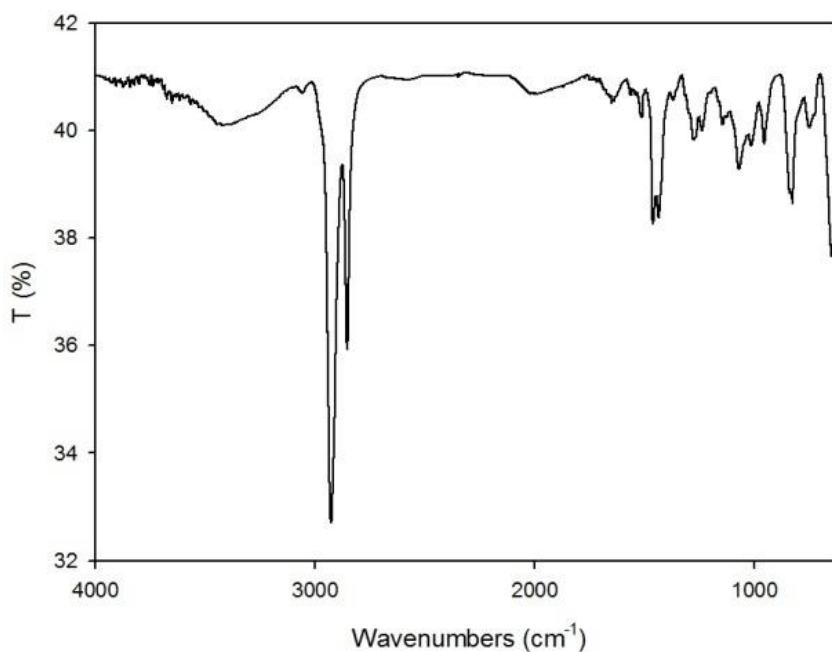


Figure 33. FT-IR spectrum of PSMc.

The spectrum was in good agreement with the expected structure, showing the following peaks (in  $\text{cm}^{-1}$ ): 3059 ( $\nu$  C-H $_{\beta}$ , thiophene); 2927 ( $\nu_{\text{as}}$  -CH $_3$ ); 2853 ( $\nu_{\text{s}}$  -CH $_3$ ); 1511 ( $\nu_{\text{as}}$  C=C); 1462 ( $\nu_{\text{s}}$  C=C); 1369 (-CH $_3$  sym. deformation); 1014 (-CH $_3$  rocking); 826 ( $\gamma$  C-H 2,3,5-trisubstituted thiophene); 648 ( $\nu$  C-S).

The UV-Vis analysis of PSMe in solution (THF) and in film is shown in Figure 34.

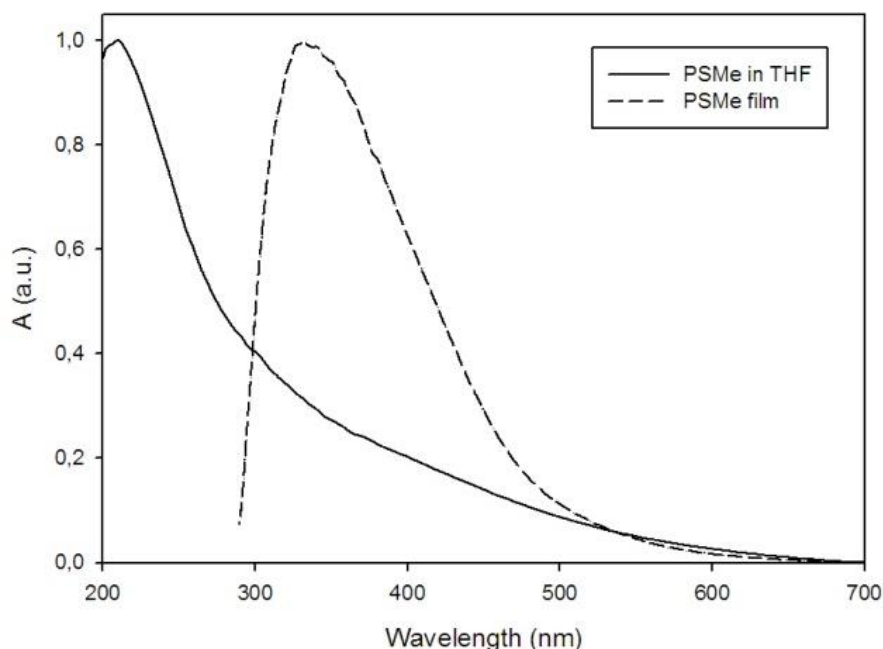
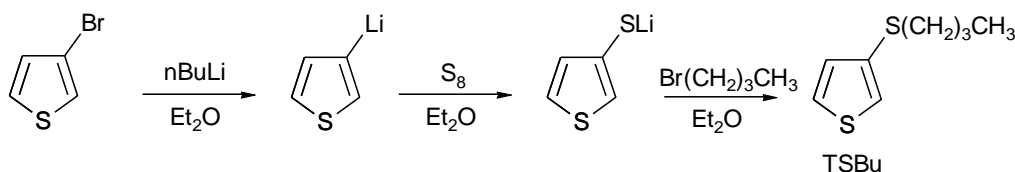


Figure 34. UV-Vis spectra of PSMe in solution and in film.

The steric hindrance of the short side-chain, the presence of Head-to-Head (H-H) linkages and the low molecular weight negatively affected the conjugation length of the polymeric backbone. In fact, even if an evident bathochromic shift of the  $\lambda_{\text{max}}$  was observable when passing from the solution to the solid state ( $\Delta\lambda_{\text{max}} = 121$  nm), the film spectrum showed a maximum absorption wavelength (332 nm) usually found in short thiophene oligomers [51]. Similar results were obtained using a different polymerization procedure which involved chloroform as a reaction solvent and an excess of iron trichloride as an oxidizing agent [52]. This time, the purification of the polymer was easier but the latter was, however, insoluble.

Taking into account the previous results, a polyalkylthiophene (PAT) derivative with a longer thioalkylic side chain was synthesized, namely poly[(3-buthylthio)thiophene] (PSBu). The monomer (3-buthylthio)thiophene (TSBu) was synthesized according to Ref. [53], starting from commercial 3-bromothiophene and using a “one pot” reaction shown in Scheme 13.

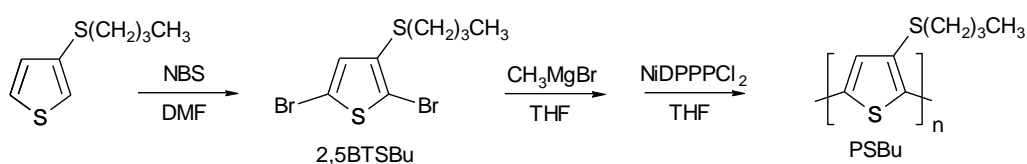




Scheme 13. Synthesis of the monomer TSBu.

TSBu was recovered with a good yield after purification and was firstly subjected to an oxidative polymerization initially with  $\text{FeCl}_3$  in  $\text{CH}_3\text{NO}_2/\text{CHCl}_3$ , a solvent mixture usually giving a good control of molecular weights as well as a low polydispersity index [54], and afterwards with  $\text{FeCl}_3$  in pure  $\text{CHCl}_3$ , a method that leads to higher molecular weights [55]. In spite of this, in both cases only short oligomers were recovered, probably because the low oxidation potential of TSBu promoted the formation of low-molecular-weight stable species [56].

TSBu was then selectively dibrominated in the 2,5-positions of the thiophenic ring by means of N-bromosuccinimide (NBS) in anhydrous N,N-dimethylformamide (DMF) by using an optimized reaction procedure involving the addition of the brominating agent in two distinct steps at room temperature. 2,5-dibromo-3-(butylthio)thiophene (2,5-BTSBu) was recovered in a good yield (70%) after chromatography column purification and exploited for organometallic coupling reactions using the McCullough procedure [57]. This method is a useful and straightforward way to synthesize regioregular Head-to-Tail (H-T) linked poly(3-alkylthiophene)s through the magnesium-halogen exchange (Grignard Metathesis Reaction, GRIM) with a preformed organometallic derivative and subsequent Ni(II) catalyzed cross-coupling reaction (Scheme 14).



Scheme 14. Synthesis of the polymer PSBu by using the GRIM reaction.

PSBu was obtained with good yield (57%) as a dark orange solid well soluble in common organic solvents. Despite its quite low molecular weight ( $M_n=11.000$ ,  $\text{PDI}=1.4$ ) it gave highly homogeneous and free-standing films. Its elemental analysis confirmed the expected chemical structure.

Table 2 show the characteristic FT-IR absorptions of the monomers TSBu and 2,5-BTSBu and of the polymer PSBu prepared with the GRIM procedure.

Table 2. FT-IR absorption bands ( $\text{cm}^{-1}$ ) and relative assignments for TSBu, 2,5-BTSTBu and PSBu samples.

Assignment	TSBu	2,5-BTSTBu	PSBu
C-H stretching (thiophene, $\alpha$ -hydrogens)	3103	-	-
C-H stretching (thiophene, $\beta$ -hydrogen)	3059	3050	3057
C-H stretching (antisymmetric, methyl)	2953	2958	2956
C-H stretching (antisymmetric, methylenes)	2928	2927	2927
C-H stretching (symmetric, methyl+methylenes)	2871	2874	2870
C=C stretching (antisymmetric, thiophene)	1492	1501	1501
C=C stretching (symmetric, thiophene)	1464	1464	1463
CH <sub>3</sub> deformation	1350	1387	1378
C-Br stretching (aromatic)	-	992	-
C-H bending out-of-plane (2,3,5-trisubstituted thiophene)	-	839	826
C-H bending out-of-plane (3-substituted thiophene)	773	-	-
CH <sub>2</sub> rocking	754	747	751
C-S stretching	686	647	714

The absorption at  $3103\text{ cm}^{-1}$ , ascribable to the stretching of the thiophene  $\alpha$ -hydrogens, was absent in 2,5-BTSTBu and PSBu samples, as well as the band at  $773\text{ cm}^{-1}$ , which was substituted by the new absorption around  $830\text{ cm}^{-1}$ . Moreover, aromatic C-Br stretching at  $992\text{ cm}^{-1}$  in the 2,5-BTSTBu spectrum was completely missing in the polymer spectrum, while the C-S stretching mode was evident in all the samples.

Table 3 shows the  $^1\text{H}$ - and  $^{13}\text{C}$ -NMR data for both the examined monomers and the PSBu polymer, together with the corresponding assignments obtained by comparing some selected references [58,59,60,61,62].

Table 3.  $^1\text{H}$ - and  $^{13}\text{C}$ -NMR signals (ppm) and relative assignments for TSBu, 2,5-BTStBu and PSBu samples.

Atom number <sup>a</sup>	TSBu		2,5-BTStBu		PSBu	
	$\delta^1\text{H}$	$\delta^{13}\text{C}$	$\delta^1\text{H}$	$\delta^{13}\text{C}$	$\delta^1\text{H}$	$\delta^{13}\text{C}$
2	7.11 (m)	122.8	-	111.6	-	132.3
3	-	132.3	-	134.7	-	129.0
4	7.00 (m)	129.7	6.91 (s)	133.0	7.37 (s)	130.3
5	7.32 (m)	126.0	-	113.5	-	134.0
6	2.82 (t)	35.0	2.81 (t)	35.7	2.81 (m)	35.0
7	1.60 (m)	31.5	1.56 (m)	32.3	1.56 (m)	31.6
8	1.43 (m)	21.8	1.44 (m)	22.4	1.43 (m)	21.7
9	0.93 (t)	13.6	0.93 (t)	14.3	0.93 (m)	13.6

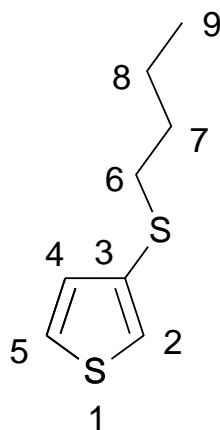
<sup>a</sup>See Figure 35

Figure 35. Adopted atoms numbering for NMR analysis.

The monomer 2,5-BTStBu was lacking in H atoms in the 2,5-positions of the thiophene therefore, its polymerization was only confirmed by the shift of the signal ascribable to the thiophene H-4 atom to a lower field. Moreover, the absence of the thiophene  $\alpha\text{CH}_2$  group prevented the determination of the percentage of regioregularity of PSBu in terms of configurational dyads. However, the presence of only

one signal in the aromatic region of the  $^1\text{H}$ -NMR spectrum of the polymer suggested that a high degree of regioregularity was achieved (Figure 36)

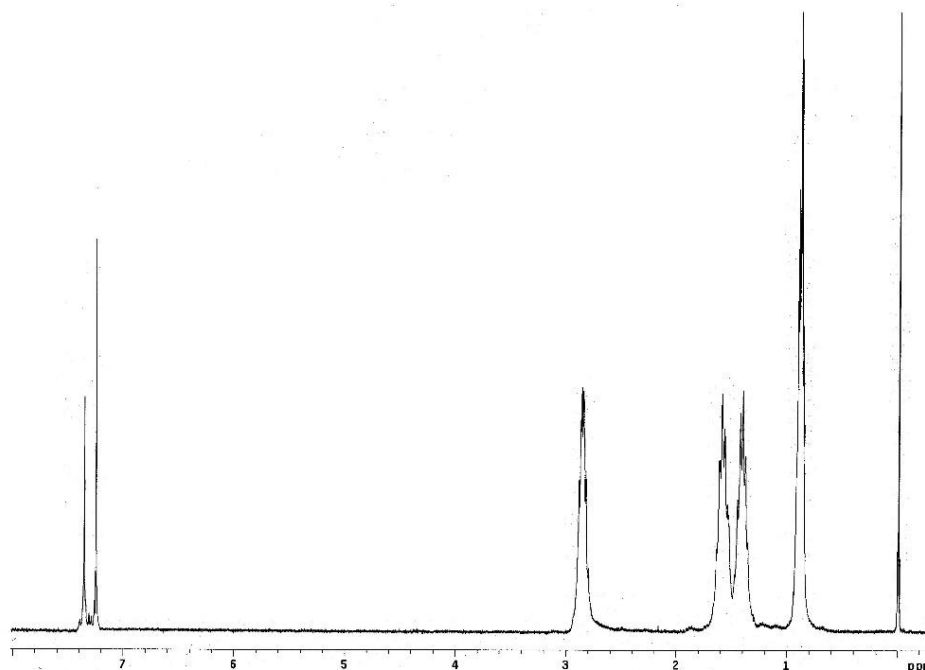


Figure 36.  $^1\text{H}$ -NMR of PSBu prepared using the McCullough procedure.

This was also confirmed by the presence of only four aromatic carbon signals in the  $^{13}\text{C}$ -NMR spectrum (Figure 37). The obtained results once again confirmed the easiness and versatility of the McCullough GRIM reaction for obtaining regioregular functionalized PATs.

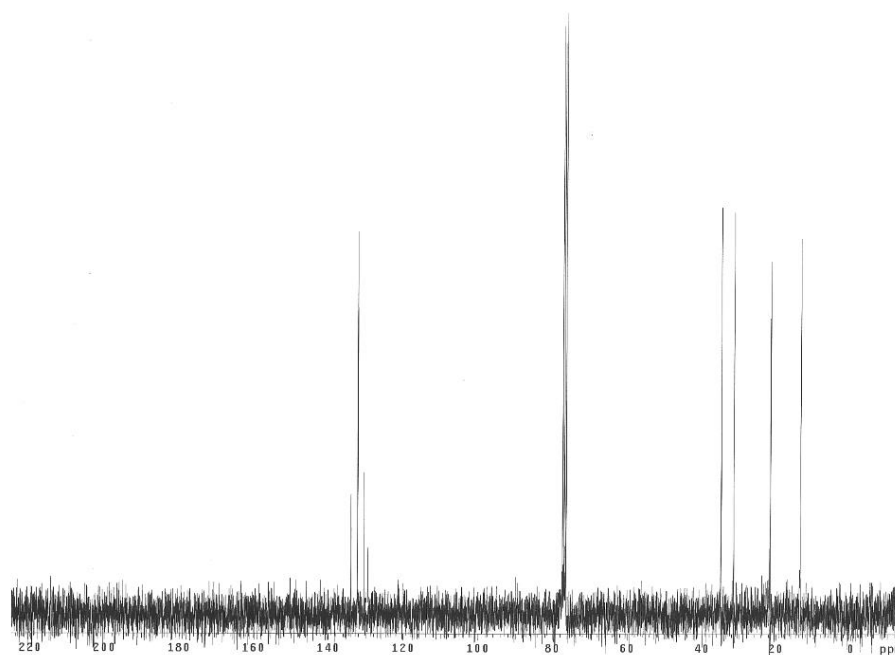


Figure 37.  $^{13}\text{C}$ -NMR of PSBu prepared using the McCullough procedure.

The high solubility of PSBu in common organic solvents made it possible to perform its UV-Vis analysis in different solvent- and non-solvent mixtures. Figure 38 shows the solvatochromic behavior of PSBu in dimethylpropyleneurea (DMPU)/methanol and tetrahydrofuran (THF)/methanol at increasing non-solvent (methanol) molar fractions.

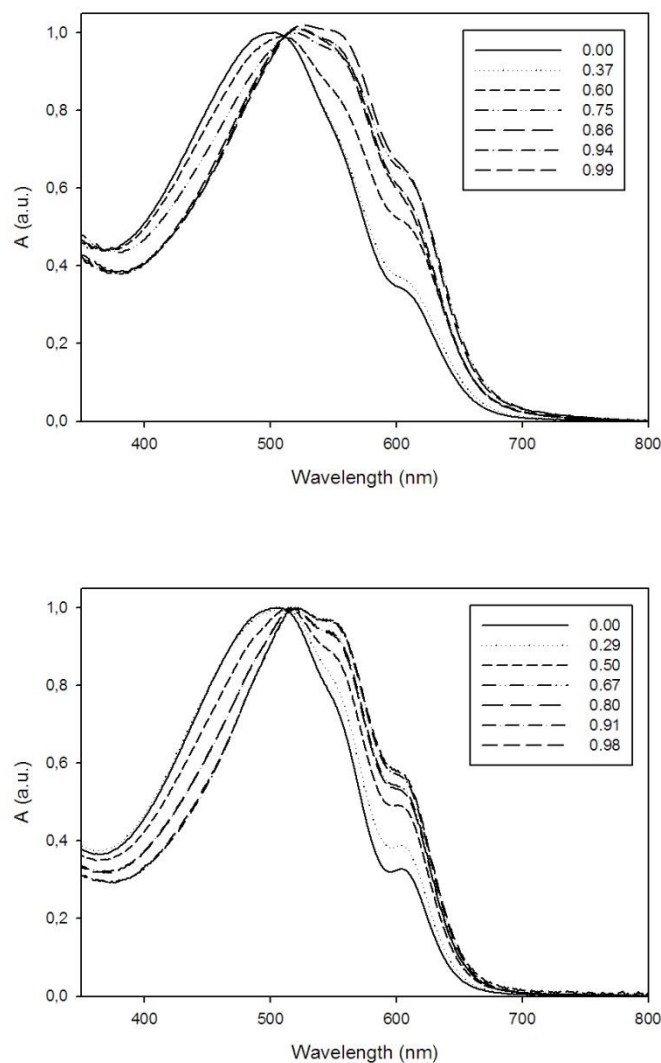


Figure 38. Solvatochromism of PSBu in DMPU/MeOH (top) and THF/MeOH (bottom) at increasing methanol molar fractions.

In both cases, the solvatochromic transition from the solvated to the less solvated conformation was clearly visible, resulting in the solution color change from dark red to violet, without any trace of macroscopic aggregation being detected even after many days. The non-solvent effect was more evident in the DMPU/MeOH system ( $\Delta\lambda_{\text{max}} = 26$  nm, from 501 to 527 nm) than in THF/MeOH ( $\Delta\lambda_{\text{max}} = 17$  nm, from 505 to 522 nm) while the polymer showed a clearly evident pure electronic transition ( $E_{0-0}$ ) around 604 nm, also visible in pure solvents. The moderate shifts of the  $\lambda_{\text{max}}$  of the polymer spectra by progressive additions of the non-solvent as well as the presence of the  $E_{0-0}$  absorption without any addition of MeOH indicated the tendency of PSBu to assume well-ordered conformations even in good

solvents, probably because the side chains possessed a high ability to self-assemble even in the solvated state. This can be a very important feature for the obtaining of concentrated solutions of preordered planar PAT chains; they are particularly useful for the preparation of homogeneous thick films which can be used either for the laser writing process or for the building up of bulk heterojunctions (BHJ) solar cells. PSBu spectrum in the film state is shown in Figure 39.

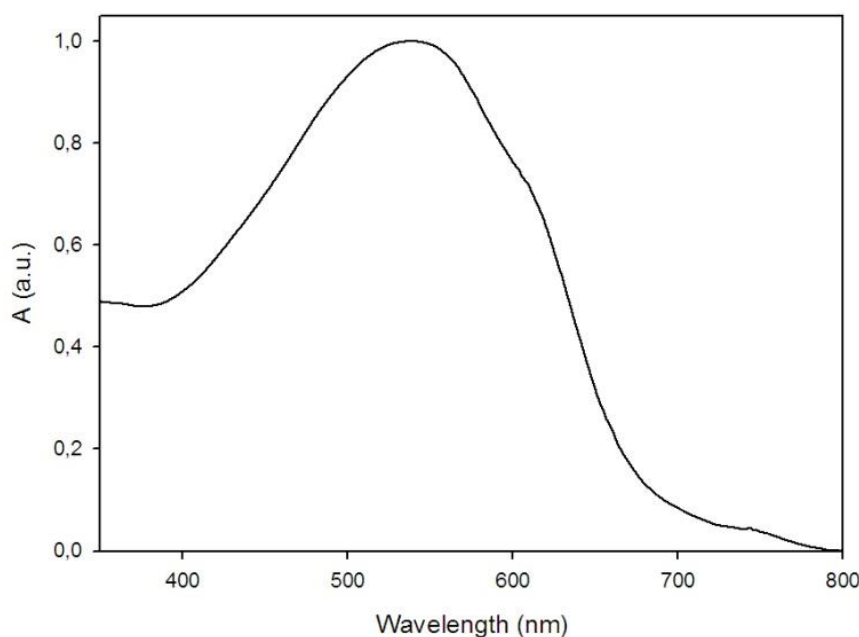


Figure 39. UV-Vis spectrum of PSBu in film.

The  $\lambda_{\max}$  of PSBu in film (538 nm) is very similar to that recorded in solution of pure solvents, thus indicating the presence of the same conformer in solution and in the solid state.

PSBu was then dissolved in THF (5 mg in 2 ml) and the solution was deposited on 10×2.5 cm preventively cleaned glass slides using the doctor blading technique. The obtained sample was annealed for 3h at 80°C in air, giving very homogeneous films with a thickness in the 5-10  $\mu\text{m}$  range. The best tracing conditions were obtained using the Krypton green laser, operating at 532 nm, a wavelength very close to the  $\lambda_{\max}$  of PSBu in film, with a scan speed of 3 cm/sec and an effective power of 600 mW, leading to a mean specific conductivity of  $5 \times 10^{-2} \text{ S} \times \text{cm}^{-1}$ . The adopted tracing speed is slower than in PATAC-Me experiments, probably because this time the longer side chain is more difficult to eliminate from the substrate, and the final conductivity lower than for the polyacetylenic derivative. PSBu, however, is a very interesting material, since it is easy to synthesize and gives very homogeneous thick films which are completely devoid of macroscopic aggregates. Moreover, PSBu is able to increase its specific electrical conductivity by 8 orders of magnitude, reaching values comparable to those obtained in doped PATs [63] but without any detrimental effect of moisture and oxygen on its time performance.

PSBu films are essentially amorphous and more elastic than those obtained using PATAC-Me, so the former can be easily applied also on flexible substrates, such as PET, cellulose acetate, polyvinylalcohol, and polyvinylchloride.

Figure 40 shows an optical microscope image of a traced sample of PSBu and the corresponding 3D elaboration.

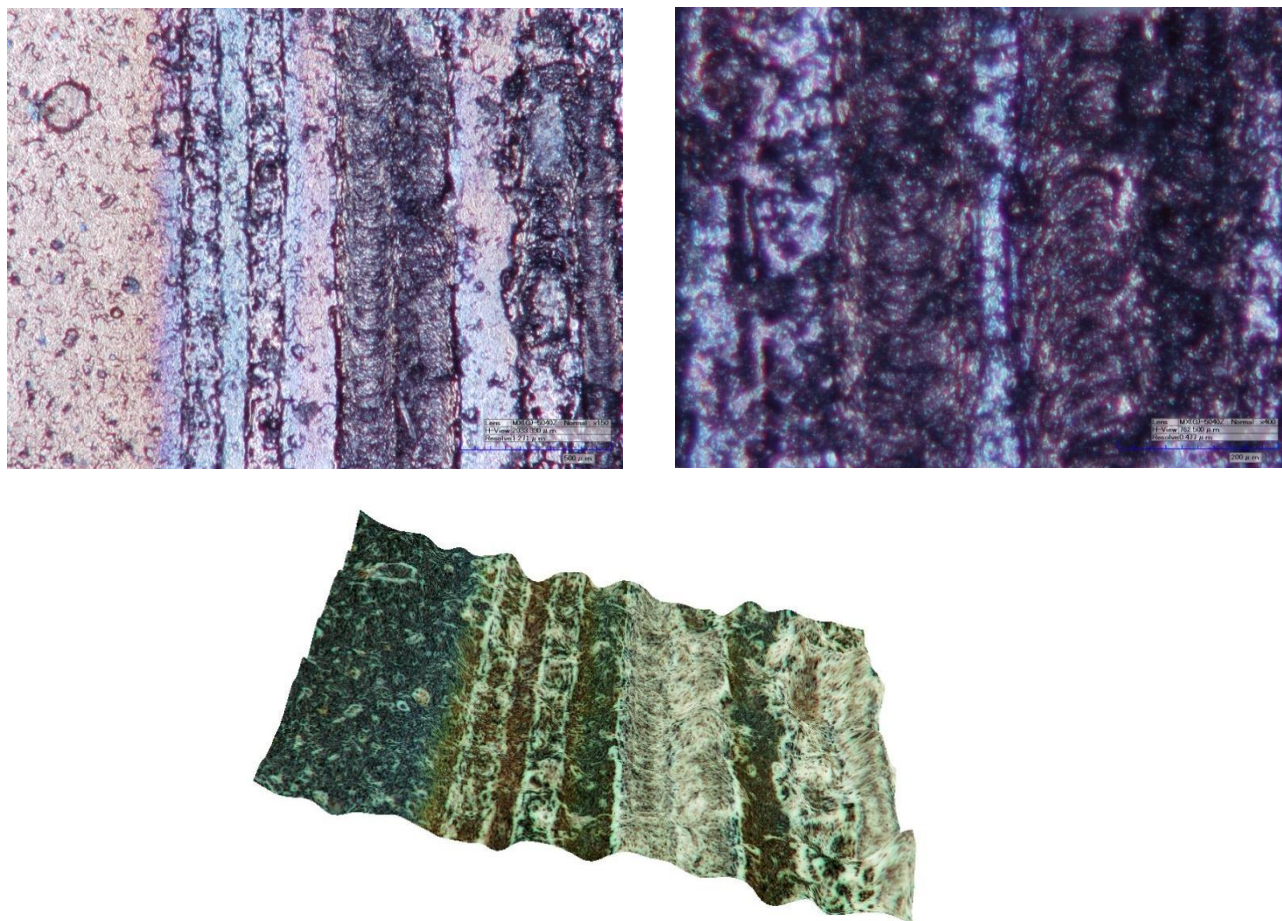


Figure 40. Optical microscope images of traced PSBu films. Top left: 50 $\times$ , right: 400  $\times$ . Bottom: 3D elaboration, 50 $\times$ .

Moving from left to right, the untreated portion of PSBu film is clearly evident and is followed first by two traces obtained with the green laser operating at reduced power (60 mW), and then by two more traces produced with full-power laser (600 mW). In all cases, the tracing speed was 3 cm/sec. The 3D image clearly shows homogeneous traces without any apparent pits or holes.

Figure 41 shows the SEM image of a traced PSBu film. The image covers an area of about 2 $\times$ 4 mm and clearly shows five parallel traces. The elemental microanalysis shows a sulfur content decreasing from 37 to 21%.



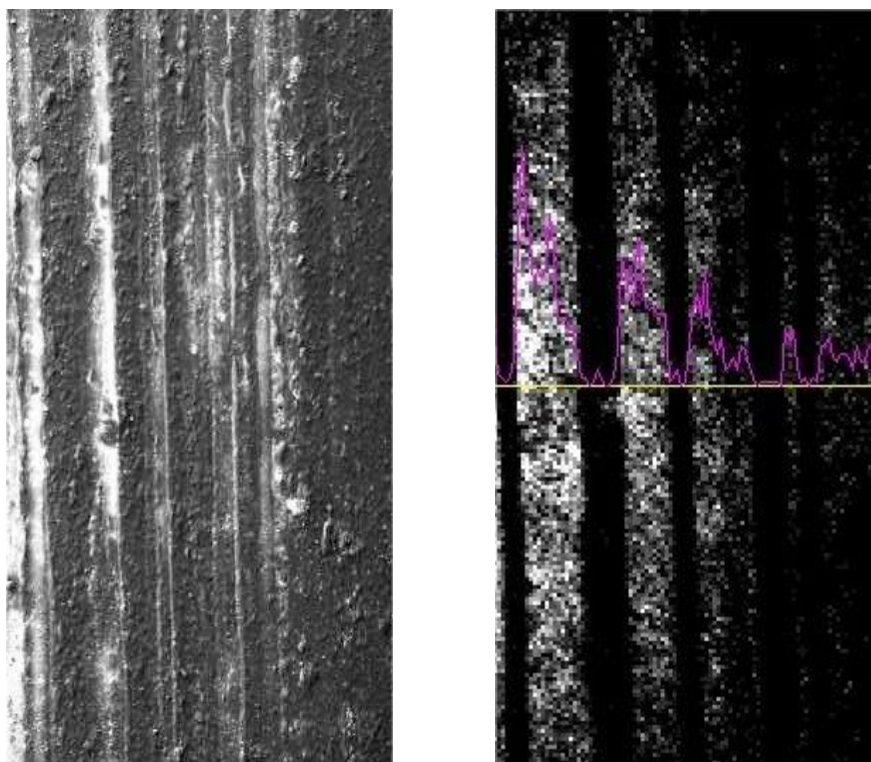


Figure 41. SEM image of a traced PSBu film (left). EDS microanalysis relative to sulfur on the same film (right).

The IR spectrum of the traced PSBu sample showed the same main absorptions of the pristine polymer at 2927, 2853, 1515, 1462, 825 and 751  $\text{cm}^{-1}$ . The band at 714  $\text{cm}^{-1}$  ( $\nu$  C-S) is absent, thus confirming the partial loss of the side chains after the photopyrolysis procedure (Figure 42).

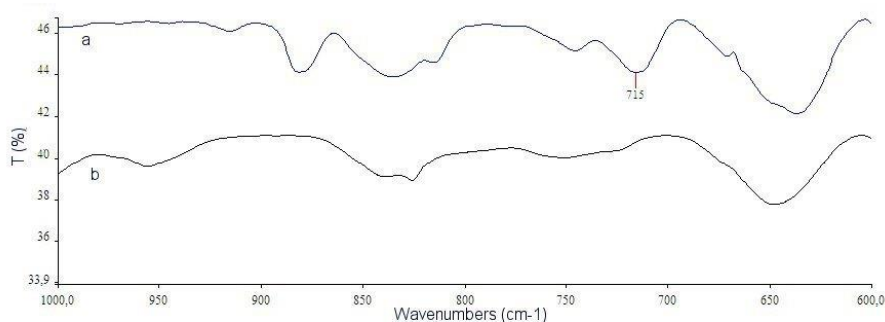


Figure 42. FT-IR spectrum of a PSBu film. a) untraced b) traced.

The thermal behavior of unexposed PATAC-Me and PSBu has been examined by means of DSC in inert atmosphere with a heating scan of 10°C/min. Thermograms are shown in Figure 43.



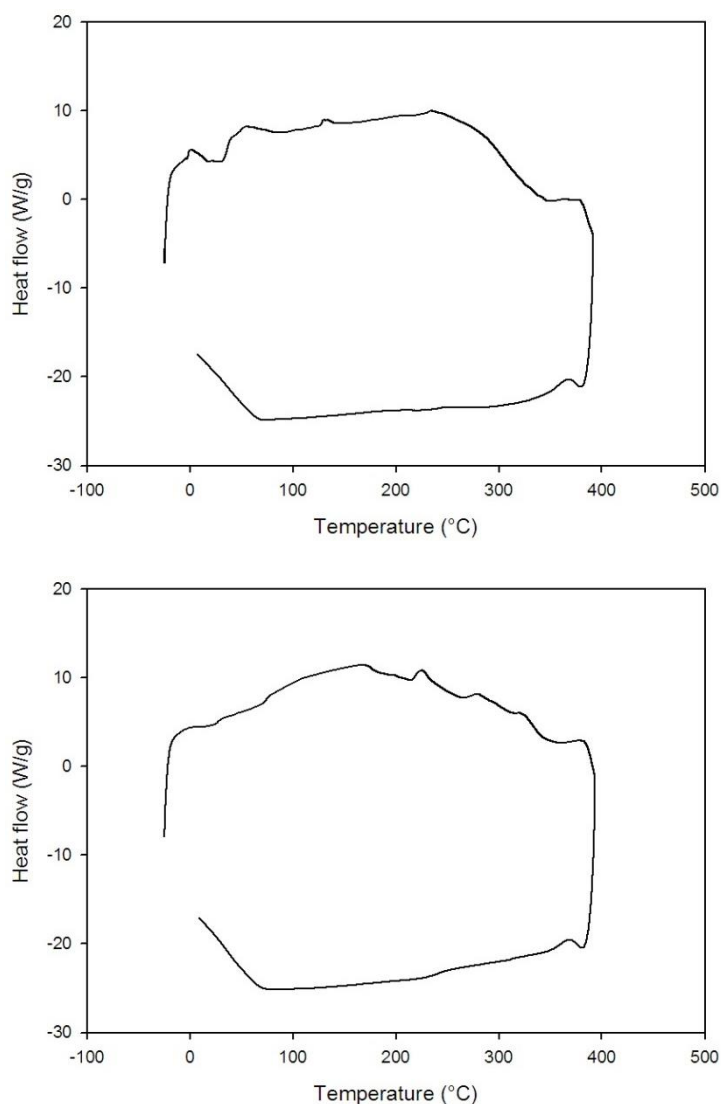


Figure 43. DSC thermograms of PATAC-Me (left) and PSBu (right).

Two second-order transitions ( $T_g$ ) were found at 42 and 80°C for PATAC-Me and PSBu respectively, and two first-order transitions ( $T_m$ ) at 131 and 166°C. After 200°C the two polymers started to decompose.

The TGA analyses of the two polymers were recorded from 25 to 600°C with a heating scan of 10°C/min in an oxidizing environment (air). PATAC-Me showed a two-phase weight loss: the first, starting around 200°C, was compatible with the loss of a thiomethylic and methylic group while the second, over 400°C, was due to the almost complete oxidation of the residual polymeric backbone (Figure 44). The PSBu behavior was more complex, showing an initial weight loss at around 200°C and ascribable to the loss of a methylic group, a second loss from 250 to 500°C compatible with the loss of the  $\text{SCH}_2\text{CH}_2\text{CH}_2$  residue and a third one over 500°C due to the cracking of the polymeric backbone.

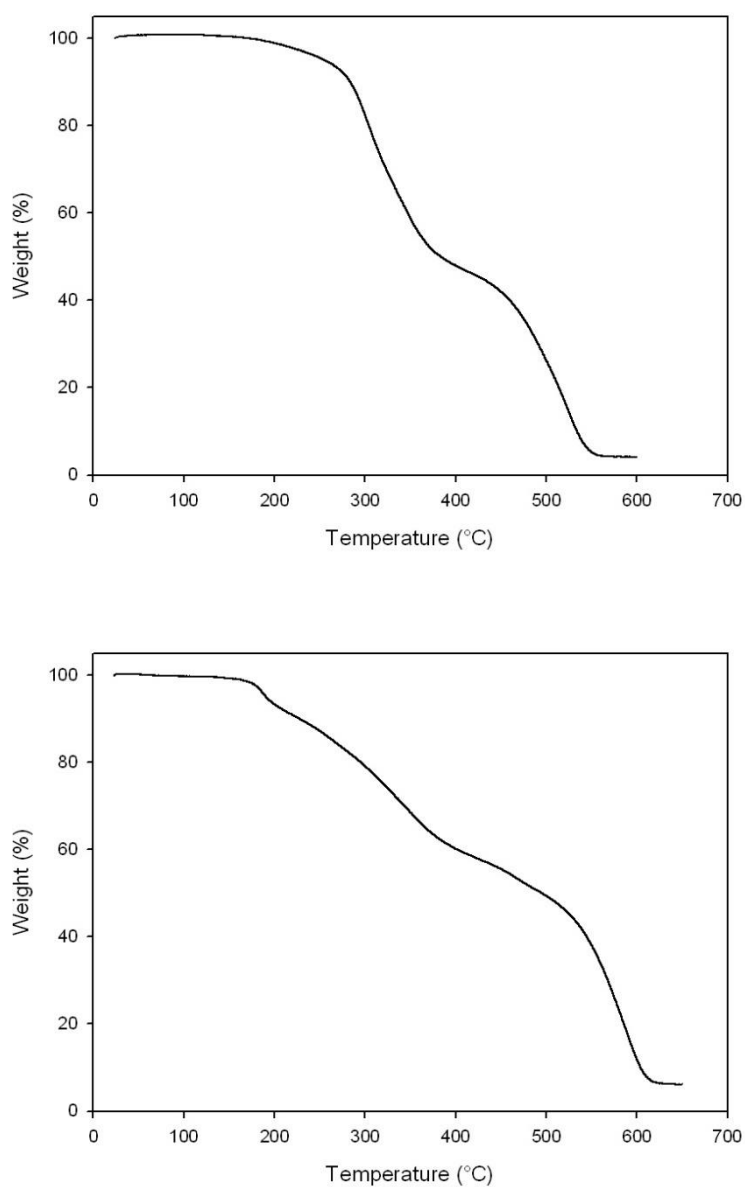


Figure 44. TGA thermograms of PATAC-Me (left) and PSBu (right).

The electrical conductivities of PATAC-Me and PSBu were also examined in the 293-453 K (20-180°C) thermal range, far enough to arrive at their decomposition temperature.

The obtained results are shown in Table 4.

Table 4. Electrical conductivity ( $\sigma$ ) of PATAC-Me and PSBu at different temperatures.

Temperature	$\sigma$ PATAC-Me	$\sigma$ PSBu
(K)	( $S \times cm^{-1}$ )	( $S \times cm^{-1}$ )
293	80	$5.0 \times 10^{-2}$
313	80	$5.2 \times 10^{-2}$
333	84	$5.2 \times 10^{-2}$
353	88	$5.5 \times 10^{-2}$
373	91	$6.1 \times 10^{-2}$
393	95	$6.3 \times 10^{-2}$
413	105	$7.1 \times 10^{-2}$
433	105	$7.2 \times 10^{-2}$
453	107	$7.6 \times 10^{-2}$

In the examined range the specific conductivity is subject to small changes, thus reflecting the polymers' thermal stability in the examined temperature range, according to DSC measurements. The observed slight increase of  $\sigma$  with temperature may indicate that polymers followed the typical behavior of inorganic semiconductors [64].

### 3.6 CONCLUSION

In this work we have successfully examined some conjugated polymers trying to find the best conditions for their laser tracing, with the aim of increasing their electrical conductivity. It is, in fact, well known that some ICPs can enhance their charge mobility, when irradiated with laser light at the suitable power and wavelength, by a photopyrolysis phenomenon which involves the partial loss of side-chain substituents. The laser-traced polymers are able to reach more planar conformations and then higher conjugation lengths since the macromolecular backbone becomes subjected to a lower degree of sterical crowding.

The first polymer examined belonged to the class of substituted polyacetylenes and was commercially available as dimethylthioderivative (PATAC-Me). After an accurate set-up of both the film deposition and the tracing conditions, we obtained pathways with an electrical conductivity similar to some metals by means of very simple procedures, involving the use of portable and inexpensive laser pointers. However, PATAC-Me films were rigid, fragile and brittle. In order to overcome this problem, we substituted the latter with the newly synthesized regioregular PSBu, a thiophenic polymer bearing a thiobutylic side chain, easily obtainable and able to give very homogeneous, flexible thick films. The high solubility of PSBu in common organic solvents, together with its flexibility, allowed for its deposition not only on glass or metal rigid substrates but also on plastic surfaces, thus leading, after laser exposure, to electrical conductivities comparable to those obtained with the best doped PATs films, but with a higher environmental and time stability.

PSBu films are thus very promising materials for the preparation of integrated circuits on rigid or flexible substrates by using the simple and rapid laser tracing technique.

## REFERENCES FOR CHAPTER 3

- [1]. Gunes S, Neugebauer H, Sariciftci NS (2007) Chem Rev 107:1324
- [2]. Murphy AR, Fréchet JMJ (2007) Chem Rev 107:1066
- [3]. Li G, Shrotriya V, Huang J, Yao Y, Moriarty T, Emery K, Yang Y (2005) Nat Mater 4:864
- [4]. Novak BM, Hegen E, Visnanathan A, Magde L (1990) Polym Prepr 31:482
- [5]. Gorman CB, Biebuyck HA, Whitesides GM (1995) Chem Mater 7:526
- [6]. Bargon J, Baumann R, Boeker P (1992) Proc SPIE 1672:441
- [7]. Roth HK, Eidner K, Roth H (1996) Circ World 22:19
- [8]. Roth HK, Gruber H, Fanghaenel E, Richter AM, Hoerig W (1990) Synth Met 37:151
- [9]. Srinivasan R, Hall RR, Wilson WD, Loehle WD, Allbee DC (1994) Synth Met 66:301
- [10]. Decker C (1987) J Polym Sci Polym Lett 25:253
- [11]. Roth HK, Baumann R, Bargon J, Schroedner M (1991) Progr Colloid Polym Sci 85:157
- [12]. Richter AM, Richter JJM, Beye N, Fanghaenel E (1987) Journal Prakt Chemie 329:811
- [13]. Okano Y, Masuda T, Hagashimura T (1982) Polymer J 14:477
- [14]. Richter AM, Laube U, Moniak F, Fanghaenel E, Hempel G, Goldenberg S, Scheler G (1991) Acta Polymerica 42:615
- [15]. Tobjork D, Kaihovirta NJ, Makela T, Pettersson FS, Osterbacka R (2008) Org Electron 9:931
- [16]. Youn H, Jeon K, Shin S, Yang M (2012) Org Electron 13:1470
- [17]. Aernouts T, Aleksandrov T, Girotto C, Genol J, Poortmans J (2008) J Appl Phys Lett 92:033306
- [18]. Hoth CN, Schilinsky P, Choulis SA, Brabec CJ (2008) Nano Letters 8:2806
- [19]. Jeong JA, Kim HK (2010) Curr Appl Phys 10:e105
- [20]. Jeong JA, Kim J, Kim HK (2011) Sol Energy Mat Sol Cells 95:1974
- [21]. Schaferling M, Bauerle P (2004) J Mater Chem 14:1132
- [22]. Su YW, Chelan S, Wei KH (2012) Materials Today 15:554
- [23]. Krebs FC, Norrman K (2010) Applied Materials & Interfaces 2:877
- [24]. Krebs FC (2009) Sol Energy Mat Sol Cells 93:394

- [25]. Sondergaard RR, Hosel M, Krebs FC (2013) J Polym Sci Part B, Polymer Physics 51:16
- [26]. Hubler A, Trnovec B, Zillger T, Ali M, Wetzold N, Mingeback M, Wagenpfahl A, Deibel C, Dyakonov V (2011) Adv Energy Mater 1:1018
- [27]. Kopola P, Aernouts T, Sliz R, Guillerez S, Yikunnari M, Cheyngs D, Valimaki M, Tuomikoski M, Hast J, Jabbour G, Myllylä r, Maaninen A (2011) Sol Energy Mater Sol Cells 95:1344
- [28]. Hambsch M, Reuter K, Stanel M, Schmidt G, Kempa H, Fugmann U, Hahn U, Hubler AC (2010) Mater Sci Eng B 170:93
- [29]. Kim A, Lee H, Lee J, Cho SM, Chae H (2011) J Nanosci Nanotechnol 11:546
- [30]. Hubler AC, Bellmann M, Schmidt GC, Zimmermann S, Gerlach A, Haentjes C (2012) Org Electron 13: 2290
- [31]. Krebs FC, Tromholt T, Jorgensen M (2010) Nanoscale 2:873
- [32] Angmo D, Hosel M, Krebs FC (2012) Sol Energy Mater Sol Cells 107:329
- [33] Sandstrom A, Dam HF, Krebs FC, Edman L (2012) Nat Commun 3:1002
- [34] Jensen J, Dam HF, Reynolds JR, Dyer AL, Krebs FC (2012) J Polym Sci Part B Polym Phys 50:536
- [35]. Galagan Y, Andriessen R, Rubingh E, Grossiord N, Blom P, Veenstra S, Verhees W, Kroon J (2010) LOPE-C 88 (ISBN 978-3-00-029955-1)
- [36] Eom SH, Senthilarasu S, Uthirakumar P, Yoon SC, Lim J, Lee C, Lim HS, Lee J, Lee SH (2009) Organic Electronics 10:536
- [37] Kwon JT, Ean SH, Moon BS, Shin JK, Kim KS, Lee SH, Lee YS (2012) Bull Korean Chem Soc 33:464
- [38] Girotto C, Rand BP, Steudel S, Genoe J, Heremans P (2009) Org Electron 10:735
- [39] Yu BK, Vak D, Jo J, Na SI, Kim SS, Kim MK, Kim DY (2010) IEEE Journal of Selected Topics in Quantum Electronics 16:1838
- [40] Tedde SF, Kern J, Sterzi T, Furst J, Lugli P, Hayden O (2009) Nano Lett 9:980
- [41] Beaujuge PM, Ellinger S, Reynolds JR (2008) Adv Mater 20:2772
- [42] Helgesen M, Carlé JE, Andreasen B, Hoesel M, Norrman K, Sondergaard R, KKrebs FC (2012) Polym Chem 3:2649
- [43]. Bargon J, Baumann R (1993) Micro Electronic Engineering 20:55

- [44]. Baumann R, Kulish U, Schroedner M, Roth HK, Sebastian D, Bargon J (1993) *Synth Met* 55-56:3643
- [45]. Roth HK, Gruber H, Fanghaenel E, Richter AM, Hoerig W (1990) *Synth Met* 37:151
- [46]. Bellamy LJ (1975) In: *The infra-red spectra of complex molecules*, Chapman and Hall, London, p. 395 ff.
- [47]. Nyquist RA (2001) In: *Interpreting Infrared Raman and NMR Spectra*, Academic Press, London.
- [48]. Lee JM, Lee SJ, Jung YJ, Kim JH (2008) *Curr Appl Phys* 8:659
- [49]. Costa Bizzarri P, Della Casa C, Lanzi M, Bertinelli F, Iarossi D, Mucci A, Schenetti L (1999) *Synth Met* 104:1
- [50]. Folli U, Iarossi D, Montorsi M, Mucci A, Schenetti L (1995) *J Chem Soc Perkin Trans* 1:537
- [51]. Bertinelli F, Costa Bizzarri P, Della Casa C, Lanzi M (2002) *Spectrochimica Acta Part A* 58:583
- [52]. Lanzi M, Costa Bizzarri P, Della Casa C (1997) *Synth Met* 89:181
- [53]. Goldoni F, Iarossi D, Mucci A, Schenetti L, Zambianchi M (1997) *J Mater Chem* 7:593
- [54]. Fraleoni Morgera A, Della Casa C, Costa Bizzarri P, Lanzi M, Missiroli A (2005) *Macromolecules* 38: 3170
- [55]. Costa Bizzarri P, Andreani F, Della Casa C, Lanzi M, Salatelli E (1995) *Synth Met* 75:141
- [56]. Roncali J (1992) *Chem Rev* 92:711
- [57]. Lowe RS, Ewbank PC, Lin J, Zhai L, McCullough RD (2001) *Macromolecules* 34:4324
- [58]. Folli U, Goldoni F, Iarossi D, Mucci A, Schenetti L (1996) *J Chem Res* 69:0552
- [59]. Cagnoli R, Mucci A, Parenti F, Schenetti L, Borsari M, Lodi A, Ponterini G (2006) *Polymer* 47:775
- [60]. Goldoni F, Iarossi D, Mucci A, Schenetti L, Costa Bizzarri P, Della Casa C, Lanzi M (1997) *Polymer* 38:1297
- [61]. Mucci A, Schenetti L (1995) *Macromol Chem Phys* 196:2687
- [62]. *New Advances in Analytical Chemistry*, Ed. Atta Ur-Rahamn, Taylor & Francis, Inc., Vol. 3, 2002, p. 1-40.
- [63]. Lanzi M, Costa Bizzarri P, Paganin L, Cesari G (2007) *Eur Polym J* 43:72
- [64] Transistor. Teoria e applicazioni. Philips semiconduttori, Milan, Italy, 1965.









# CHAPTER 4: USE OF

## POLY(3-METHYLTHIO)THIOPHENE BLENDS FOR

### DIRECT LASER TRACING AND BULK

### HETEROJUNCTION SOLAR CELLS

#### *4.1. INTRODUCTION*

The need for flexible, lightweight, easily processable new materials for electronics has pushed research toward the synthesis of organic materials able to compete with the “classic” inorganic semiconductors in their own application fields. Organic semiconductors, such as conjugated polymers, are promising candidates for this replacement, as demonstrated both by the number of patent applications in 2013 (more than 100 on polythiophenes) and by the growing number of newly launched companies and existing manufacturers of materials or devices that have added organic photovoltaics to their portfolio.

In this context, polythiophenes are intriguing materials which have now been studied for a long time thanks to their electric and electronic properties. In fact, in the charged (doped) state they are very effective conductors of electricity, while in the neutral (undoped) state they are mainly employed in optoelectronic devices - for the construction of organic light emitting diodes (OLEDs), low-voltage field effect transistors and bulk heterojunction (BHJ) solar cells - and in devices such as optical filters, signal modulators and polarization rotators. Alkyl-substituted polythiophenes (PATs) are very soluble in common organic solvents and can be easily filmed and processed using a number of different techniques, e.g. spincoating [1], doctor blading [2], screen printing [3], inkjet printing [4] and roll-to-roll methods [5], making them very interesting materials from an industrial standpoint.

Structurally, PATs belong to the class of conjugated polymers the precursor of which is polyacetylene (PAC). PAC shows electronic characteristics similar to those of PATs; recently some researchers have reported that PACs functionalized with a thioalkylic group (PAC-SR) are photosensitive polymers [6]. In fact, thin insulating films of PAC-SR can be traced by laser operating at suitable speed, power, and wavelength leading to electroconductive patterns on the film surface [7]. This approach is particularly intriguing since it makes it technically feasible to obtain high resolution patterns for electronic circuits while strongly limiting the number of processing steps and chemicals required. In fact, the line

patterning of an insulating polymeric matrix by a laser-induced photopyrolysis process makes it possible to rapidly develop custom conductive circuits from a schematic drawing, by using simple CAD (computer aided design) systems to drive the laser source [8]. Various advantages are evident: over conventional inorganic conductors (metals, oxides, silicon), since no multiple etching and lithographic steps are required to obtain the final circuit, and over the most synthesized conjugated polymers, as no redox processes are necessary to make the polymer conductive, thus avoiding the well-known problems of time and environmental stability.

But conjugated polymers are also intensively studied for other technological applications. In fact, in recent years, conjugated polymers-fullerene mixtures have been widely investigated for use in organic solar cells. Bulk heterojunction (BHJ) polymer solar cells have been reported using either poly(p-phenylenevinylene) derivatives [9], poly(3-alkylthiophene)s [10,11], or low-bandgap polymers [12,13] as electron-donors combined with PCBM ([6,6]-phenyl-C61-butyric acid methyl ester), a soluble fullerene derivative, as the electron acceptor thus creating the photoactive blend. In the standard architecture, the photoactive blend is sandwiched between a glass covered with indium tin oxide (ITO), acting as the anode, and a cathode made of a low-workfunction metal (usually Al). The light incident on the BHJ cell through the ITO electrode is mainly absorbed by the conjugated polymer, thus leading to the creation of bound excitons (holes/electrons couples). If the polymer and fullerene components are phase-segregated on a nanoscale length, the excitons can split into separated electrons and positive holes, which are transported along PCBM and conjugated polymer toward the metal and ITO electrode, respectively, thus generating the photocurrent and photovoltage.

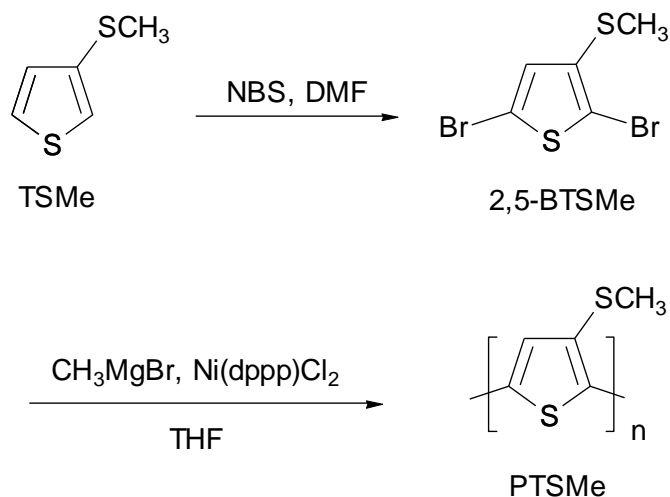
One factor that strongly limits the efficiency of this kind of cell is the low exploitation of the sunlight due to the narrower absorption band of the absorption spectrum of the conjugated polymer in comparison to the solar spectrum; however some strategies have been adopted to overcome this limitation, in particular the synthesis of low band-gap polymers [14, 15, 16] and the preparation of polythiophenes containing chromophores in the side chain [17, 18].

Therefore, the aim of this work is to synthesize a regioregular polythiophenic derivative functionalized with thiomethylic groups - namely the poly(3-methylthio)thiophene (PTSM<sub>e</sub>) - and to study its electrical behavior before and after laser tracing. For this purpose, PTSM<sub>e</sub> was blended with regioregular poly(3-hexyl)thiophene (P3HT) to overcome its poor filmability caused by its incomplete solubility in organic solvents. The obtained blend showed a wider absorption spectrum than conventional P3HT and was employed for the preparation of BHJ solar cells. The assembled cells were fully characterized from the morphological and electronic standpoint and their performances was compared with a reference cell made of only P3HT.

## 4.2. EXPERIMENTAL

### 4.2.1. Synthesis and polymerization

Scheme 15 outlines the experimental route from monomer to polymer.



Scheme 15. Synthesis of the monomer 2,5-BTSMc and polymer PTSMc.

### 4.2.2 Synthesis of the monomer 2,5-dibromo-3-methylthiophene (2,5-BTSMc)

2.73 g (15.4 mmol) of N-bromosuccinimide (NBS) in 15.5 ml of N,N-dimethylformamide (DMF) were added dropwise - under stirring and in an inert atmosphere - to a solution of 2.0 g (15.4 mmol) of 3-methylthiophene (TSMc, Atlantic Chemical Co., USA) in 15.5 ml of DMF. The mixture was reacted for 6 h at room temperature. 3.02 g (17.05 mmol) of NBS in 17.1 ml of DMF were added dropwise and the mixture was reacted for another 24 h at room temperature and under nitrogen. The reaction mixture was then poured into 500 ml of an aqueous solution of NaCl and the organic phase was extracted with 4×150 ml of n-pentane. The collected organic phases were washed with a 5% solution of  $\text{NaHCO}_3$  (2×300 ml) and with water to neutrality. The organic phase was then dried and concentrated at reduced pressure thus giving the crude product, which was purified with column chromatography ( $\text{SiO}_2$ /n-heptane) leading to 3.19 g of pure 2,5-BTSMc (72% yield).

$^1\text{H-NMR}$  ( $\text{CDCl}_3$ , ppm)  $\delta$ : 6.91 (s, 1H, H4); 2.55 (s, 3H,  $\text{CH}_3$ ).

FT-IR (Ge disk,  $\text{cm}^{-1}$ ): 3051 ( $\nu$  C-H, thiophene  $\beta$ -hydrogen); 2960 ( $\nu$  C-H, antisymmetric methyl); 2875 ( $\nu$  C-H, symmetric methyl); 1503 ( $\nu$  C=C, antisymmetric thiophene); 1468 ( $\nu$  C=C, symmetric

thiophene); 1368 (symmetric deformation  $\text{CH}_3$ ); 991 ( $\nu$  C-Br, thiophenic); 840 ( $\gamma$  C-H 2,3,5-trisubstituted thiophene); 690 ( $\nu$  C-SMe).

#### 4.2.3 Synthesis of the regioregular poly(3-methylthio)thiophene (PTSM<sub>e</sub>)

4.2 ml (4.2 mmol) of a 1 M solution of methylmagnesium bromide in di-n-buthyl ether were added to a solution of 1.20 g (4.16 mmol) of 2,5-BTSM<sub>e</sub> in 25 ml of anhydrous THF. The mixture was refluxed for 2 h under stirring and under Ar atmosphere and then 24.83 mg (0.0458 mmol) of Ni(dppp)Cl<sub>2</sub> were added and the reaction refluxed for 1 h more. The mixture was cooled down to room temperature, poured into 40 ml of methanol and filtered on a Teflon septum (0.45  $\mu\text{m}$  pore size). The recovered polymer was washed several times with methanol and dried, resulting in 0.320 g of PTSM<sub>e</sub> (60 % yield).

<sup>1</sup>H-NMR ( $\text{CDCl}_3$ , ppm)  $\delta$ : 7.26 (s, 1H, H<sub>4</sub>); 2.49 (s, 3H, CH<sub>3</sub>).

FT-IR (Ge disk,  $\text{cm}^{-1}$ ): 3059 ( $\nu$  C-H, thiophene  $\beta$ -hydrogen); 2957 ( $\nu$  C-H, antisymmetric methyl); 2853 ( $\nu$  C-H, symmetric methyl); 1511 ( $\nu$  C=C, antisymmetric thiophene); 1462 ( $\nu$  C=C, symmetric thiophene); 1369 (symmetric deformation  $\text{CH}_3$ ); 1014 (rocking  $\text{CH}_3$ ); 823 ( $\gamma$  C-H 2,3,5-trisubstituted thiophene); 716 ( $\nu$  C-SMe).

#### 4.2.4 Preparation of the PTSM<sub>e</sub>-P3HT blend (PB)

120 mg (0.94 mmol) of PTSM<sub>e</sub> and 60 mg (0.36 mmol) of regioregular poly(3-hexylthiophene) (P3HT, 92% HT,  $M_n=32$  KDa, PDI=1.18), previously synthesized using the same procedure used for the preparation of PTSM<sub>e</sub>, were dissolved in 10 ml of  $\text{CHCl}_3$  at room temperature and the obtained solution was sonicated for 10 min. The solution was then filtered over a Teflon septum (0.20  $\mu\text{m}$  pore size) and concentrated at reduced pressure producing the PB blend.

### 4.3 MEASUREMENTS

<sup>1</sup>H-NMR were recorded on a Varian Mercury Plus spectrometer (400 MHz) using TMS as a reference. FT-IR spectra of the monomers (pure liquids) and polymers (films) were obtained on Ge disks using a Perkin Elmer Spectrum One spectrophotometer. Molecular weights were determined by gel permeation chromatography (GPC) using polystyrene standards and THF as an eluent on a HPLC Lab Flow 2000 apparatus equipped with a PL Gel MXL column and a Linear Instrument UV-Vis detector model UVIS-200 working at 263 nm. UV-Vis spectra were recorded on a Perkin Elmer Lambda 19

spectrophotometer using polymer films on quartz slides cast from chloroform solutions (ca.  $10^{-3}$  M). Cyclic voltammetry (CV) was performed on a Autolab PGSTAT 30 (EcoChemie, The Netherlands) with a three electrode system in a solution of 0.1 M  $\text{Bu}_4\text{NPF}_6$  in  $\text{CH}_3\text{CN}$ , at a scan rate of  $50 \text{ mV s}^{-1}$ . Polymer films were coated on a Pt plate electrode ( $1 \text{ cm}^2$ ) by dipping the electrode into the corresponding solution ( $5 \times 10^{-3}$  M in  $\text{CHCl}_3$ ) and then drying, obtaining films of the approximatively same thickness (0.4-0.5  $\mu\text{m}$ ). A Pt wire was used as the counter electrode and an aqueous saturated calomel electrode (SCE) as the reference electrode.

Electrical measurements were performed in air at room temperature using a Keithley 2101 electrometer (traced films) and an Alpha Lab teraohmmeter (pristine films). The reported values were the mean of five measurements performed on different parts of the same sample as well as on five different samples prepared using the same experimental conditions. In all cases, differences did not exceed 5% of the final value. The laser source was a Wicked Lasers Spyder III Arctic class 4 diode laser, operating at 445 nm with a nominal power of 750 mW. The effective power of the laser beam on the polymer surface was measured with a Coherent FieldMax II laser power meter giving an effective power of 600 mW. Samples were mounted on a computer-controlled positioning system (Thorlabs L490MZ) and moved on a plane perpendicular to the focused laser beam by using two Thorlabs MTS TDC001 controllers thus making it possible to control both the tracing speed on the x-y plane and the laser-sample distance for the correct focus of the beam on the sample surface, while operating on the z-axis. Films thickness was measured using an AFM Burleigh Vista 100 as a profilometer. SEM analyses were performed on a Phenom-world ProX SEM apparatus, equipped with an EDS microanalysis probe. AFM of the blend was performed on a Burleigh Vista Atom Force Microscope equipped with a silicon-nitride tip and operating in a non-contact tapping mode. Optical 2D and 3D microscopy was performed using a Hirox KH-7700 Digital microscope.

#### *4.3.1 ITO/PEDOT/PB:PCBM/Al solar cell assembly*

ITO glass (Delta Technologies, Stillwater, Minnesota, USA; 2.5 x 2.5 cm; code CG-41IN-0107) was first cleaned in an ultrasonic bath using a non-foaming glass detergent in deionized water. ITO glass was then rinsed sequentially in double distilled water, isopropanol, and acetone reaching a final resistance of  $6 \Omega/\text{sq}$ . PEDOT:PSS (Aldrich Chemical Co.) was diluted 1:1 with isopropanol and deposited by doctor blading (DB) on top of the cleaned ITO glass using a Sheen Instruments Model No. S265674 (film thickness about 80 nm). Anhydrous chloroform was used to prepare solutions of P3HT or PB and PCBM (1:1 weight ratio), which were deposited by DB on the PEDOT:PSS layer. After baking films in a vacuum at  $130^\circ\text{C}$  for 30 min, the active layer film thickness measured by AFM was about 100 nm.

Lastly, to create the OPV devices, 50 nm of Al was thermally deposited under a vacuum of  $6 \times 10^{-7}$  mmHg by means of an Edwards E306A vacuum coating apparatus equipped with a dual-stage mechanical vacuum pump Edwards 2 E2H2 and with a selectable diffusion pump or turbo-molecular pump. The current-voltage characteristics were measured using a Keithley 2401 source meter under the illumination of a Abet Technologies LS 150 Xenon Arc Lamp Source AM1.5 Solar Simulator, calibrated with an ILT 1400-BL photometer.

#### 4.4. RESULTS AND DISCUSSION

Polyacetylenes functionalized with thiomethylic (PAc-SMe) or thioethylic (PAc-SEt) groups were the first photosensitive polymers examined for laser patterning applications. In fact, they were able to increase their electrical conductivity by many orders of magnitude (up to 16) when exposed to a correctly focused laser radiation of a suitable wavelength (351 or 488 nm) without need for a chemical doping. The best conditions for the tracing of PAc derivatives were quite difficult to find but, when the system was correctly set-up, conducting traces became insoluble in common solvents and insensitive to humidity, chemical vapors and high temperature. When exposed to a coherent light source, these polymers undergo a photopyrolysis process, with the partial loss of the thioalkylic substituent, which leads to the formation of unsaturated backbones mainly made up of  $sp_2$  hybridized carbon atoms which are only partly linked with sulfur substituents in side chains [19]. This process leads to an extended  $\pi$ -system delocalized over the polymeric chain with an enhanced main chain mean conjugation length (MCL), which explains the higher electrical conductivity.

In this work, we tried to substitute PAc-SMe [20] with an easier synthesizable polythiophenic derivative, i.e. poly(3-methylthio)thiophene (PTSM<sub>e</sub>), which possesses a photosensitive functional group and a polyconjugated backbone, similar to the acetylene-based polymer, but also shows an increased solubility, filmability and environmental resistance in the non-traced pristine state. Since regioregularity is a fundamental prerequisite for obtaining PATs with high electron mobility [21], PTSM<sub>e</sub> was prepared using the McCullough Grignard Metathesis (GRIM) polymerization procedure (Scheme 1), which generally leads to regioregular and soluble thiophenic polymers [22].

This procedure starts from a 2,5-dihalothiophene derivative and leads to the obtainment of functionalized polythiophenes with a good yield and a high degree of regioregularity through a simple and effective organometallic group exchange (Grignard Metathesis) reaction. With this aim, the monomer 2,5-dibromo-3-(methylthio)thiophene (2,5-BTSM<sub>e</sub>) was prepared through the dibromination of TSM<sub>e</sub> with N-bromosuccinimide (NBS) in anhydrous N,N-dimethylformamide (DMF). The halogenation conditions were accurately optimized, providing for the addition of NBS in two separate amounts while



operating at room temperature, thus leading to a satisfying yield (72%) of 2,5-BTSM<sub>e</sub>. We tried also a faster way, which consisted of the one-step addition of the entire amount of NBS and a reaction time of only 4h at 60°C. This time, however, we observed a partial bromination of the –CH<sub>3</sub> in the side chain. The two bromine atoms in the  $\alpha$ -positions of 2,5-BTSM<sub>e</sub> were exploited for the organometallic coupling involving the magnesium-halogen exchange (metathesis reaction) with a preformed Grignard derivative (1<sup>st</sup> reaction step), followed by a Ni(II) catalyzed cross-coupling reaction (2<sup>nd</sup> reaction step), thus leading directly to the regioregular polymer. These two steps are consecutive and the polymerization is a simple and fast one-pot process.

PSM<sub>e</sub> was then obtained as a red-brownish powder highly soluble in aromatic chlorinated solvents (chlorobenzene and o-dichlorobenzene) up to 30 mg/ml, but its solubility decreases to about 5-10 mg/ml in common organic solvents (CHCl<sub>3</sub>, THF) at room temperature. This can be ascribed to PTSM<sub>e</sub> short side chains, which are not able to produce a strong plastifying effect, and not to the polymer main chain lengths, since its molecular weight was not particularly high (M<sub>n</sub>=18.000, PDI=1.2).

Films of PTSM<sub>e</sub> cast on glass slides or PET foils show poor homogeneity, some dots, and brittleness and do not have good and permanent adhesion on different surfaces. In order to overcome this problem, we blended the prepared PTSM<sub>e</sub> with a previously synthesized P3HT sample prepared with the same polymerization technique (GRIM procedure), since P3HT is well soluble in common organic solvents, from which it produces thick, homogeneous free-standing films, while its optical and electrical properties have been well known for a long time now.

The polymeric blend (PB) was prepared starting from a 2:1 weight ratio (about 7:3 molar ratio) between PTSM<sub>e</sub> and P3HT. The FT-IR analysis of PB was performed on a thin film cast on a Ge disk from CHCl<sub>3</sub> solution (Figure 45).

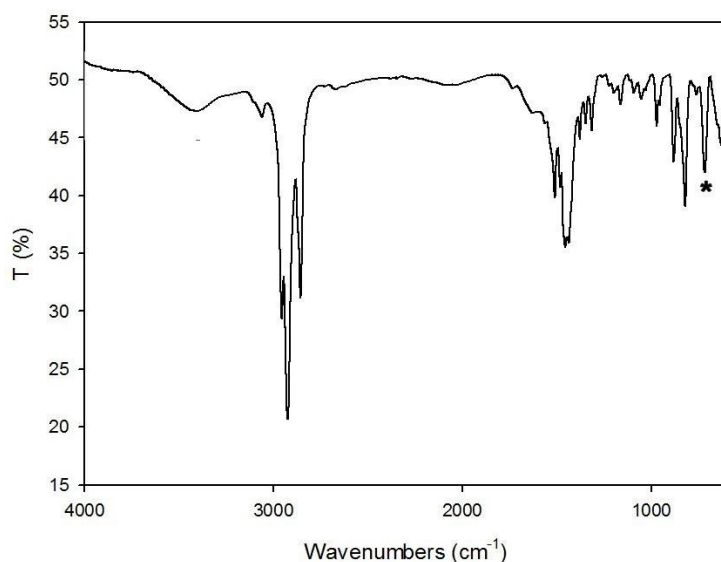


Figure 45. FT-IR spectrum of PB in film cast on Ge disk from  $\text{CHCl}_3$  solution. The C-SMe stretching band is evidenced by an asterisk.

The spectrum clearly shows the peaks ascribable to the presence of both polymers. Most of them are common to both the polymers but some peaks can be ascribed to each single structure. In detail, the signals (in  $\text{cm}^{-1}$ ) at 3055 ( $\nu$  C-H, thiophene  $\beta$ -hydrogen), 2955 ( $\nu$  C-H, antisymmetric methyl), 2856 ( $\nu$  C-H, symmetric methyl), 1510 ( $\nu$  C=C, antisymmetric thiophene), 1455 ( $\nu$  C=C, symmetric thiophene), 1377 (symmetric deformation  $\text{CH}_3$ ) and 820 ( $\gamma$  C-H 2,3,5-trisubstituted thiophene) are common to both the polymers while the signals at 2925 ( $\nu$  C-H, antisymmetric methylenes) and 757 ( $\text{CH}_2$  rocking) are characteristics of P3HT and that at 716 ( $\nu$  C-SMe) is exclusive to PTSMc.

$^1\text{H}$ -NMR spectrum of PB in  $\text{CDCl}_3$  is reported in Figure 46.

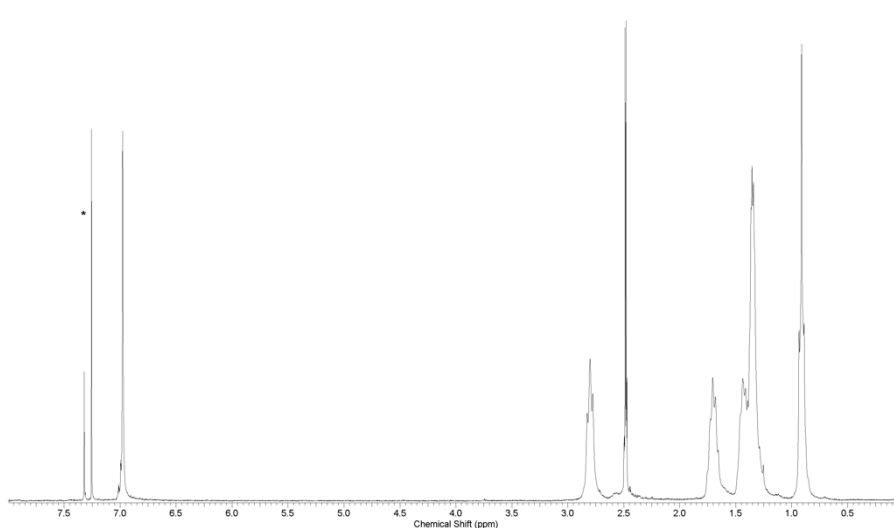


Figure 46.  $^1\text{H}$ -NMR spectrum of PB in  $\text{CDCl}_3$ .  $\text{CHCl}_3$  peak is indicated by an asterisk.

Starting from the aromatic region, the peak at 7.26 ppm is ascribable to the thiophenic H-4 proton of the TSM<sub>e</sub> monomer and the fact that it is a singlet confirms that we obtained a regioregular PTSM<sub>e</sub> polymer. The signal at 6.99 ppm is ascribable to the aromatic H-4 protons of the T6H moieties; this time also, the spectrum confirms the high regioregularity of the P3HT sample, since the intensity of the peak attributable to the HT-HT dyads is strongly prevalent over those belonging to the other kinds of linkages, also visible at about 7.00 ppm. The singlet at 2.49 ppm is ascribable to the thiomethylic protons, while the triplet at 2.80 ppm (-CH<sub>2</sub>  $\alpha$  to the thiophene ring), the multiplet at 1.73 ppm (-CH<sub>2</sub>  $\beta$  to the thiophene ring), the broad multiplet in the 1.50-1.20 ppm range (-CH<sub>2</sub> of the central units) and, lastly, the triplet at 0.90 ppm (-CH<sub>3</sub>) are due to the protons of the P3HT side chains. The composition of the blend can be determined by means of the normalized integral ratio of the signals at 2.49 and 0.90 ppm and, alternatively, by the normalized integral ratio of the two signals at 7.26 and 6.99 ppm. The real composition of PB was quite different from the starting ratio of the two polymers. In fact, the final molar ratio between PTSM<sub>e</sub> and P3HT was around 1:2 instead of the 7:3 feed ratio used. This can be ascribed to the low solubility of PTSM<sub>e</sub> in common organic solvents which caused a kind of fractionation when we filtered the PB solution on the Teflon septum.

However, PB was well soluble in CHCl<sub>3</sub>, producing homogeneous and glossy dark-red films.

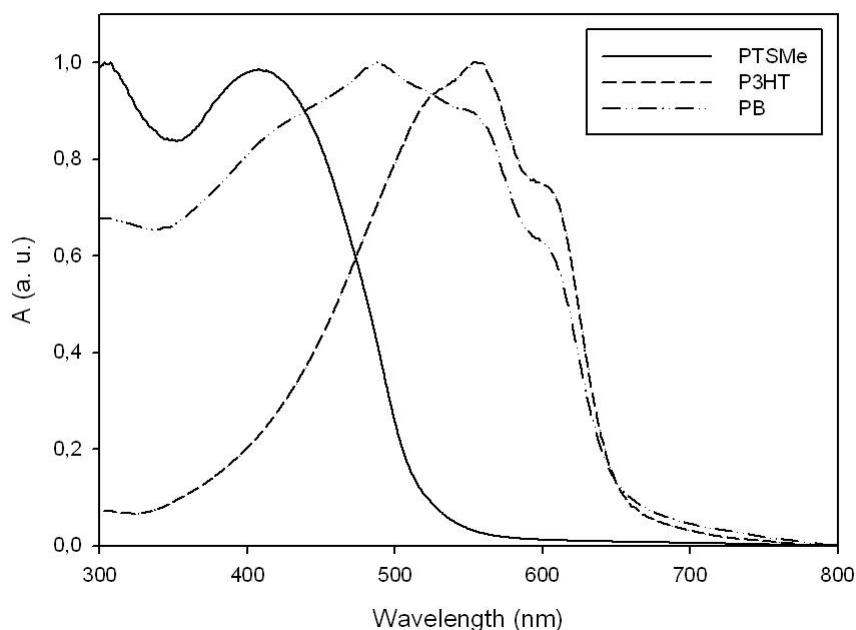


Figure 47. UV-Vis spectra of polymers in film cast from CHCl<sub>3</sub> solutions.

Figure 47 shows the UV-Vis spectra of the polymers in film cast from CHCl<sub>3</sub> solutions. Regioregular P3HT shows a  $\lambda_{\text{max}}$  at 554 nm, corresponding to the first vibronic quantum, and an evident shoulder at 595 nm, corresponding to the pure electronic transition E<sub>0-0</sub> [23] which derives from the

vibronic absorption of ordered P3HT crystalline regions in films [24]. PTSMe shows only one peak at 415 nm, blue-shifted with respect to the  $\lambda_{\text{max}}$  of P3HT and does not show any evident vibronic transition, since short side chains are not able to interact with themselves, thus giving more ordered main chains conformations [25]. The spectrum of the blend shows a very large absorption region, starting at 350 nm and ending at about 650 nm. The blend spectrum clearly evidences the main absorptions of its two components: the PTSMe absorption maximum is now embedded in the spectrum and becomes visible as a shoulder at 410 nm, while the transitions ascribable to the P3HT component are found at 599 nm ( $E_{0-0}$ ), 546 nm (first vibronic quantum), and 488 nm ( $\lambda_{\text{max}}$ ). The broad absorption range of the blend can be very useful for polymeric solar cells, since a wider light absorption in the visible region of the solar spectrum can generate more excitons in the BHJ active layer, thus increasing the  $J_{\text{sc}}$  of the final device [26].

A few drops of PB solution (5 mg in 5 ml) in  $\text{CHCl}_3$  were deposited on a quartz slide ( $4.0 \times 4.0$  cm) using the DB technique thus giving a homogeneous  $1.5 \mu\text{m}$  thick film that was used for the laser tracing procedure. The best tracing conditions were found at a  $1.0 \text{ mm/s}$  tracing speed, by making three contiguous parallel lines with an inter-trace distance of  $0.33 \text{ mm}$  (Figure 48).

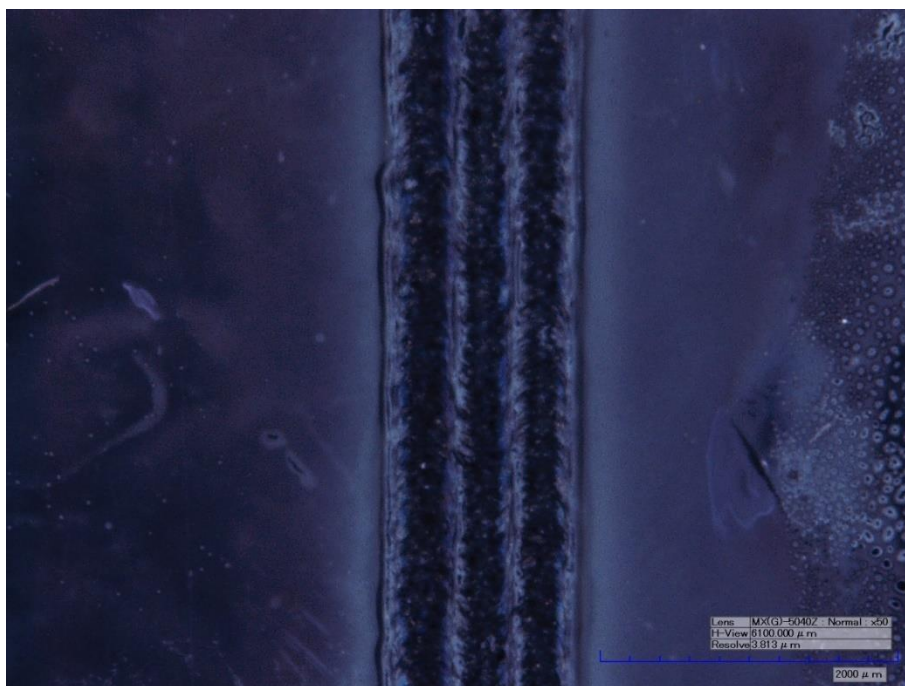


Figure 48. Optical microscope image of a traced PB sample ( $\times 50$ ). The film was cast from the polymer solution in  $\text{CHCl}_3$ .

The obtained traces are clearly visible since the polymer surface changed notably after the laser exposure, going from a very smooth, homogeneous surface to a rough, porous surface. This is also evident in the 3D image and in the SEM micrograph of Figures 49 and 50, respectively.

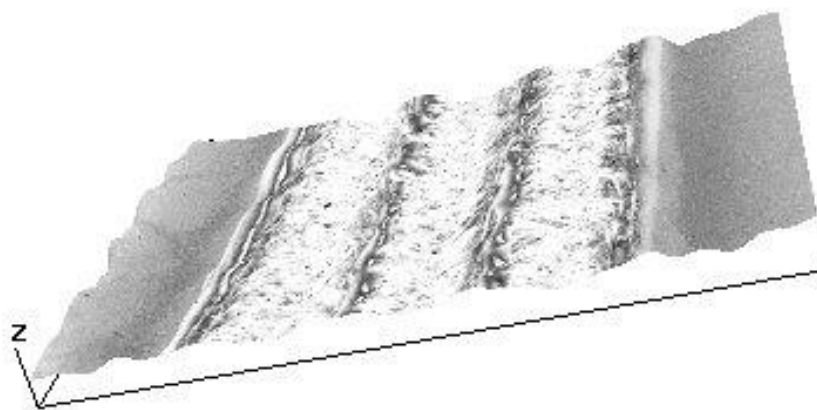


Figure 49. 3D image of PB traces on the polymer film cast from  $\text{CHCl}_3$  solution.

Film porosity is determined by the outflow of gaseous reaction products - mainly sulfides and mercaptanes [27] - which leaves the polymer surface during the laser patterning.

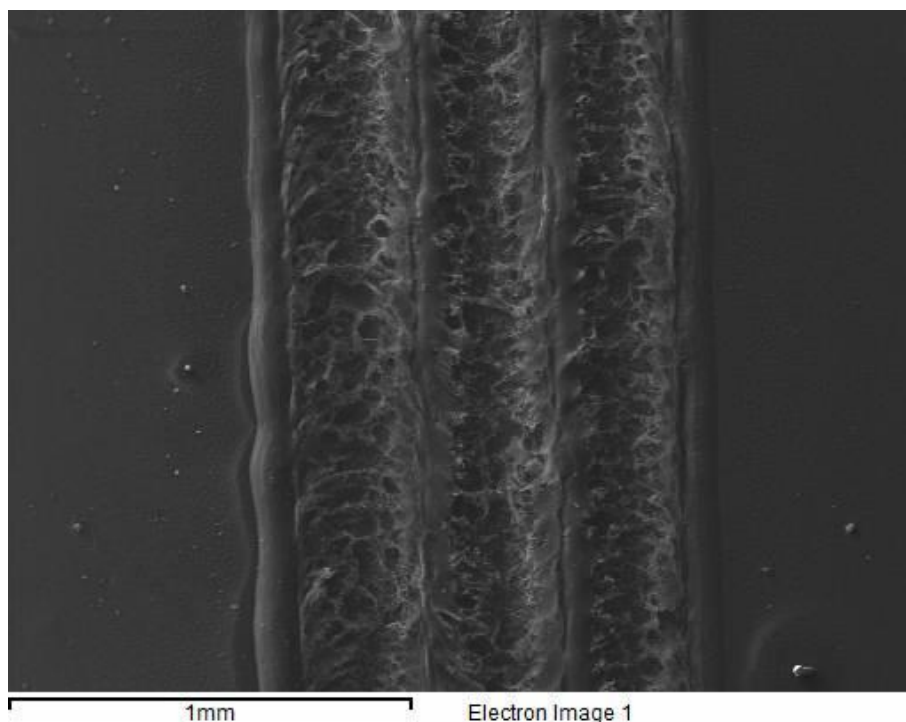


Figure 50. SEM micrograph of a PB film after laser tracing. The polymer film was cast from PB solution in  $\text{CHCl}_3$ .

The band at  $716\text{ cm}^{-1}$  in the IR spectrum of PB, ascribable to C-S stretching [28], decreases in intensity after the laser tracing, thus confirming the partial loss of the thiomethylic group after the photopyrolysis procedure (Figure 51).

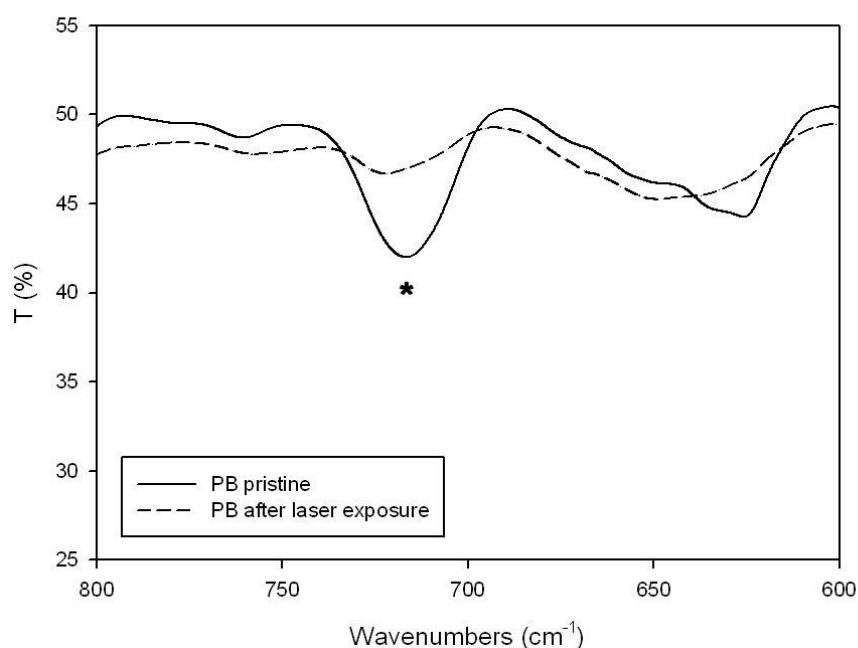


Figure 51 FT-IR spectrum (expansion) of a PB film on Ge disk from  $\text{CHCl}_3$  solution before and after the laser tracing procedure. The C-SMe stretching band is evidenced by an asterisk.

We observed that the resistance of the sample decreases as the number of contiguous traces increases, rapidly reaching an asymptotic value corresponding to about three lines. A droplet of an Ag conductive paint (Ted Pella Inc., USA) was then applied to the two ends of the 3-cm-long trace and the resistance was measured with a Keithley 2401 source meter. We prepared five samples of the traced PB blend and measured their surface resistance, which was  $150 \text{ k}\Omega/\text{sq}$  with a very good reproducibility of this value among the samples, with a deviation from the reported value of 3%.

The surface resistance of the samples before tracing was  $210 \text{ G}\Omega/\text{sq}$  ( $\pm 5\%$ ) and was measured with a teraohmmeter (Alpha Lab Inc., USA) using a two probe measuring system. Samples and probes were carefully shielded from surrounding EMF with a Faraday-cage homemade device.

We then prepared another series of samples under the same experimental conditions, i.e. by depositing the  $\text{CHCl}_3$  solution of PB on a quartz slide using DB technique. This time, samples were annealed for 2 h at  $130^\circ\text{C}$  under a vacuum (0.5 mmHg) by using a Büchi B-585 glass oven before the laser tracing. Even if their initial resistance was essentially unchanged (about  $200 \text{ G}\Omega/\text{sq}$  ( $\pm 4\%$ )), the final resistance of the traced samples was  $27 \pm 2\% \text{ k}\Omega/\text{sq}$ . This time, the laser treatment of samples enabled a resistance decrease of six orders of magnitude. It must be stressed that the annealing procedure was also performed on the previously traced samples but - this time - it was ineffective, since no evident changes in the final resistance values were found. In fact, the exposure to the laser light makes the traced polymer apparently harder, more scratch-resistant, and insoluble in organic solvents, thus suggesting that the

exposed polymer no longer has the characteristics of a substituted polythiophene but rather those of a system of  $\pi$ -conjugated C atoms. Figure 52 shows the SEM micrograph of an annealed PB sample, prepared by DB technique using PB chloroform solution, after laser tracing. Its appearance is nearly identical to the unannealed film sample, because the laser exposure converted the polymer into worm-like dull traces, devoid of a fine texture, which are always apparently identical one to another.

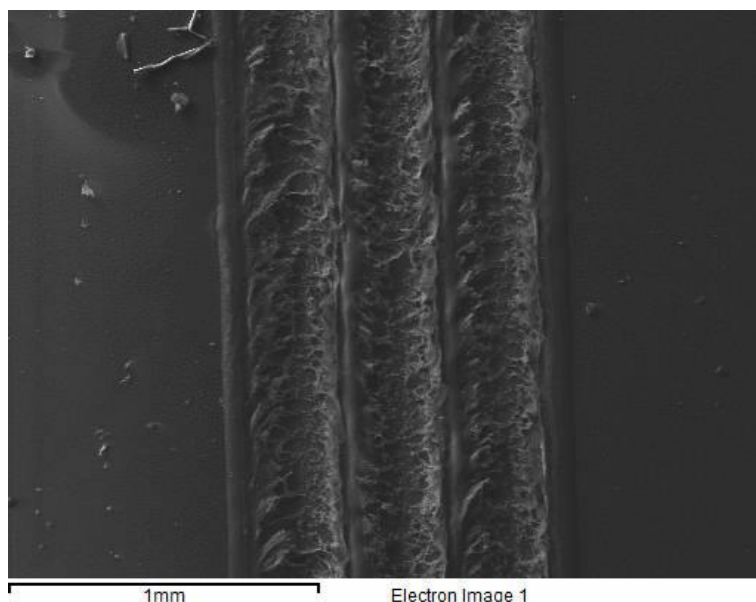


Figure 52. SEM micrograph of a pre-annealed PB film, cast from  $\text{CHCl}_3$  solution, after laser tracing.

Figure 53 shows the topographic microanalysis of the sample shown in Figure 52 in relation to the C and S elements recorded using an energy-dispersive spectrometer (EDS) probe.

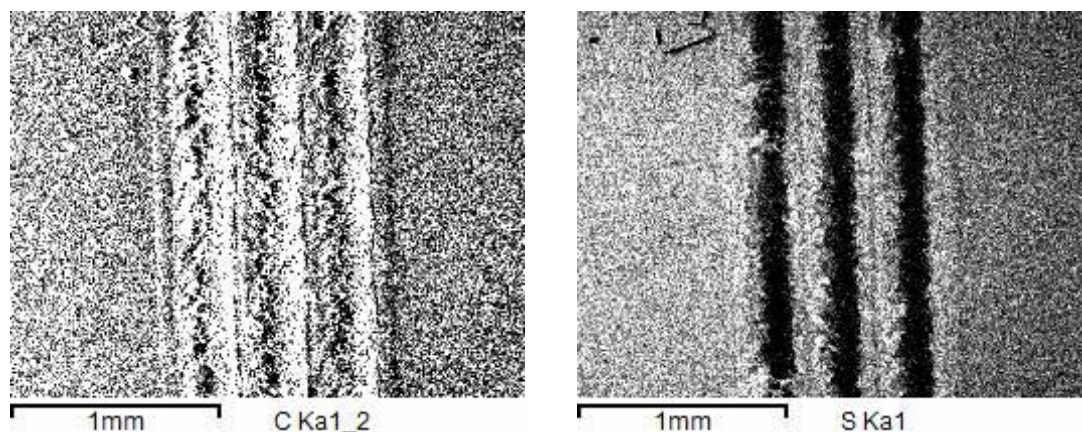


Figure 53. EDS topographic microanalysis of PB film reported in Figure 8. Left: Carbon; Right: Sulfur.

In Figure 9 it is evident that the laser-exposed polymer has a higher amount of C and a lower amount of S in the traces, since the concentration of the examined element is proportional to the intensity of white. More deeply, C and S concentration passed from 65% and 28% of the unexposed area to 68% and 25% of the laser-treated portions, respectively, thus confirming the partial loss of thiomethylic side



chains. It is worth noting that this slight changes in the PB composition due to the laser exposure is capable of determining such a high surface resistivity change.

Lastly, we prepared a new set of samples made of P3HT alone, in order to evaluate whether the laser treatment was capable of decreasing their electrical resistance. P3HT films were deposited by DB using a polymer solution in  $\text{CHCl}_3$ . In this case, the surface resistance of these samples was the same before and after the exposure to laser radiation i.e.  $220 \text{ G}\Omega/\text{sq}$  ( $\pm 6\%$ ). This test confirms that the electrical conductivity enhancement is ascribable to the presence of the photo-sensitive thiomethylic groups, which are involved in a laser-induced photocleavage which leaves the polythiophenic backbone able to partially crosslink and, then, to rearrange in a more planar and more conjugated conformation, thus aiding the electroconductivity of the final material [29].

Figure 54 shows the J-V characteristic curves of solar cells which have the structure of ITO/PEDOT:PSS/composite (photoactive polymer:PCBM)/Al. PEDOT:PSS acts as a hole-transporting layer, the photoactive polymer (P3HT or PB) as an electron donor, and PCBM as an electron acceptor, while the Al electrode is the cathode of the solar cell and the ITO layer the anode [30]. The operational procedures followed for the preparation of cells are described in the experimental section. We used a polymer/PCBM 1:1 weight ratio since some studies have shown that devices with this ratio achieve the highest power conversion efficiency [31, 32] and the film thicknesses of the blend absorber layers were each about 100 nm, in order to make the measurement of the photocurrent independent of the thickness of the samples.

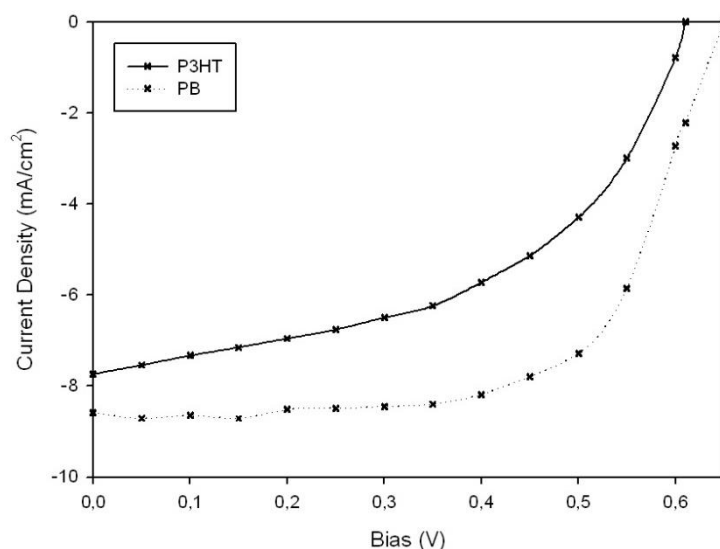


Figure 54. J-V characteristic curves for the prepared solar cells under AM 1.5 irradiation with an intensity of 1 sun ( $100 \text{ mW}/\text{cm}^2$ ) from a calibrated solar simulator.

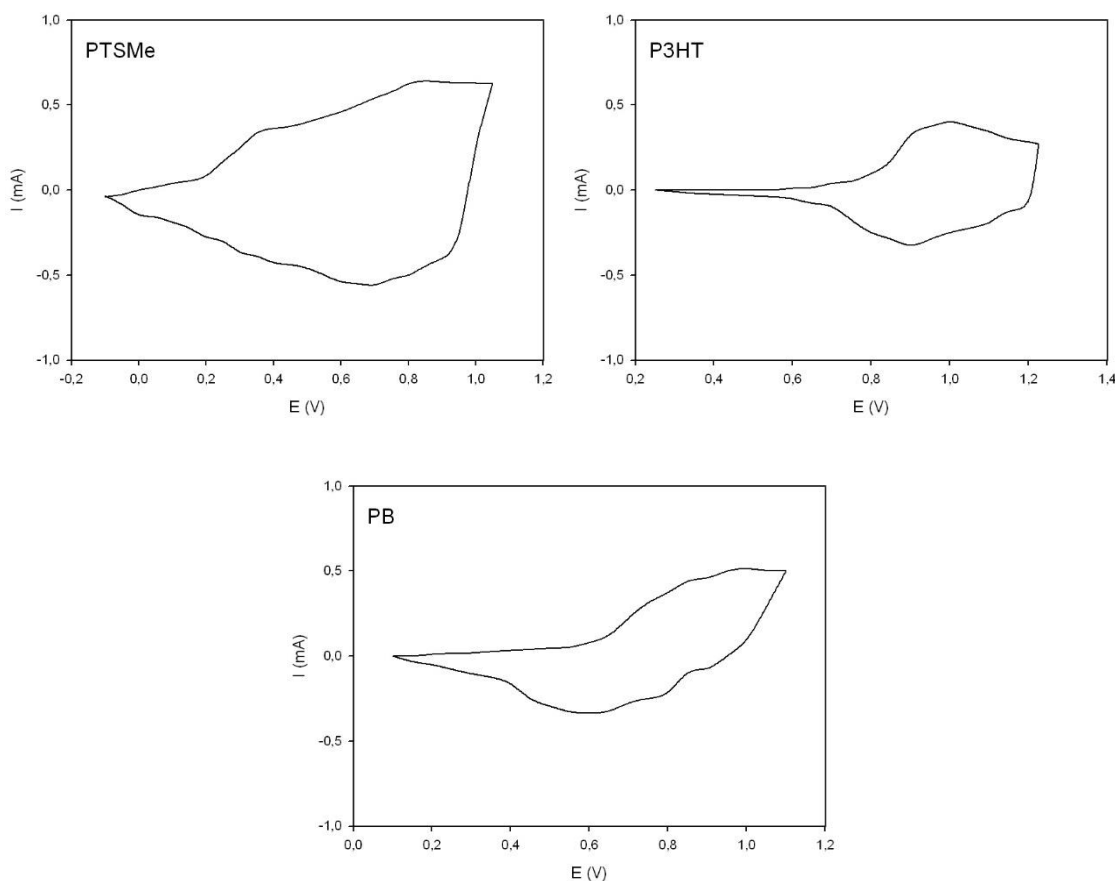
The device parameters: short circuit current ( $J_{sc}$ ), open circuit voltage ( $V_{oc}$ ), Fill Factor (FF), and power conversion efficiency (PCE) are summarized in Table 5.



Table 5. Photovoltaic parameters for the devices obtained using the two different photoactive blends.

Polymer	$J_{sc}$ (mA/cm <sup>2</sup> )	$V_{oc}$ (V)	FF (%)	PCE (%)
<b>P3HT</b>	7.73	0.61	52.8	2.48
<b>PB</b>	8.58	0.65	56.7	3.16

The electrochemical behavior of the three examined polymers has been evaluated performing cyclic voltammetry (CV) on their thin films cast on a Pt electrode from CHCl<sub>3</sub> solutions (Figure 55). We decided to characterize also a film of PSMe even if, as already mentioned, this polymer was not employed as active layer for solar cells since its adhesion to the ITO-glass coated with PEDOT-PSS was very poor and prevented the homogeneous deposition of the Al cathode.

Figure 55. Cyclic voltammograms of the polymer films on Pt recorded in 0.1 M Bu<sub>4</sub>NPF<sub>6</sub> acetonitrile solution at a scan rate of 50 mV s<sup>-1</sup>.

All voltammograms exhibited reversible oxidation and a quite good symmetry for the p-doping/undoping process, and this can be useful for practical applications based on the charge/discharge process since the required potential range needed for passing between neutral and doped states is limited. The HOMO levels of the polymers were measured by CV, while the LUMO energies were calculated

indirectly, taking into account that they correspond to the HOMO energies plus the optical energy gaps ( $E_{\text{opt}}$ ) evaluated from the onsets of the UV-Vis spectra of the polymers in film [33]. The obtained values are reported in Table 6. PSMe showed the lower oxidation potential, according to the electron-donor character of its thiomethylic side chain directly linked to the thiophene ring [34], and the higher bandgap, probably determined by disorder phenomenon like steric effects, cross linking or chain terminations [35].

Table 6. Optical and electrochemical properties of the films cast from  $\text{CHCl}_3$  solutions.

Polymer	$\lambda_{\text{edge}}^{\text{abs}}$ (nm)	$E_{g,\text{opt}}$ (eV)	$E_{\text{ox}}^{\text{onset}}$ (V)	HOMO (eV)	LUMO (eV)
PSMe	520	2.38	0.18	-4.58	-2.20
P3HT	655	1.89	0.76	-5.16	-3.27
PB	655	1.89	0.55	-4.95	-3.06

In Figure 56 is reported the band diagram with HOMO/LUMO levels of the ED polymers used for the solar cells in relation with the levels of PCBM and the work function of ITO and Al, according to Ref. [36].

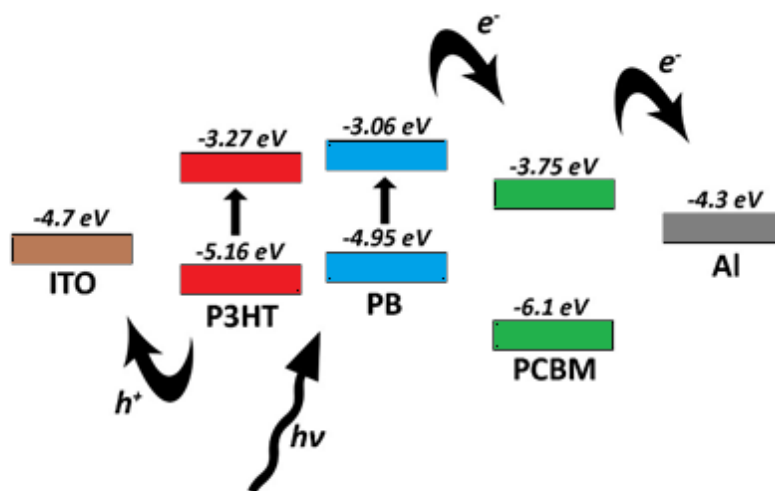


Figure 56. Band diagram with HOMO/LUMO levels of the ED polymers and EA PCBM in relation to the work functions of ITO and Al electrodes.

PB sample showed an energy difference between its LUMO level and the LUMO of the EA molecule ( $\Delta E_{\text{LUMO}}$ ) higher than P3HT (0.69 vs 0.48 eV) and this can be favorable for the photoinduced charge separation. In fact, it has been reported that a  $\Delta E_{\text{LUMO}} = 0.3$  eV is the minimum value required to overcome the binding energy of the excitons generated in organic semiconductor polymeric films [37,

38]. The total photovoltage of the organic solar cells is ideally equal to the band gap value of the conjugated polymer employed in the light-absorbing (active) layer. In the examined case, the theoretical values should be the same for P3HT and PB since they have the same bandgap (1.89 eV). However, there exists a loss factor related to the high exciton binding energy in organic materials which determines the need for a LUMO-LUMO Donor/Acceptor offset in D/A cells to polarize the exciton [39, 40]. Practically, the LUMO offset should be large enough to obtain an effective and fast charge transfer and the loss factor is inversely proportional to the  $\Delta E_{\text{LUMO}}$  value. This could explain the  $V_{\text{OC}}$  value of PB slightly higher than that of the reference cell.

The factors limiting the PCE of polymeric solar cells include the low exploitation of the sunlight mainly due to the narrower absorption band of the absorption spectra in the polyconjugated materials used in the photoactive layer, in comparison with the solar spectrum and the mismatch of the two spectra [41]. The increased efficiency of PB:PCBM solar cells compared to the reference cell made of the normally used regioregular P3HT could be ascribed to the stronger absorbance of PB blend in the 350-500 nm range. Our results are very much in line with those reported in literature. In fact, Li et al. [42] reported that a series of solar cells prepared with polythiophene derivatives functionalized with bi(thienylenevinylene) side chains (biTV-PTs), reached a maximum PCE of 3.18% under AM 1.5, 100 mW/cm<sup>2</sup>, with a 38% efficiency increase compared to that of the cells based on P3HT under the same operative conditions. The enhanced performance was attributed to the increased absorption of (biTV-PTs) in the region between 350 and 450 nm [43]. In fact, the  $J_{\text{SC}}$  represents the maximum photocurrent density produced by a solar cell under solar illumination at short circuit condition. This current is directly related to the external quantum efficiency (EQE) which depends on the absorption efficiency of the photoactive layer [44]. When the organic cells are made of a conjugated polymer and PCBM, a wider and more intense absorption spectrum of the photoactive blend can raise the PCE of the device acting on its photocurrent density. In our case, since the integrated intensity of the UV-Vis spectra of P3HT, PSMe and PB in film are in a 1:0.95:1.57 ratio respectively, and the thicknesses of the active layers in the cells are almost the same (about 100 nm), the higher value of  $J_{\text{SC}}$  observed for PB (if compared with the reference cell) can be ascribed to its more extended absorption range.

To analyze the morphology of solar cells, we chose to use atomic force microscopy (AFM). Figure 57 shows the surface morphology of P3HT or PB and PCBM (1:1 weight ratio) photoactive blends. Films were prepared by casting the chloroform solutions of the polymers on ITO glasses using the DB technique. The support had been cleaned beforehand using the same procedure used for the preparation of solar cells. After the blend deposition, samples were subjected to the annealing procedure (30 min at 130°C under vacuum) and the surface images were recorded using an AFM in a non-contact (tapping) mode in height-modulated (HMM) and phase-modulated (PMM) modes.

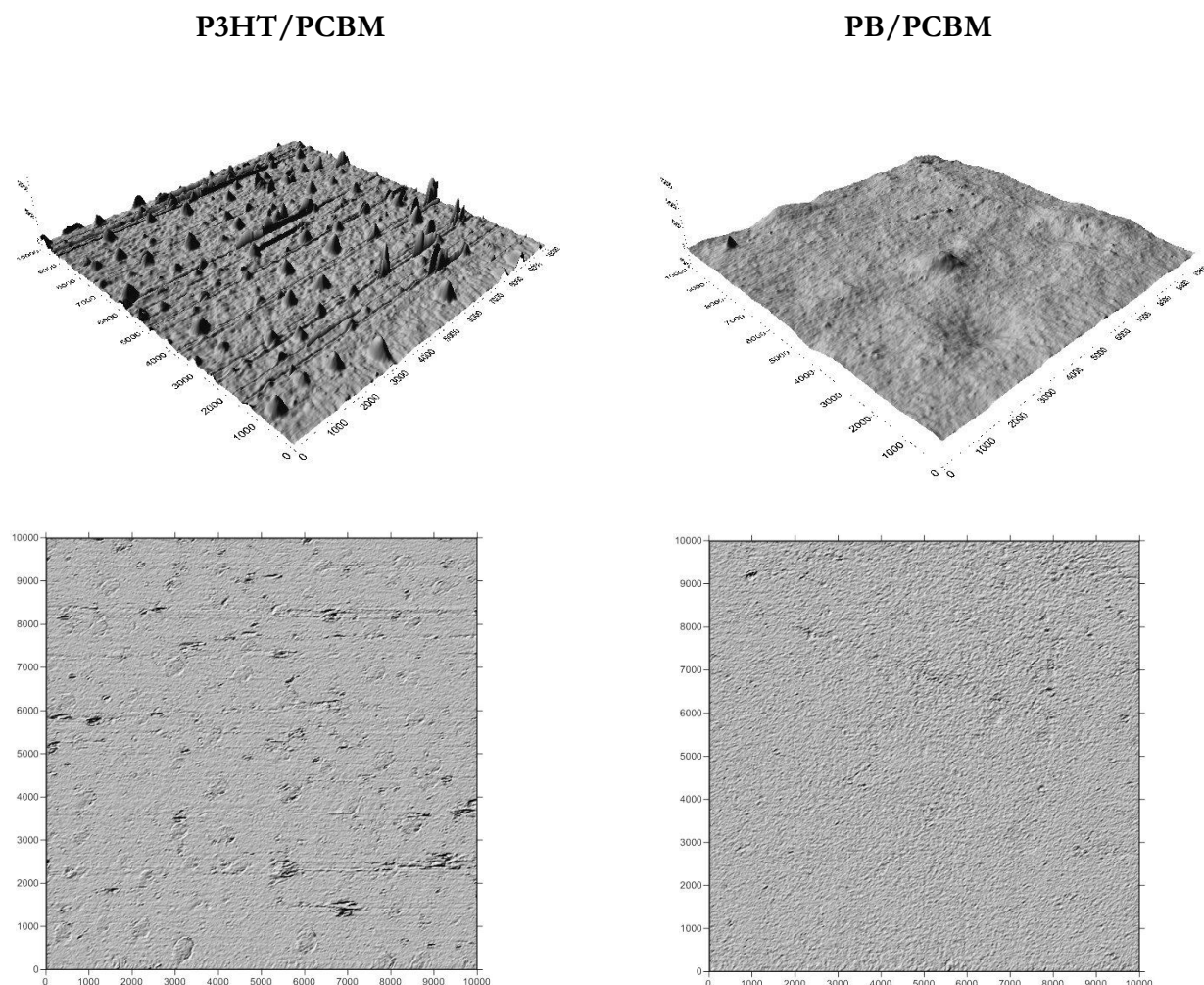


Figure 57. AFM images of the examined blends (tapping mode, scale in nm; top: height modulated images; bottom: phase modulated images). The blends were obtained by casting the polymer/PCBM solutions in  $\text{CHCl}_3$  on ITO glasses.

The AFM images of the surfaces of the two prepared films (100 nm thick) are quite different; in fact the surface rms (root-mean-square) roughness is 5.4 nm for the P3HT:PCBM film (with an average 18 nm diameter of grains) and 2.2 nm for PB:PCBM (average 11 nm diameter grains). The large black features in PMM, which correspond to bumps in topography (HMM), are ascribable to PCBM-rich domains. The rough surface indicates a P3HT self-organization in the blend, enhancing the ordered structure formation in the film [45]. However, an excessively rough surface morphology can cause poorer contact between the photoactive layer and the metallic cathode [46], leading to a decrease in the  $V_{OC}$  values as the shunt resistance of the cell increases [47]. Surface roughness was found to be a critical parameter also in polymer solar cells based on inkjet-printed PEDOT:PSS layers, where irregular surface morphologies of the layers led to very poor device performance in terms of  $J_{sc}$ , FF and PCE [48].

All devices showed good reproducibility and stability in time in terms of final PCE: the cells stored in vacuo, at room temperature, showed an average approximate 5% PCE decrease in the initial value after 30 days. The best solar cell performance was obtained using the PB/PCBM system as the

active blend. This can be ascribed not only to the enhanced absorption spectrum of this blend, which acts positively on its generated photocurrent, but also to its very smooth surface and to the nanoscale homogeneous separation of its components, leading to a high interfacial area of the electron donor-acceptor domains, which acts positively on the final  $V_{oc}$  and FF, as confirmed by the data reported in Table 1. The obtained results are very promising since they demonstrate that it is possible to produce highly efficient active layers of polymer solar cells with good sunlight absorption by using a simple mixture of easily synthesizable polymers, thus avoiding the long and complex synthesis usually required to obtain low-bandgap conjugated polymers [49].

## 4.5 CONCLUSIONS

This work demonstrated the possibility to enhance the electroconductivity of some films made of thioalkylic-substituted polythiophene derivatives through laser light exposure. In particular, a blend made of regioregular poly(3-methylthio)thiophene (PTSM<sub>e</sub>) and poly(3-hexyl)thiophene (P3HT) proved to be an optimal solution for overcoming the incomplete solubility and poor filmability of the thioalkyl-substituted polythiophenic derivative alone. The blend used strategically combines the plastifying properties of the alkylthiophene polymer with the ability of the photosensitive polythiophene to increase its electrical conductivity by means of a fast, simple laser treatment. This way, we obtained very homogeneous polymeric films which were easily cast from common organic solvents and which proved to be capable of increasing their electrical conductivity by about  $7 \times 10^6$  times after tracing. The final electrical conductivity of the conductive traces can be easily modulated by working on the blend composition, laser power, and tracing speed, thus making the preparation of integrated circuits faster and simpler. We also demonstrated that the performance of the BHJ solar cell prepared using the blend as the photoactive layer is higher than in the reference cell made of P3HT alone, thanks to the wider absorption spectrum and the more homogeneous morphology of the films obtained from P3HT/PTSM<sub>e</sub> mixtures. These results indicate that PTSM<sub>e</sub> and, in particular, its blends with P3HT, are promising multifunctional polymeric materials for application in electronics and in plastic solar cells.

## REFERENCES FOR CHAPTER 4

- [1] K. Norrman, A. Ghanbari Siahkali, N. B. Larsen, *Annu. Rep. Prog.Chem. Sect. C.*, 101 (2005) 174-201.
- [2] P. Schilinsky, C. Waldauf, C. J. Brabec, *Adv. Funct. Mater.* 16 (2006) 1669-1672
- [3] F. C. Krebs, M. Jorgensen, K. Norman, O. Hagemann, J. Alstrup, T. D. Nielsen, J. Fyenbo, K. Larsen, J. Kristensen, *Sol. Energy Mater. Sol. Cells* 93 (2009) 422-441.
- [4] A. Lange, M. Wegener, C. Boeffel, B. Fischer, A. Wedel, D. Neher, *Sol. Energy Mater. Sol. Cells* 94 (2010) 1816-1821
- [5] F. C. Krebs, *Sol. Energy Mater. Sol. Cells* 93 (2009) 465-475.
- [6] H. K. Roth, K. Eidner, H. Roth, *Circ. World*, 22(2) (1996) 31-32.
- [7] R. Baumann, U. Kulish, M. Schroedner, H. K. Roth, D. Sebastian, J. Bargon, *Synth. Met.*, 55-56, (1993) 3643-3648.
- [8] M. Lanzi, F. P. Di Nicola, M. Livi, L. Paganin, F. Cappelli, F. Pierini, *J. Mater. Sci.*, 48 (2013) 3877-3893
- [9] H. Hoppe, M. Niggemann, C. Winder, J. Kraut, R. Hiesgen, A. Hinsch, D. Meissner, N. S. Sariciftci, *Adv. Funct. Mater.*, 14 (2004), 1005-1011.
- [10] R. Hegde, N. Henry, B. Whittle, H. Zang, B. Hu, J. Chen, K. Xiao, M. Dadmun, *Sol. Energy Mat. Sol. Cells*, 107 (2012) 112-124.
- [11] A. J. Moulé, S. Allard, N. M. Kronenberg, A. Tsumi, U. Scherf, K. Meerholz, *J. Phys. Chem. C*, 112 (2008) 12583-12589
- [12] J. Hou, H. Y. Chen, S. Zhang, G. Li, Y. Yang, *J. Am. Chem. Soc.*, 130 (2008) 16144-16145
- [13] Y. Li, Y. Zou, *Adv. Mater*, 20 (2008) 2952-2958.
- [14] E. Bundgaard, F. C. Krebs, *Sol. Energy Mater. Sol. Cells* 91 (2007) 954-985
- [15] D. Muehlbauer, M. Scharber, M. Morana, Z. G. Zhu, D. Waller, R. Gaudiana, C. Brabec, *Adv. Mater.*, 18 (2006) 2884-2889.
- [16] N. Blouin, A. Michaud, M. Leclerc, *Adv. Mater*, 19 (2007) 2295-2300.

- [17] K. Takahashi, Y. Takano, T. Yamaguchi, J. Nakamura, C. Yokoe, K. Murata, *Synth. Met.*, 155 (2005) 51-55.
- [18] L. Angiolini, T. Benelli, V. Cocchi, M. Lanzi, E. Salatelli, *React. Funct. Polym.*, 73 (2013) 1198-1206.
- [19] H. K. Roth, H. Gruber, E. Fanghaenel, A. M. Richter, W. Hoerig, *Synth. Met.* 37 (1990) 151-164.
- [20] B. M. Novak, E. Hegen, A. Visnanathan, L. Magde, *Polym. Prepr.* 31 (1990) 482-483.
- [21] I. Zergioti, M. Makrygianni, P. Dimitrakis, P. Normand, S. Chatzandroulis, *Appl. Surf. Sci.*, 257 (2011) 5148-5151
- [22] R. S. Lowe, P. C. Ewbank, J. Lin, L. Zhai, R. D. McCullough, *Macromolecules* 34 (2001) 4324-4333.
- [23] M. Lanzi, L. Paganin *Eur. Polym. J.*, 44 (2008) 3987-3996.
- [24] S. P. Singh, C. Pavan Kumar, G. D. Sharma, R. Kurchania, M. S. Roy, *Adv. Funct. Mater.*, 22, 2012, 4087-4095.
- [25] F. Bertinelli, P. Costa Bizzarri, C. Della Casa, M. Lanzi, *Spectrochimica Acta Part A*, 58 (2002) 583-592.
- [26] A. Mikroyannidis, P. Suresh, G. D. Sharma, *Org. Electron.*, 11, 2010, 311-321.
- [27] H. K. Roth, R. Baumann, J. Bargon, M. Schroedner, *Progr. Colloid. Polym. Sci.*, 85 (1991) 157-162.
- [28] J.B. Lambert, D.A. Lightner, H.F. Shurvell, R.G. Cooks in "Introduction to Organic Spectroscopy", Macmillan Ed., New York (1987).
- [29] M. Lanzi, L. Paganin, *Eur. Polym. J.* 45 (2009) 1118-1126.
- [30] M. Lanzi, L. Paganin, *React. Funct. Polym.*, 70 (2010) 346-360.
- [31] D. Chirvase, J. Parisi, J.C. Hummelen, V. Dyakonov, *Nanotechnology*, 15 (2004) 1317-1323.
- [32] G. Li, V. Shrotriya, Y. Yao, Y. Yang, *J. Appl. Phys.*, 98 (2005) 043704
- [33] M. Lanzi, F. P. Di Nicola, F. Errani, L. Paganin, A. Mucci, *Synth. Met.*, 195 (2014) 61-68.
- [34] J. Roncali, *Chem. Rev.*, 92 (1992) 711-738.
- [35] A. J. Nelson, S. Glenis, A. J. Frank, *J. Chem. Phys.* 87 (8) (1987) 5002-5006.

- [36] M. Al-Ibrahim, H. Klaus Roth, U. Zhokhavets, G. Gobsch, S. Senfuss, *Sol. Energy Mater. Sol. Cells* 85 (2005) 13-20.
- [37] T. M. Clarke, J. R. Durrant, *Chem. Rev.* 110 (2010) 6736-6767.
- [38] M. C. Scharber, D. Wuhlbacher, M. Koppe, P. Denk, C. Waldhauf, A. J. Heeger, C. L. Brabec, *Adv. Mater.*, 18 (2006) 789-794.
- [39] M. Zhang, H. Wang, C. W. Tang, *Appl. Phys. Lett.*, 97 (2010) 143503-506.
- [40] A. Gadisa, M. Svensson, M. R. Andersson, O. Ingänas, *Appl. Phys. Lett.*, 84 (2004) 1609-1611.
- [41] Y. Li, Y. Zou, *Adv. Mater.*, 20 (2008) 2952-2958.
- [42] J. Hou, Z. Tan, Y. Yan, Y. He, C. Yang, Y. Li, *J. Am. Chem. Soc.*, 128 (2006) 4911-4916.
- [43] B. Carsten, F. He, H.J. Son, T. Xu, L. Yu, *Chem. Rev.*, 111, (2011), 1493-1528.
- [44] X. Yang, A. Uddin, *Renewable and Sustainable Energy Reviews*, 30 (2014) 324-336.
- [45] G. Li, V. Shrotriya, J. S. Huang, Y. Yao, T. Moriarty, K. Emery, Y. Yang, *Nat. Mater.*, 4 (2005) 864-868.
- [46] G. Zhao, Y. He, Y. Li, *Adv. Mater.*, 22 (2010) 4355-4358
- [47] A. Moliton, J. M. Nunzi, *Polym. Int.*, 55 (2006) 583-600.
- [48] S. H. Eom, S. Senthilarasu, P. Uthirakumar, S. C. Yoon, J. Lim, C. Lee, H. S. Lim, J. Lee, S. H. Lee, *Organic Electronics*, 10 (2009) 536-542.
- [49] N. Blouin, A. Michaud, D. Gendron, S. Wakim, E. Blair, R. Neagu-Plesu, M. Belletete, G. Durocher, Y. Tao, M. Leclerc, *J. Am. Chem. Soc.*, 130 (2008) 732-742.



# CHAPTER 5: SOLVENTLESS DEPOSITION OF OLIGO- AND POLYTHIOPHENES FOR BHJ SOLAR CELLS

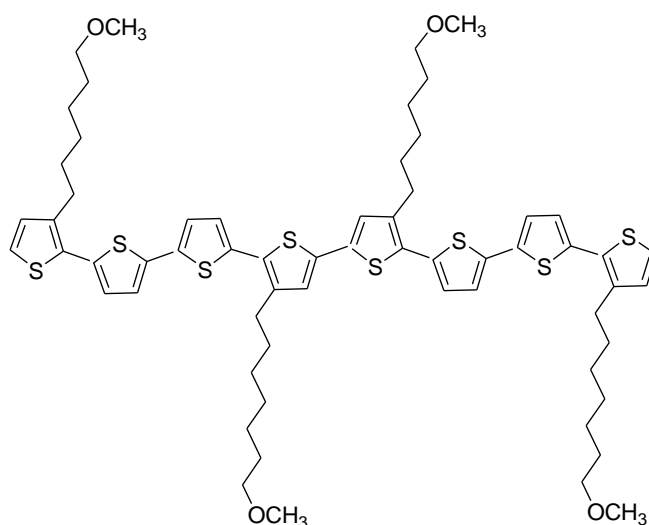
## *5.1. INTRODUCTION*

Organic semiconductors are particularly attractive for low cost electronic applications, especially when characteristics such as lightness, flexibility and inexpensiveness have a dominant role if compared with electrical performances. Most organic semiconductors described in literature are thiophene-based oligomers [1,,3], homopolymers [4,,6] and copolymers [7]. These materials have been effectively used for optoelectronic applications such as either organic light-emitting diodes (OLEDs) or organic solar cells (OSCs) [8,9] and for electronic applications such as organic field-effect transistors [10] or for laser tracing aimed at obtaining conductive patterns on polymeric insulating thin films [11]. At present, a certified power conversion efficiency (PCE) on the order of 4-5% has been obtained using polythiophenes as active materials for the fabrication of OSCs with an architecture called Bulk Heterojunction Junction (BHJ) [12]. For this type of cells, the active layer is a blend of a polythiophene derivative (usually poly(3-hexyl)thiophene, P3HT [13,14]) used as electron-donor material and a high electron-affinity molecule (usually C<sub>60</sub>-fullerene or [6,6]-phenyl-C<sub>61</sub>-butyric acid methyl ester (PCBM)). P3HT ensures high charge mobility and, with the addition of selected additives, has been effectively used in the preparation of highly efficient solar cells by ink-jet printing [15].

Recently, some researchers have demonstrated the possibility of obtaining thin, homogeneous and well adherent films from a polythiophene derivative (i.e. poly[3-(4-octyloxyphenyl)thiophene]) by means of the Matrix Assisted Pulsed Laser Evaporation technique [16]; however, the molecular weight of the evaporated polymer was not determined. Wei et al. [17] have reported on the deposition of P3HT using an electron-beam heated effusion cell and concluded that the chemical composition and structure of the polymer was largely conserved, basing their assumptions on FT-IR and XPS characterizations. More recently, Kovacik et al. [18] investigated the deposition of some P3HT samples by vacuum thermal evaporation (VTE) in depth, using <sup>1</sup>H-NMR, FT-IR UV-Vis absorption spectroscopy and GPC. They observed both a strong reduction in P3HT molecular weight during the deposition process ( $M_w$  decreased from 36000 to 1500 g/mol) and how some side chains broke away from the backbone. In a 2012 paper [19], the same authors reported the thermal evaporation both of P3HT and of a non-substituted polythiophene sample (PTh). The latter gave homogeneous films with a high degree of crystallinity,

without any evidence of chemical decomposition and made it possible to obtain some planar heterojunction solar cells with improved overall photoconversion efficiency (+70%) if compared to P3HT.

In view of the above, in this work we investigated the possibility of VTE co-depositing two thiophenic derivatives (a regioregular P3HT sample and a functionalized thiophenic octamer, OCT Scheme 16) and the electron-acceptor molecule ( $C_{60}$ -fullerene) in order to obtain a final architecture of the photoactive layer as close as possible to the BHJ type.



*Scheme 16. Structure of 3,3',4'',4''',3''''-tetra(6-methoxyhexyl)-2,2':5',2'':5'',2''':5''',2''''-octithiophene (OCT).*

We decided to examine the evaporation of both the most used and studied thiophenic polymer (P3HT) for comparison purpose and a previously synthesized oligothiophene [20] in order to take advantage of its higher volatility and the presence of methoxy groups in side chains. In fact, it is well known for polythiophene that the introduction of alkoxy side chains on thiophene units makes an increase in the coplanarity of the thienylene moieties all along the polymer side chain possible [21,22].

## 5.2. EXPERIMENTAL

All the solvents and reagents used for the synthesis were purchased from Aldrich Chemical Company. NMR spectra were run on a Varian Gemini 300 (300 MHz) FT-NMR spectrometer using TMS as reference. FT-IR spectra were obtained using a Perkin Elmer Spectrum One FT-IR spectrophotometer. Molecular weights were determined by size exclusion chromatography (SEC) relative

to polystyrene standards on a HPLC Lab Flow 2000 apparatus equipped with a Phenogel mixed MXL column and a Linear Instrument UV-Vis detector (model UVIS-200) working at 263 nm, with THF being used as an eluent at a flow rate of 1.0 ml/min. The UV-Vis spectra were recorded with a Perkin Elmer Lambda 19 spectrophotometer. Thermal analysis was performed on a TA Instruments TGA-2050 at a heating rate of 10°C/min under inert atmosphere (30 Nml/min of N<sub>2</sub>). Cyclic voltammetry (CV) was performed on a Autolab PGS 30 (EcoChemie, The Netherlands) with a three-electrode system in a solution of 0.1 M Bu<sub>4</sub>NPF<sub>6</sub> in CH<sub>3</sub>CN at a scan rate of 50 mV/sec. Oligomer film was prepared by evaporating OCT on a ITO glass obtaining a 0.25 µm thick film. A Pt wire was used as the counter electrode and SCE was used as the reference electrode.

Solar cells were prepared according to the following procedure: the ITO-glass substrate (area 1.0 × 1.0 cm<sup>2</sup>, surface resistance 21 Ω/sq, Alphalab Inc., USA) was firstly etched on three sides by using a concentrated Piranha solution, in order to obtain a final 0.75 × 0.75 cm<sup>2</sup> area covered by ITO. The glass was then cleaned in a ultrasonic bath filled with a diluted solution (1% w/w) of a Roth detergent for ultrasonic cleaners (RBS-Viro) and subsequently washed several times with distilled water, isopropyl alcohol, acetone and, lastly, diethyl ether. It was then dried overnight at 70°C in an oven previously filled with dry silica gel. The final surface resistance of the ITO layer on glass was 15 Ω/sq.

The glass was then prepared for the VTE by covering a small 0.25 × 1.0 cm area with insulating tape on the side opposite to the previously etched area, in order to leave this small portion of conductive glass uncovered by the active layer. The final active area of the cell was 0.25 cm<sup>2</sup>. The active layer was evaporated by heating a tungsten boat (Edwards Co., USA) previously filled with a 1:1 (wt/wt) polymer/C<sub>60</sub>-fullerene (99% pure) powder using an Edwards E306A coating system operating at 1×10<sup>-6</sup> mmHg. The temperature of the boat was monitored using an Italmec Elettronica Srl (Italy) temperature controller equipped with a Julabo Pt-100 probe (Code No. 8981005) placed in contact with the evaporation boat. The P3HT/ C<sub>60</sub> mixture was evaporated at 320±5°C at a rate of about 10 nm/min, while the OCT/ C<sub>60</sub> mixture was deposited at 270±5°C at a rate of about 15 nm/min. Cells were annealed at 130°C for 30 min at 20 mmHg using a Büchi GKR-50 micro glass oven.

The layers obtained were characterized by AFM and then a 50 nm thick Al contact was deposited using the above mentioned apparatus.

The electrical parameters of the photovoltaic cells were measured at room temperature using a Keithley 2401 Source Meter and a Abet Technologies Solar Simulator (AM 1.5, 70 mW/cm<sup>2</sup>) calibrated with an ILT 1400-BL radiometer photometer.

The film thickness was measured by means of a FTPadvanced FTPadv-2 (Sentech GmbH, Germany) film thickness probe equipped with FTP Expert software. This apparatus was calibrated by

measuring some reference films whose thickness was previously determined using a Burleigh Vista AFM system. The thickness of the active layer was 45 nm for P3HT/  $C_{60}$  and 55 nm for OCT/  $C_{60}$ .

The described deposition procedure was also used to obtain the polymeric samples that have been chemically and spectroscopically characterized, using a glass or a quartz slide instead of the ITO glass as a substrate.

X-ray diffraction data were recorded at room temperature by using a  $CuK\alpha$  ( $\lambda=1.5406$  Å) radiation source (Philips PW 1050) and a Bragg-Brentano diffractometer (Philips PW 1710) equipped with a graphite monochromator in the diffracted beam. The  $2\theta$  range between  $2.0$  and  $90.0^\circ$  was scanned by 881 steps of  $0.1^\circ$  with a counting time of 15 sec for each step. The XRD characterization was carried out on films on glass slides obtained both by casting OCT solution in  $CHCl_3$  and by direct VTE of the oligomer.

Poly(3-hexylthiophene) (P3HT:  $M_n=32000$ ,  $PDI=1.2$ , 92% HT) was synthesized from commercial 3-hexylthiophene using the Grignard Metathesis (GRIM) procedure described by McCullough et al. [23], while the octamer was prepared according to the procedure described in a previous work [20].

### 5.3. RESULTS AND DISCUSSION

The main purpose of this work was to find a fast and effective system to deposit the photoactive layer onto the ITO substrate for the preparation of polymeric BHJ solar cells. We decided to use the vacuum thermal evaporation (VTE) system applied on a thiophenic oligomer. There are only a few examples in the literature of Bulk Hetero-Junction (BHJ) Solar Cells made of evaporated oligothiophenes. In fact, the performances of devices made with oligomers are usually rather inferior relative to cells made with blends of polythiophenes and fullerene derivatives and this can be ascribed to the reduced conjugation length of the oligomers and to the difficulty in maintaining a suitable and reproducible  $C_{60}$ /oligomer ratio in the evaporated blend [24]. The first BHJ solar cells made with evaporated oligothiophenes were prepared by Aso, Otsubo and Harima [25] and showed a power conversion efficiency (PCE) of 0.4%.

The standard BHJ architecture (i.e. ITO/PEDOT-PSS/ED polymer-EA molecule/Al, where the electron-donor polymer is usually a polythiophene and the EA molecule a fullerene derivative) was recently improved by Bäuerle and co-workers in a series of papers dealing with the preparation and the structure-property relationships of vacuum-processed small molecules based OSCs. In particular, they prepared some cells with planar heterojunction (PL) and bulk heterojunction (BHJ) architecture using a

mixture of  $C_{60}$ -fullerene and a dicyanovinyl-substituted oligothiophene deposited by VTE as the photoactive layer. The active layer was the central layer of the cell and was surrounded by many other organic layers in a complex but effective architecture called Stacked Layer (SL). PLSL solar cells gave efficiencies of 1.2-2.8% while BHJSL solar cells up to 5.2% [26]. Other stacked layer vacuum deposited bulk heterojunction solar cells were made using dicyanovinylene-substituted selenophene-thiophene co-oligomers (PCE up to 3.09% [27]), oligothiophenes incorporating benzothiadiazole units (PCE up to 2.76% [28-29]) and methyl-substituted dicyanovinyl-capped quinquethiophenes (PCE up to 6.1% [30]). We can therefore conclude that conjugated thiophene oligomers with a well-defined length are versatile photoactive materials for the preparation of heterojunction solar cells and worthy of further investigations.

In this work, the first attempt to evaporate a conjugated polymer was made on a regioregular P3HT sample. In fact, this polymer, thanks to its high electronic mobility [31], is usually used as hole-transporting material in organic solar cells [32] and represents a reference p-donor material. Moreover, we decided to study the VTE of a regioregular sample of P3HT since some researchers reported that this polymer withstood the thermal evaporation process while largely retaining its chemical composition [15]. The thermal stability of P3HT was preliminarily examined using thermogravimetric analysis (TGA) in an inert ( $N_2$ ) atmosphere. The main weight loss was identified at around 400°C with a weight loss of 58% while two very small shoulders in the baseline can be found at around 150 and 300°C (Fig. 58).

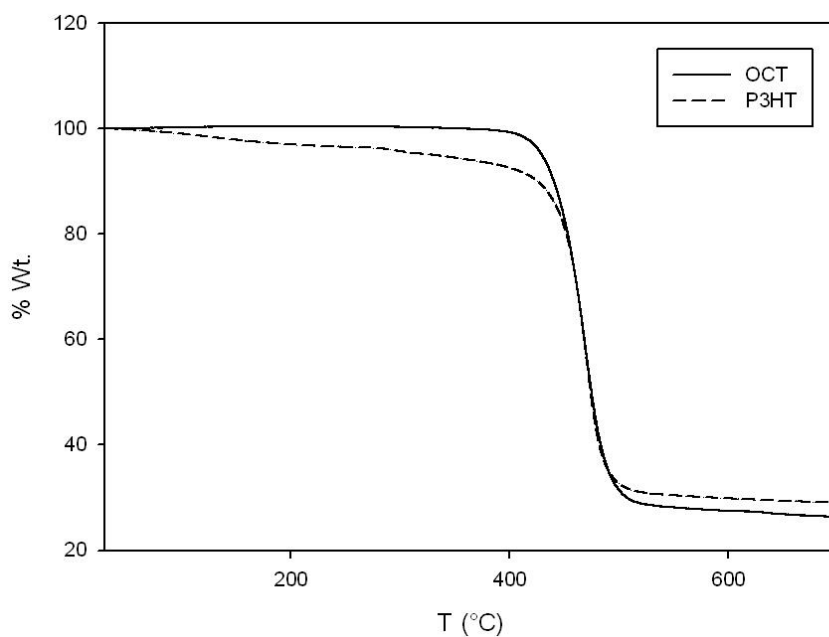


Figure 58. TGA thermogram of P3HT and OCT under nitrogen.

A thin yellow film of P3HT (70 nm thick) was obtained on a  $2.5 \times 2.5$  cm quartz slide by evaporating the polymer at a temperature of  $350 \pm 5$  °C after 4 minutes at a pressure of  $1 \times 10^{-6}$  mmHg. The VTE of P3HT was repeated many times in order to obtain an amount of evaporated polymer sufficient for its analysis. It is to underline that the deposition of P3HT was also attempted at lower temperatures, as 350°C is quite close to the temperature at which the decomposition of the polymer starts, but no evidences of film formation were found. The  $^1\text{H}$ -NMR spectrum of the evaporated P3HT is shown in Fig. 59 together with the spectrum of the pristine sample.

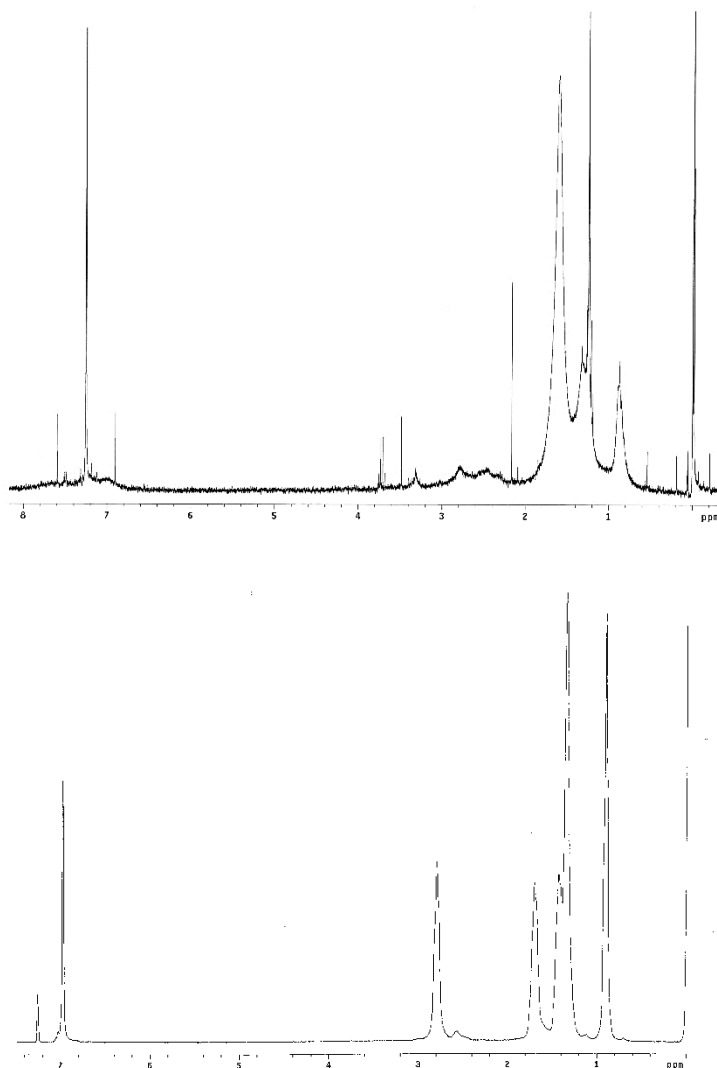


Figure 59.  $^1\text{H}$ -NMR spectrum of P3HT. Up: evaporated polymer redissolved in  $\text{CDCl}_3$ . Down: the same polymer before vacuum evaporation, dissolved in  $\text{CDCl}_3$ .

The spectrum shows the main signals ascribable to this kind of polymer, i.e. 7.00 ppm (thiophene H-4); 2.80-2.35 ppm ( $-\text{CH}_2$   $\alpha$  to the thiophene ring); 1.90-1.10 ppm (central  $-\text{CH}_2-$  of the side chain); 0.90 ppm ( $-\text{CH}_3$ ) together with a plethora of signals which are hardly ascribable to the P3HT structure.

Even when the P3HT was evaporated both under a controlled temperature, below the decomposition temperature determined by TGA analysis, and under high vacuum, the polymer underwent a pyrolysis reaction, with the consequent possible removal of small fragments and molecules. This hypothesis was also supported by the observation that the pressure in the Edwards evaporation system chamber tended to increase during polymer evaporation. The evaporated P3HT was also subjected to GPC analysis, which confirmed the partial loss of the polymeric structure of P3HT, giving a  $M_n$  of 1800 g/mol with a PDI of 3.5.

Since the attempt to evaporate the P3HT sample was not completely successful, we decided to use the oligomer as an active layer for the OPV cell. We then tried to prepare an OCT film using the same evaporation procedure used for P3HT. The TGA of OCT is shown in Fig. 1 and highlights the total stability of this oligomer up to 400°C under inert atmosphere.

At 400°C a very rapid weight loss was seen, leaving only 26% of the initial weight of the sample.

OCT was then evaporated operating at  $270 \pm 5^\circ\text{C}$  and  $1 \times 10^{-6}$  mmHg for 3 min. Even if the thermograms of OCT and P3HT are similar, their deposition temperatures are quite different probably because their thermal decomposition was examined under a nitrogen flux while their VTE was performed under high vacuum. A red-orange 80 nm thick film of OCT was obtained on the  $2.5 \times 2.5$  cm quartz substrate. This time, the film showed metallic lusters and a very smooth and homogeneous surface.

$^1\text{H}$ -NMR spectrum of evaporated OCT (Fig. 60, up) showed a group of signals in the aromatic region which can be attributed to thiophenic protons according to the numeric system used in the Fig.60.

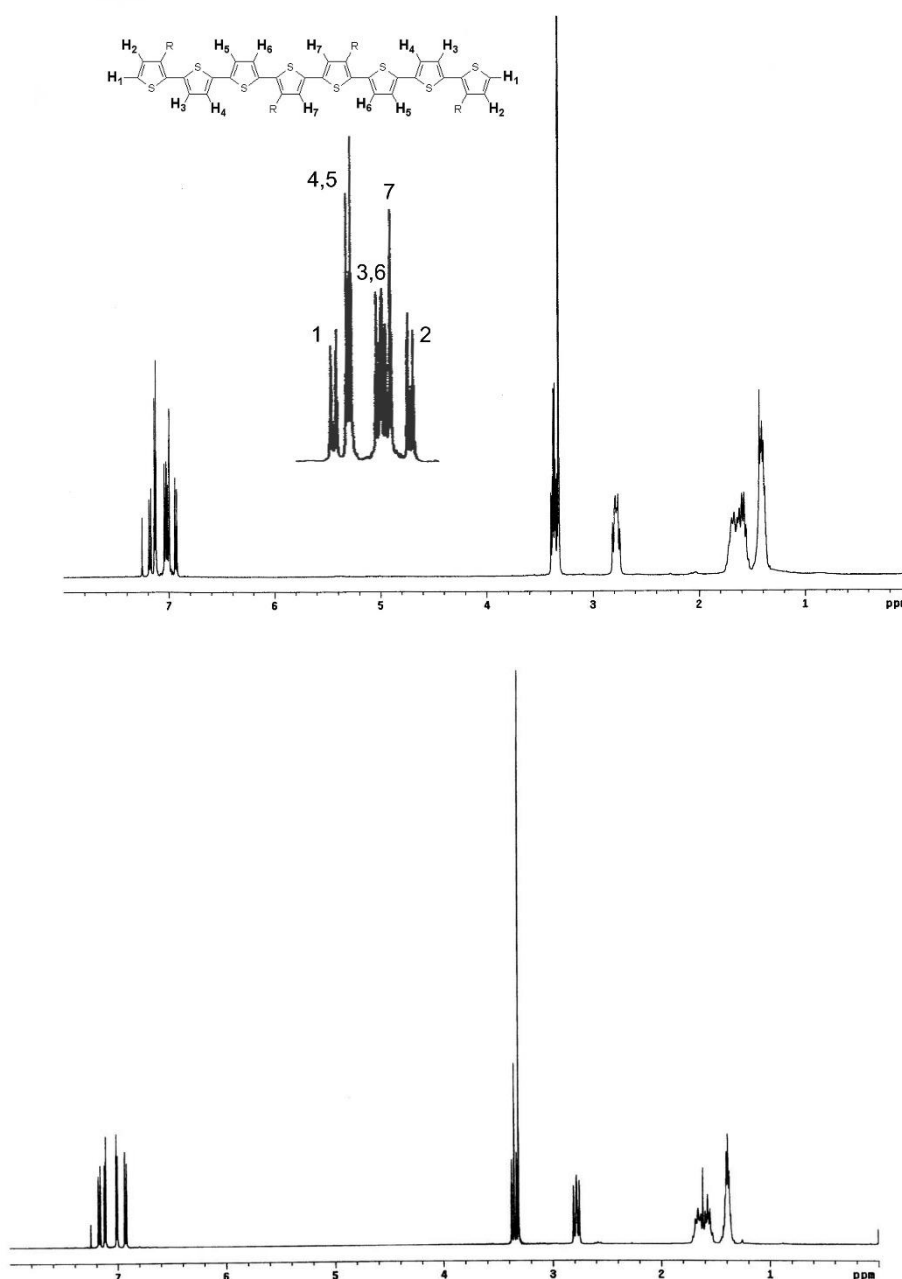


Figure 60. <sup>1</sup>H-NMR spectrum of OCT. Up: evaporated oligomer redissolved in CDCl<sub>3</sub>. Down: the same oligomer before vacuum evaporation, dissolved in CDCl<sub>3</sub>.

In detail, signals at 6.94 and 7.00 ppm can be related to protons 2 and 7; signals at 7.02 and 7.04 ppm to protons 3 and 6; the signal at 7.13 ppm to protons 4 and 5, respectively, while the doublet at 7.18 ppm to proton 1. At 3.32 and 3.37 ppm the signals ascribable to -CH<sub>2</sub>- and -CH<sub>3</sub> protons  $\alpha$  to the oxygen atoms of the ether groups are clearly evident, and at 2.78 ppm the triplet deriving from the -CH<sub>2</sub>- groups  $\alpha$  to the thiophene rings can be found. Signals in the 1.75-1.15 ppm range stem from protons of the central methylene units in the side chains.



The chemical identity of the evaporated OCT sample is also confirmed by its FT-IR analysis made by dissolving the deposited film in  $\text{CHCl}_3$  and by casting it on a Ge disk.

Frequencies and assignments of IR absorption bands of OCT are listed in Table 7, while the spectrum is shown in Fig. 61 together with that of the pristine sample.

Table 7. IR absorption bands and relative assignments for evaporated OCT.

Assignment	Wavenumber ( $\text{cm}^{-1}$ )
$\nu_{\text{C-H}}$ $\beta$ thiophene	3063
$\nu_{\text{as}}$ $\text{CH}_3$	2979
$\nu_{\text{as}}$ $\text{CH}_2$	2930
$\nu_{\text{sym}}$ $\text{CH}_2$	2859
$\nu_{\text{as}}$ $\text{CH}_2\text{-O}$	2825
$\nu_{\text{sym}}$ $\text{CH}_2\text{-O}$	2806
$\nu_{\text{as}}$ $\text{C}=\text{C}$	1500
$\delta_{\text{C-H}}$ $\text{CH}_3$	1464
$\nu_{\text{sym}}$ $\text{C}=\text{C}$	1444
$\nu_{\text{as}}$ $\text{C-O-C}$	1118
$\gamma_{\text{C-H}}$ thioph. $\alpha$ , $\alpha'$ disubst.	789
rocking $-\text{CH}_2-$	730
$\gamma_{\text{C-H}}$ thioph. $\alpha$ , $\beta$ disubst.	691

$\nu$  = stretching;  $\delta$  = on plane bending;  $\gamma$  = out of plane bending

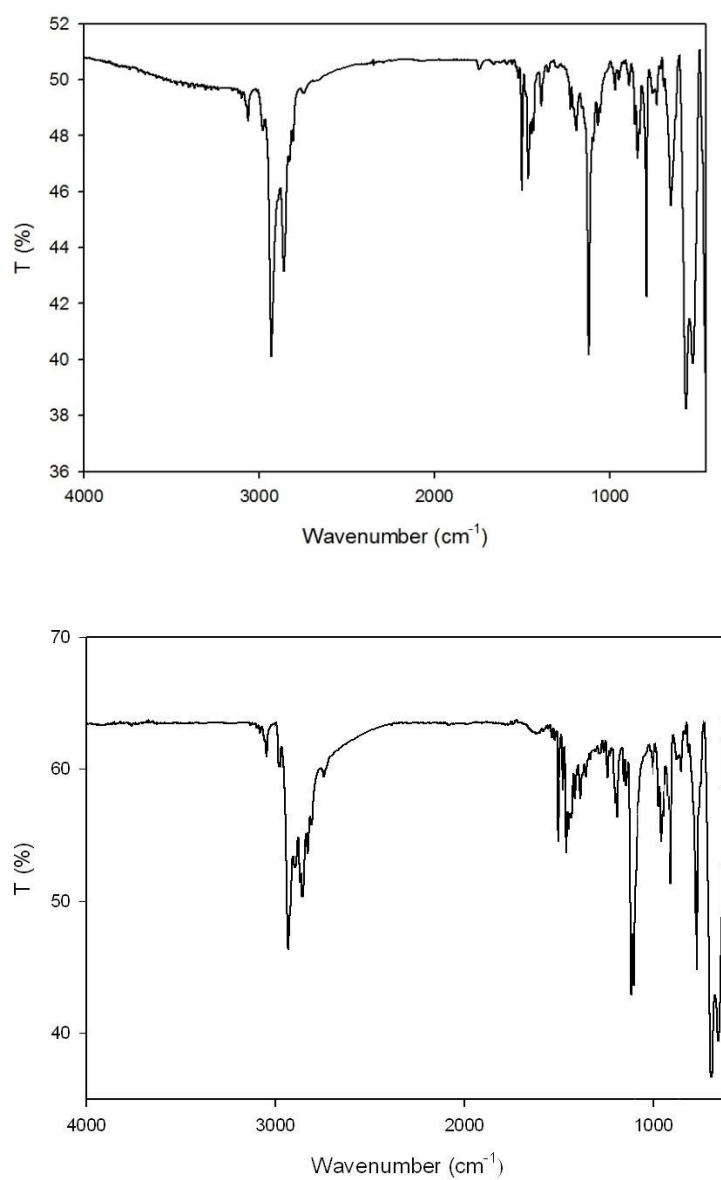


Figure 61. IR spectrum of evaporated (up) and pristine (down) OCT.

These findings comply with the expected structure of the vacuum deposited octamer.

The UV-Vis spectra of OCT in film on quartz slide are shown in Fig. 62.

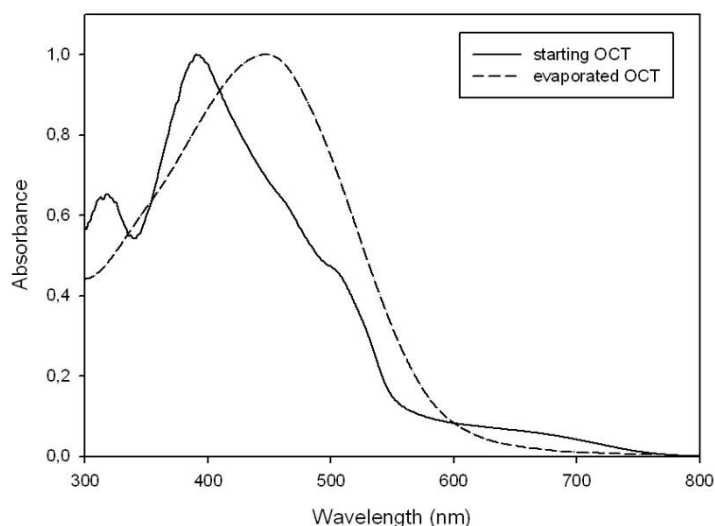


Figure 62. UV-Vis spectra of pristine and evaporated OCT (film on quartz).

The two curves are normalized to their maximum intensity. The pristine sample, cast from its solution in chloroform, shows a structured profile, with a  $\lambda_{\max}$  at 391 nm, and two shoulders at 462 and 500 nm, corresponding to the second and to the first vibronic quantum, respectively.

The  $E_{0-0}$  (pure electronic) transition is hard to find since the spectrum does not show any evident peak at low energies but the deconvolution of the spectrum profile allowed us to locate it at 612 nm.

The presence of clear absorption in the 600-770 nm range can be ascribed to the presence of high intermolecular  $\pi$ - $\pi$  stacking and indicates the existence of inter-chain aggregates [33-36]. On the basis of  $\lambda_{\max}$  values, the mean conjugation length (MCL) of pristine OCT in the film state can be calculated using the Jiang formula [37] and corresponds to about four thiophene conjugated units. The UV-Vis spectrum of the evaporated sample is quite different from the pristine one. In fact, the spectrum profile is broader and the  $\lambda_{\max}$  is red-shifted of 56 nm. Moreover, the spectrum does not show any evident structure and its onset is 584 nm ( $E_g^{\text{opt}} = 2.12$  eV).

The MCL of the evaporated sample is higher than the pristine one and corresponds to about six conjugated thiophenic rings: a good value taking into account that the oligomer is composed of only eight thiophenic units. We can conclude that the pristine sample of OCT has better aggregation and stacking in film than the evaporated sample; the latter, however, shows a higher conjugation length, a parameter which directly affects electron mobility over the polymeric backbone [38].

The XRD patterns of OCT samples are shown in Fig. 63.

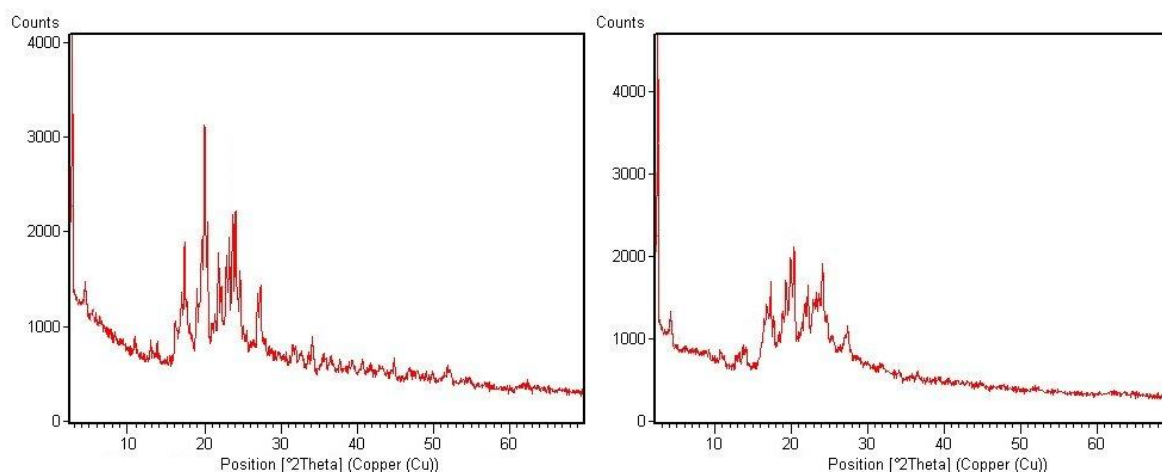


Figure 63. X-Ray diffractograms of OCT films obtained by casting (left) and VTE (right).

Diffraction patterns display a set of strong peaks in the central region ( $2\theta = 17^\circ$ - $28^\circ$ ) and some peaks of lower intensity in the remaining regions. For the cast sample, low angle peaks are found at  $2\theta = 2.49^\circ$  and  $5.00^\circ$  ( $d = 3.54$  and  $1.77$  nm, respectively) and correspond to the (100) and (200) peaks observed in poly(3-octylthiophene) [39]. Moving to higher angles, three peaks at  $2\theta = 19.6^\circ$ ,  $22.8^\circ$  and  $28.0^\circ$  ( $d = 4.52$ ,  $3.90$  and  $3.18$  Å, respectively) can be found. The latter have been previously ascribed to the (110), (200) and (210) reflections of unsubstituted polythiophene [40,41]. The evaporated sample shows a diffractogram with a less detailed fine structure, with broader and less intense peaks according to a lower degree of crystallinity, as already observed from its UV-Vis spectrum in film.

The electrochemical behaviour of OCT was evaluated by means of cyclic voltammetry. A film of evaporated OCT on a ITO glass (55 nm thick) was examined and its voltammogram is reported in Fig. 64.

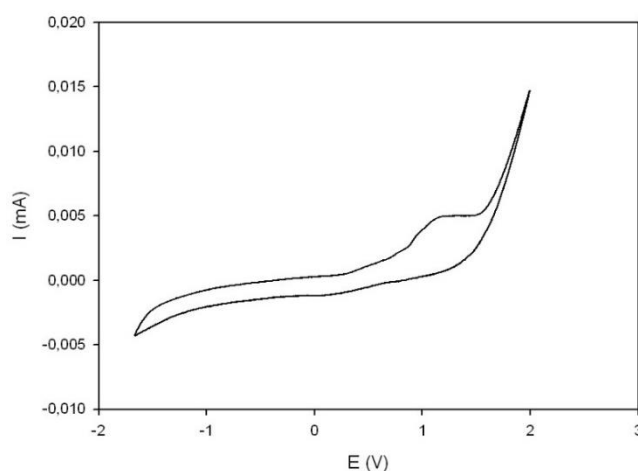


Figure 64. Cyclic voltammogram of an OCT film obtained by VTE (1st scan).

Unfortunately, the absence of any evident peak in the negative bias range made it impossible to evaluate both the reduction potential of OCT ( $E_{red}^{onset}$ ) and its electrochemical bandgap ( $E_g^{ec}$ ). The energy of the HOMO level was estimated according to the following relation [42,43]:

$$I_p (HOMO) (eV) = -e(E_{ox}^{onset} + 4.4)$$

Since  $E_{ox}^{onset}$  was 0.45 V, the HOMO level of evaporated OCT was  $-4.85$  eV and, since  $E_g^{opt}$  was 2.12 eV, the LUMO level was  $-2.73$  eV.

The HOMO level energy is very close to the standard reference P3HT ( $-4.8$  eV, [44]) thus indicating that OCT can be effectively used as an electron-donor material for organic solar cells [45].

The bandgap of evaporated OCT (2.12 eV) is lower than that of P3HT [40] and this could favour the final photoconversion efficiency of the device [46,47].

BHJ solar cells were prepared by evaporating the electron-donor material (P3HT and OCT) and the electron-acceptor ( $C_{60}$ -fullerene) at the same time, as detailed in the experimental section. The final architecture of the cells was: ITO (100 nm)/Photoactive blend/Al cathode (50 nm) while the thickness of the active layers made of evaporated P3HT/ $C_{60}$  or OCT/ $C_{60}$  was 45 and 55 nm, respectively. The active area of the cells was  $0.25 \text{ cm}^2$  and both devices were annealed in a vacuum at  $130^\circ\text{C}$  for 30 min using a Büchi GKR-50 micro glass oven before the cathode deposition. I/V measurements were performed at room temperature with a Keithley 2401A source meter operating in the  $-2/+2$  V range. For the photovoltaic characterization, the cells were illuminated with  $70 \text{ mW/cm}^2$  power intensity of AM 1.5 radiation provided by an Abet Technologies LS150 Xenon Arc Lamp Source calibrated with an ILT 1400-BL radiometer photometer. The recorded J/V curves under illumination are shown in Fig. 65 while photovoltaic properties are listed in Table 8.

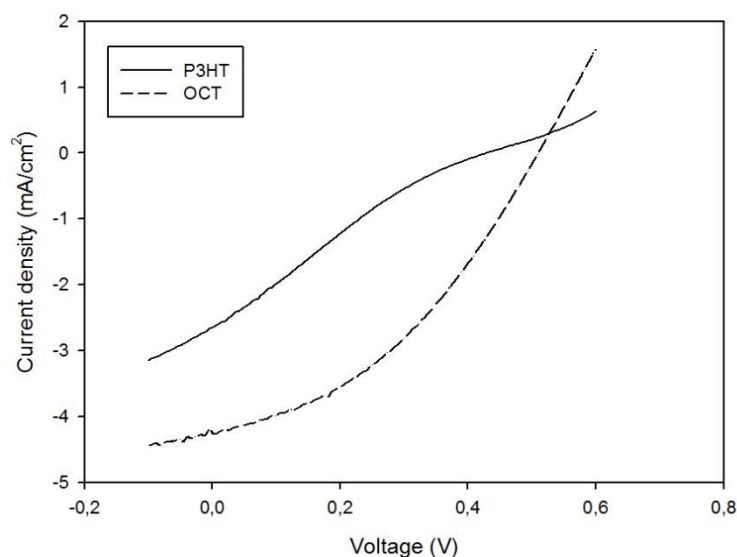


Figure 65.  $J/V$  curves under AM 1.5 illumination of the prepared cells.

Table 8. Photovoltaic properties of the assembled solar cells.

Property <sup>a</sup>	P3HT	OCT
$V_{oc}$ (V)	0.43	0.51
$J_{sc}$ (mA/cm <sup>2</sup> ) <sup>a</sup>	2.66	4.19
FF	0.22	0.40
$\eta$ (%)	0.35	1.21

a) under  $70 \text{ mW/cm}^2$  simulated AM 1.5 illumination through the ITO electrode

Very promising results were obtained using the co-evaporated mixture of OCT/ $C_{60}$ : in this case, the shape of the  $J/V$  curve was the same usually observed in this kind of devices [48] while the power conversion efficiency was notably higher than in the previously prepared cells ( $\eta=1.21\%$  vs  $0.35\%$ ), when a photoactive blend of OCT and SWCNT in  $\text{CHCl}_3$  was deposited by spin-coating on the ITO glass and was used as an active layer [20]. The PCE of the OCT cell is comparable with the values obtained with PLSL solar cells (but lower than those reported for BHJSL solar cells) [26] prepared using VTE system.

Even if the obtained efficiency is not very high in absolute terms, OCT seems to be particularly prone to evaporation by VTE in one single step together with fullerene, with a rapid and straightforward procedure, without the need to prepare the electron donor/acceptor solution and also avoiding the

deposition of the PEDOT-PSS buffer layer, the use of solvents and, above all, the deposition of many layers as reported for the stacked layer solar cells. Moreover, the adopted deposition procedure was particularly efficient, since no residues were found on the tungsten source. Therefore, the use of OCT seems very promising in continuous coating systems using roll to roll (R2R) or reel to reel coating techniques [49,50].

Unfortunately, the good results shown by OCT were not obtained when the active layer was prepared by the evaporation of the P3HT/C<sub>60</sub> mixture. In fact, in this case the power conversion efficiency was only 0.35% while a reference cell prepared using the same batch of P3HT and fullerene in chlorobenzene and spin-coated on a ITO glass, with a final architecture ITO (100 nm)/PEDOT (50 nm)/P3HT- C<sub>60</sub> (50 nm)/Al (50 nm), led to a PCE of 1.10%. This is not surprising, since the VTE of a polymer is harder than for an oligomer and then the polymer thermal degradation cannot be completely avoided.

Fig. 66 shows the surface morphology of OCT/C<sub>60</sub> and P3HT/C<sub>60</sub> blends made by thermal evaporation of components on ITO glass and annealed at 130°C for 30 minutes.

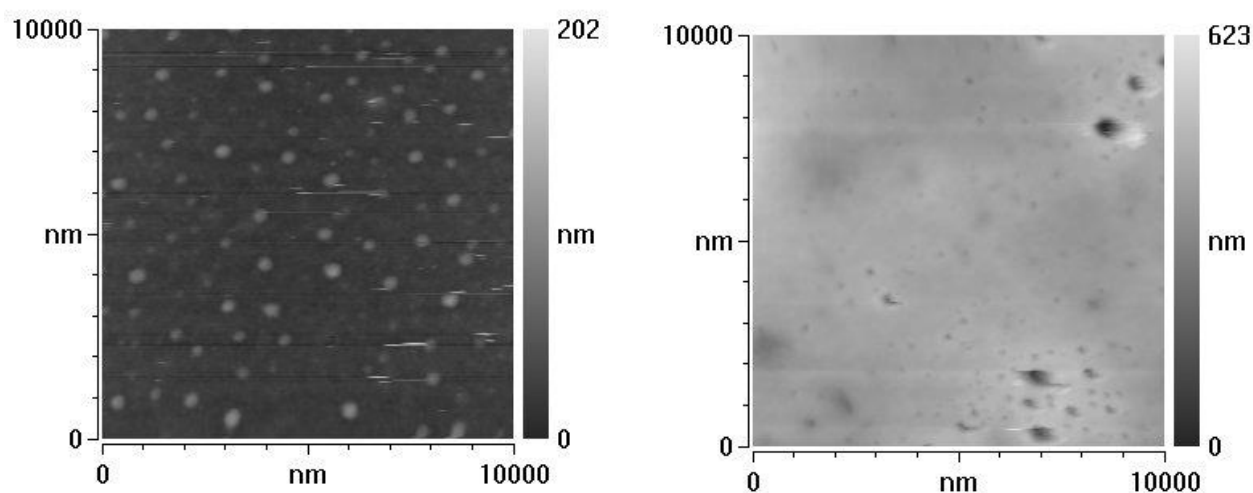


Figure 66. AFM images of OCT/C<sub>60</sub> (left) and P3HT/C<sub>60</sub> (right) evaporated blends.

AFM non-contact tapping mode images allowed the surface parameters to be determined: OCT/C<sub>60</sub> roughness (nm) 0.40, diameter (nm) 12; P3HT/C<sub>60</sub> roughness (nm) 0.66, diameter (nm) 16. The OCT blend showed the lowest root mean square (RMS) roughness and average diameter of grains, while the P3HT blend evidenced the highest roughness and diameter of crystallites, and this is probably due to the presence of nanoaggregated fullerene. Moreover, the latter sample showed the less uniform distribution of aggregates as well as the less homogeneous thickness of the polymeric layer and this fact could be ascribed to the poor chemical resistance of P3HT to the evaporation deposition system.

## ***5.4. CONCLUSIONS***

In this work we have successfully demonstrated that the VTE technique can be suitable for the deposition of photoactive blends for the construction of polymeric solar cells. This deposition method is very fast and effective since it facilitates the simultaneous deposition of the two components in the blend and does not require the presence of a buffer layer, such as PEDOT-PSS. However, this method cannot be applied to the entire range of conjugated polymers. In our experiments P3HT, unlike a tetrasubstituted octithiophene oligomer (OCT), was damaged during the evaporation procedure, thus leading to a final device with low photoconversion efficiency (0.35%). On the contrary, the low molecular weight oligothiophene derivative made it possible to obtain a polymeric solar cell with an acceptable efficiency (1.21%), notably higher than that showed by a sample prepared using conventional deposition techniques.

The VTE system is compatible with continuous manufacturing processes and can be effectively used in the preparation of a number of electronic or optoelectronic devices.



## REFERENCES FOR CHAPTER 5

- [1] W. Porzio, S. Destri, M. Pasini, A. Bolognesi, A. Angiulli, P. Di Gianvincenzo, D. Natali, M. Sampietro, M. Caironi, L. Fumagalli, S. Ferrari, E. Peron, F. Perissinotti *Mat. Sci. Eng. C* 26 (2006) 996-1001.
- [2] E. Mena-Osteritz *Adv. Mat.* 14 (2002) 609-616.
- [3] T. Kirschbaum, R. Azumi, E. Mena-Osteritz, P. Bauerle *New J. Chem.* (1999) 241-250.
- [4] V. C. Gonçalves, B. M. Nunes, D. T. Balogh, C. A. Olivati *Phys. Status Solidi A* 207 (2010) 1756-1759.
- [5] L. Ricciotti, F. Borbone, A. Carella, R. Centore, A. Roviello, M. Barra, G. Roviello, C. Ferone, C. Minarini, P. Morvillo *J. Polym. Sci. A Polym. Chem.* 51 (2013) 4351-4360.
- [6] B. B. M. Torres, D. T. Balogh *J. Appl. Polym. Sci* 124 (2012) 3222-3228.
- [7] P. Costa Bizzarri, C. Della Casa, M. Lanzi, F. Bertinelli, D. Iarossi, A. Mucci, L. Schenetti *Synth. Met.* 104 (1999) 1-7.
- [8] S. Günes, H. Neugebauer, N. S. Sariciftci *Chem. Rev.* 107 (2007) 1324-1338.
- [9] M. Lanzi, L. Paganin *React. Funct. Polym* 70 (2010) 346-360.
- [10] C. Shi, Y. Yao, Y. Yang, Q. Pei *J. Am. Chem. Soc.* 128 (2006) 8980-8986.
- [11] M. Lanzi, F. P. Di-Nicola, M. Livi, L. Paganin, F. Cappelli, F. Pierini *J. Mater. Sci* 48 (2013) 3877-3893.
- [12] Fang-Chung Chen, Chu-Jung Ko, Jyh-Lih Wu, Wei-Chi Chen *Sol. Energy Mater. Sol. Cells*, 94 (2010) 2426-2430.
- [13] M. T. Dang, L. Hirsch, G. Wantz, J. D. Wuest *Chem. Rev.* 113 (2013) 3734.
- [14] M. T. Dang, L. Hirsch, G. Wantz *Adv. Mater.* 23 (2011) 3597.
- [15] S. H. Eom, H. Park, S. H. Mujawar, S. C. Yoon, S. S. Kim, S. I. Na, S. C. Kang, D. Khim, D. Y. Kim, S. H. Lee *Organic Electronics* 11 (2010) 1516-1522.
- [16] F. Bloisi, A. Cassinese, R. Papa, L. Vicari, V. Califano *Thin Solid Films*, 516 (2008) 1594-1598.
- [17] H. Wei, L. Scudiero, H. Eilers *Appl. Surf. Sci* 255 (2009) 8593-8597.

- [18] P. Kovacik, G. Sforazzini, A. G. Cook, S. M. Willis, P. S. Grant, H. E. Assender, A. A. R. Watt *Applied Materials and Interfaces* 3 (2011) 11-15.
- [19] P. Kovacik, S. M. Willis, J. D. Matichak, H. E. Assender, A. A. R. Watt *Organic Electronics* 13 (2012) 687-696.
- [20] M. Lanzi, L. Paganin, D. Caretti *Polymer* 49 (2008) 4942-4928.
- [21] I. McCulloch, M. Heeney, C. Bailey, K. Genevicius, I. McDonald, M. Shkunov, D. Sparrowe, S. Tiemey, R. Wagner, W. Zhang, M. I. Chabinyc, R. J. Kline, M. D. McGehee, M. F. Toney *Nat. Mater.* 5 (2006) 328-333.
- [22] B. S. Ong, Y. Wu, P. Liu, S. Gardner *J. Am. Chem. Soc.* 126 (2004) 3378-3379.
- [23] R. S. Lowe, P. C. Ewbank, J. Liu, L. Zhai, R. D. McCullough *Macromolecules* 34 (2001) 4324-4333.
- [24] J. L. Segura, N. Martin, D. M. Guldi *Chem. Soc. Rev.* 34 (2005) 31.
- [25] N. Negishi, K. Yamada, Y. Takimiya, Y. Aso, T. Otsubo, Y. Harima *Chem. Lett.* 32 (2003) 404.
- [26] R. Fitzner, E. Reinold, A. Mishra, E. Mena-Osteritz, H. Ziehlke, C. Koerner, K. Leo, M. Riede, M. Weil, O. Tsaryova, A. Weiss, C. Uhrich, M. Pfeiffer, P. Bäuerle *Adv. Funct. Mater.* 21 (2011) 897.
- [27] S. Haid, A. Mishra, C. Uhrich, M. Pfeiffer, P. Bäuerle *Chem. Mater.* 23 (2011) 4435.
- [28] S. Steinberger, A. Mishra, E. Reinold, C. M. Mueller, C. Uhrich, M. Pfeiffer, P. Bäuerle *Org. Lett.* 13 (2011) 90.
- [29] S. Steinberger, A. Mishra, E. Reinold, J. Levichov, C. Uhrich, M. Pfeiffer, P. Bäuerle *Chem. Commun.* 47 (2011) 1982.
- [30] R. Fitzner, E. Mena-Osteritz, A. Mishra, G. Schulz, E. Reinold, M. Weil, C. Koerner, H. Zielke, C. Elschner, K. Leo, M. Riede, M. Pfeiffer, C. Uhrich, P. Bäuerle *J. Am. Chem. Soc.* 134 (2012) 11064.
- [31] T. C. Nason, J. A. Moore, T. M. Lu *Appl. Phys. Lett.* 60 (1992) 1866.
- [32] J. Y. Kim, K. Lee, N. E. Coates, D. Moses, T. Q. Nguyen, M. Dante, A. J. Heeger *Science* 317 (2007) 222-225.
- [33] P. J. Brown, D. S. Thomas, A. Kohler, J. S. Wilson, J. S. Kim, C. M. Ramsdale, H. Sirringhaus, R. H. Friend *Physical Review B*. 67 (6) (2003).

- [34] Y. D. Park, D. H. Kim, Y. Jang, J. H. Cho, M. Hwang, H. S. Lee, J. A. Lim, K. Cho *Organic Electronics* 7(6) (2006) 514-520.
- [35] F. Bertinelli, P. Costa Bizzarri, C. Della Casa, M. Lanzi *Synth. Met.* 122 (2001) 267-273.
- [36] F. Bertinelli, P. Costa Bizzarri, C. Della Casa, M. Lanzi *Spectrochimica Acta Part A* 58 (2002) 583-592.
- [37] M. Q. Jiang in *Rule of homologous linearity of organic compounds*, Science Press, Beijing, 1980, p. 184.
- [38] Y. H. Chou, S. Takasugi, R. Goseki, T. Ishizone W. C. Chen, *Polym. Chem.* 5 (2014) 1063-1071.
- [39] J. Abad, N. Espinosa, P. Ferrer, R. Garcia-Valverde, C. Miguel, J. Padilla, A. Alcolea, G. R. Castro, J. Colchero, A. Urbina *Sol. Energy Mater. Sol. Cells* 97 (2012) 109-118.
- [40] Z. Mo, K. B. Lee, Y. B. Moon, M. Kobayashi, A. J. Heeger, F. Wudl *Macromolecules* 18(10) (1985) 1972-1977.
- [41] P. Hermet, J. L. Baintignies, R. Almairac, J. L. Sauvajol, F. Serein, J. P. Lère-Porte *J. Phys. Chem. B* 112 (40) (2008) 12662.
- [42] Y. Li, Y. Cao, J. Gao, D. Wang, G. Yu, A. J. Heeger *Synth. Met.* 99 (1999) 243-248.
- [43] F. Parenti, P. Morvillo, E. Bobeico, R. Diana, M. Lanzi, C. Fontanesi, F. Tassinari, L. Schenetti, A. Mucci *Eur. J. Org. Chem* (2011) 5659-5667.
- [44] T. V. Richter, C. H. Braun, S. Link, M. Scheuble, E. J. W. Crossland, F. Stelzl, U. Wuerfel, S. Ludwigs *Macromolecules* 45 (2012) 5782-5788.
- [45] M. Dante, J. Peet, T. Q. Nguyen *J. Phys. Chem. C* 112 (2008) 7241-7249.
- [46] F. Ouhib, R. C. Hiorns, R. De Bettignies, S. Bailly, J. Desbrières, C. Dagron-Lartigau *Thin Solid Films* 516 (2008) 7199-7204.
- [47] T. L. Wang, Y. T. Shieh, C. H. Yang, T. H. Ho, C. H. Chen *Express Polym. Lett.* 7(1) (2013) 63-75.
- [48] L. Angiolini, T. Benelli, V. Cocchi, M. Lanzi, E. Salatelli *React. Funct. Polym.* 73 (2013) 1198-1206.
- [49] F. C. Krebs *Sol. Energy Mater. Sol. Cells* 93 (2009) 394-412.
- [50] R. R. Sondergaard, M. Hosel, F. C. Krebs *J. Polym. Sci. B* 51 (2013) 16-34.



## CHAPTER 6: A REGIOREGULAR

### POLYTHIOPHENE-FULLERENE FOR POLYMERIC

### SOLAR CELLS

#### *6.1 INTRODUCTION*

Organic photovoltaic (OPV) solar cells are devices based on either small organic semiconducting molecules or conjugated polymers capable of converting sunlight into electrical power. They are prepared by sandwiching a thin (from tens to a few hundred nanometers) film of an organic semiconductor between two electrodes. In the usual geometry, the electrons exit from the top electrode (usually Al) and positive holes from the bottom electrode (usually ITO which, thanks to its high transparency, allows for a good illumination of the photo-active layer); however, an inverted geometry has also been reported, in which electrons exit at the bottom and holes at the top.[1,2,3] The active layer, made by intermixing an electron-acceptor and an electron-donor material, is usually deposited either by spin-coating a solution of conjugated polymer/electron acceptor molecule on the ITO electrode or by vacuum-evaporating small organic molecules on the same substrate. In the latter case, some active materials can be easily synthesized and purified, thus increasing the photoconversion efficiency, while the processing speed is usually lower than for solution-processed conjugated polymers.[4] In any case, OPV solar cells are very attractive devices, being cost-effective, light-weight and particularly suitable for being scaled-up from a laboratory scale (usually a few square centimeters) to a commercial scale (many square meters) using roll-to-roll printing techniques.[5]

Among the different possible techniques for fabricating OPV cells, bulk heterojunction (BHJ) architecture has been studied intensively in recent years for its potential to obtain high efficiency at low costs. BHJ is essentially based on a bi-continuous network of an electron-donor (a conjugated polymer) and acceptor (fullerene or its derivatives) in which the two components are separated at a micro- or nanoscale level, with a high internal surface area where the ultrafast photoinduced charge transfer can occur; this way mobile holes in the donor phase and mobile electrons in the acceptor phase can be generated. The carriers produced are then driven to the electrodes by the cell internal field before they recombine in the photoactive layer.

The carrier generation and transport process is the key- mechanism which determines the main parameters of the BHJ solar cell, directly acting on the short-circuit current density ( $J_{sc}$ ), the fill factor (FF) and then the final power conversion efficiency (PCE).

The morphology and microstructure of the active layer are thus of primary importance, even if how to control them and at what degree of separation remain unclear, since a compromise is required between the need for a nanoscale separation (i.e. high interfacial area) for efficient exciton quenching, and the presence of larger domains (macrophase separation) for both the efficient transport of charges to the electrodes and an increased carrier lifetime [6].

With the aim of producing optimal phase segregation between the donor and acceptor molecules for charge generation while, at the same time, maintaining a continuous path in each phase for the efficient transport of electrons and holes, a number of strategies have been adopted. Among them, the synthesis of donor-acceptor double-cable polymers appears particularly intriguing. In fact, this architecture leads to the homogeneous distribution of the electron donor-acceptor (ED-EA) domains, at the same time maximizing the interface between them.[7] In these systems, the fullerene group is usually linked to the conjugated polymer (CP) main chain (generally a polythiophene derivative, exploiting the 3-position of the thiophenic units) by means of either an aromatic substituent<sup>8</sup> or an alkylic spacer which enhances the solubility of the final polymer by increasing the mobility of the EA group and, at the same time, electronically insulates the conjugated backbone from the C<sub>60</sub> aromatic molecule.[9,10]

Double-cable polymers allow for the optimized nanoscale phase separation of the EA/ED domains whose length scale must be comparable to exciton diffusion distance (10-20 nm [11]) by avoiding spontaneous phase separation; the latter is usually observed in conventional BHJ blends, and is caused by the very low entropy of mixing for high molecular weight polymers [12].

On these bases, the making of a “molecular heterojunction” by covalently grafting fullerene to polythiophene backbone may be considered a suitable alternative to the conventional BHJ architecture of OPV solar cells; in fact, this system exploits the same ED/EA moieties while retaining the positive electronic and photophysical properties of CP/fullerene composites but limiting phase separation and clustering phenomena. A drawback of double-cable polymer way to build polymeric solar cells is, indeed, the more complex synthetic route necessary to obtain the fullerene-functionalized monomers; this usually makes the conventional BHJ architecture - based on the simple mixing of the ED/EA components even if on a nanoscale separation - preferable when final power conversion efficiencies are essentially the same.

In this paper, we report on both the synthesis of a new thiophenic monomer bearing the C<sub>60</sub>-fullerene at the end of a hexylic side chain, and the preparation of a soluble thiophenic copolymer using the same procedure used for the monomer on a reactive polymeric precursor. The synthesis employed is

particularly interesting since it involves a very simple and straightforward procedure based on the Grignard-coupling between  $\omega$ -bromoalkyl-derivatives and C<sub>60</sub>-fullerene. The prepared copolymer was widely characterized using IR, NMR, GPC, UV-Vis spectroscopy, and DSC-TGA thermal analysis. The molecular arrangement of its thin films was studied by AFM measurements. Lastly, the current density/voltage (J/V) characteristics of the prepared solar cell were determined under one-sun illumination, in order to evaluate PCE when using the newly synthesized double-cable copolymer as a photoactive layer; these characteristics were also compared with those of a reference OPV solar cell made with BHJ conventional architecture.

## **6.2 EXPERIMENTAL**

### **6.2.1 Materials**

All reagents were purchased from Sigma-Aldrich Chemical Co. and used without further purification where not expressly indicated otherwise. All solvents used (HPLC grade) were dried and purified by normal procedures, stored under molecular sieves, and handled in a moisture-free atmosphere.

The reference polymer for solar cells, i.e. poly(3-hexylthiophene) (P3HT), was synthesized starting from 3-hexylthiophene (T6H) purchased from Sigma-Aldrich (CAS No. 1693-86-3, Product No. 399051) using the McCullough procedure, [13] regioregularity in HT dyads 96%, Mn 30.0 KDa, PDI 1.2.

### **6.2.2 Measurements**

<sup>1</sup>H NMR and <sup>13</sup>C NMR were recorded on a Varian Mercury Plus spectrometer using TMS as a reference. IR spectra were taken on KBr pellets (model compound and alkylthiophene-fullerene derivative) and Ge disk (thin polymer films) using a Perkin Elmer Spectrum One spectrophotometer. Molecular weights were determined by gel permeation chromatography (GPC) using polystyrene standards and THF as an eluent on a HPLC Lab Flow 2000 apparatus equipped with a PL Gel MXL column and a Linear Instrument UV-Vis detector model UVIS-200 working at 263 nm. Mass spectra were recorded on a Thermo Finnigan MAT95XP spectrometer. The elemental analysis of the prepared copolymers was performed by Redox Laboratory, Monza, Italy. UV-Vis spectra were recorded on a Perkin Elmer Lambda 19 spectrophotometer using polymer films on quartz slides cast from o-dichlorobenzene (ODCB) solutions using the doctor blading (DB) technique (average thickness: 150 nm). A DSC TA Instruments 2920 was used for the thermal analysis of the polymer by varying the

temperature from -50 to 200°C at a rate of 10°C min<sup>-1</sup> in a nitrogen atmosphere. A TGA TA Instruments 2050, operating in either an inert or an oxidizing atmosphere, was used to determine the decomposition temperatures of the polymer by heating samples from 30° to 900°C at a heating scan rate of 20°C min<sup>-1</sup>. AFM measurements were made on a Burleigh Vista instrument in a non-contact tapping mode using high resolution silicon-nitride tips.

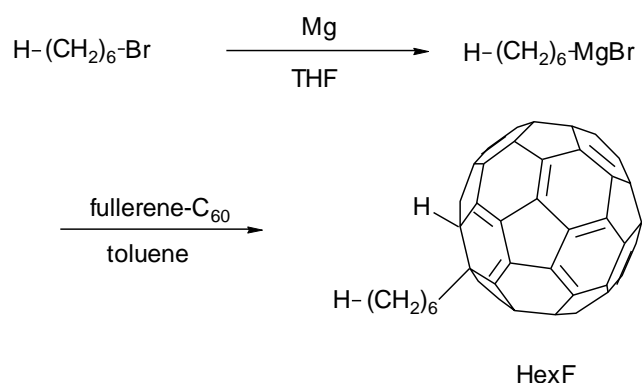
For the preparation of the solar cells, ITO glass (1×1 cm) was first cleaned in an ultrasonic bath using a non-foaming glass detergent in deionized water. ITO glass was then rinsed sequentially in double distilled water, isopropanol, and acetone. PEDOT:PSS (Aldrich Chemical Co.) was diluted 1:1 with isopropanol, filtered on a Gooch filter G2 and deposited by doctor blading on top of the cleaned ITO glass (film thickness about 80 nm) by means of a Sheen Instruments S265674. The glass slide was baked under a vacuum at 120°C for 2 h using a Büchi GKR-50 Micro Glass Oven. Anhydrous ODCB was used to prepare solutions of COP2 (7, 10, 13, and 15 mg ml<sup>-1</sup>), which were deposited by doctor blading on the PEDOT:PSS layer. More concentrated solutions of COP2 in ODCB determined the formation of a dark-red precipitate on the bottom of the vial. After baking films in a vacuum at 130°C for 15 min, the active layer film thicknesses measured by AFM were respectively 80, 100, 150 and 180 nm. Lastly, to create PSCs, 50 nm of Al were thermally deposited under a vacuum of  $6 \times 10^{-7}$  mmHg using an Edwards E306A vacuum coating apparatus. The active area of the cell was 0.25 cm<sup>2</sup>. The current-voltage characteristics were measured using a Keithley 2401 source meter under the illumination of a Abet Technologies LS 150 Xenon Arc Lamp Source AM1.5 Solar Simulator, calibrated with an ILT 1400-BL photometer. The reported PCE results were the averaged values obtained from 5 different devices prepared under the same operative conditions. The spectral response of the solar cells was measured using a SCSpecIII (SevenStar Optics, Beijing, PRC) incident photon to charge carrier efficiency (IPCE) setup.

## 6.3 SYNTHESSES OF MONOMERS

### 6.3.1 Synthesis of the model compound 1-fullerenylhexane (HexF)

Scheme 17 outlines the experimental route for the preparation of HexF.





*Scheme 17. Synthesis route for the preparation of HexF*

A solution of 0.837 g (5.07 mmol) of 1-bromohexane in 6 ml of anhydrous THF was added dropwise to 0.141 g (5.80 mmol) of Mg under stirring and in an inert atmosphere. The mixture was refluxed for 5h, cooled down to room temperature, and then transferred via cannula to a solution of 1.22 g (1.69 mmol) of C<sub>60</sub>-fullerene in 400 ml of anhydrous toluene and 2.30 ml of anhydrous N,N-dimethylformamide (DMF). The final mixture was reacted for 30 min under stirring at room temperature and in an inert atmosphere. The reaction was quenched with a solution of 100 mg of NH<sub>4</sub>Cl in 10 ml of distilled water and then added to 200 ml of brine. The organic phase was washed with distilled water to neutrality, dried with MgSO<sub>4</sub>, and concentrated. The crude product was dissolved in 50 ml of toluene and precipitated by adding 100 ml of MeOH dropwise to the solution. After filtration on a Teflon septum (0.45 μm pore size), 1.05 g of 1-fullerenylhexane (HexF) were recovered as a dark brown powder (77% yield).

<sup>1</sup>H NMR (400 MHz, CDCl<sub>3</sub>, δ): 6.48 (s, 1H, C<sub>60</sub>H), 3.45 (m, 2H, C<sub>60</sub>CH<sub>2</sub>), 2.60 (q, 2H, C<sub>60</sub>CH<sub>2</sub>CH<sub>2</sub>), 1.92-1.45 (bm, 6H, central methylenes), 1.05 (t, 3H, CH<sub>3</sub>).

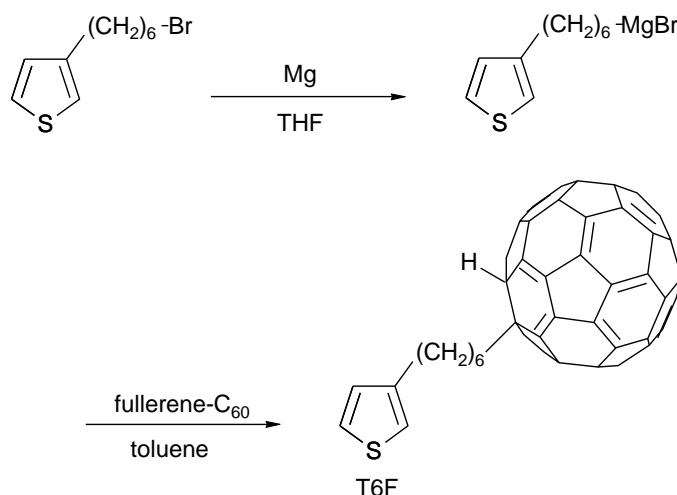
<sup>13</sup>C NMR (100 MHz, CDCl<sub>3</sub>, δ): 157.45 (2C, C<sub>60</sub>), 153.91 (2C, C<sub>60</sub>), 147.45 (1C, C<sub>60</sub>), 147.42 (1C, C<sub>60</sub>), 146.90 (2C, C<sub>60</sub>), 146.31 (2C, C<sub>60</sub>), 146.25 (2C, C<sub>60</sub>), 146.15 (2C, C<sub>60</sub>), 146.00 (2C, C<sub>60</sub>), 145.78 (2C, C<sub>60</sub>), 145.65 (2C, C<sub>60</sub>), 145.41 (2C, C<sub>60</sub>), 145.31 (2C, C<sub>60</sub>), 145.25 (2C, C<sub>60</sub>), 145.21 (2C, C<sub>60</sub>), 144.77 (2C, C<sub>60</sub>), 144.45 (2C, C<sub>60</sub>), 143.22 (2C, C<sub>60</sub>), 142.45 (2C+2C, C<sub>60</sub>), 142.10 (2C, C<sub>60</sub>), 141.95 (2C, C<sub>60</sub>), 141.85 (2C, C<sub>60</sub>), 141.78 (2C, C<sub>60</sub>), 141.68 (2C, C<sub>60</sub>), 141.55 (2C, C<sub>60</sub>), 141.45 (2C, C<sub>60</sub>), 140.44 (2C, C<sub>60</sub>), 140.00 (2C, C<sub>60</sub>), 137.22 (2C, C<sub>60</sub>), 135.85 (2C, C<sub>60</sub>), 61.03 (1C, C<sub>60</sub>CH<sub>2</sub>), 41.82 (1C, C<sub>60</sub>CH<sub>2</sub>), 31.03 (1C, CH<sub>2</sub>CH<sub>3</sub>), 29.98 (1C, CH<sub>2</sub>), 26.93 (1C, CH<sub>2</sub>), 22.88 (1C, CH<sub>2</sub>), 14.22 (1C, CH<sub>2</sub>CH<sub>3</sub>).

IR (KBr): ν = 2952, 2921, 2850, 1428, 1384, 1182, 577, 526 cm<sup>-1</sup>.

EIMS m/z (%): 807 (10) [M<sup>+</sup>], 806 (25) [M<sup>+</sup> - H].

### 6.3.2 Synthesis of 3-(6-fullerenylhexyl)thiophene (T6F)

Scheme 18 outlines the experimental route for the preparation of T6F.



*Scheme 18. Synthesis route for the preparation of T6F.*

1.24 g (5.07 mmol) of 3-(6-bromohexyl)thiophene prepared according to Ref. 14 in 6 ml of anhydrous THF was added dropwise to 0.141 mg (5.80 mmol) of Mg under stirring in an inert atmosphere. The mixture was refluxed for 5 h, cooled down to room temperature, and then transferred via cannula to a solution of 1.22 g (1.69 mmol) of C<sub>60</sub>-fullerene in 400 ml of anhydrous toluene and 2.30 ml of anhydrous N,N-dimethylformamide (DMF). The final mixture was reacted for 30 min under stirring and in an inert atmosphere. The reaction was quenched with a solution of 100 mg of NH<sub>4</sub>Cl in 10 ml of distilled water and then added to 300 ml of brine. The organic phase was washed with distilled water to neutrality, dried with MgSO<sub>4</sub> and concentrated. The crude product was dissolved in 75 ml of toluene and precipitated by adding 150 ml of n-pentane dropwise to the solution. After filtration on a Teflon septum (0.45 μm pore size), 1.20 g of 3-(6-fullerenylhexyl)thiophene (T6F) were recovered as a black powder with metallic lusters (80% yield).

<sup>1</sup>H NMR (400 MHz, ODCB-*d*<sub>4</sub>, δ): 7.21 (m, 1H, H5Th), 6.93 (m, 2H, H2Th+H4Th), 6.48 (s, 1H, C<sub>60</sub>H), 3.45 (m, 2H, C<sub>60</sub>CH<sub>2</sub>), 2.85 (m, 2H, ThCH<sub>2</sub>), 2.60 (m, 2H, C<sub>60</sub>CH<sub>2</sub>CH<sub>2</sub>), 2.00-1.25 (bm, 6H, central methylenes).

<sup>13</sup>C NMR (100 MHz, ODCB-*d*<sub>4</sub>, δ): 157.33 (2C, C<sub>60</sub>), 153.22 (2C, C<sub>60</sub>), 147.55 (1C, C<sub>60</sub>), 147.33 (1C, C<sub>60</sub>), 146.80 (2C, C<sub>60</sub>), 146.42 (2C, C<sub>60</sub>), 146.22 (2C, C<sub>60</sub>), 146.11 (2C, C<sub>60</sub>), 146.00 (2C, C<sub>60</sub>), 145.75 (2C, C<sub>60</sub>), 145.62 (2C, C<sub>60</sub>), 145.45 (2C, C<sub>60</sub>), 145.31 (2C, C<sub>60</sub>), 145.22 (2C, C<sub>60</sub>), 145.00 (2C, C<sub>60</sub>), 144.67 (2C, C<sub>60</sub>), 144.45 (2C, C<sub>60</sub>), 143.18 (2C, C<sub>60</sub>), 142.35 (2C+2C, C<sub>60</sub>), 142.10 (2C, C<sub>60</sub>), 141.95 (2C, C<sub>60</sub>),

141.85 (2C, C<sub>60</sub>), 141.78 (2C, C<sub>60</sub>), 141.68 (2C, C<sub>60</sub>), 141.53 (2C, C<sub>60</sub>), 141.43 (2C, C<sub>60</sub>), 140.65 (2C, C<sub>60</sub>), 140.11 (2C, C<sub>60</sub>), 139.92 (1C, ThC3), 137.28 (2C, C<sub>60</sub>), 135.98 (2C, C<sub>60</sub>), 135.70 (1C, ThC5), 128.91 (1C, ThC2), 125.85 (1C, ThC4), 61.22 (1C, C<sub>60</sub>CH<sub>2</sub>), 41.62 (1C, C<sub>60</sub>CH<sub>2</sub>), 30.60 (1C, CH<sub>2</sub>Th), 29.88 (1C, CH<sub>2</sub>), 29.60 (1C, CH<sub>2</sub>), 26.20 (2C, CH<sub>2</sub>).

IR (KBr):  $\nu$  = 3101, 3051, 2924, 2851, 1512, 1461, 1427, 1173, 766, 671, 576, 526 cm<sup>-1</sup>.

EIMS m/z (%): 889 (35) [M<sup>+</sup>], 888 (60) [M<sup>+</sup> - H].

## 6.4 SYNTHESSES OF POLYMERS

### 6.4.1 Synthesis of Poly[3-hexylthiophene-co-3-(6-bromohexyl)thiophene] (COP1)

1.02 ml of a CH<sub>3</sub>MgCl 3.0 M solution in anhydrous THF was added to 0.80 g (2.45 mmol) of 2,5-dibromo-3-hexylthiophene (2,5BT6H) and 0.25 g (0.61 mmol) of 2,5-dibromo-3-(6-bromohexyl)thiophene (2,5BT6Br) in 20 ml of anhydrous THF. The mixture was refluxed for 2 h under stirring in inert atmosphere and then 8.29 mg (0.015 mmol) of NiDPPPCl<sub>2</sub> were added and the reaction refluxed for 1 h. After cooling down to room temperature, the copolymer was recovered by adding 30 ml of methanol to the solution and subsequent filtration on a PTFE membrane (0.45  $\mu$ m pore size). The copolymer was dissolved in 15 ml of CHCl<sub>3</sub> and reprecipitated with 50 ml of methanol, leading to 0.455 g (2.50 mmol, 82% yield) of dark-red COP1.

<sup>1</sup>H NMR (400 MHz, CDCl<sub>3</sub>,  $\delta$ ): 6.98 (s, H4Th), 3.43 (t, CH<sub>2</sub>Br), 2.90-2.45 (2bm, ThCH<sub>2</sub>), 1.90-1.25 (bm, central methylenes), 0.89 (t, CH<sub>3</sub>).

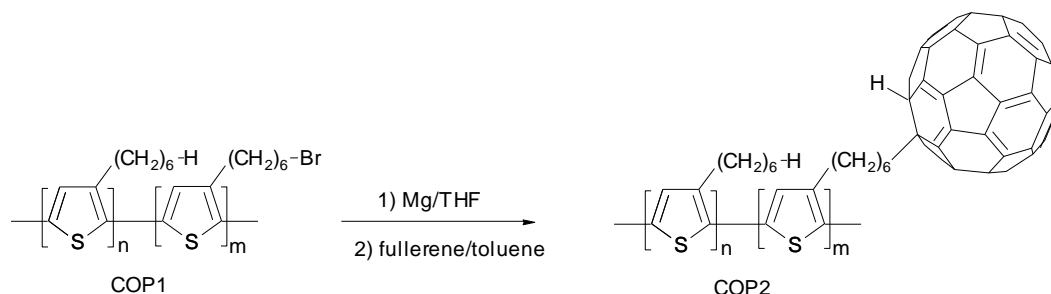
<sup>13</sup>C NMR (100 MHz, CDCl<sub>3</sub>,  $\delta$ ): 140.29 (ThC3), 134.35 (ThC5), 131.30 (ThC2), 129.25 (ThC4), 34.63 (CH<sub>2</sub>Br), 33.91 (CH<sub>2</sub>CH<sub>2</sub>Br), 30.91 (CH<sub>2</sub>Th), 29.94 (CH<sub>2</sub>), 29.30 (CH<sub>2</sub>), 27.15 (CH<sub>2</sub>), 22.91 (CH<sub>2</sub>CH<sub>3</sub>), 15.10 (CH<sub>3</sub>).

IR (Ge):  $\nu$  = 3050, 2955, 2927, 2853, 1560, 1510, 1458, 1375, 1260, 1235, 1089, 830, 729, 643, 561 cm<sup>-1</sup>.

Anal calcd for [(C<sub>10</sub>H<sub>13</sub>BrS)<sub>0.2</sub> (C<sub>10</sub>H<sub>14</sub>S)<sub>0.8</sub>]<sub>n</sub>: C 65.97, H 7.64, Br 8.78, S 17.61; found: C 65.15, H 7.55, Br 8.95, S 18.35.

### 6.4.2 Synthesis of Poly[3-hexylthiophene-co-3-(6-fullerenylhexyl)thiophene] (COP2)

Scheme 19 shows the synthesis of the copolymer COP2.



Scheme 19. Synthesis of copolymer COP2

0.407 g (2.24 mmol) of COP1 in 10 ml of anhydrous THF was added dropwise to 0.062 mg (2.56 mmol) of Mg under stirring in an inert atmosphere. The mixture was refluxed for 5 h, cooled down to room temperature, and then transferred via cannula to a solution of 0.539 g (0.747 mmol) of C<sub>60</sub>-fullerene in 200 ml of anhydrous toluene and 1.10 ml of anhydrous N,N-dimethylformamide (DMF). The final mixture was reacted for 30 min under stirring in an inert atmosphere. The reaction was quenched with a solution of 50 mg of NH<sub>4</sub>Cl in 5 ml of distilled water and then added to 150 ml of brine. The organic phase was washed with distilled water to neutrality, dried with MgSO<sub>4</sub> and concentrated. The copolymer was then fractionated by redissolving it in 75 ml of toluene and then slowly adding the solution to 150 ml of n-pentane. After filtration through a Teflon membrane (0.45 μm pore size), 0.571 g of fractionated COP2 were obtained (81% yield).

<sup>1</sup>H NMR (400 MHz, ODCB-*d*<sub>4</sub>, δ): 7.00 (m, H4Th), 6.40 (s, C<sub>60</sub>H), 3.45 (m, C<sub>60</sub>CH<sub>2</sub>), 2.80-2.55 (bm, ThCH<sub>2</sub> + C<sub>60</sub>CH<sub>2</sub>CH<sub>2</sub>), 2.00-1.25 (bm, central methylenes), 0.95 (t, CH<sub>3</sub>).

<sup>13</sup>C NMR (100 MHz, ODCB-*d*<sub>4</sub>, δ): 157.43 (C<sub>60</sub>), 153.50 (C<sub>60</sub>), 147.92 (C<sub>60</sub>), 147.15 (C<sub>60</sub>), 146.95 (C<sub>60</sub>), 146.52 (C<sub>60</sub>), 146.31 (C<sub>60</sub>), 146.15 (C<sub>60</sub>), 146.05 (C<sub>60</sub>), 145.85 (C<sub>60</sub>), 145.65 (C<sub>60</sub>), 145.50 (C<sub>60</sub>), 145.35 (C<sub>60</sub>), 145.25 (C<sub>60</sub>), 145.05 (C<sub>60</sub>), 144.75 (C<sub>60</sub>), 144.35 (C<sub>60</sub>), 143.10 (C<sub>60</sub>), 142.45 (C<sub>60</sub>), 142.20 (C<sub>60</sub>), 141.90 (C<sub>60</sub>), 141.80 (C<sub>60</sub>), 141.70 (C<sub>60</sub>), 141.62 (C<sub>60</sub>), 141.55 (C<sub>60</sub>), 141.40 (C<sub>60</sub>), 140.95 (ThC3), 140.68 (C<sub>60</sub>), 140.15 (C<sub>60</sub>), 137.25 (C<sub>60</sub>), 135.95 (C<sub>60</sub>), 135.15 (ThC5), 129.80 (ThC2), 126.80 (ThC4), 61.22 (C<sub>60</sub>CH<sub>2</sub>CH<sub>3</sub>), 42.65 (C<sub>60</sub>CH<sub>2</sub>), 31.95 (CH<sub>2</sub>CH<sub>3</sub>), 30.55 (CH<sub>2</sub>Th), 29.88 (CH<sub>2</sub>), 29.63 (CH<sub>2</sub>), 26.22 (CH<sub>2</sub>), 14.55 (CH<sub>2</sub>CH<sub>3</sub>).

IR (Ge): ν = 3049, 2954, 2923, 2851, 1538, 1460, 1428, 1377, 1173, 829, 576, 526 cm<sup>-1</sup>.

Anal calcd for [(C<sub>70</sub>H<sub>14</sub>S)<sub>0.2</sub> (C<sub>10</sub>H<sub>14</sub>S)<sub>0.8</sub>]<sub>n</sub>: C 85.12, H 4.55, S 10.33; found: C 84.85, H 4.65, S 10.50.

## 6.5 RESULTS AND DISCUSSION

The control of the morphology of the active layer in the polymeric photovoltaic cells is a very important parameter since it is necessary to maximize the surface area of the p-n junction in order to achieve a high energy conversion efficiency [15,16]. In fact, the blend morphology can directly influence the conformational order of the conjugated backbone, while it is well known that a low degree of the polythiophene intra- and inter-chain disorder [17] may lead to a strong increase in hole mobility and, consequently, in charge carrier generation and extraction efficiency [18].

Moreover, recently, some thin films of organic polymers have been deposited on ITO glass or plastic surfaces by ink-jet printing [19] or screen printing [20], thus demonstrating that the development of fast, reproducible, homogeneous and stable film-forming techniques is of the utmost interest.

In addition to a physical (thermal) approach, several chemical methods may also be used for controlling the morphology within the photoactive layer, in order to minimize the separation of the donor-acceptor compounds. One of these methods consists of synthesizing a conjugated p-type macromolecule bearing a fullerene molecule linked to its backbone. This method is particularly interesting and chemically elegant, since a single polymeric material would possess the ability to transport both the electrons and the holes (double-cable polymer). This would then lead to a fast inter- and intra-chain transport of positive holes and also to a more rapid displacement of the electrons along the fullerenes [21]. In addition, the interfacial area between the donor and acceptor would be maximized and segregation would be avoided. In this regard, J. R. Durrant et al. in a very recent paper [22], stress the fact that the use of donor copolymers with a high degree of D-A character can be particularly effective in reducing the energy offset requirement for an efficient charge separation, thus leading to high efficient organic solar cell devices.

In this work, a new thiophenic monomer containing fullerene in the side chain was synthesized using the Grignard-coupling reaction; this synthesis method made it possible to use C<sub>60</sub>-fullerene directly as the starting material, without either resorting to its expensive derivatives (e.g. PCBM) or preparing fulleropyrrolidine intermediates [23]. Moreover, the Grignard reaction involves few simple and straightforward steps, making the preparation of the monomer particularly easy, efficient, and interesting. Before proceeding to the synthesis of the fullerene-substituted thiophenic monomer, i.e. 3-(6-fullerenylhexyl)thiophene (T6F), we attempted to synthesize a model compound, in order to verify the actual feasibility of synthesis. The monoaddition of the Grignard reagent to C<sub>60</sub>-fullerene was inspired by the paper of Nakamura et al. [24] We started from 1-bromohexane, which is quite similar to 3-(6-bromohexyl)thiophene, but devoid of the thiophene moiety.

The reaction was carried out in an inert atmosphere using freshly distilled anhydrous THF, by reacting 1-bromohexane with Mg turnings. The obtained mousey-gray Grignard solution was transferred via a PTFE cannula into a second flask containing the C<sub>60</sub>-fullerene solubilized in toluene/DMF. The reaction mixture was left at room temperature for 15 min and then quenched with ammonium chloride; subsequently, the solvent was evaporated at reduced pressure. HexF was purified by fractionation using a toluene/methanol solution and recovered, after filtration, as a dark brown powder with a good yield.

The product obtained was characterized by <sup>1</sup>H and <sup>13</sup>C NMR, IR, and mass spectroscopy (see Experimental section).

The <sup>1</sup>H NMR spectrum shows the expected signals; in details, the triplet ascribable to the terminal -CH<sub>3</sub> protons can be found at 1.05 ppm, the two quintets attributable to the internal -CH<sub>2</sub>- protons of the alkyl chain between 1.45 and 1.92 ppm and the quintet due to the -CH<sub>2</sub>- protons β to the fullerene group at 2.60 ppm. The multiplet at 3.45 ppm is relative to the -CH<sub>2</sub>- directly linked to the fullerene: it is not a triplet due to the conformational stability of the alkyl chain linked to the fullerene; in fact, even if the bridge methylenic group is able to rotate, most of the time it maintains a specific conformation. This results in two hydrogen atoms which are chemically identical but magnetically different, whose couplings may be described by an AA'BB' system, giving the observed characteristic peak profile [25]. Lastly, the singlet due to the directly fullerene-linked hydrogen can be found at 6.48 ppm. The <sup>13</sup>C NMR spectrum, the IR spectroscopy and the mass analysis also confirm the HexF expected structure.

Once the ability to bind an alkyl halide directly to the fullerene via the Grignard reaction was confirmed, we proceeded with the synthesis of the monomer of interest (T6F). The reaction conditions used were analogous to those reported for the model compound, except for the purification conditions.

This time the <sup>1</sup>H NMR spectrum was recorded in deuterated o-dichlorobenzene, since T6F is more soluble in this solvent than in chloroform (25 mg/ml vs 8 mg/ml). Thanks to the previous study of the model compound, it was possible to state that the reaction was successful in this case also.

In particular, the singlet relative to the proton directly linked to fullerene is clearly visible at 6.48 ppm, the multiplet relative to the -CH<sub>2</sub>- α and β to the fullerene group at 3.45 and 2.60 ppm respectively, and the multiplet of the methylenic protons α to the thiophenic ring at 2.85 ppm. Lastly, the last three multiplets in the 1.25-2.00 ppm range are related to the central methylene groups of the alkylic side chain. Thiophenic aromatic protons appear partially embedded with the solvent signals and are found at 7.21 (H5) and 6.93 ppm (H2+H4).

The <sup>13</sup>C NMR spectrum of the monomer is also in good agreement with the expected structure.

The presence of head-to-head (HH) couplings among the repeating units of poly(3-alkylthiophene)s affects the polymer conformation, leading to poor electrical conductivity,<sup>26</sup> low values of conjugation length<sup>27</sup> and then low power conversion efficiencies in BHJ solar cells<sup>28</sup>. Therefore we decided to polymerize T6F using a regiospecific procedure, namely the Grignard Metathesis (GRIM)<sup>29</sup> polymerization reaction, which involves the cross-coupling of organomagnesium intermediates prepared by reacting a 2,5-dibromothiophene derivative with a pre-formed Grignard's reactive (usually methylmagnesium chloride or isopropylmagnesium bromide) in the presence of a Ni(II) catalyst. Unfortunately, the dibromination of T6F to obtain 2,5-dibromo-3-(6-fullerenylhexyl)thiophene did not give any acceptable results since the bromination of the fullerene moiety was unavoidable even using mild reaction conditions, i.e. adding the N-bromosuccinimide in two subsequent steps and operating at 0°C in anhydrous N,N-dimethylformamide.

An alternative procedure was then used, namely the insertion of the fullerenic substituent on a pre-synthesized polymeric precursor: a technique known as post-polymerization functionalization (PPF) [30].

As it may be inferred from the data reported in Table 9, a satisfactory yield of the regioregular polymeric precursor COP1 was obtained by reacting 2,5-dibromo-3-hexylthiophene and 2,5-dibromo-3-(6-bromohexyl)thiophene in a 80:20 molar ratio with one equivalent of CH<sub>3</sub>MgCl in anhydrous THF. The adopted synthetic strategy is not only easy to perform, but it also produces a polymer with appreciable molecular weight and microstructural features. COP1 is, in fact, characterized by a good DP<sub>n</sub> (185 r.u.) and a high degree of regioregularity (96% in HT dyads content), as determined by the integral ratio of the signals at 2.90 and 2.45 ppm in the <sup>1</sup>H-NMR spectrum [31].

Table 9. Copolymers characteristics.

Polymer	Yield <sup>a</sup> [%]	HT dyads <sup>b</sup> [%]	M <sub>n</sub> <sup>c</sup> [KDa]	M <sub>w</sub> /M <sub>n</sub>
<b>COP1</b>	82	96	33.7	1.3
<b>COP2</b>	81	96	55.0	1.2

<sup>a</sup> In fractionated polymer

<sup>b</sup> Regioregularity expressed as Head-to-Tail dyads percentage

<sup>c</sup> Determined by GPC relatively to polystyrene standards

COP1 was then dissolved in anhydrous THF and reacted with metallic Mg and then with a solution of fullerene in toluene using the same procedure used for the preparation of T6F from T6Br.

After filtration, the resulting black powder was brought to dryness at 50°C in a vacuum oven. The high content of the non-functionalized monomer in COP2 allowed for both its good solubility in common organic solvents and its high post-polymerization functionalization reaction yield (86%).

The solubility of COP2 was 15 mg/ml in ODCB and 5 mg/ml in CHCl<sub>3</sub> and its molecular weight, determined via GPC with respect to polystyrene standards, was:  $M_n=55.000$  g/mol with a polydispersity index (PDI) of 1.2.

Figure 67 shows the <sup>1</sup>H NMR spectrum of COP2.

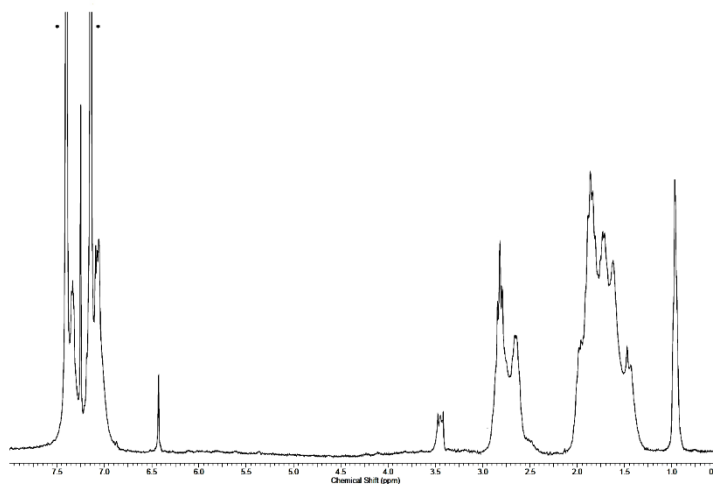


Figure 67. <sup>1</sup>H NMR spectrum of COP2 in ODCB-*d*<sub>4</sub>.

The <sup>1</sup>H NMR spectrum of COP2 shows the signals ascribable to both the monomers but some of them are superimposed since the two repeating units differ only in the final group of the side chain. However, some peaks can be unequivocally ascribed, like those at 0.95 ppm (protons of the terminal -CH<sub>3</sub> group of the alkyl chain of the non-functionalized monomer) and at 3.45 ppm (-CH<sub>2</sub> directly linked to the fullerene). All signals between 1.25 and 2.00 ppm are due to the central methylenic groups of the alkyl chains of the two monomers. The multiplet in the range between 3.00 and 2.55 ppm is attributable to the signals of methylenic protons α- and β- to thiophene and fullerene, respectively. The overlapping of these signals makes it impossible to directly determine the regioregularity of the copolymer using <sup>1</sup>H-NMR.

At 6.40 ppm the signal of the proton directly attached to the fullerene group is evident and, lastly, in the aromatic region, the signal ascribable to thiophene H-4 can be found at 7.00 ppm.

The composition of COP2 was determined by comparing the integral of the signal of the -CH<sub>3</sub> group belonging to the alkyl monomer at 0.95 ppm with the integral of the peak at 3.45 ppm, concerning



methylenes  $\alpha$  to fullerene (this time, also, a multiplet and not a triplet), which is present only in the functionalized monomer. COP2 has a 20% molar content of T6F, thus proving the effectiveness of the employed PPF reaction, since all –Br groups have been substituted by the C<sub>60</sub> moiety.

As evidenced by <sup>13</sup>C-NMR analysis of COP2 (Figure 1 in the Supporting Information section), the signals at 34.63 and 33.91 ppm, ascribable to the presence of the –Br group in the side chains, clearly observable in COP1 spectrum, are completely missing in COP2 spectrum, thus confirming the complete bromine atom substitution by the fullerene group.

The signals reported in the Experimental section confirm what was said about the proton spectrum. Moreover, the presence of only four evident signals ascribable to thiophenic carbons suggests the prevalence of one kind of configurational triad in the COP2 structure. This is not surprising, since the PPF reaction does not involve the polymer main chain but only the reactive functional groups at the end of the side chains.

Figure 68 shows the IR spectrum of T6F, COP1 and COP2 as a thin film on the Ge disk, while the main IR bands of the model compound, T6F, and copolymers COP1 and COP2 are listed in Table 10 together with their respective assignments.

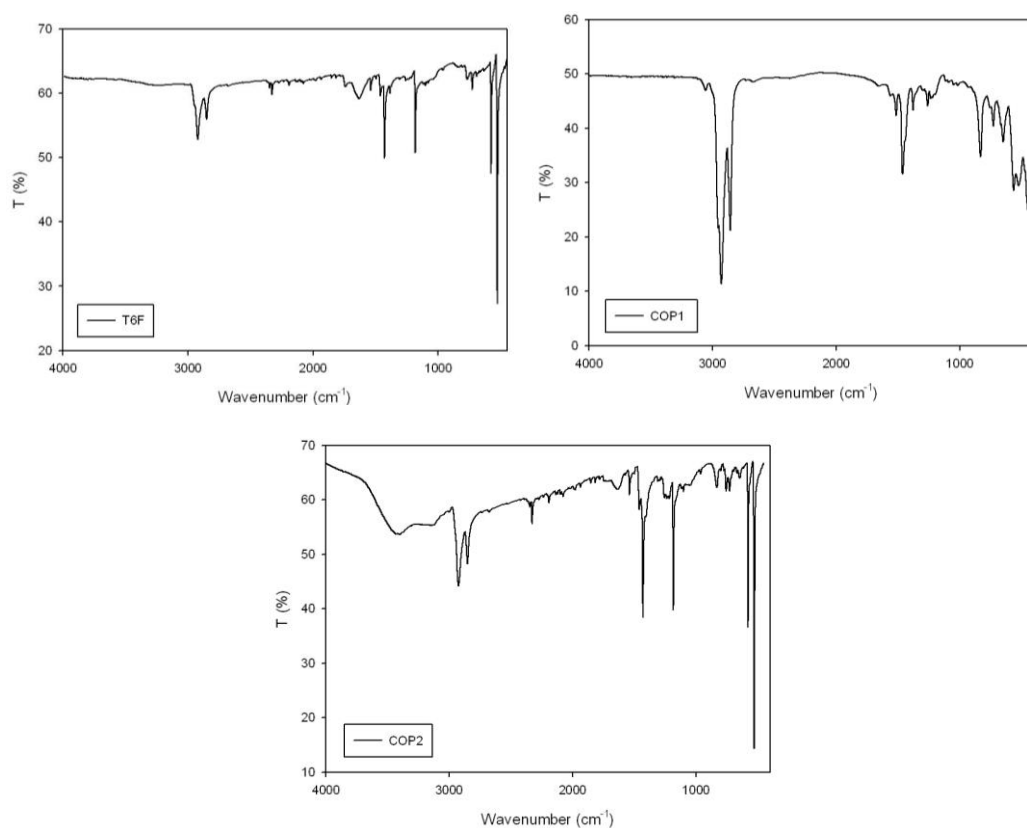


Figure 68. IR spectra of T6F, COP1 and COP2.

Table 10. IR absorption bands (in cm<sup>-1</sup>) and respective assignments for the synthesized materials

Assignment	HexF	T6F	COP1	COP2
$\nu$ C-H $\alpha$ thiophene	-	3101	-	-
$\nu$ C-H $\beta$ thiophene	-	3051	3050	3049
$\nu_{as}$ CH <sub>3</sub>	2952	-	2955	2954
$\nu_{as}$ CH <sub>2</sub>	2921	2924	2927	2923
$\nu_{sym}$ CH <sub>2</sub>	2850	2851	2853	2851
$\nu_{as}$ C=C thiophene	-	1512	1510	1538
$\nu_{as}$ C=C thiophene	-	1461	1458	1460
fullerene	1428	1427	-	1428
-CH <sub>3</sub> deformation	1384	-	1375	1377
fullerene	1182	1173	-	1173
$\gamma$ C-H thioph. 2,3,5-trisubstituted	-	-	830	829
$\gamma$ C-H thioph. 3-substituted	-	766, 671	-	-
$\nu$ C-Br			643, 561	
fullerene	577, 526	576, 526		576, 526

$\nu$  = stretching;  $\gamma$  = out of plane bending

The IR analysis of the copolymers confirmed the expected structures. In fact, the characteristic absorptions of the 3-alkylthiophenic system are clearly evident, as well as those related to the particular functional groups, i.e. the halogen at 643 and 561 cm<sup>-1</sup> and the fullerene moiety at about 1428, 1180, 576 and 526 cm<sup>-1</sup>. Moreover, in the copolymers spectra, the band at 3101 cm<sup>-1</sup> is absent, while that at about 3050 cm<sup>-1</sup> is evident and the bands at 766 and 671 cm<sup>-1</sup> are replaced by that at 829 cm<sup>-1</sup>. These observations

confirm that the repeating units of copolymers are linked through the  $\alpha$  positions of thiophene rings (absence of  $\alpha$ - $\beta$  and  $\beta$ - $\beta$  couplings), thus benefiting the structural regularity and electron delocalization.

Figure 69 shows the UV-Vis spectrum of COP2 and of P3HT/PCBM blend on a quartz slide cast from ODCB solution.

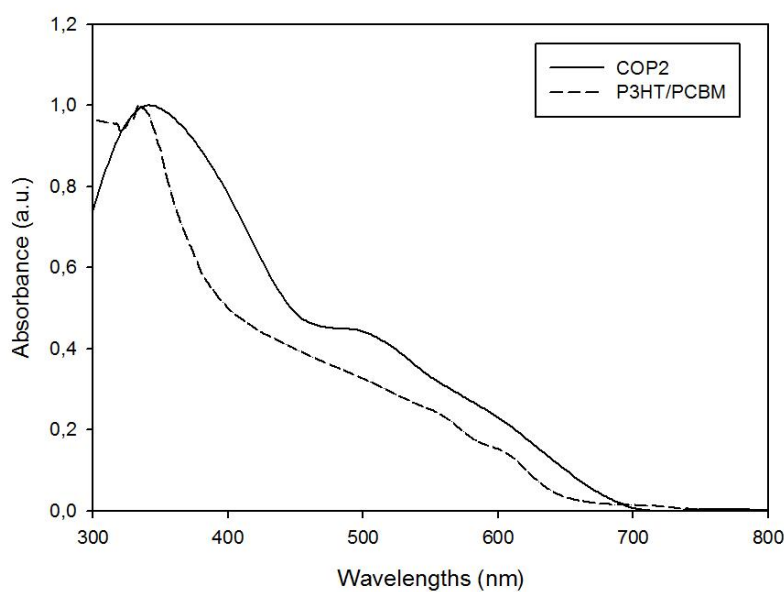


Figure 69. UV-Vis spectrum of COP2 and P3HT/PCBM blend in film

The absorbance around 340 nm is attributable to the fullerene derivative [32,33] (in the side chain, for COP2, and in the blend for P3HT) which, given the intense absorbance, appears to be a particularly efficient chromophoric system. The shoulder around 500 nm, particularly evident in COP2 spectrum, is attributable to the polythiophenic system while the presence of a further shoulder at 600 nm, albeit of weak intensity, indicates the formation of  $\pi$ -stacking between thiophene rings [34]. Even if COP2 is a copolymer between two thiophenes bearing different groups in the side chain - one of which is particularly bulky - the structured profile of the spectrum clearly evidences the presence of a conformational order among the polymeric main chains.

The DSC thermogram of COP2 (Figure 70) shows an evident endothermic flexure at 29°C (glass transition temperature) and two endothermic peaks at 95°C and 155°C which are ascribable to the melting of crystalline domains determined by the packing of side chains and backbones, respectively.

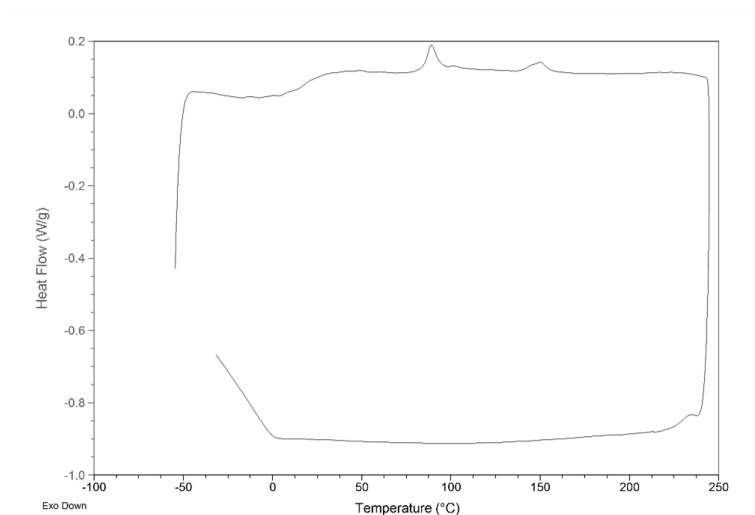


Figure 70. DSC curve of COP2.

It is interesting to note that, for the usually employed poly(3-hexylthiophene) (rrP3HT, Aldrich Chemical Co., %HT dyads >95%, Mn: 15000-45000, CAS No. 156074-98-5, Code No. 698989), the main chain melting transition occurs at around 200°C and the  $T_g$  at -4.7°C,<sup>35,36</sup> while COP2 has a lower  $T_m$  but a higher  $T_g$  than the reference polymer; the selection of polymers with the highest possible glass transition temperature is an important prerequisite for the thermal stability of the photoactive blend in order to avoid the demixing of its components.<sup>37,38</sup> The lower  $T_m$  of COP2 with respect to the reference polymer can be ascribed to the higher steric hindrance of the substituent of the former, since bulky groups in polythiophene side chains generally hinder the crystallization process of the polymer.<sup>39</sup> Moreover, the higher  $T_g$  of COP2 can be explained in terms of the reduced mobility of the side chains, as already evidenced in the <sup>1</sup>H-NMR section (vide infra).

The COP2 thermal stability was investigated by the TGA analysis both under nitrogen and in air at a heating scan of 20°C min<sup>-1</sup>. The thermograms obtained are shown in Figure 71.

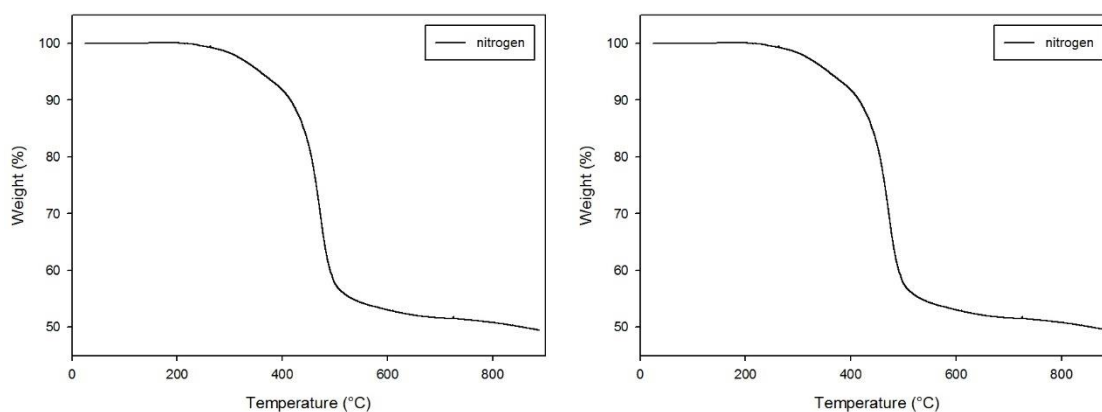


Figure 71. TGA graphs of COP2 under nitrogen and in air.

In nitrogen, COP2 is stable up to around 300°C, after which the thermal decomposition begins with a two-step weight loss. The second step begins at around 400°C. In air, the decomposition starts at around 275°C and the second step always at 400°C. This time, a third degradation step can be observed and, over 600°C, no residual product can be found. These results agree with those obtained by Kumar et al., [40] showing that the addition of carbon nanotubes or C<sub>60</sub> fullerene to poly(3-hexylthiophene) reduces its thermal stability.

Figure 72 shows the J-V characteristic curves of solar cells which have the structure of ITO/PEDOT:PSS/photoactive layer/Al under AM 1.5 one sun illumination (100 mW cm<sup>-2</sup>).

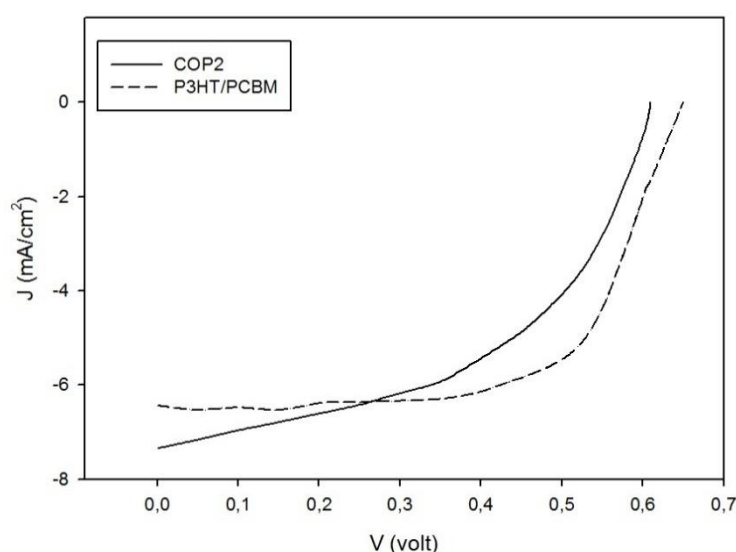


Figure 72. Current density-voltage for tested cells under AM 1.5 one sun illumination.

As reference cell we used a P3HT/PCBM 1:1 weight ratio, since some studies have shown that devices with this ratio achieve the highest power conversion efficiency [41,42]. The cell made with COP2 did not require the use of PCBM, since fullerene was already present in this copolymer, at a loading of approximately 46% wt. We tried to optimize the deposition conditions of the active layers by acting both on the thickness of the blend and on the annealing temperature. In fact, these important parameters directly affect the PCE of the final device through the light absorption efficiency as well as the morphology of the photoactive blend, mainly acting on the J<sub>sc</sub> of the PSC [43]. The effect of the thickness of the active layer was examined by depositing, using the doctor blade, COP2 solutions in ODCB at different concentrations (Table 2). The thermal annealing of the photoactive layer was performed at 130°C for 15 min in a vacuum, since these conditions gave the best results. The best conditions for the reference cell were found to be: P3HT:PCBM 1:1 (w/w) and 15 wt% solution in ODCB, leading to a 160 nm-thick film after doctor blade deposition.

A summary of the averaged J-V characteristics, based on the analysis of 5 devices, is given in Table 11.

Table 11. Photovoltaic parameters for the devices obtained using the two different photoactive polymers.

Polymer	$J_{sc}$ [mA cm <sup>-2</sup> ]	$V_{oc}$ [V]	FF [%]	PCE [%]
<b>COP2</b>	10.7	0.58	52.0	3.21
<b>P3HT/PCBM</b>	7.20	0.63	55.1	2.50

The results obtained for the P3HT/PCBM device are in good agreement with those reported in the literature; in fact, we obtained a 3.53% of PCE with a 160 nm thick film, after an annealing time of 15 min at 130°C, whereas the best conditions reported for the same system were an annealing time of 10 min at 130°C using a 150 nm thick film, giving a 3.60% of PCE.<sup>43</sup> In the COP2 case, the best results were obtained with a 150 nm thick film with the same annealing conditions used for the reference cell, leading to a superior PCE performance of 4.19%.

The IPCE plots of the best devices under short circuit conditions are shown in Figure 73.

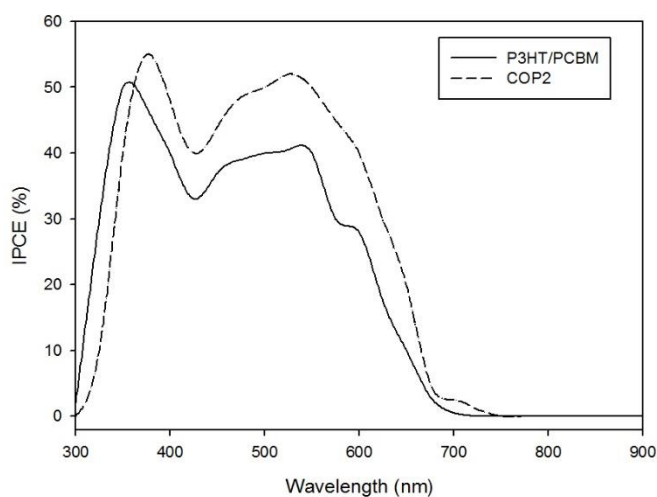


Figure 73. IPCE curves of the prepared OPV solar cells.

The photo-current response wavelength of the cells based on the P3HT/PCBM photoactive blend and on the COP2 layer range from 290 to 700 nm and 310 to 750 nm, respectively. The curve of the device based on the reference cell has two feature peaks at 355 and 575 nm and a shoulder at 600 nm, whereas the device based on the copolymer shows only two peaks at 400 and 580 nm. The IPCE

profile of COP2 follows the trend observed in the absorption spectra of the copolymer in film, indicating that the harvested photons over the whole absorption spectrum contribute to the photocurrent. Moreover, an enhanced quantum efficiency is observed in the device made with COP2 as compared to the device made with P3HT/PCBM, thus suggesting an improved charge collection efficiency of the copolymer.

The results obtained clearly show that the performance of the double-cable based solar cells is higher than that of the device prepared following the conventional bulk-heterojunction approach, and reaches a PCE higher than the value reported in literature for BHJ solar cells made with poly(alkyl)thiophenes (P3ATs)/PCBM with a conventional architecture (3.57%) [44].

To analyze the morphology of solar cells, we chose to use atomic force microscopy (AFM). Figure 74 shows the surface morphology of the reference blend, i.e. P3HT and PCBM (1:1 weight ratio), as well as of a film of COP2 on ITO glass. The two films had similar thickness (about 150 nm) and were prepared by filming with doctor blade the ODCB solutions of polymers on ITO glasses that had been cleaned beforehand using the same procedure used for the preparation of solar cells. After the film deposition, samples were subjected to an annealing procedure (15 min at 130°C under vacuum) and surface images were recorded using an AFM in a non-contact (tapping) mode in height-modulated (HMM) mode.

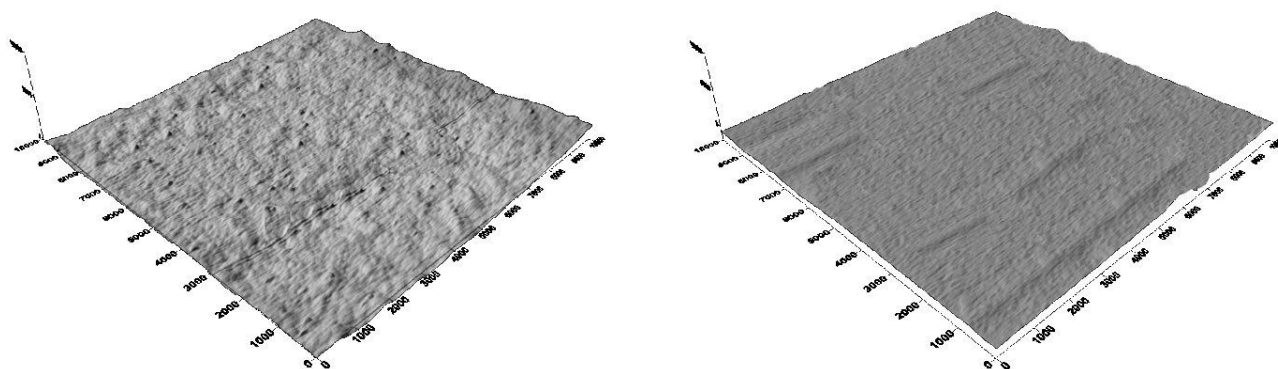


Figure 74. AFM images of a P3HT/PCBM blend (left) and of a COP2 film (right).

The AFM images of the surfaces of the two prepared films are quite different; in fact the surface rms (root-mean-square) roughness is 16.1 nm for the P3HT:PCBM film (with an average 25.6 nm diameter of grains) and 5.7 nm for COP2 (average 7.1 nm diameter grains). The bumps in topography are ascribable to PCBM-rich domains. P3HT has a rougher surface than COP2, thus suggesting a higher degree of self-organization in the blend, which could foster the formation of ordered structure in the film [45] However, fullerene derivatives that have a strong tendency to self-crystallize (such as PCBM) do not mix well with P3HT, thus producing inhomogeneous composite films with a less efficient photoinduced

charge-transfer [46] and then a lower  $J_{SC}$  [47]. Therefore, the use of COP2 as a photoactive blend, with no need for other EA species, is very promising, since the copolymer produces films with a very smooth surface, a more uniform molecular distribution, and a high interfacial area of the electron donor-acceptor domains, which acts positively on the final  $J_{SC}$  and PCE, as confirmed by the data shown in Table 10. Further studies are in progress, with the aim to prepare regioregular copolymers with a fullerene content higher than COP2.

## 6.6 CONCLUSIONS

In this work, we have obtained important results toward the optimization and production of polymeric solar cells. The first goal we had set provided for the synthesis of a model compound that confirmed the feasibility of the direct functionalization of a bromoalkane with the fullerene moiety. After the confirmation that the model could be obtained, the synthesis was modified by replacing 1-bromohexane with 3-(6-bromohexyl)thiophene, thus obtaining the monomer 3-(6-fullerenylhexyl)thiophene with a good yield and via a simple and straightforward synthesis procedure. The designed synthesis was adopted to prepare a soluble and filmable copolymer functionalized with 20% (in moles) of fullerene which provided a 4.19% photovoltaic efficiency when used as the photoactive layer in a polymeric solar cell, after a suitable optimization of the layer thickness and of the annealing procedure. The PCE obtained is higher than that of the reference cell and also of the values reported in literature for conventional BHJ solar cells based on the P3AT/PCBM system. The results obtained are especially encouraging. In fact, they show the possibility to obtain a photoactive polymer that is directly usable, without resorting to the preparation of the EA/ED blend (polymer/fullerene, carbon nanotubes or PCBM), thus avoiding the problems associated with the aggregation, segregation, and inhomogeneity of the components in the photoactive layer.



## REFERENCES FOR CHAPTER 6

- [1]. White, M. S.; Olson, D. C.; Shaheen, S. E.; Kopidakis, N.; Ginley, D. S. *Appl. Phys. Lett.* **2006**, *89*, 143517.
- [2]. Waldauf, C.; Morana, M.; Denk, P.; Schilinsky, P.; Coakley, K.; Choulis, S. A.; Brabec, C. J. *Appl. Phys. Lett.* **2006**, *89*, 233517.
- [3]. Niggemann, M.; Glatthaar, M.; Lewer, P.; Mueller, C.; Wagner, J.; Gombert, A. *Thin Solid Films* **2006**, *511-512*, 628.
- [4]. Carlé, J. E.; Krebs, F. C. *Sol. Energy Mater. Sol. Cells* **2013**, *119*, 309.
- [5]. Liu, Y.; Larsen-Olsen, T. T.; Zhao, X.; Andreasen, B.; Sondergaard, R. R.; Hegelsen, M.; Norrman, K.; Jorgensen, M.; Krebs, F. C.; Zhan, X. *Sol. Energy Mater. Sol. Cells* **2013**, *112*, 157.
- [6]. Vandewal, K.; Himmelberger, S.; Salleo, A. *Macromolecules* **2013**, *46*, 6379.
- [7]. Tan, Z.; Hou, J.; He, Y.; Zhou, E.; Yang, C.; Li, Y. *Macromolecules* **2007**, *40*, 1868.
- [8]. Li, M.; Xu, P.; Yang, J.; Yang, S. *J. Mater. Chem.* **2010**, *20*, 3953.
- [9]. Cravino, A.; Sedar Sariciftci, N. *J. Mater. Chem.* **2002**, *12*, 1931.
- [10]. Lanzi, M.; Paganin, L.; Errani, F. *Polymer* **2012**, *53*, 2134.
- [11]. Moon, J. S.; Takacs, C. J.; Cho, S.; Coffin, R. C.; Kim, H.; Bazan, G. C.; Heeger, A. J. *Nano Lett.* **2010**, *10*, 4005.
- [12]. Glowacki, E. D.; Sariciftci, N. S.; Tang, C. W. in *Solar Energy*; C. Richter et al. Eds., Springer: New York, **2013**.
- [13]. Jeffries, M.; Sauvé, G.; McCullough, R. D. *Adv. Mater.* **2004**, *16*, 1017.
- [14]. Lanzi, M.; Paganin, L. *React. Funct. Polym.* **2010**, *70*, 346.
- [15]. Moulé, A. J.; Meerholz, K. *Adv. Funct. Mat.* **2009**, *19*, 3028.
- [16]. Jorgensen, M.; Norman, K.; Krebs, F. C. *Sol. Energy Mater. Sol. Cells* **2008**, *92*, 686.
- [17]. Zerbi, G.; Radaelli, R.; Veronelli, M.; Brenna, E.; Sannicolò, F.; Zotti, G. *J. Chem. Phys.* **1993**, *98*, 4531.
- [18]. Turner, T. S.; Pingel, P.; Steyrleuthner, R.; Crossland, E. J. W.; Ludwigs, S.; Neher, D. *Adv. Funct. Mat.* **2011**, *21*, 4640.
- [19]. Jørgensen, M.; Norman, K.; Gevorgyan, S. A.; Tromholt, T.; Andreasen, B.; Krebs, F. C. *Adv. Mater.* **2012**, *24*, 580.

- [20]. Krebs, F. C.; Jørgensen, M.; Norman, K.; Hagemann, O.; Alstrup, J.; Nielsen, T. D.; Fyenbo, J.; Larsen, K.; Kristensen, J. *Sol. Energy Mater. Sol. Cells* **2009**, *93*, 422.
- [21]. Falkenberg, C.; Uhrich, C.; Olhof, S.; Maennig, B.; Riede, M.; Leo, K. *J. Appl. Phys.* **2008**, *104*, 34506.
- [22]. Dimitrov, S. D.; Durrant, J. R. *Chem. Mater.* **2014**, *26*, 616.
- [23]. Prato, M.; Maggini, M. *Acc. Chem. Res.* **1998**, *31*, 519.
- [24]. Matsuo, Y.; Iwashita, A.; Abe, Y.; Li, C. Z.; Matsuo, K.; Hashiguchi, M.; Nakamura, E. *J. Am. Chem. Soc.* **2008**, *130*, 15429.
- [25]. Bax, A. in *Two-Dimensional Nuclear Magnetic Resonance in Liquids*; Springer Verlag: Berlin, Germany, **1982**.
- [26]. Ho H.; Leclerc M. *J. Am. Chem. Soc.* **2003**, *125*, 4412.
- [27]. Brédas, J. L. *J. Chem. Phys.* **1985**, *82*, 3809.
- [28]. Kudret, S.; Kesters, J.; Janssen, S.; Van den Brande, N.; Defour, M.; Van Mele, B.; Manca, J.; Lutsen, L.; Vanderzande, D.; Maes, W. *React. Funct. Polym.* **2014**, *75*, 22.
- [29]. McCullough, R. D.; Lowe, R. D. *J. Chem. Soc. Chem. Commun.* **1992**, 70.
- [30]. Lanzi, M.; Paganin, L.; Costa Bizzarri, P.; Della Casa, C.; Fraleoni, A. *Macromol. Rapid Commun.* **2002**, *23*, 630.
- [31]. Sato, M.; Morii, H. *Macromolecules* **1991**, *24*, 1196.
- [32]. Bondouris, B. W.; Molins, F.; Blank, D. A.; Frisble, C. D.; Hillmyer, M. A. *Macromolecules* **2009**, *42*, 4118.
- [33]. Cugola, R.; Giovanella, U.; Di Gianvincenzo, P.; Bertini, F.; Catellani, M.; Luzzati, S. *Thin Solid Films* **2006**, *511*, 489.
- [34]. Lanzi, M.; Paganin, L. *Eur. Polym. J.* **2008**, *44*, 3987.
- [35]. Motaung, D. E.; Malgas, G. F.; Arendse, C. J.; Mavundla, S. E.; Oliphant, C. J.; Knoesen, D. *Sol. Energy Mater. Sol. Cells* **2009**, *93*, 1674.
- [36]. Bertho, S.; Haeldermans, L.; Swinnen, A.; Moons, W.; Martens, T.; Lutsen, L.; Vanderzande, D.; Manca, J.; Senes, A.; Bonfiglio, A. *Sol. Energy Mater. Sol. Cells*, **2007**, *91*, 385.
- [37]. Ma, W.; Yang, C.; Gong, X.; Lee, K.; Heeger, A. J. *Adv. Func. Mater.* **2005**, *15*, 1617.
- [38]. Lindqvist, C.; Wang, E.; Andersson, M. R.; Mueller, C. *Macromol. Chem. Phys.* **2014**, *215*, 530.

- [39]. Schopf, G.; Kossmehl, G. in *Polythiophenes-Electrically Conductive Polymers*, Springer Verlag: Berlin, Germany, **1997**.
- [40] Kumar, J.; Singh, R. K.; Kumar, V.; Rastogi, R. C.; Singh, R. *Diamond Rel. Mater.* **2007**, *16*, 446.
- [41] Chirvase, D.; Parisi, J.; Hummelen, J. C.; Dyakonov, V. *Nanotechnology* **2004**, *15*(9), 1317.
- [42]. Li, G.; Shrotriya, V.; Yao, Y.; Yang, Y. *J. Appl. Phys.* **2005**, *98*(4), 043704.
- [43]. Ho, C.; Huang, E.; Hsu, W.; Lee, C.; Lai, Y.; Yao, E.; Wang, C. *Synth. Met.* **2012**, *162*, 1164.
- [44]. Chi, D.; Qu, S.; Wang, Z.; Wang, J. *J. Mater. Chem. C* **2014**, *2*, 4383.
- [45]. Li, G.; Shrotriya, V.; Huang, J. S.; Yao, Y.; Moriarty, T.; Emery, K.; Yang, Y. *Nat. Mater.* **2005**, *4*, 864.
- [46]. Hiramoto, M.; Fujiwara, H.; Tokoyama, M. *Appl. Phys. Lett.* **1991**, *58*(10), 1062.
- [47]. Savagatrup, S.; Printz, A. D.; Rodriguez, D.; Lipomi, D. J. *Macromolecules* **2014**, *47*, 1981.





## **PART 2: FKM**







Table 12. *List of ABBREVIATIONS and SYMBOLS*

BTTPC	Benzyltriphenylphosphonium chloride
CTFE	Chlorotrifluoroethylene
DBU	1,8-Diazabicyclo[5-4-0]-undec-7-ene
DETA	Diethylene triamine
DMAC	Dimethylacetamide
d.o.g.	Degree of grafting
DSC	Differential scanning calorimetry
DTA	Differential thermal analysis
EDA (-C)	Ethylene diamine (carbamate)
HBTP	Hexamethylene-N,N'bis(tert-butyl
HFP	Hexafluoropropene
HMDA	Hexamethylene diamine
HMDA-C	Hexamethylene diamine carbamate
HPFP	1H-pentafluoropropene
MBTBP	Methylene bis-4-cyclohexyl-N,N'(tert-butylperoxycarbamate)
ODR	Oscillating disc rheometer
PMVE	Perfluoro(methyl vinyl ether)
PVDF	Polyvinylidene fluoride
t <sub>1/2</sub>	Half life
TAC	Triallylcyanurate
TAIC	Triallylisocyanurate
TFE	Tetrafluoroethylene
THF	Tetrahydrofurane
VDF	Vinylidene fluoride

## CHAPTER 1: INTRODUCTION

### *1.1 INTRODUCTION ON FLUOROPOLYMERS*

Fluorinated polymers are particularly interesting and attractive compounds because of their properties. Indeed, the electronegativity of the fluorine atom implies strong C-F bonds (about 110 kcal.mol<sup>-1</sup>), and a higher strength of the C-C bonds in fluorinated compounds (97 kcal.mol<sup>-1</sup>). It also supplies to fluoropolymers strong Van Der Waals forces between hydrogen and fluorine atoms [1-3], and it confers a lot of good properties to the fluorinated polymers such as:

- Chemical, thermal, electric stabilities [4-6],
- Inertness to acids, bases, solvents and oils,
- Low dielectric constant,
- Low refractive index,
- No flammability,
- High resistance to ageing, and to oxidation,
- Low surface tension.

Fluorinated polymers also range as a wide scope of thermoplastics, elastomers, plastomers, thermoplastic elastomers [7-14], and can be semi-crystalline or totally amorphous. Hence, fluorinated polymers have been used in many applications: building industries (paints and coatings resistant to UV and to graffiti), petrochemical and automotive industries, aerospace and aeronautics (use of elastomers as seals, gaskets, O-rings used in extreme temperature for tanks of liquid hydrogen for space shuttles), chemical engineering (high-performance membranes), optics (core and cladding of optical fibers), treatment of textile, stone protection (especially for old monuments), microelectronics [8-14], and for cable insulation.

As a matter of fact, the performance of fluoropolymers, especially insolubility and fusibility can be improved by crosslinking. Indeed, the crosslinking reaction takes advantage of the base-sensitive characteristic of the VDF-based polymer [15]. The crosslinking is a chemical reaction between the polymer backbone and an ex-situ agent that possesses both same fonctions in order to couple covalently the polymeric chains together, to produce a network structure, and to increase the molecular weight.

Sulphur has been the predominant curing agent in the rubber industry, and in 1840, rubber was with sulphur [16]. Many efforts have been devoted over the 40 years of existence of fluoroelastomers toward the development of practical crosslink systems.

Fluoroelastomers are now usually cured by nucleophiles such as diamines [17-31], or bisphenols [3,32-38], or with peroxides [3,35,39-43], by chemical reactions when the polymers based on VDF contain cure-site monomer, such as thiol function [44], by radiation, such as electron beam [45-52].

The cure chemistry of VDF based fluoroelastomers is connected with the strong polarity of the C-F bond and specific polarisation of molecules, which determine their selective ability to split off hydrogen fluoride under the influence of internal factors.

## ***1.2 PVDF***

Among fluoropolymers, polyvinylidene fluoride (PVDF) is a semi-crystalline and thermoplastic polymer, with a glass transition temperature of  $-40^{\circ}\text{C}$  [53,54]. This polymer exhibits interesting thermal, chemical and physical properties, especially when it is co- or ter- polymerised with a fluorinated alkene [14,35,50,55-59]. Its main drawback is its sensitivity to base that can degrade it by creating insaturations. PVDF homopolymer is a long chain macromolecule endowed with a high crystallinity rendering it unsuitable as elastomer, and unsuitable for curing. So, copolymers of VDF with various comonomers can fall into three categories:

1. when the amount of comonomers in the copolymer is small about that of VDF, the resulting materials are thermoplastics with a lower crystallinity than that of the PVDF [60,61];
2. for a bit higher content of comonomer, thermoplastic elastomers are obtained;
3. for higher proportion of comonomers, the produced copolymers are elastomeric and amorphous with low intermolecular forces [35,50,57,58,62-66].

In the case of the poly(VDF- co-HFP) copolymer, when the molar percentage of VDF is higher than 85%, the copolymer is a thermoplastic, whereas for a smaller content, the copolymer is an elastomer [35,50].

## ***1.3 COPOLYMER BASED ON VDF***

VDF has been involved in radical copolymerisation with many monomers [14,60,61,67], listed in Table 1 [44,68-94].

Most common co- or termonomers of VDF [14,50] are hexafluoropropene (HFP) [80,82,83,95-97], tetrafluoroethylene (TFE) [78,80,81,98,99], chlorotrifluoroethylene (CTFE) [78,79,100-102], trifluoroethylene (and in that case, interesting piezoelectrical materials have been obtained) [75], perfluoro(methyl vinyl ether) (PMVE) [77,84,103-105], and 1H-pentafluoropropene (HPFP)

[67,106,107]. Interestingly, functional fluoromonomers (also called cure site monomers) useful for further crosslinking, have been successfully used, bearing OH [86], CO<sub>2</sub>H [71,89], Si(OR)<sub>3</sub> [94] functions, or bromine [87] and iodine atoms. Table 13 supplies a non-exhaustive list of fluoromonomers that were copolymerised with VDF, and their reactivity ratios  $r_i$ , when assessed.

Table 13. Monomer reactivity ratios for the radical copolymerization of VDF (A) with other fluoroalkenes (B) (and vinyl acetate and ethylene)

Monomer B	$r_A$	$r_B$	$r_A r_B$	$1/r_A$	Ref.
CH <sub>2</sub> =CH <sub>2</sub>	0.05	8.5	0.42	20.00	[68]
CH <sub>2</sub> =CHOCOCH <sub>3</sub>	-0.40	1.67	-0.67	-2.5	[69]
	0.50	2.0	1.00	2.0	[70]
CH <sub>2</sub> =C(CF <sub>3</sub> )COOH	0.33	0	0	3.03	[71]
CHF=CH <sub>2</sub>	0.17	4.2-5.5	0.71-0.94	5.88	[72]
	0.20-0.43	3.8-4.9	0.76-2.11	2.33-5.00	[73]
CH <sub>2</sub> =CFCF <sub>2</sub> ORF	0.38	2.41	0.92	2.63	[74]
CF <sub>2</sub> =CHF	0.70	0.50	0.35	1.43	[75]
CF <sub>2</sub> =CHCF <sub>3</sub>	9.0	0.06	0.54	0.11	[76]
CF <sub>2</sub> =CHC <sub>6</sub> F <sub>13</sub>	12.0	0.90	10.80	0.08	[77]
CFCI=CF <sub>2</sub>	0.73	0.75	0.55	1.37	[78]
	0.17	0.52	0.09	5.88	[79]
CFBr=CF <sub>2</sub>	0.43	1.46	0.63	2.33	[78]
CF <sub>2</sub> =CF <sub>2</sub>	0.23	3.73	0.86	4.35	[78,80]
	0.32	0.28	0.09	3.13	[81]
CF <sub>3</sub> -CF=CF <sub>2</sub>	6.70	0	0	0.15	[82]
	2.45	0	0	0.40	[80]
	2.90	0.12	0.35	0.34	[83]
CF <sub>2</sub> =CFOCF <sub>3</sub>	3.40	0	0	0.29	[84]
CF <sub>2</sub> =CFOC <sub>3</sub> F <sub>7</sub>	1.15	0	0	0.86	[84]
CF <sub>2</sub> =CFO(HFP)OC <sub>2</sub> F <sub>4</sub> SO <sub>2</sub> F	0.57	0.07	0.04	1.75	[85]
CF <sub>2</sub> =CFCH <sub>2</sub> OH	0.83	0.11	0.09	1.02	[86]
CF <sub>2</sub> =CF(CH <sub>2</sub> ) <sub>2</sub> Br	0.96	0.09	0.09	1.0	[87]
CF <sub>2</sub> =CF(CH <sub>2</sub> ) <sub>3</sub> OAc	0.17	3.26	0.59	5.56	[88]
CF <sub>2</sub> =CF(CH <sub>2</sub> ) <sub>3</sub> SAc	0.60	0.41	0.25	4.07	[44]
CF <sub>2</sub> =CFCOOCH <sub>3</sub>	0.30	0	0	3.33	[89]
CF <sub>2</sub> =C(CF <sub>3</sub> )OCOC <sub>6</sub> H <sub>5</sub>	7.60	0.02	0.15	0.13	[90]

Although it is difficult to compare their reactivities (since 1) the copolymerisations were not carried out under similar conditions, 2) certain articles do not mention if the kinetics of copolymerisation were realised at low monomer conversion, and 3) various kinetic laws were used], it was worth examining a reactivity series of fluorinated monomers with VDF. The traditional method for the determination of a reactivity of a macroradical to several monomers was used. Indeed, it is common to compare the value  $1/r_A = k_{AB}/k_{AA}$ , as the ratio of rate constants of co-propagation ( $k_{AB}$ ) to that of homo-propagation ( $k_{AA}$ ). Thus, the higher the  $1/r$  value, the higher the copropagation reactivity of the radical. Based on the data in Table 13, the increasing order of relative reactivities of monomers to  $\sim$ VDF macroradicals is as follows

$\text{CF}_2=\text{CHC}_6\text{F}_{13} < \text{CF}_2=\text{CHCF}_3 < \text{HFP} < \text{PMVE} < \text{PPVE} < \text{CF}_2=\text{CFC}_2\text{H}_4\text{Br} < \text{VDF} < \text{CF}_2=\text{CFCH}_2\text{OH} < \text{CF}_2=\text{C}(\text{CF}_3)\text{OCOC}_6\text{H}_5 < \text{TrFE} < \text{CTFE (recent value)} \approx \text{BrTFE} < \text{CH}_2=\text{CFCH}_2\text{ORF} < \text{CF}_2=\text{CFCOOCH}_3 < \text{TFE} < \text{CF}_2=\text{CFC}_3\text{H}_6\text{SCOCH}_3 < \text{CF}_2=\text{CFC}_3\text{H}_6\text{OAc} < \text{CH}_2=\text{CHF} \approx \text{CTFE (old value)} < \text{CH}_2=\text{CH}_2$

## 1.4 OVERVIEW

In order to improve their properties, poly(VDF-co-HFP) copolymers or poly(VDF-ter-HFP-ter-TFE) terpolymers can be crosslinked by bisnucleophiles, such as diamines or bisphenols, or by irradiation. On the other hand, poly(VDF-ter-HFP-ter-termonomer containing an iodine or bromine atom) terpolymer can be crosslinked by peroxides/coagent systems. Those three main ways of crosslinking exhibit two main crosslinking mechanisms (ionic and radical mechanisms) and different properties.

### 1.4.1 Different crosslinking agents

Several curing systems have been investigated or developed for the crosslinking of fluoroelastomers. Some of them are [35,108]

- high energy radiation [19, 45-52],
- peroxide with or without coagent [3,35,39-43],
- dithiols in combination with amines [19],
- aromatic polyhydroxy compounds [3, 32-38],
- diamines and their derivatives [17-31],
- thiol-ene systems [44,50].

Each curing system exhibits a different crosslinking mechanism, and results in different mechanical properties and crosslinking densities. Indeed, Table 14 [35] shows different mechanical properties for bisphenols and peroxides cured systems.

Table 14. Improvement of mechanical properties of bisphenol, and peroxide-cured poly(VDF-ter-HFP-ter-TFE) terpolymer with post cure step.

Properties	Bisphenol		Peroxide	
	Press cure <sup>1</sup>	Post cure <sup>2</sup>	Press cure <sup>1</sup>	Post cure <sup>2</sup>
<b>Modulus at 100% strain (MPa)</b>	5.0	7.9	5.0	7.9
<b>Tensile strength at break (MPa)</b>	10.0	13.8	9.7	15.9
<b>Elongation at break (%)</b>	225	175	165	150
<b>Compression set (200°C, 70h)</b>				
<b>O-rings (%)</b>	63	25	50	27
<b>Pellets (%)</b>	85	20	52	20

<sup>1</sup> press cure at 177°C for 10 min

<sup>2</sup> post cure at 232°C for 24 h

### 1.4.2 Compounding

In order to improve the properties of the raw elastomer, many materials that enable to facilitate mixing or processing may be compounded with the vulcanizing agent [28,55], accelerators and accelerator activators to increase the rate of vulcanization and to improve product properties; fillers to enhance physical properties and /or to reduce costs; softeners enable to aid processing or to plasticize the product; antioxidants and other materials which slow down decomposition of the product by oxidation; heat and/or radiation; pigments and blowing agents.

For the main additional materials, the proportions (in part per hundred of polymer) are [55]:

- Raw Polymer 100;
- Curing agent 1-6;
- Basic metallic oxide 6-20;
- Filler > 60.

### *1.4.3 Press-cure and Post-cure steps for crosslinking*

The best vulcanisate properties are obtained by a two step-process [35,58,109]. Fluoroelastomers and additives are generally molded in a press and then post cured in an oven [28].

First, the materials are press cured at different times and temperatures, depending on the size of the product, the structure of the polymer, the curing systems, and on end-use requirements (paints, O-rings, membranes, seals) [28]. Press cure conditions vary from 4 minutes at temperatures approaching 200°C for thin cross sections, to 30 min at 150-170°C for thick sections [28,110]. The purpose of this step is to develop sufficient crosslinks in the sample to prevent the formation of bubbles due to the release of trapped air during the early stages of the subsequent oven cure [111].

Then, the second step (post cure or oven-cure) is carried out in air or under nitrogen at higher temperature than that of the press cure, and under atmospheric pressure [35,58].

This post cure step is required to reach the best vulcanisate properties (tensile strength, modulus at 50 or 100% elongation, compression set resistance, elongation at break) [28,40,108,111]. Table 15 [35] shows the improvement of compression set resistance with post curing, for four samples containing poly(VDF-ter-HFP-ter-TFE) terpolymer crosslinked with a peroxide [2,5-bis(t-butylperoxy)-2,5-dimethylhexyne] in the presence of triallyl/isocyanurate [35,108,112,113]. Table 2 [35] presents the improvement of some mechanical properties of bisphenol and peroxide cured systems with post cure.

An improvement in compression set resistance is observed after post cure under nitrogen compared to that realised under air (Table 15). The C=C double bond of the polymeric backbone undergoes an oxidation from the oxygen of air atmosphere, that prevents from good compression set resistance. Table 15 shows a 50% increase in modulus at 100% elongation (M<sub>100</sub>) and tensile strength at break, and a 50% decrease in elongation at break.



Table 15. Compression set resistance measured at 204°C for 70h, of a peroxide cured VDF/HFP/TFE terpolymer.

Compound	Compression set %		
	Press Cured <sup>1</sup>	Post Cured <sup>2</sup>	
	Air	Air	N <sub>2</sub>
<b>A</b>	71	38	20
<b>B</b>	70	37	25
<b>C</b>	59	27	12
<b>D</b>	52	21	9

Compound A: 100 phr polymer, 3 phr peroxide, 3 phr TAIC, 3 phr PbO

Compound B: 100 phr polymer, 3 phr peroxide, 3 phr TAIC, 2 phr MgO, 2 phr ZnO

Compound C: 100 phr polymer, 3 phr peroxide, 3 phr TAIC, 3 phr PbO

Compound D: 100 phr polymer, 3 phr peroxide, 6 phr Ca(OH)<sub>2</sub>, 3 phr MgO

Bromo cure site in A and B differed from that in C and D.

<sup>1</sup> press cure in air at 177°C for 15 min

<sup>2</sup> post cure in air or N<sub>2</sub> at 232°C for 24 h [35]

During the step of crosslinking of fluoroelastomers, water is formed, and post cure removes this water, whose presence prevents from full development of the diamine cure and causes reversion of the bisphenol cure [3,23,40,114]. Indeed, during press cure, water is formed from the reaction between the acid acceptor and HF, caused by dehydrofluorination.

For thick sections, the temperature of the post cure oven is usually raised in several steps to prevent from fissuring of the part. Generally, 12-24h reaction time at a temperature of 200-260°C is used [28,35,58,110]. Typically, 200°C is sufficient for amines [59,111], whereas bisphenol and peroxide cures need higher temperatures (230 to 260°C).

All these results suppose a difference in the crosslinking mechanism of bisphenols, peroxides and diamines cured systems, that are the most important crosslinking agents for VDF-based fluoroelastomers. The crosslinking mechanisms and the properties of the resulting crosslinked polymers are the subject of the following parts.

## ***1.5 CROSSLINKING OF VDF-BASED FLUOROELASTOMERS***

### ***1.5.1 Crosslinking with Amines and Diamines***

The curing by diamines, originally introduced in late 1950s, was a predominant way of crosslinking of raw fluoroelastomers until late 1960s, when bisphenol curing was introduced [55,58]. The polyamine system is the best for general use because of easier processing [96]. Indeed, it only needs the presence of hydrogen atoms in the polymer backbone. Moreover, the mechanism of crosslinking can be a simple addition on this backbone [96].

The diamine curing system generally results in relatively poor processing, safety concerns, thermal and ageing resistance, and compression set resistance. However, this cure system has demonstrated specific properties, such as excellent adhesion to metal [115].

The curing of elastomer with an amine or a diamine usually takes place in the three following steps [24,114,116,117]:

- (1) an elimination of HF (dehydrofluorination) from VDF segments adjacent to HFP in the main chain to generate internal double bonds,
- (2) a Michael addition of the diamine onto the resulting double bonds to form crosslinks,
- (3) an elimination of HF from the crosslinks, during post cure to form further double bonds.

Although amine curing is no more used, it is useful to describe it in order to better understand what is happening during the crosslinking process. Amine curing is reported as an example.

### ***1.5.2 Dehydrofluoruration of the Fluoropolymer***

The dehydrofluorination of a solution of Viton poly(VDF-co-HFP) copolymer treated with several amines, or heated at high temperature can be monitored by measurement of hydrogen fluoride elimination (titration of the HF in the solution) [5,15,19,116], infrared study [19,24,118], viscosity [19], solubility and determination of the gel content [5].

Solutions of Viton in tetrahydrofurane were treated with primary, secondary and tertiary monoamines for periods of several weeks at room temperature. The reaction was followed by the measurement of HF elimination by a titration of the hydrogen fluoride in the solution. Figure 75 [19] shows the evolution of the quantity of HF in the solution of THF as a function of time for primary, secondary and tertiary monoamines. All of the monoamines used caused dehydrofluorination of the polymer to some degree. Tertiary amines are the least efficient, primary amines by far are the most active.

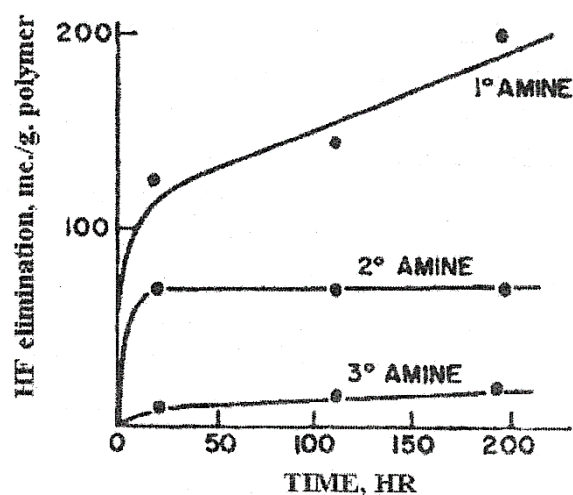


Figure 75. Amount of elimination of HF from primary, secondary and tertiary amines cured Viton A.

Figure 76 [24,118] shows the infrared spectrum of uncured poly(VDF-co-HFP) copolymer (FKM gum), before and after a thin film of polymer is heated in air at 300°C. Two new bands centered at 1580 and 1750  $\text{cm}^{-1}$  appeared after heating, which are assigned to the conjugated double bonds and to the  $-\text{CH}=\text{CF}_2$  end groups, respectively. Unsaturation is likely to be caused by elimination of HF from PVDF block of the FKM chain, in particular from the head- to-tail position of the structure.

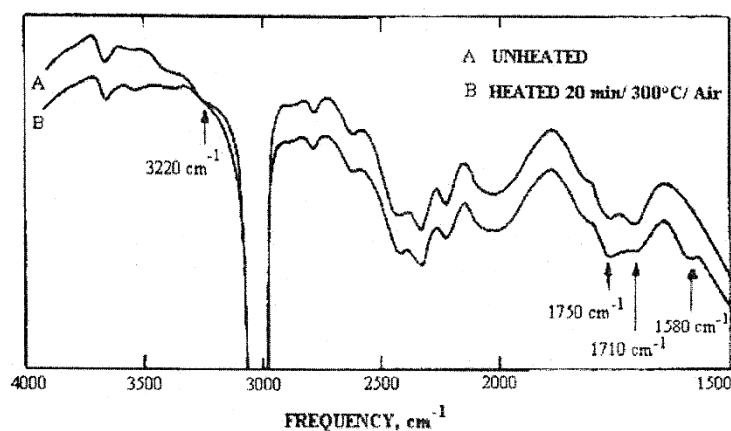
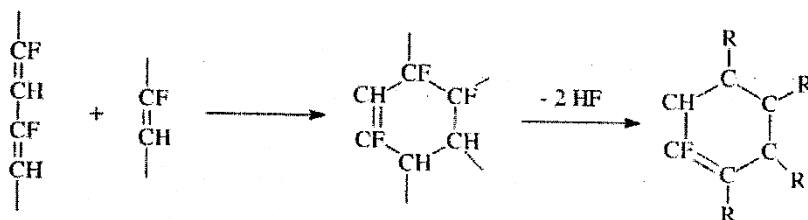


Figure 76. Infrared spectra of an uncured poly(VDF-co-HFP) copolymer before (A) and after (B) heating at 300°C for 20 min in air.

So, in the presence of a base or under heating, the VDF-based fluoroelastomers are submitted to dehydrofluorination.

The conjugated double bonds evidenced by infrared measurements allowed us to interpret a new mechanism. Figure 2 [118] exhibits the presence of isolated double bonds (1710  $\text{cm}^{-1}$ ), and the presence of conjugated double bonds (1580  $\text{cm}^{-1}$ ). It is proposed that the initial double bond (1710  $\text{cm}^{-1}$ ) activates the elimination of HF from neighboring atoms leading to conjugated double bonds (1580  $\text{cm}^{-1}$ ). This process would lead to the formation of a brown color [20,24,118]

Such a conjugate site would then be expected to react with a double bond, in an adjacent chain by a Diels Alder reaction, leading to a fluorinated cyclohexene which should readily loses HF to form an aromatic ring (Scheme 20) [19,119].



*Scheme 20. Diels-Alder reaction during post-curing forms aromatic ring with loss of HF.*

The observed absorption at  $1580\text{ cm}^{-1}$  could be ascribed to such a site.

The evolution of the solubility of a raw poly(VDF-co-HFP) copolymer heated in air at  $250^{\circ}\text{C}$  is shown in Table 16 [24]. Indeed, there is an initial rapid decrease in solubility, and then it proceeds to rise slowly. This type of variation of solubility, together with the formation of a swollen gel, indicates the simultaneous occurrence of crosslinking and chain scission in the polymer [5,114]

*Table 16. Soluble fraction in acetone of a poly(VDF-co-HFP) copolymer heated in air at  $250^{\circ}\text{C}$ .*

Time (hours)	Fraction soluble in acetone at $28^{\circ}\text{C}$	Volume fraction of polymer in swollen gel fraction at equilibrium in acetone at $28^{\circ}\text{C}$
3	0.78	Not determined
24	0.52	0.02
42	0.47	0.02
48	0.48	0.02
137	0.53	0.01

During heating or attack with a base, the polymer undergoes a dehydrofluorination, creating conjugated double bonds that can be involved in a Diels Alder reaction. But, at higher temperature or in the presence of a stronger base, it also creates degradation such as oxidation or scissions that can be evidenced by the measurements of the decrease in the intrinsic viscosity, caused by the decrease in molecular weight [19]. In order to avoid any degradation, the created double bonds can become the site of the addition of several agents like diamines, bisphenols or peroxides, that can increase the mechanical and chemical properties.

In VDF-based fluoropolymers, and especially poly(VDF-co-HFP) copolymer, dehydrofluorination occurs on special sites.

Paciorek et al. [23] studied the crosslinking of amines on several fluoro-compounds models. The model of addition of butylamine onto 1,5,5-trihydro-4-iodoperfluorooctane and 4-hydroperfluoroheptene-3, in diethylether at room temperature, is the only one known. It proceeds according to the following scheme:



The reaction occurs mainly on the carbon adjacent to the iodine atom, because dehydrofluorination is the main process under the selected conditions.

From  $^{19}\text{F}$  NMR characterisation, Schmiegel [3,15,32,33] showed that a polymer based on VDF units with HFP, TFE, PMVE co- or ter-monomers in solution of DMAC can undergo dehydrofluorination from the  $\text{n-Bu}_4\text{N}^+\text{OH}^-$  in specific sites.

Figure 77 [33] represents the 294.1 MHz  $^{19}\text{F}$  NMR spectra of poly(VDF-co-HFP) copolymer before (top) and after (bottom) treatment with hydroxylic base in DMAC at 20°C. Peaks A and B are assigned to  $\text{CF}_3$  group, peaks C, D, E, F, G, H, I, J, K, and L are attributed to  $\text{CF}_2$  of VDF, peaks M and N are assigned also to  $\text{CF}_2$  of the HFP, and finally peaks O and P are assigned to  $\text{CF}$ . The small resonances A, G and O correspond to HFP inversions, whereas F, J, K, and L are attributed to VDF inversions. Spectrum at the bottom exhibits selective intensity reduction of resonance B, H, I, M, N and P after addition of  $\text{Bu}_4\text{N}^+\text{OH}^-$ . A peak assigned to  $\text{CF}_3$  groups of  $-\text{C}=\text{C}(\text{CF}_3)-\text{C}$  appears also at -55 ppm. These observations can be accommodated to the highly selective dehydrofluorination of isolated VDF units, i.e. HFP- VDF-HFP structures [3,32-34]. The concentration of this site in a 3.5 poly(VDF-co-HFP) copolymer is about 0.6 mol/kg. The same results were observed in poly(VDF-co-TFE) and poly(VDF-co-PMVE) copolymers, and poly(VDF-ter-HFP-ter-TFE) and poly(VDF-ter-PMVE-ter-TFE) terpolymers [33]. For example, in poly(VDF-co-TFE) copolymer, dehydrofluorination occurs on VDF units having a TFE-VDF-TFE triad, or in poly(VDF-ter- HFP-ter-TFE) terpolymer, it occurs on HFP-VDF-TFE structure.

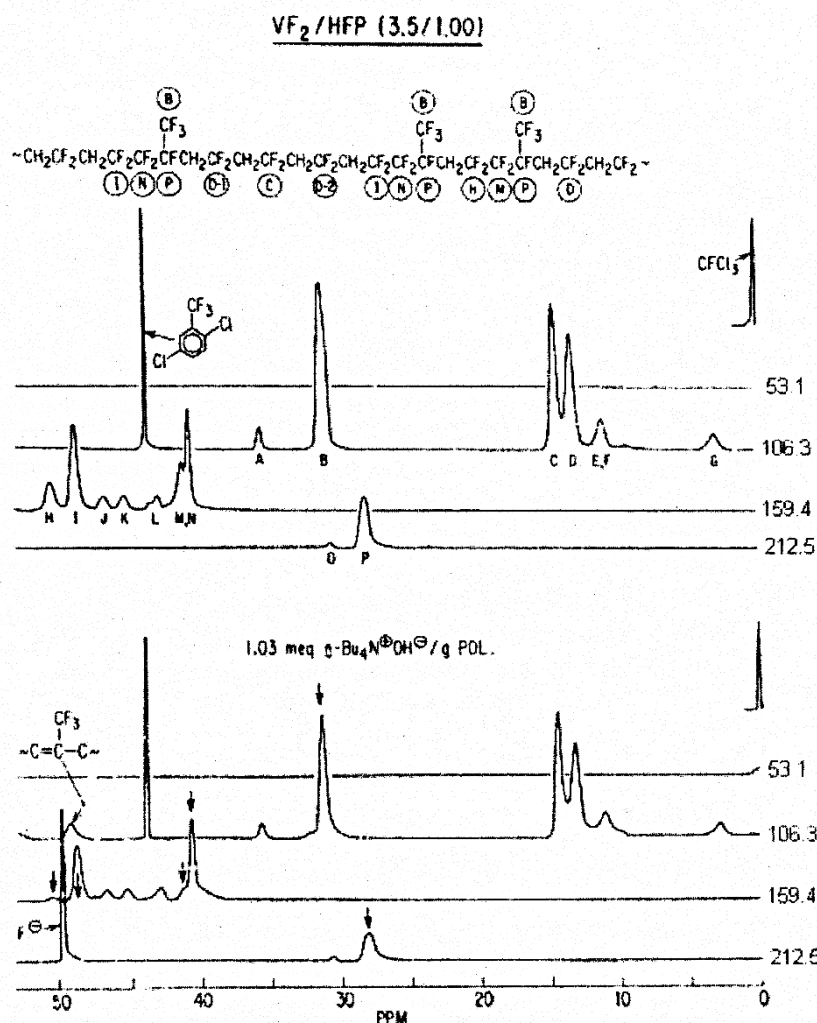
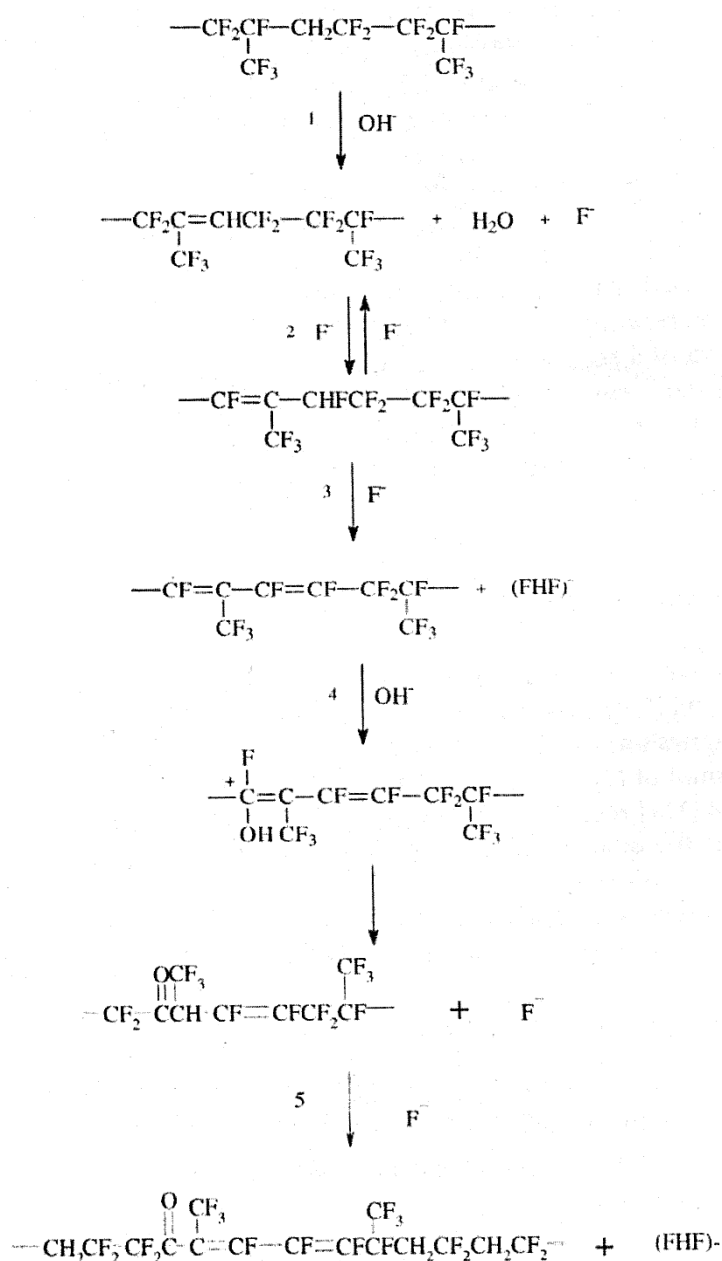


Figure 77. <sup>19</sup>F-NMR spectra of a poly(VDF-co-HFP) copolymer before (top) and after (bottom) treatment with hydroxyl base (2,5-trifluorobenzotrifluoride internal standard). Changes in peak intensities are indicated.

A reaction scheme of dehydrofluorination of poly(VDF-co-HFP) copolymer in the presence of a base was given by Schmiegel (Scheme 21) [32,33].

First, the attack of hydroxide creates a double bond on VDF units in VDF-HFP diad. Then, a fluoride ion rearrangement of the initial double bond occurs. The resulting allylic hydrogen is abstracted by fluoride, followed by an elimination of a second fluoride. So, a bifluoride and a formally conjugated non-coplanar diene are formed. Then, a nucleophilic attack by the hydroxide on the diene forms an enone and subsequent attack of fluoride ion onto the highly acidic hydrogen of the tertiary carbon atom. The final product is the dienone [32,33].



Scheme 21. Dehydrofluorination mechanism of poly(VDF-co-HFP) copolymer in the presence of base.

### 1.5.2.1 Role of the acid acceptor

An acid acceptor of metal oxide type is a necessary ingredient of all VDF-based polymer curing formulations. No cure is obtained without any metal oxide which did not contain magnesium oxide, and the state of cure developed is directly related to the amount of MgO [111,114,120].

Figure 78 [111] represents the evolution of the tensile strength and the modulus versus the quantity of MgO, for a trimethylamine hydrochloride cured poly(VDF-co-HFP) copolymer. Indeed, there is an evidence by infrared that MgO contributes to the elimination of HF from the polymer during irradiation, and probably also in the course of the chemical cures.

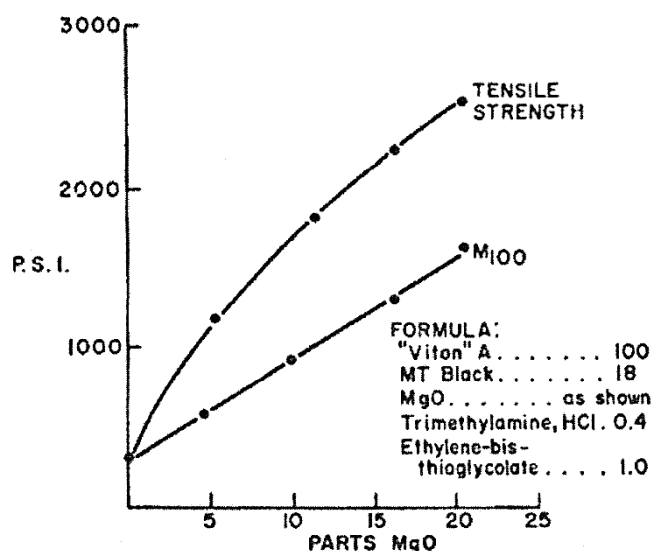


Figure 78. Effect of MgO on the mechanical properties of a formula comprising Viton A cured with dithiol.

Figure 79 [116] shows the variation of the amount of fluoride ions at 200°C with MgO content. The presence of MgO does not prevent from HF elimination; it merely reduces its rate of evolution from the elastomer, a 15% addition giving a result comparable with that of the raw polymer alone.

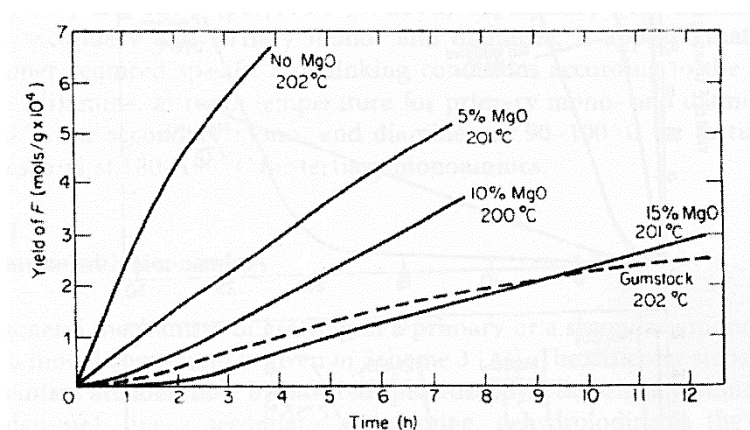
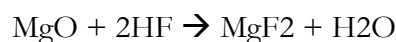


Figure 79. Evolution of the yield of fluoride atom of VDF-based fluoropolymer heated at 200°C versus time and amount of MgO (acid acceptor)

The reaction between MgO and HF is given in the following scheme [114]:

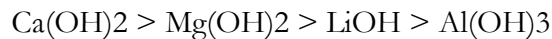


Several metal oxides can be used as HF scavengers for VDF-based polymers. The relative efficiencies of a number of basic oxides, hydroxides and carbonates as HF acceptors at approximately 275°C are illustrated in Figure 80 [116]. It is apparent that there are many variations in the efficiencies of the different compounds. The decreasing order of efficiencies is as follows:





The hydroxides are significantly better acceptors than their analogous oxides. The decreasing order of efficiencies is [116]:



Finally, the decreasing order of efficiencies for carbonates is [116]:



The most commonly used acid acceptor is MgO.

Thus, dehydrofluorination of VDF comonomer in the diad is the first step of crosslinking mechanism with diamine. The second step consists in the addition of the amine or the diamine onto that unsaturation.

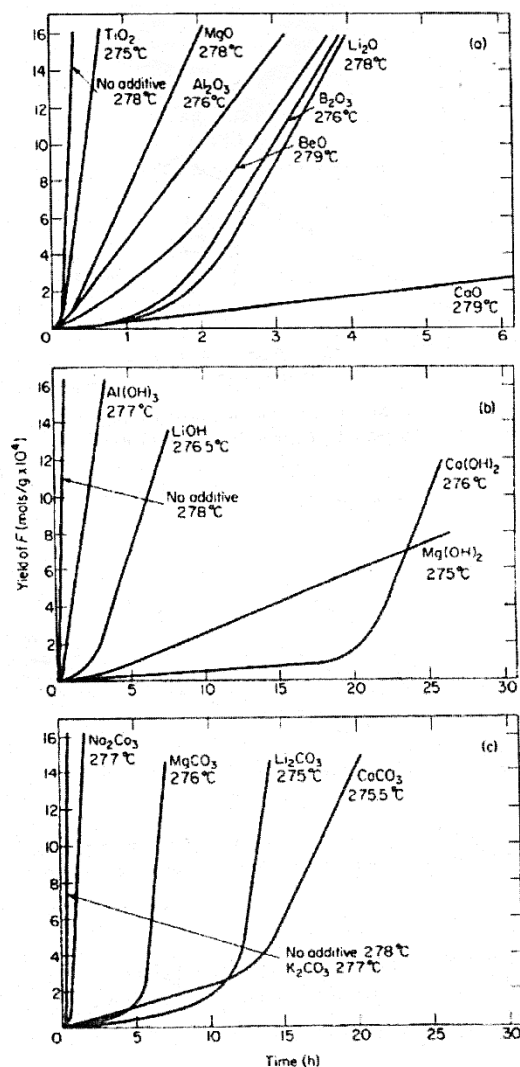


Figure 80. Comparison of the efficiency of acid acceptors: a) metal oxide at 275°C, b) hydroxide acceptors at 275°C and c) carbonate acceptors at 275°C.

## 1.6 CROSSLINKING WITH BISPHENOLS

Bisphenols are presently the predominant crosslinking agents for curing fluorocarbon-based elastomers. Bisphenols curing was developed in the late 1960ies and started replacing the diamine cure in the early 1970ies [109,135-138]. Because of processing and property advantages, the most commonly used compound is bisphenol AF (2,2-bis(4-hydroxyphenyl) hexafluoropropane). Others, like substituted hydroquinone, and 4,4'-disubstituted bisphenols also work well and are used commercially to a lesser degree [35,36,38,58]. As in cases above, crosslinking reaction was evidenced by  $^{19}\text{F}$  NMR.

### 1.6.1 Crosslinking mechanism

The crosslinking mechanism takes place in three steps: elimination of HF creating double bonds, then reorganisation of the double bonds, such as in Scheme 2, and finally substitution of the bisphenol onto the double bond.

Crosslinking agent require accelerators to make that reaction more efficient. For example, to enable the dehydrofluorination of a VDF/HFP diad, bisphenols need to react with a metal oxide to give the phenolate ion, which in turn reacts with the phosphonium or tetraalkylammonium ion to give intermediates I and II.



These intermediates are strong bases [35]. The crosslinking mechanism proposed by Schmiegel is shown in Scheme 81 [33,35,64,139].

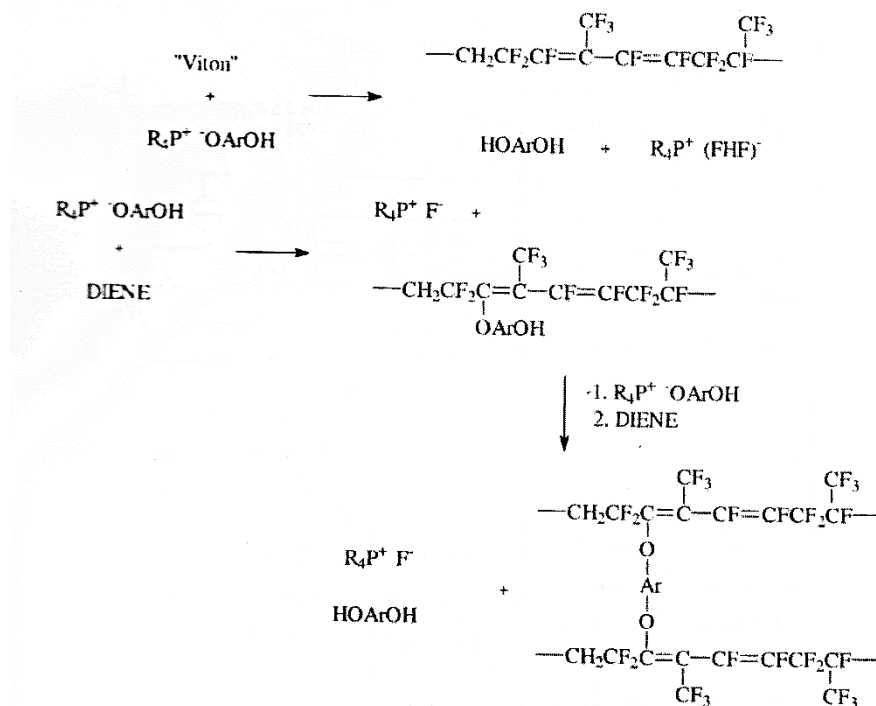


Figure 81. Crosslinking mechanism with bisphenol.

In the first step (the dehydrofluorination) Viton copolymer is attacked by the intermediate described below, creating diene. Then, the bisphenol-derived phenolate ( $\text{OArOH}$ ) attacks the intermediate diene and finally leads to the dienic phenyl ether crosslinks [32,33]. This reaction is a substitution. The resulting product surprisingly shows good properties, particularly with regard to oxidative and hydrophilic stability.

### 1.6.2 $^{19}\text{F}$ NMR study

The mechanism of crosslinking was evidenced by  $^{19}\text{F}$  NMR, and Schmiegell et al. [3,32,33] studied the  $^{19}\text{F}$  NMR spectra of poly(VDF-co-HFP) copolymer treated in dimethylacetamide (DMAC), with DBU (1,8-diazabicyclo[5.4.0]-undec-7-ene) and bisphenol AF. DBU is strong enough to enable a dehydrofluorination of the polymer and to ionise the phenol, but is sterically hindered for being an efficient competitor of phenoxide for the fluoroolefin [33]. Figure 82 [33,34] represents the  $^{19}\text{F}$  NMR spectra of a base (DBU)-treated soluble polymer (upper spectrum), and the gel produced by base in the presence of bisphenol-treated polymer (lower spectrum). Both spectra exhibit two new peaks at  $-55$  and  $-62$  ppm, assigned to  $-\text{C}=\text{C}(\text{CF}_3)-\text{C}-$  isomeric structure of the  $\text{CF}_3$ . So, poly(VDF-co-HFP) copolymers treated with DBU and with DBU/bisphenol system undergo at least dehydrofluorination and rearrangement, such as in Scheme 2. However, to prove the crosslinking of bisphenol-AF onto the copolymer, a  $^{19}\text{F}$  NMR spectrum of the same sample after precipitation must be recorded.

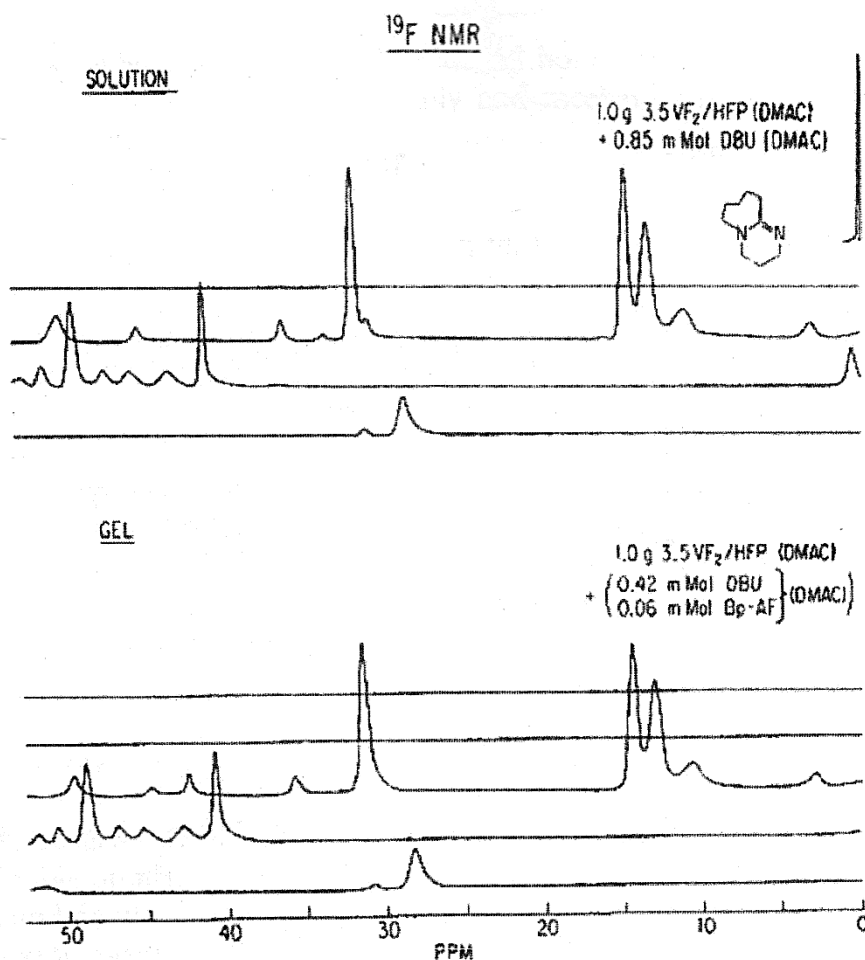


Figure 82. <sup>19</sup>F-NMR spectra of a poly(VDF-co-HFP) copolymer treated with DBU in a solution of DMAC (top) and the gel which results from this reaction in the presence of BAF (bottom).

Figure 83 [33,34] shows two <sup>19</sup>F NMR spectra of poly(VDF-co-HFP) copolymers. The first one (top) deals with the spectrum of poly(VDF-co-HFP) copolymer treated with DBU and the bisphenol AF in DMAC, while the other one (bottom) represents the same sample but precipitated twice from an appropriate solvent for free phenol or any unreacted phenolate (acetonitrile). The <sup>19</sup>F NMR spectra of the washed polymer (bottom) clearly shows the presence of the geminal trifluoromethyl groups. So, after precipitation in acetonitrile of all the phenol and phenolate that did not react with the copolymer, the peak at -55 ppm was still noted. It proves that a part of the bisphenol-AF enabled the crosslinking of the copolymer. Under those conditions, about 40% of the phenolate were incorporated based on the internal p-fluoroanisole standard.

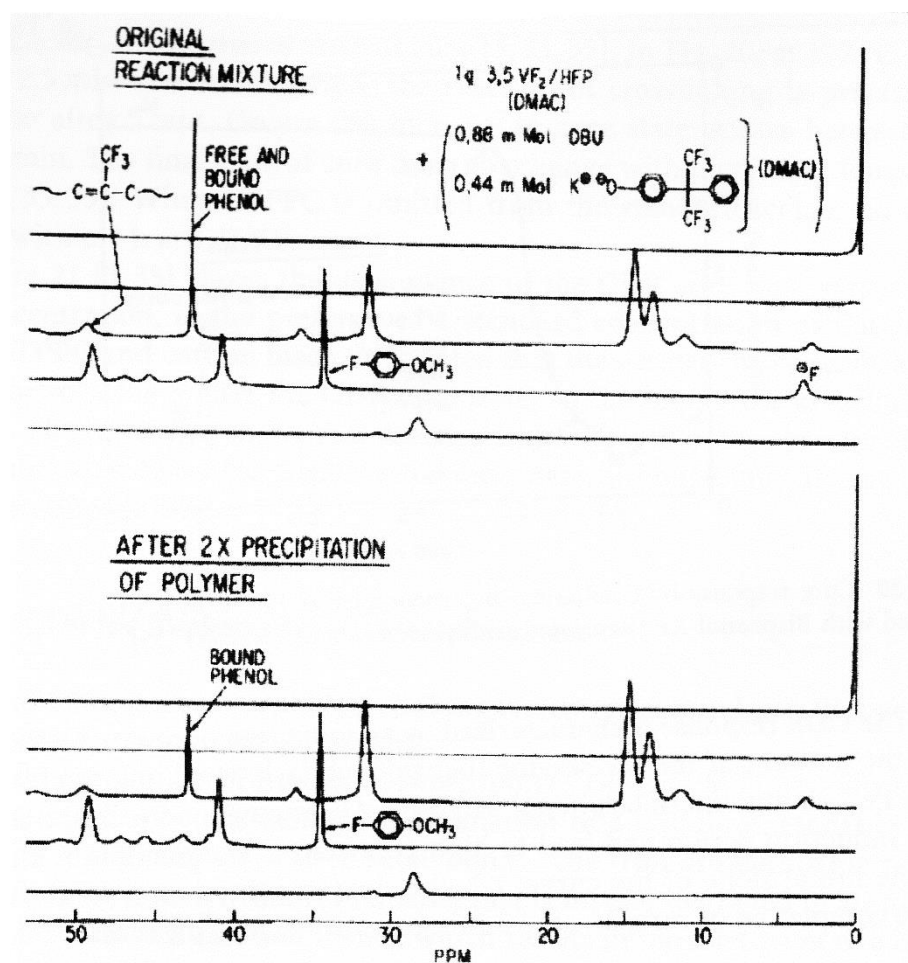


Figure 83.  $^{19}\text{F}$ -NMR spectra of a poly(VDF-co-HFP) copolymer treated with DBU and BAF in as solution of DMAC (top) and the same sample after several purifications (bottom).

Hence,  $^{19}\text{F}$  NMR results allowed us to evidence that crosslinking was achieved.

### 1.6.3 Oscillating Disc Rheometer (ODR) response

Bisphenol-cured fluoropolymers are usually analysed by ODR. Reaction time and crosslinking density can be deduced from ODR curve.

This equipment can plot the evolution of the torque (in Nm) as function of time (in min), at a given temperature, for a crosslinkable mixing (copolymer, crosslinking agent, accelerators, coagent...). Usually, the torque starts to decrease (during an induction period), and when the crosslinking reaction occurs it increases rapidly, reaching a maximum when the reaction is finished.

Bisphenols curing systems are usually used for O-ring applications [26]. Indeed, they exhibit a high resistance to high temperature compression set. Figure 84 [3,33,35] depicts the evolution of a 177°C cure response by ODR, of a bisphenol AF (BAF) curing poly(VDF-co-HFP) copolymer.

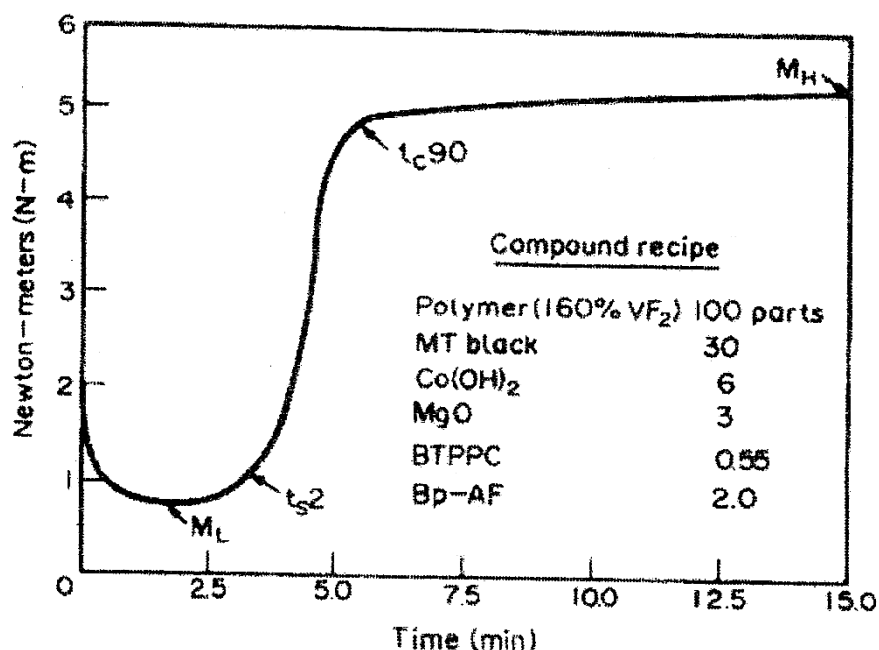


Figure 84. Cure response by ODR at 177°C of a VDF-based polymer cured with BAF.

The ODR response is characterised by an induction period, which depends on the amount of the accelerator (benzyltriphenylphosphonium chloride or BTPPC), or amount of bisphenol. High Bp-AF amounts increase the length of the induction period and lead to high cure states. The maximum cure state is the initial slope of the curve;  $t_{s2}$ , the time to initiation;  $t_{c90}$ , the time to 90% completion of cure;  $M_L$ , the minimum torque;  $M_H$ , the maximum torque; and  $M_H - M_L$ , the degree of state of cure [3,33,35]. In Figure 20, at 177°C, and after a 2.5 minutes induction period, the reaction of crosslinking is practically complete after 5 min. Only a 2% increase in cure state occurs between 13 and 60 min. The final state of cure does not change with increasing temperature [3,33,35]. When BTPPC is omitted from the standard recipe, no cure occurs within one hour at 177°C.

Figure 85 [3,33] shows the dependence of the ODR cure state versus Bp-AF concentration, in the presence of standard concentration of Ca(OH)<sub>2</sub>, MgO, BTPPC and carbon black. It is noted that the greater the concentration in bisphenols, the higher the ODR cure state, so the higher the crosslinking density. The lower line shows that the accelerator BTPPC in the absence of the bisphenol can also lead to a substantial cure state, although only at very high concentrations [3,33].

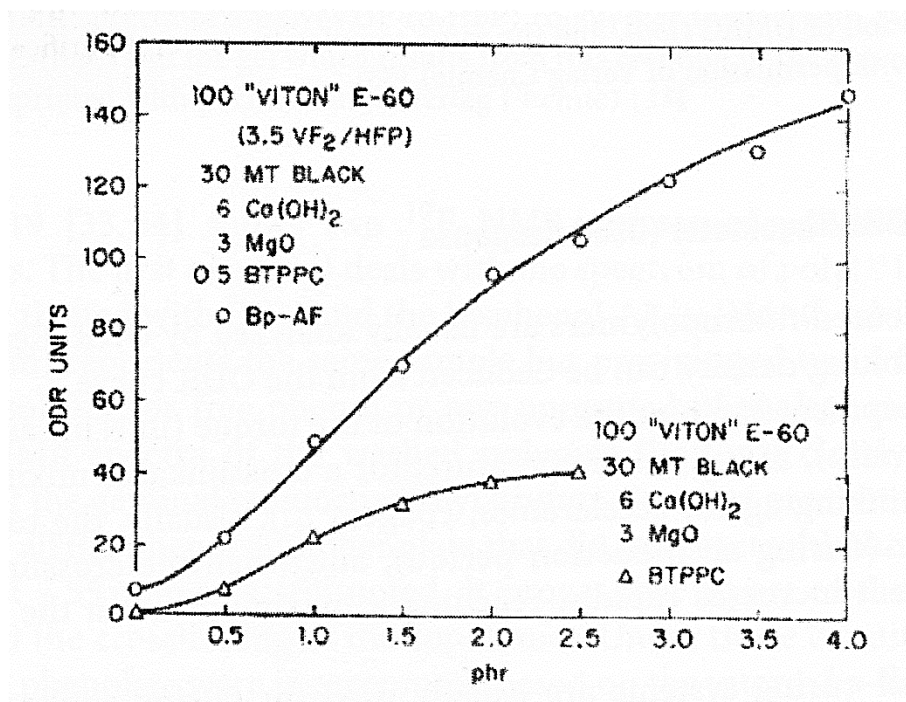


Figure 85. Evolution of the ODR units (crosslink density) at 177°C: (○) with variation of BAF concentration (in phr), in the presence of BTPPCl and (Δ) with BTPPCl concentration in the absence of BAF.

#### 1.6.4 Limitations of the bisphenol-cured fluoroelastomers

Bisphenol-cure is a very rapid crosslinking system, as shown by ODR, but this system presents also some limitations.

The crosslinking mechanism between poly(VDF-ter-PMVE-ter-TFE) terpolymer and bisphenols generates elimination of a trifluoromethoxide and a fluoride ion, giving a CF=CF double bonds. The trifluoromethoxide reacts with hydrogen, giving trifluoromethanol that is further degraded in air to hydrogen fluoride and carbon dioxide, which results in the formation of a large amount of volatiles [3,33,35]. The cured system, therefore, shows excessive porosity and poor vulcanisate properties due to volatiles produced during the curing process. For this reason, it is advisable that VDF-based polymers containing perfluoroalkyl vinyl ethers have a special cure site with curing chemistry different from nucleophilic attack on the backbone. Such a chemistry is the peroxide induced crosslinking which was specially developed to bypass these kinds of problems.

### 1.7 CROSSLINKING WITH PEROXIDES

Another technique to crosslink VDF containing fluoropolymers requires peroxides.

The first peroxide cure agents were used in 1929. But the vulcanisates obtained had poor physical properties, and poor resistance to heat ageing when compared to sulphur-cured vulcanisates.

Braden and Fletcher [140] described the vulcanisation of natural rubber with dicumyl peroxide using different compounding ingredients and comparing it with sulphur-cured compounds.

Since 1950s, peroxides/triallylisocyanurate systems, which enable crosslinking of fluoropolymers through a free radical mechanism, have been established as the best-known non sulfurated crosslinking agent.

### *1.7.1 Reaction conditions*

That kind of crosslinking is more easily achieved when the polymer bears specific group. This group or atom can be introduced into the polymer from the direct terpolymerisation of VDF and fluoroalkene.

A fluorinated monomer susceptible to copolymerise or terpolymerise vinylidene fluoride is needed to undergo free-radical attack to render peroxide curable the elastomeric co- or terpolymers of VDF [35]. So, this monomer must be functionalized or halogenated to ensure a free-radical crosslinking. The main used monomers are bromine-containing fluoroolefins such as [42,43]:

- Bromotrifluoroethylene,  $\text{BrCF}=\text{CF}_2$  [42,141,142]
- 1-bromo-2,2-difluoroethylene,  $\text{BrCH}=\text{CF}_2$  [143-145]
- 4-bromo-3,3,4,4-tetrafluorobutene-1,  $\text{CH}_2=\text{CHCF}_2\text{CF}_2\text{Br}$  [146-148]
- 3-bromoperfluoropropylene,  $\text{BrCF}_2\text{CF}=\text{CF}_2$  [149]
- Fluorobutylene  $\text{BrCF}_2\text{CF}_2\text{CF}=\text{CF}_2$ ,  $\text{BrCF}_2\text{CF}_2\text{CH}=\text{CF}_2$ ,  $\text{F}_2\text{C}=\text{CFOCF}_2\text{F}_4\text{Br}$  [150-152]
- 1,1,2-trifluoro-4-bromobutene,  $\text{F}_2\text{C}=\text{CFC}_2\text{H}_4\text{Br}$  [87]

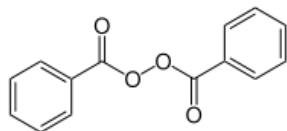
The VDF-based polymer containing the brominated monomer gives free radical intermediates on its polymeric backbone upon attack by peroxides [3,35,40,41,62-65,134]. Fluoroelastomers containing iodine or bromine atoms can be cured with peroxides. Indeed, modifications of fluorocarbon elastomers with perfluoroalkyl iodides allow to introduce iodine end groups on the polymeric chain [35,153-158]. These polymers also lead to free radical intermediates upon attack by peroxides, which in turn crosslink into a network in the presence of a radical trap. Thus, the peroxide needs a coagent to trap the polymeric radicals.

Aromatic as well as aliphatic peroxides can be used. Diacyl peroxides give low crosslinking efficiency and usually require 10 phr for adequate curing. Some dialkyl peroxides and peresters give high crosslinking efficiencies. However, mainly di-tertiary butyl peroxide and dicumyl peroxide are able to cure compounds containing reinforcing carbon black fillers [16].

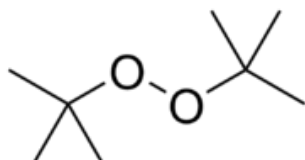


The main used peroxides are:

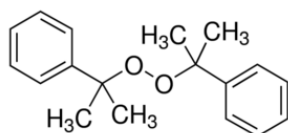
- dibenzoyl peroxide,  $t_{1/2} = 1\text{ h}$  at  $92^{\circ}\text{C}$  [16]:



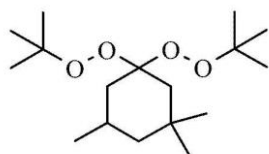
- di-*t*-butyl peroxide,  $t_{1/2} = 1\text{ h}$  at  $132^{\circ}\text{C}$  [16]:



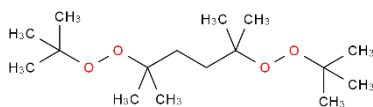
- dicumyl peroxide,  $t_{1/2} = 1\text{ h}$  at  $132^{\circ}\text{C}$  [16,159]:



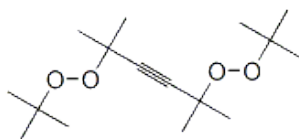
- 1,1-bis(*tert*-butylperoxy)-3,3,5-trimethylcyclohexane,  $t_{1/2} = 1\text{ h}$  at  $105^{\circ}\text{C}$  [16]:



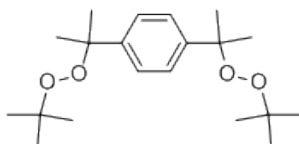
- 2,5-bis-(*t*-butylperoxy)-2,5-dimethylhexane,  $t_{1/2}=1\text{ h}$  at  $134^{\circ}\text{C}$  [40,159]:



- 2,5-bis-(*t*-butylperoxy)-2,5-dimethylhexyne,  $t_{1/2}=1\text{ h}$  at  $141^{\circ}\text{C}$  [40,159]:

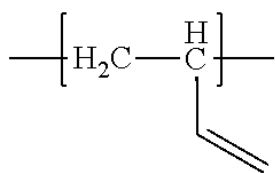


- $\alpha,\alpha'$ -bis(*t*-butylperoxy)diisopropylbenzene,  $t_{1/2} = 1\text{ h}$  at  $134^{\circ}\text{C}$  [39,159]:

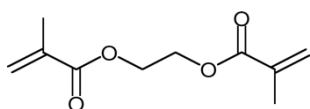


The coagents are used to enhance the crosslinking efficiency of peroxide cured compounds. They are generally di- and trifunctional vinyl compounds, such as:

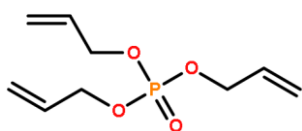
- 1,2-polybutadiene [16,159]:



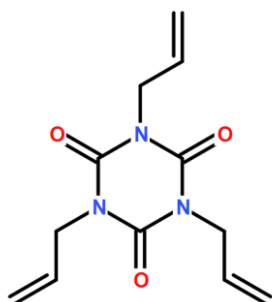
- ethylene glycol dimethacrylate [16,159]:



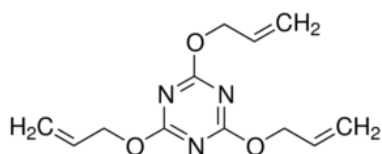
- triallyl phosphate [16]:



- triallylisocyanurate (TAIC) or triallyl-1,2,5-triazine-2,4,6-(1H,3H,5H)-trione [35,40,95,97,160]:



- triallylcyanurate (TAC), or 2,4,6-triallyloxy-1,2,5-triazine [16]:



The triazine ring is chemically and thermally stable. So, it reinforces the crosslinking network. But the best coagent is TAIC.

The crosslinking reaction also needs metal oxides such as  $\text{Ca}(\text{OH})_2$ ,  $\text{CaO}$ ,  $\text{MgO}$ ,  $\text{ZnO}$ , and  $\text{PbO}$  to absorb traces of  $\text{HF}$  generated during the curing process [35],  $\text{MgO}$ , being the most efficient one, as shown in a case above.

### 1.7.2 Importance of the coagent

The coagent, whose most efficient one is TAIC, is essential in the peroxide-cure mechanism. Indeed, it permits the reaction of crosslinking and improves the compression set resistance.

A poly(TFE-alt-P) copolymer is mixed with the  $\alpha,\alpha'$ -bis(*t*-butylperoxy)-*p*-diisopropylbenzene (5 phr), different coagents, such as divinylbenzene, N,N'-*m*-phenylenedimaleimide, 1,2- polybutadiene, trimethylolpropane trimethacrylate, diallylmelamine, TAC, TAIC (3 phr), MgO as acid acceptor (10 phr), and carbon black (35 phr), to investigate the influence of the different coagents on the gel fraction and the compression set resistance [39]. Each sample is press cured at 160°C for 30 min, and oven cured at 200°C for 2h.

Table 17 [39] exhibits the effects of the coagent on peroxide vulcanisation. By considering the compression set percentage, TAIC is found to exhibit the lowest compression set, so it is the most efficient coagent. Basic metal also contributes to improve the compression set resistance. Indeed, the percentage of compression decreases from 75 to 62% thanks to calcium carbonate in the presence of TAIC.

Table 17. Influence of the coagent on the gel fraction and the compression set resistance of a peroxide-cured poly(VDF-co-HFP) copolymer ( $M_n=100000$  g/mol).

Coagent	Gel fraction	Compression set (%)
None	0.44	100
Divinylbnzene	0.50	100
N,N'- <i>m</i> -phenylenedimaleimide	0.70	98
1,2-polybutadiene ( $M_w=2000$ )	0.66	100
Trimethylolpropane trimethacrylate	0.77	94
Diallylmelamine	0.76	95
Triallyl cyanurate (TAC)	0.80	85
Triallyl isocyanurate (TAIC)	0.84	75
Triallyl isocyanurate + CaCO <sub>3</sub>	0.89	62

Compound (phr): polymer 100,  $\alpha,\alpha'$ -bis(*t*-butylperoxy)-*p*-diisopropylbenzene 5, MgO 10, carbon black 35.  
Vulcanization conditions: press cure at 160°C for 30 min, and oven cure at 200°C for 2 h.

Figure 86 [39,40] shows the gel formation as a function of the peroxide level. The gel fraction gradually increases with the peroxide level, when coagent is not present. The cure-promoting effect of the TAIC is remarkable, yielding a gel fraction of nearly 90% at low peroxide dose. So, the crosslinking density is not really influenced by the level of peroxide when coagent (TAIC) is introduced.

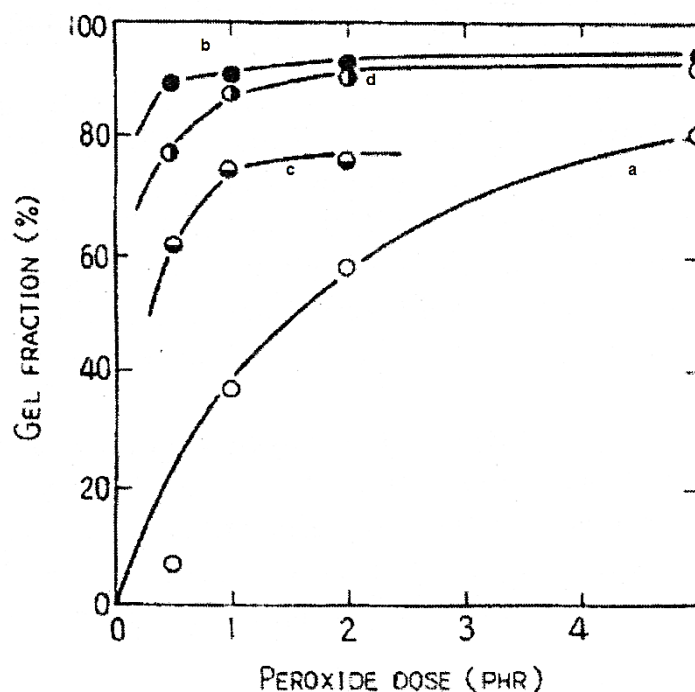


Figure 86. Evolution of the gel fraction as a function of peroxide dose (phr) for a peroxide-cured poly(TFE-alt-P) copolymer (a) without any coagent; (b) with 3 phr of TAIC; (c) with 2.4 phr of divinylbenzene; (d) with 3 phr of TAC.

The same result is obtained in the presence of the 2,5-bis-(t-butylperoxy)-2,5-dimethylhexane [40]. A poly(VDF-co-HFP) copolymer was crosslinked by this peroxide in the presence of TAIC, by oscillating disk rheometer (ODR) at 177°C for 30 min. MH-M<sub>L</sub> represents the measured cure state (or crosslinking density in N.m).

Figure 87 [40] shows that cure state tends to be more drastically influenced by coagent concentration than peroxide concentration. Indeed, Figure 87 shows that with an unchanged amount of 3 phr for the coagent, and by increasing the quantity of peroxide, the cure state remains constant, whereas with a constant amount of 3 phr of the peroxide, and by increasing the amount of the coagent, the cure state increases. However, cure rate is influenced by both TAIC concentration and peroxide concentration.

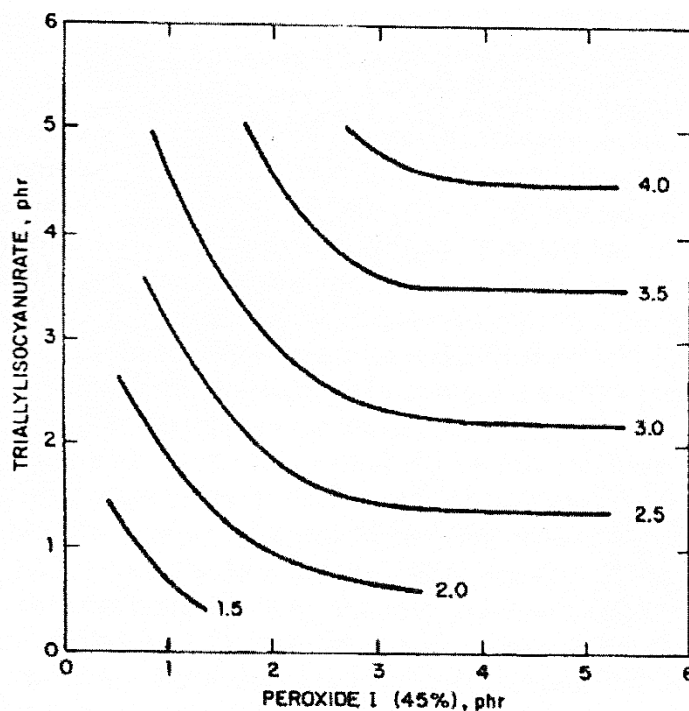


Figure 87. Interactions between peroxide and coagent, in the evolution of initial cure state (Nm) of a poly(VDF-co-HFP) copolymer, measured by ODR at 177°C for 30 min.

### 1.7.3 Influence of the nature and the amount of the peroxide

Lots of peroxides enable the curing of VDF-based fluoropolymers, but the nature of the peroxides, and the molar amount can influence many different factors such as the curing temperature and the gel fraction.

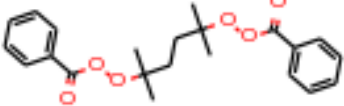
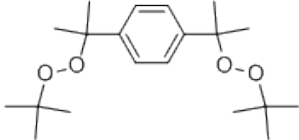
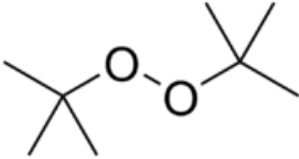
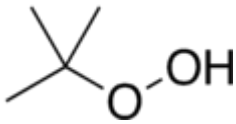
Identical cure systems are crosslinked, with either 2,5-bis-(*t*-butylperoxy)-2,5-dimethylhexane, or 2,5-bis-(*t*-butylperoxy)-2,5-dimethylhexyne [35,40]. Table 18 [35] shows the different cure state obtained when changing the peroxide and the temperature. For both peroxides, the cure state exhibits a maximum at a fixed temperature. For 2,5-bis-(*t*-butylperoxy)-2,5-dimethylhexane, the cure state is maximum at 177°C, whereas with 2,5-bis-(*t*-butylperoxy)-2,5-dimethylhexyne, it is maximum at 182°C. Moreover, 2,5-bis-(*t*-butylperoxy)-2,5-dimethylhexane is also more efficient than 2,5-bis-(*t*-butylperoxy)-2,5-dimethylhexyne. Indeed, the first peroxide reaches a cure state of 8.6 Nm, whereas it is 7.7 Nm for the second one.

Table 18. Crosslinking of two peroxides onto poly(VDF-co-HFP) copolymer and the influence of their cure temperature on ODR values.

Cure temperature (°C)	Peroxide half-life (min)	ODR Values		
		t <sub>s2</sub> (min)	t <sub>c90</sub> (min)	Cure state, M <sub>H</sub> - M <sub>L</sub> (Nm)
2,5-bis-(t-butylperoxy)-2,5-dimethylhexane				
160	4.80	4.0	24.0	8.0
177	0.80	1.6	8.3	8.6
190	0.24	1.4	4.6	8.2
204	0.07	0.8	2.8	7.9
2,5-bis-(t-butylperoxy)-2,5-dimethylhexyne-3				
160	18.7	7.1	41.0	-
177	3.4	3.4	14.0	7.7
190	1.0	2.1	7.5	7.7
204	0.3	1.2	4.2	7.5

Gel fractions were measured from different poly(TFE-*alt*-P) copolymers cured by peroxide. In Table 19 [39], 30 eq.mol<sup>-1</sup> polymer of peroxide (acyl-, alkyl- or hydro-) are added to a poly(TFE-*alt*-P) copolymer and vulcanised in mold at 160°C for 30 min, and post cure at 200°C for 2h. Gel fraction results indicate that these peroxides achieve vulcanisation, except for the hydroperoxide which tends to decompose ionically. The best result was obtained with  $\alpha,\alpha'$ -bis(t-butylperoxy)diisopropylbenzene, but even in this case, the gel fraction was only 44% because of the absence of a coagent.

Table 19. Half-life and gel fraction values of poly(TFE-co-P) copolymers ( $M_n=100000$  g/mol) cured with acyl-, alkyl- or hydroperoxides.

Peroxides	Type	Peroxide group	$t_{1/2}$ (min)	Gel fraction
	Acyl	2	1.2	0.05
	Alkyl	2	4.0	0.44
	Alkyoxy or methyl	1	12.0	0.10
	Hydroxy	1	6.0	0.00

The samples are press cured at 160°C for 30min and post cured at 200°C for 2 h.

A rheometric study [159] was carried out by different tested poly(VDF-ter-HFP-ter-TFE) terpolymers cured by peroxides (dicumyl peroxide (40%) for P-1; 1,3-bis(tert-butylperoxyisopropyl)-benzene (40%) for P-2; 1,1-bis(tert-butylperoxy)-3,3,5-trimethylcyclohexane (40%) for P-3; 2,5-bis-(tert-butylperoxy)-2,5-dimethylhexane (45%) for P-4; 2,5-bis-(tert-butylperoxy)-2,5-dimethylhexyne (45%) for P-5) with the same coagent (TAIC). Table 20 [159] gives the composition of the compounds used in the study. Compounds (FP-1 to FP-5) differ only from the type and the amount of the peroxide.

Table 20. Composition of different Viton GF compounds cured with peroxide.

Component	Compound				
	FP-1	FP-2	FP-3	FP-4	FP-5
<b>Viton GF<sup>1</sup></b>	100	100	100	100	100
<b>Carbon black</b>	30	30	30	30	30
<b>PbO</b>	3	3	3	3	3
<b>TAIC</b>	3	3	3	3	3
<b>P-1<sup>2</sup></b>	3				
<b>P-2<sup>3</sup></b>		4.8			
<b>P-3<sup>4</sup></b>			3.4		
<b>P-4<sup>5</sup></b>				3	
<b>P-5<sup>6</sup></b>					3

<sup>1</sup>poly(VDF-ter-HFP-ter-TFE) terpolymer<sup>2</sup>P-1 = dicumylperoxide<sup>3</sup>P-2 = *a,a'*-bis(*t*-butylperoxy)diisopropylbenzene,<sup>4</sup>P-3 = 1,1-bis(*tert*-butylperoxy)-3,3,5-trimethylcyclohexane<sup>5</sup>P-4 = 2,5-bis-(*t*-butylperoxy)-2,5-dimethylhexane<sup>6</sup>P-5 = 2,5-bis-(*t*-butylperoxy)-2,5-dimethylhexyne-3

Figure 88 [159] is the cure response of an oscillating disc rheometer of the compounds mentioned in Table 20. Figure 88 demonstrates that the rate of crosslinking varies drastically for the industrial peroxides. Efficiencies of P-4 and P-5 are outstanding as compared to the three other peroxides, but in the presence of P-3, no crosslinking could be detected by rheometric curve.

So, the following decreasing activity series of the peroxides can be suggested:  
P-5  $\approx$  P-4  $\gg$  P-1  $\approx$  P-2.



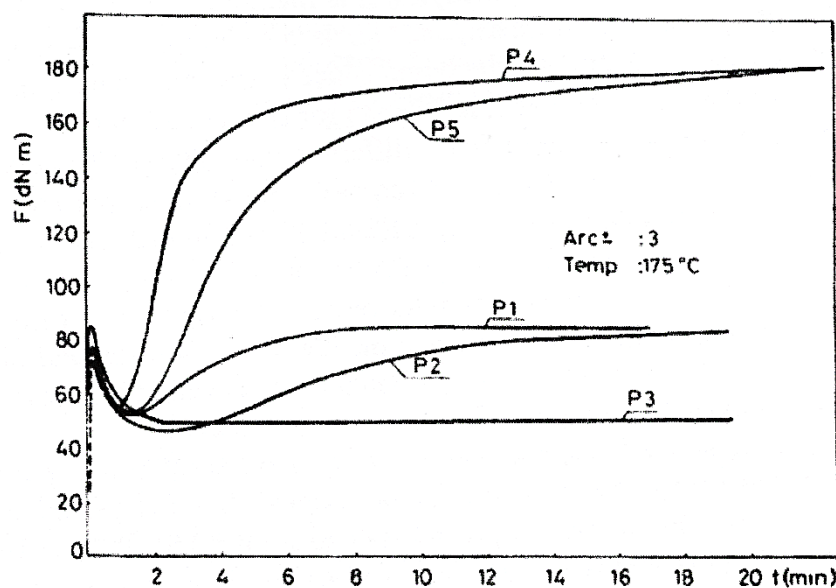


Figure 88. Rheometer curve of the compounds containing different peroxides.

#### 1.7.4 Mechanism of crosslinking

The crosslinking mechanism with peroxide/ TAIC system is slightly different from these of diamine or bisphenol ones.

Scheme 22 [3,16,35] shows the most probable reaction taking place in a fully compounded stock. An initial process is the thermally induced homolytic cleavage of a peroxide molecule to yield two oxy radicals. The primary decomposition of the 2,5-bis-(*t*-butylperoxy)-2,5- dimethylhexane leads to the formation of a *t*-butoxy radical, which may, in a minor reaction, abstract a hydrogen atom to give a *t*-butanol, and in a major reaction (usually from 120°C), decomposes into acetone and methyl radical. The methyl radical, in turn, can abstract a bromine atom from the polymer, to give methyl bromine, or add to the triallyl(iso)cyanurate to give a more stable radical intermediate. These intermediate radicals abstract bromine from the polymer to generate polymeric radicals. The driving force for the chain reaction during propagation is the transfer of a bromine atom from the electron-poor fluoropolymer to an electron-rich hydrocarbon radical on the coagent. Crosslinking takes place when the polymeric radicals add to allylic bonds of the trifunctional coagent. The coagent, therefore becomes the crosslinker.



The cure temperature chosen in peroxide formulations depends on the stability, and the half-life of the peroxide. Peroxides with acid groups decompose at lower temperatures than those involving dialkyl or diaryl peroxide. Thus, dicumyl peroxide offers better processing safety than dibenzoyl peroxide does. According to Bristow [161], to obtain peroxide cured natural vulcanisates endowed with the best properties, cure times should not be less than one hour at 160°C, 3h at 150°C, and 8h at 140°C.

Peroxide and bisphenol or diamine- cured systems are differentiating by the type of reaction of crosslinking. Bisphenols or diamines exhibit a dehydrofluorination of the fluoropolymer backbone, followed by a Michael addition for the diamine, and a substitution of the fluorine atom for the bisphenols. Peroxide-cure reaction is a free radical attack, and so this system needs special cure site monomers. Another important crosslinking system that implies radical is the radiation crosslinking.

### ***1.8 COMPARISON OF PHYSICAL AND MECHANICAL PROPERTIES***

All the different cured systems mentioned previously differ from the crosslinking agents and mechanism, but also from the crosslinking density, and the mechanical properties, such as compression set resistance, elongation at break, modulus at 100 and 200%, tensile strength, hardness of the cured material, etc... The comparison of the crosslinking density and the different mechanical properties for the main cured systems (diamines, bisphenols and peroxides) is the subject of this part.

Regarding resistance to acids ( $\text{H}_2\text{SO}_4$ ,  $\text{HNO}_3$ ), to bases ( $\text{NaOH}$ ,  $\text{NaClO}$ ), and to water, by measuring the volume increase after immersion, it is clear that peroxide-cured elastomers are more resistant to acids, to bases and to water than those from diamine one. Indeed, this last system decomposes when immersed in a strong base or an acid solution.

Nevertheless, diamine-cured systems have a lower percentage of volume increase after immersion in oil and fuel oil than peroxide ones.

Figure 89 [3,35,134] compares the crosslinking density of post cure diamine, bisphenol or peroxide cured systems at 204°C under nitrogen. The vulcanisate crosslinking density of bisphenol and peroxide cured systems, before and after post curing remains the same, whereas that of the diamine vulcanisate increases substantially. This implies that diamine is a better crosslinking agent than bisphenol or peroxide regarding crosslinking densities.

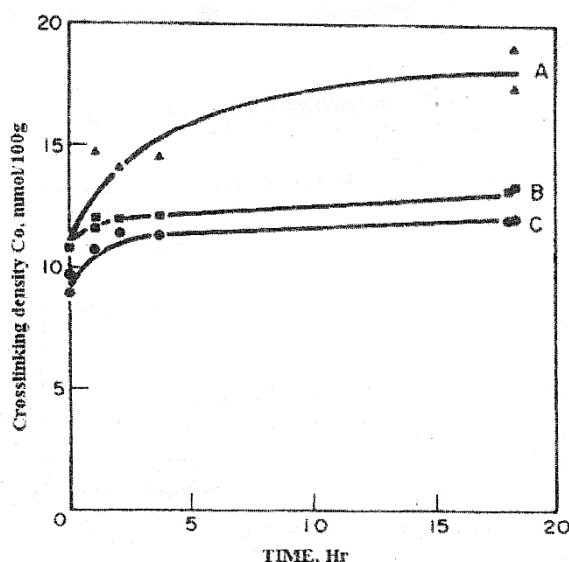


Figure 89. Crosslinking density of cured gum stocks versus post cure time at 204°C, under nitrogen: (A) diamine cured system; (B) peroxide cured system and (C) bisphenol cured.

A Viton A-HV (poly(VDF-co-HFP) copolymer) is crosslinked with a same amount of a diamine (biscinnamylidene hexamethylene diamine or LD-214) and a peroxide (benzoyl peroxide), in the presence of Maglite D (MgO) [23]. Different mechanical properties (tensile strength, elongation at break, and hardness) are evaluated for both press cure and post cure systems. Tables 21 I and II [23] shows that peroxide cure system leads to materials which exhibit higher tensile strengths, whereas diamine improves the elongation and hardness of the resulting crosslinked macromolecules. Table 16 II also shows that post cure step improves readily each mechanical property (tensile strength, elongation and hardness). So, this step is essential in the crosslinking mechanism.

Table 21. Composition of vulcanizates I and II.

Components	Vulcanisate I (phr)	Vulcanisate II (phr)
Viton A-HV <sup>1</sup>	100	100
Maglite D <sup>2</sup>	15	15
LD-214 <sup>3</sup>	4	-
Benzoyl peroxide, 95%	-	4

<sup>1</sup>Viton A-HV = poly(VDF-co-HFP) copolymer

<sup>2</sup>Maglite D = MgO

<sup>3</sup>LD-214 = biscinnamylidene hexamethylene diamine

Other mechanical properties and resistance to bases and to acids are studied for a poly(TFE-*alt*-P) elastomer cured with a peroxide ( $\alpha,\alpha'$ -bis-(*t*-butylperoxy)-*p*-diisopropylbenzene), and a poly(VDF-*ter*-HFP-*ter*-TFE) terpolymer cured with a diamine (N,N' dicinnamylidene-1,6- hexanediamine) (Table 22) [39].

As in Table 21 II, peroxide-cured systems exhibit a better tensile strength, and a better compression set resistance, whereas diamines exhibit higher elongation at break and hardness.

Table 22. Mechanical properties of vulcanizates I (diamine cure) and II (peroxide cure) after press cure at 150°C for 30min and post cure from 120°C to 200°C at heating rate of 25°C/h then heat at 200°C for 24h.

Properties	Vulcanisate I		Vulcanisate II	
	Press cure	Post cure	Press cure	Post cure
<b>Tensile strength (psi)</b>	2230	3250	3550	3650
<b>Elongation (%)</b>	460	310	460	420
<b>Hardness, shore A</b>	64	68	60	63

Table 14 [35] displays different mechanical properties (modulus at 100%, tensile strength, elongation at break and compression set for O-rings and pellets) for bisphenol-cured and peroxide-cured poly(VDF-*ter*-HFP-*ter*-TFE) terpolymer, after press cure at 177°C for 10 min and after post cure at 232°C for 24h. As in Table 22 II, Table 2 shows an improvement of the mechanical properties after post cure. Moreover, bisphenol-cured system has a better compression set resistance than peroxide-cured system, whereas peroxide-cured system has better modulus at 100%, better tensile strength, better elongation than those resulting from bisphenol crosslinking.

A study of several mechanical properties (100% Modulus, tensile strength, elongation at break, and compression set resistance) of bisphenol AF and peroxide (2,5-dimethyl-2,5-di-*t*-butylperoxyhexane)-cured poly(VDF-*co*-HFP) copolymers is supplied in Table 23 [40]. First, the post cure step improves all mechanical properties. Then, bisphenol post cure systems exhibit a better compression set resistance than peroxide one, whereas peroxide- cured polymer exhibits better modulus at 100%, better tensile strength, and better elongation at break than bisphenol-cured polymer.

Table 23. Mechanical and chemical properties of a peroxide-cured poly(TFE-alt-P) elastomer and a diamine-cured poly(VDF-ter-HFP-ter-TFE) elastomer

Properties	Peroxide <sup>1</sup> cured TFE/P elastomer	Diamine <sup>2</sup> cured VDF/HFP/TFE terpolymer
<i>Physical properties:</i>		
Specific gravity (g/cm <sup>3</sup> )	1.60	1.93
Tensile strength (MPa)	20-25	14-17
Elongation at break (%)	200-400	400-500
Tensile modulus at 100% (MPa)	2.5-3.5	4.0-5.0
Hardness, shore A	70	83
Compression set <sup>3</sup> (%)	35	49
Brittle point (°C)	-40	-45
Retraction temperature (°C)	3	-20
<i>Chemical resistance</i>		
Volume increase after immersion (%)		
96% H <sub>2</sub> SO <sub>4</sub> , 100°C, 3 d	4.4	45
60% HNO <sub>3</sub> , 70°C, 3 d	10.0	Decomposed
50% NaOH, 100°C, 3 d	1.1	Decomposed
10% NaClO, 100°C, 7 d	1.0	Decomposed
H <sub>2</sub> O, 100°C, 3 d	1.1	5.9
Steam, 160°C, 7 d	4.6	12.8
Oil #1, 150°C, 3 d	2.0	0.5
Oil #3, 150°C, 3 d	10.0	2.0
Fuel oil, 25°C, 7 d	38	3.0

Flisi [131] studied the evolution of elongation at break and tensile strength for a poly(VDF- co- HFP) Tecnoflon N copolymer cured with a bisphenol AF and diamines (melting of piperazine carbamate and trimethylene diamine carbamate). Figures 90 and 91 [131] represent elongation at break and tensile strength versus time for those samples. This author showed that elongation at break (Figure 34) decreased continuously because the network chains became shorter. Moreover, crosslinking with bisphenol yielded materials with a higher elongation than those achieved from diamine. Tensile strength (Figure 35) decreased slowly in bisphenol vulcanisate during the whole period of 32 days, while the curve of the diamine vulcanisate presents an irregular trend. Indeed, the curve first decreased, then increased, and finally decreased again.

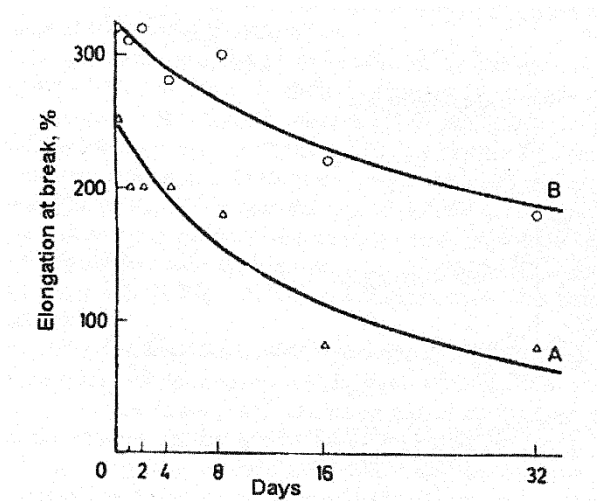


Figure 90. Dependence of elongation at break versus aging time of a poly(VDF-co-HFP) copolymer crosslinked with piperazine carbamate and trimethyl diamine carbamate (curve A) and cured with Bisphenol AF (curve B).

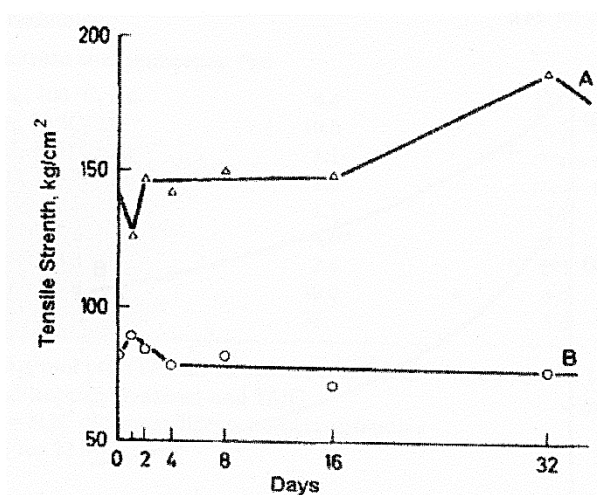


Figure 91. Dependence of tensile strength versus ageing time of the same sample than Fig. 90.

First, the best compression set resistance was obtained for curve 4 (biphenol-AF cured poly(VDF-co-HFP) copolymer). Second, little improvement was obtained in Tecnoflon T by changing

the curing agent from HMDA-C (curve 1) to piperazine carbamate (curve 2). Finally, no practical difference was observed by changing the polymer with the same formulation, since curves 2 and 3 have the same behaviour.

Table 24 summarizes the efficiency of bisphenol, peroxide and diamine cure systems regarding each mechanical property. Bisphenols and peroxides-cured fluorinated polymer exhibit better tensile strength, and resistance to bases and acids than diamine-cured systems. However, diamine-cured VDF-based polymers show a higher hardness and resistance to oil than those of peroxide- and bisphenol-cured systems. Indeed, bisphenol was shown to be the best crosslinking agent for a high compression set resistance. By regarding the thermostability of each cure system, the diamine (biscinnamylidene hexamethylene diamine) cure copolymer decomposes at 457°C whereas the peroxide one decomposes at 472°C [23,184]. The diamine cure is thermally more stable than the hydroquinone one [29].

Table 24. Mechanical properties for press cure and post cure VDF/HFP copolymer cured with BAF or peroxide.

Compounds	VDF/HFP copolymer cured by BAF <sup>1</sup>		VDF/HFP copolymer cured by peroxide <sup>1</sup>	
Post cure <sup>2</sup>	No	Yes	No	Yes
<b>Stress-strain, 25°C</b>				
<b>100% Modulus (MPa)</b>	4.5	6.3	5.3	11.4
<b>Tensile strength (MPa)</b>	11.7	14.5	10.4	15.9
<b>Elongation at break (%)</b>	250	185	200	140
<b>Compression set<sup>3</sup> (%)</b>				
<b>Pellets</b>	85	15	45	18
<b>O-ring</b>	40	16	44	25

<sup>1</sup>both cured samples are press cured at 177°C for 30 min

<sup>2</sup>post cured at 232°C for 24 h

<sup>3</sup>at 200°C for 70 h



## ***1.9 APPLICATIONS***

The chemical, physical and mechanical properties mainly depend on the crosslinking agent. Those properties are crucial for the applications.

The thermal stability, sealing capability and chemical resistance of fluoroelastomers have led to increase their use in a broad variety of industries. Applications for fluorocarbon elastomers in automotive, petroleum, and energy related industries illustrate the potential for those high- performance elastomer [115].

Fluoroelastomers are nowadays widely used in the industry as O-rings, V-rings, gaskets and other types of static and dynamic seals, as diaphragms, valve seals, hoses, coated clothes, shaft seals [185], expansion joints, etc [186]. They are also used in cars as O-rings for fuel, shaft seals and other components of fuel and transmission systems [35,58,63-66].

Moreover, some properties of fluoroelastomers, and especially those of VDF-based elastomers can be improved by crosslinking. Those better properties allow one to use cured fluoroelastomers in new applications as mentioned below.

The elastomeric poly(VDF-co-HFP) copolymers crosslinked with polyamine possess high temperature stability, good resistance to a wide variety of solvents, oils, and fuels [187]. So, these cured elastomers are particularly suitable for use in the manufacture of tubing employed as aircraft hoses, used to carry fuel lubricants, at high temperature and under high pressure [188]. Moreover, poly(VDF-co-HFP) copolymers crosslinked with aminosilane are used in the aircraft construction industry because they are also odorless [189].

Other applications of cured fluoroelastomers are sealings, O-rings [26] and oil seals [26,115,131,190]. It is mentioned above that a cured VDF-based copolymer has a better compression set resistance than a raw rubber. This property is essential for the sealing application.

Peroxide curable VDF-based copolymer and terpolymer offer improved extrusion characteristics. They can be vulcanised at atmospheric pressure and eliminates fissuring in thick sections. They have applications as cords, tubes or irregular-profile items of any dimension [40,191].

A poly(VDF-co-HFP) copolymer is applied to a metallic substrate, as coating composition and crosslinked with amine, diamine, or ethoxysilane [192]. This cured polymer used as thick or thin free standing films, or thick or thin films with good adhesion to metallic or other rigid surfaces [192]. Moreover, diamine-cured PVDF can be used as strong adhesive joints without prior surface modification [31].

Crosslinkable fluoropolymers based on TFE, TrFE, HFP, VDF, CTFE, and perfluoro(alkylvinylether) can form corrosion resistant structures [193].

Another application of cured fluoroelastomer is a multi-layer insulator system for electrical conductors. This system possesses an extruded crosslinked fluoroelastomer outer layer with the fluoropolymer selected from copolymer or terpolymer of ethylene and TFE.

Irradiated PVDF and poly(VDF-co-TrFE) copolymer possess ferroelectric properties that allow the use of such fluorinated polymer in the domain of captors, sensors, and detectors [47,194]. Another interesting property of crosslinked poly(VDF-co-HFP) copolymer is their insolubility in organic solvent [195]. Cured fluorinated polymers can be processed as membranes for many electrochemical applications such as fuel cell and batteries [196]. For example, a poly(VDF-co-HFP) copolymer has been crosslinked with polyamines, polyols, by irradiation with electron beam or  $\gamma$ -rays in order to elaborate a solid polymer electrolyte for non-aqueous lithium battery [197]. This electrolyte is particularly interesting for its ionic conductivity, its adhesion with an electroconductive substrate and also remarkably enhanced heat resistance.

## REFERENCES FOR CHAPTER 1

- [1]. Montermoso JC (1961) Rubber Chem Techn 34:1521
- [2]. Cooper JR (1968) High Polymers 23:273
- [3]. Schmiegel WW, Logothetis AL (1984) ACS Symposium Series, No. 260, Polymers for Fibers and Elastomers 260:159
- [4]. Anderson RF, Punserson JO (1979) Organofluorine Chemicals and Their Industrial Applications, Banks RE (ed), Horwood, Chichester
- [5]. Abu-Isa IA, Trexler HE (1985) Rubber Chem Techn 58:326
- [6]. Frapin B (1987) Revue Generale des Caoutchoucs & Plastiques 672:125
- [7]. Wall L (1972) Fluoropolymers. Wiley, New York
- [8]. Banks RE, Smart BE, Tatlow JC (1994) (eds) Organofluorine Chemistry: Principles and Commercial Applications, Wiley, New York
- [9]. Scheirs J (1997) Modern Fluoropolymers, Wiley, New York
- [10]. Ajroldi G (1997) Chimica e l'Industria 79:483
- [11]. Hougham G, Cassidy PE, Johns K, Davidson T (1999) (eds) Fluoropolymers 2: Properties, Kluwer Academic/Plenum Publishers, New York
- [12]. Johns K, Stead G (2000) J Fluorine Chem 104:5
- [13]. Imae T (2003) Current Opinion in Colloid & Interface Science 8:307
- [14]. Ameduri B, Boutevin B (2004) Well-Architected Fluoropolymers: Synthesis, Properties and Applications. Elsevier, Amsterdam
- [15]. Schmiegel WW (2004) Kaut Gum Kunst 57:313
- [16]. Ogunniyi DS (1999) Prog Rubber Plastics Techn 15:95
- [17]. Pruett RL, Barr JT, Rapp KE, Bahner CT, Gibson JD, Lafferty RH (1950) J Amer Chem Soc 72:3646
- [18]. Moran AL, Kane RP, Smith JF (1959) J Ind Eng Chem (Washington, D. C.) 51:831
- [19]. Smith JF (1960) Rubber World 142:102
- [20]. Paciorek KL, Mitchell LC, Lenk CT (1960) J Polym Sc 45:405
- [21]. Smith JF, Perkins GT (1961) Rubber and Plastics Age 42:59

- [22]. Paciorek KL, Merkl BA, Lenk CT (1962) J Org Chem 27:266
- [23]. Paciorek KL, Lajiness WG, Lenk CT (1962) J Polym Sc 60:141
- [24]. Thomas DK (1964) J Appl Polym Sc 8:1415
- [25]. Thomas DK (1969) GB Patent 1 175 417
- [26]. Moran AL, Pattison DB (1971) Rubber Age 103:37
- [27]. Smith TL, Chu WH (1972) J Polym Sc, Polym Phys Ed 10:133
- [28]. Arnold RG, Barney AL, Thompson DC (1973) Rubber Chem Techn 46:619
- [29]. Knight GJ, Wright WW (1973) British Polym J 5:395
- [30]. Ogunniyi DS (1988) Rubber Chem Techn 61:735
- [31]. Schonhorn H, Luongo JP (1989) J Adh Sc Techn 3:277
- [32]. Schmiegel WW (1978) Kaut Gum Kunst 31:137
- [33]. Schmiegel WW (1979) Angew Makromol Chem 76/77:39
- [34]. Pianca M, Bonardelli P, Tato M, Cirillo G, Moggi G (1987) Polymer 28:224
- [35]. Logothetis AL (1989) Progress in Polymer Science 14:251
- [36]. Carlson DP, Schmiegel WW (1989) Eur Patent 333062
- [37]. Arcella V, Brinati G, Apostolo M (April 1997) Chem Ind p 490
- [38]. Schmiegel WW (2002) US Patent 2003065132
- [39]. Kojima G, Wachi H (1978) Rubber Chem Techn 51:940
- [40]. Finlay JB, Hallenbeck A, MacLachlan JD (1978) J Elast Plast 10:3
- [41]. Apothecker D, Krusic PJ (1980) US Patent 4214060
- [42]. Ameduri BM, Armand M, Boucher M, Manseri A (2001) PCT WO2001096268
- [43]. Coggio WD, Scott PJ, Hintzer K, Hare ED (2004) US Patent 2004014900
- [44]. Ameduri B, Boutevin B, Kostov GK, Petrova P (1999) Designed Monomers and Polymers 2:267
- [45]. Clark DT, Brennan WJ (1988) J El Spectr Rel Phen 47:93
- [46]. Suther JL, Laghari JR (1991) J Mat Sc Let 10:786
- [47]. Betz N, Petersohn E, Le Moel A (1996) Nuclear Instruments & Methods in Physics

Research, Section B: Beam Interactions with Materials and Atoms 116:207

[48]. Banik I, Bhowmick AK (2000) Rad Phys Chem 58:293

[49]. Banik I, Bhowmick AK (2000) J Mat Sc 35:3579

[50]. Ameduri B, Boutevin B, Kostov G (2001) Prog Polym Sc 26:105

[51]. Nasef MM, Dahlan KZM (2003) Nuclear Instruments & Methods in Physics Research, Section B: Beam Interactions with Materials and Atoms 201:604

[52]. Soresi B, Quartarone E, Mustarelli P, Magistris A, Chiodelli G (2004) Solid State Ionics 166:383

[53]. Lee WA, Rutherford RA (1975) The glass transition temperatures of polymers. In: Brandrup J, Immergut EH (eds) Polymer Handbook, Wiley-Interscience, New York

[54]. Seilers DA (1997) PVDF in the chemical processing industry. In: Scheirs J (ed) Modern Fluoropolymers. Wiley, New York, chap 25 p 487

[55]. Smith S (1982) Fluorelastomers. In: Banks RE (ed) Preparation, Properties, and Industrial Applications of Organofluorine Compounds. Ellis Harwood. Chichester, chap 8 p 235

[56]. England DC, Uschold RE, Starkweather H, Pariser R (1983) Proceedings of the Robert A. Welch Foundation Conference on Chemical Research, Houston, Texas vol 26 p 192

[57]. Uschold RE (1985) Polym J (Tokyo, Japan) 17:253

[58]. Logothetis AL (1994) Fluoroelastomers In: Banks RE, Tatlow JC (eds) Organofluorine Chemistry: Principles and Commercial Applications. Wiley, New York chap 16 p 373

[59]. Bowers S (1997) Proceedings of Fluoroelastomers. In: Scheirs J (ed) Modern Fluoropolymers. Wiley, New York chap 5 p 115

[60]. Tournut C (1994) Macromol Symp 82:99

[61]. Tournut C (1997) Thermoplastic copolymers of vinylidene fluoride, Modern Fluoropolymers. In: Scheirs J (ed) Modern Fluoropolymers, Wiley, New York Chap 31 p 577

[62]. Lynn MM, Worm AT (1987) Encycl Polym Sci Eng 7:257

[63]. Cook D, Lynn M (1990) Rapra Review Reports 3:32/1

- [64]. Arcella V, Ferro R (1997) Fluorocarbon elastomers. In: Scheirs J (ed) Modern Fluoropolymers, Wiley, New York, Chap2 p71
- [65]. Van Cleeff A (1997) Fluoroelastomers In: Scheirs J (ed) Modern Fluoropolymers. Wiley, New York Chap 32 p 597
- [66]. Logothetis AL (1997) Perfluoroelastomers and their Functionalization Macromolecular Design of Polymeric Materials. M. Dekker Inc., New York, Chap 26 p 447
- [67]. Sianesi D, Bernardi C, Regio A (1967) US Patent 3331823
- [68]. Sorokin AD, Volkova EV, Naberezhnykh RA (1972) Radiat Khim 2:295
- [69]. Baradie B, Shoichet MS (2002) Macromolecules 35:3569
- [70]. Guiot J (2003) PhD Thesis, University of Montpellier
- [71]. Souzy R, Ameduri B, Boutevin B (2004) Macromol Chem Phys 205:476
- [72]. Sianesi D, Caporiccio G (1968) J Polym Sc, PartA1: Polym Chem 6:335
- [73]. Caporiccio G, Sianesi D (1970) Chimica e l'Industria 52:37
- [74]. Ameduri B, Bauduin G (2003) J Polym Sc, Part A: Polym Chem 41:3109
- [75]. Yagi T, Tatemoto M (1979) Polym J (Tokyo, Japan) 11:429
- [76]. Usmanov KU, Yul'chibaev AA, Mukhamadaliev N, Sarros TK (1975) Izvestiya Vysshikh Uchebnykh Zavedenii, Khimiya i Khimicheskaya Tekhnologiya (Chem. Abstr. 83, 28687) 18:464
- [77]. Otazaghine B, Ameduri B (2000 (July 16-20) The 16th International Symposium in Fluorine Chemistry. Durham, United Kingdom and Otazaghine B, Sauguet L, Ameduri B (2005) J Fluorine Chem (in press)
- [78]. Moggi G, Bonardelli P, Bart JCJ (1984) J Polym Sc, Polym Phys Ed 22:357
- [79]. Dohany RE, Dukert AA, Preston SS (1989) Encycl Polym Sci Technol 17:532
- [80]. Bonardelli P, Moggi G, Turturro A (1986) Polymer 27:905
- [81]. Naberezhnykh RA, Sorokin AD, Volkova EV, Fokin AV (1974) Izvestiya Akademii Nauk SSSR, Seriya Khimicheskaya:232
- [82]. Moggi G, Bonardelli P, Russo S (1983) Con Ital Sci Macromol 6th 2:405
- [83]. Gelin MP, Ameduri B J Fluorine Chem 126:577
- [84]. Otazaghine B, Sauguet L, Ameduri B Eur Polym J (in press)

- [85]. Ameduri BM, Manseri A, Boucher M (2002) PCT WO2002050142
- [86]. Guiot J, Ameduri B, Boutevin B (2002) J Polym Sc, Part A: Polym Chem 40:3634
- [87]. Sauguet L, Guiot J, Neouze MA, Ameduri B, Boutevin B (2005) J Polym Sc Polym Chem 43:917
- [88]. Ameduri B, Bauduin G, Boutevin B, Kostov G, Petrova P (1999) Macromolecules 32:4544
- [89]. Souzy R, Guiot J, Ameduri B, Boutevin B, Paleta O (2003) Macromolecules 36:9390
- [90]. Khodzhaev SG, Yusupbekova FZ, Yul'chibaev AA (1981) Sbornik Nauchnykh Trudov - Tashkentskii Gosudarstvennyi Universitet im. V. I. Lenina (Chem. Abstr. 97, 163545) 667:34
- [91]. Guiot J, Ameduri B, Boutevin B, Lannuzel T (2003) Eur Polym J 39:887
- [92]. Souzy R, Ameduri B, Boutevin B (2004) J Polym Sc, Part A: Polym Chem 42:5077
- [93]. Souzy R, Ameduri B, Boutevin B, Capron P, Gebel G (2005) Fuel Cell (in press)
- [94]. Lannuzel T, Ameduri B, Guiot J, Boutevin B (2004) French Patent 20042852316
- [95]. Dittman AL, Passino HJ, Wrightson JM (1954) US Patent 2689241
- [96]. Dixon S, Rexford DR, Rugg JS (1957) J Indus Eng Chem (Washington, D. C.) 49:1687
- [97]. Rugg JS, Stevenson A.C., Rexford D.S. (1957) Rubber World 82:102
- [98]. Pailthorp JR, Schroeder HE (1961) US Patent 2968649
- [99]. Rexford DR (1962) US Patent 3051677
- [100]. Conroy ME, Honn FJ, Robb LE, Wolf DR (1955) Rubber Age 76:543
- [101]. Griffis CB, Montermoso JC (1955) Rubber Age 77:559
- [102]. Jackson WW, Hale D (1955) Rubber Age 77:865
- [103]. Watanabe T, Momose T, Ishigaki I, Tabata Y, Okamoto J (1981) J Polym Sc, Polym Let Ed 19:599
- [104]. Ohmori A, Tomihashi N, Inukai H, Shimizu Y (1985) Eur Patent 138091
- [105]. Ameduri B, Boutevin B, Kostov GK, Petrova P (1998) J Fluorine Chem 92:69
- [106]. Sianesi D, Bernardi C, Diotallevi G (1967) US Patent 3333106

- [107]. Migmierina A, Ceccato G (1969) 4th Int. Sun. Rubber Symposium 2:65
- [108]. Ogunniyi DS (1989) Prog Rubber Plast Techn 5:16
- [109]. Schmiegel WW (2000) US Patent 2000011072
- [110]. Barney AL, Kalb GH, Khan AA (1971) Rubber Chem Techn 44:660
- [111]. Smith JF (1959) Rubber World 140:263
- [112]. Hepburn C, Ogunniyi DS (1985) Proceeding of the International Rubber Conference. Kyoto, Japan
- [113]. Ogunniyi DS, Hepburn C (1986) Plastics and Rubber Processing and Applications 6:3
- [114]. Smith J (1961) J Appl Polym Sc 5:460
- [115]. Albin LD (1982) Rubber Chem Techn 55:902
- [116]. Wright WW (1974) British Polym J 6:147
- [117]. Bryan CJ (1977) Rubber Chem Techn 50:83
- [118]. Kalfayan SH, Silver RH, Liu SS (1976) Rubber Chem Techn 49:1001
- [119]. Ogunniyi DS, Hepburn C (1995) Iranian Journal of Polymer Science & Technology (English Edition) 4:242
- [120]. Barton JM (1978) British Polym J 10:151
- [121]. Bentley FE (1957), PhD Thesis, University of Florida
- [122]. Mullins L (1959) J Appl Polym Sc 2:1
- [123]. Smith TL (1967) J Polym Sc, Polym Symp 841
- [124]. Van der Hoff BME, Buckler EJ (1967) J Macromol Sci, Part A 1:747
- [125]. Moran AL, Kane RP, Smith JF (1959) J Chem Eng Data 4:276
- [126]. O'Brien EL, Beringer FM, Mesrobian RB (1957) J Amer Chem Soc 79:6238
- [127]. Pedersen CJ (1958) J Org Chem 23:255
- [128]. Pedersen CJ (1958) J Org Chem 23:252
- [129]. O'Brien EL, Beringer FM, Mesrobian RB (1959) J Amer Chem Soc 81:1506
- [130]. Spain RG (1958) Division of Rubber Chemistry, American Chemical Society Meeting. Cincinnati



- [131]. Flisi U, Giunchi G, Geri S (1976) Kaut Gum Kunst 29:118
- [132]. Schmiegel WW (1985) US Patent 4496682
- [133]. Taguet A, Ameduri B, Boutevin B submitted in J Polym Sci, Part A: Polym Chem
- [134]. Apotheker D, Finlay JB, Krusic PJ, Logothetis AL (1982) Rubber Chem Techn  
55:1004
- [135]. Schmiegel WW (1975) US Patent 3872065
- [136]. Schmiegel WW (1975) US Patent 1413837
- [137]. Schmiegel WW (1984) US Patent 127318
- [138]. Hung MH, Schmiegel WW (2001) US Patent 2001081464
- [139]. Arcella V, Albano M, Barchiesi E, Brinati G, Chiodini G (1993) Rubber World 207:18
- [140]. Braden M, Fletcher WP (1955) Transactions, Institution of the Rubber Industry 31:155
- [141]. Udagawa R (2001) Eur Patent 2001081391
- [142]. Staccione A, Albano M (2003) Eur Patent 1347012
- [143]. Davis RA, Tigner RG (1970) US Patent 3505416
- [144]. Kryukova AB, Demidova NM, Khmelevskaya VM, Sankina GA, Dontsov AA, Chulyukina AV, Kosteltsev VV, Zavyalova AD, Savchenkova GL, et al. (1993) Russ. Patent 1815268
- [145]. Shimizu T, Enokida T, Naraki A, Tatsu H (2000) Jpn Patent 2000230096
- [146]. Saito M, Kama H, Miwa T, Hirai H (1994) Jpn Patent 06306245
- [147]. Bowers S, Schmiegel WW (2000) PCT WO2000011050
- [148]. Schmiegel WW (2003) US Patent 2003208003
- [149]. Banks RE, Birchall JM, Haszeldine RN, Nicholson WJ (1982) J Fluorine Chem  
20:133
- [150]. Gafurov AK, Isamukhamedov SI, Yul'chibaev AA, Usmanov KU (1978) Uzbekskii  
Khimicheskii Zhurnal:25
- [151]. Funaki A, Kato K, Takakura T, Myake H (1994) Jpn Patent 06306196
- [152]. Tamura M, Miyake H (1998) Jpn Patent 10158376
- [153]. Tatamoto M, Nagakawa T (1979) US Patent 4158678

- [154]. Tatemoto M (1979) IX International Symposium on Fluorine Chemistry, Avignon, France
- [155]. Tatemoto M, Suzuki T, Tomota M, Furukawa Y, Ueta Y (1981) US patent 4243770
- [156]. Tatemoto M, Morita S (1982) US Patent 4361678
- [157]. Oka M, Tatemoto M (1984) Contemp Top Polym Sc 4:763
- [158]. Ishiwari K, Sakakura A, Yuhara S, Yagi T, Tatemoto M (1985) International Rubber Conference, Kyoto, Japan
- [159]. Erdos P, Balazs G, Doszlop S, Varga J (1985) Periodica Polytechnica, Chemical Engineering 29:165
- [160]. Oggunniyi DS, Hepburn C (2003) Iranian Polymer Journal 12:367
- [161]. Bristow GM (1976) Natural Rubber Technology 7 3:61

## CHAPTER 2: BISPHENOL-BASED CURING SYSTEMS

### *2.1 INTRODUCTION*

The most common curing system based on bisphenol consists of two components, Bisphenol AF [2,2-bis-(4-hydroxyphenyl)-hexafluoropropane] and benzyltriphenylphosphonium chloride (BTPPCL) (Fig. 92).

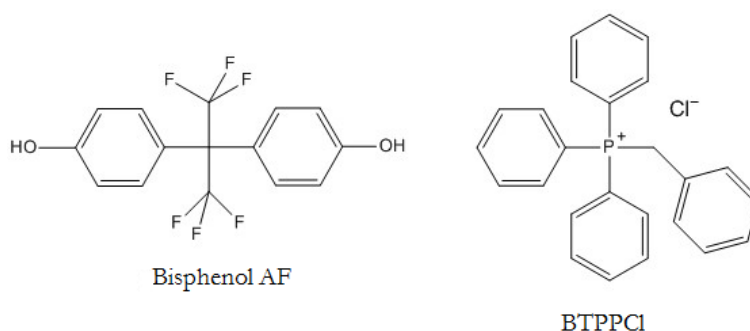


*Figure 92. Bisphenol AF and BTPPCL curing system.*

As explained in the previous chapter, the bisphenol AF (BAF) is the crosslinking agent while the phosphonium (or ammonium) salt act as an accelerator of the reaction.

The study of the curing system involves the synthesis and the characterization of different systems, each of them based on a different phosphonium salt. As mentioned above, the most commonly used is a completely aromatic salt; in this work we investigated the possibility of using different ligands for the P<sup>+</sup> cation, such as aliphatic chains or aromatic and aliphatic mixed systems. Lastly we studied the possibility of varying also the anionic counterpart of the salt.

In particular, we used four different salt in order to obtain our crosslinking systems (Fig. 93):

1. Benzyltriphenylphosphonium chloride;
2. Tetrabutylphosphonium bromide;
3. Butyltriphenylphosphonium bromide;
4. Tetrabutylphosphonium hexafluorophosphate.

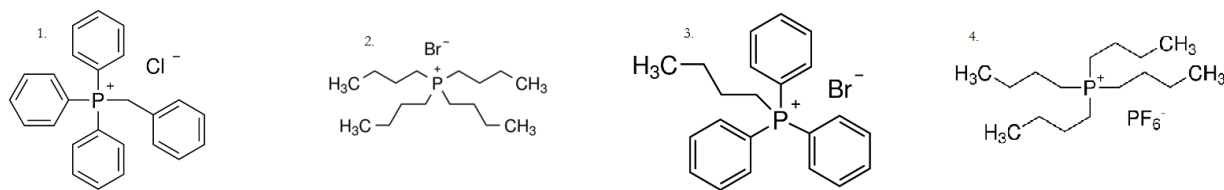


Figure 93. Different salts used in the curing systems.

Each salt was mixed with bisphenol AF and the obtained mixture was used as the crosslinking agent for a standard VDF/HFP copolymer.

## 2.2 EXPERIMENTAL

### 2.2.1 Typical preparation of the crosslinking system

Bisphenol AF and the examined phosphonium salt are mixed in a 4:1 molar ratio. The powders are mixed together then they are melted with a heat gun, avoiding boiling or smoking. Once chilled, an orange-pinkish glass-like solid is obtained.

The systems obtained with salts 2 and 4 are slightly sticky, probably because the aliphatic chains decrease the melting point of the whole system.

### 2.2.2 Preparation of the rubber compounds

The four systems are then used in a rubber compound that is prepared by mixing 100 phr of virgin polymer, 30 phr of carbon black, 6 phr of  $\text{Ca}(\text{OH})_2$ , 3 phr of  $\text{MgO}$ , 2.6 phr of the examined catalytic system in exam, 1 phr of waxes.

### 2.2.3 Instruments used

NMR spectra are recorded on a Varian Mercury Plus VX 400 spectrometer using 3-5% solution in  $\text{CD}_3\text{OH}$ . Chemical shifts are expressed in ppm using TMS as reference.

ODR analysis were performed with Gibitre Reocheck Profile Oscillating Disk at  $180^\circ\text{C}$  for 12 minutes.

Stress-strain curves were obtained by means of Gibitre Tensor Check Profile at room temperature, after a post curing performed at  $230^\circ\text{C}$  for 24h.

### 2.3 $^1\text{H}$ -NMR ANALYSIS

First of all, bisphenol AF, the four salts and obtained the four systems were characterized by  $^1\text{H}$ -NMR analysis.

The BAF spectrum is reported in figure 94.

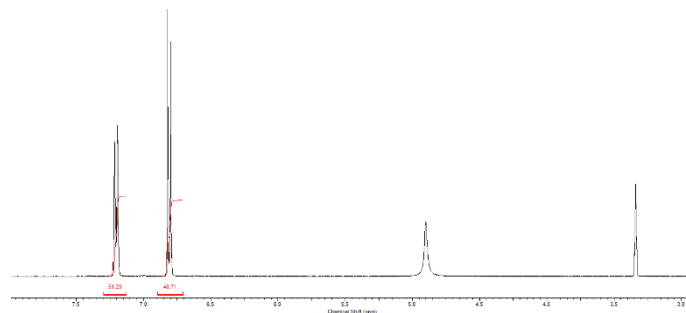


Figure 94.  $^1\text{H}$ -NMR spectrum of bisphenol AF.

Since the BAF molecule is symmetrical, in the spectrum ( $\text{CD}_3\text{OD}$ ) there are only two doublets in the aromatic region: that at 6.85 ppm is attributable to the two protons near the hydroxyl groups while the other signal, at 7.17 ppm, is ascribable to the protons near the  $\text{CF}_3$  central groups.

Figure 95 shows the spectrum of the benzyltriphenylphosphonium chloride (Salt 1, top) and the crosslinking system 1 obtained with this salt (bottom).

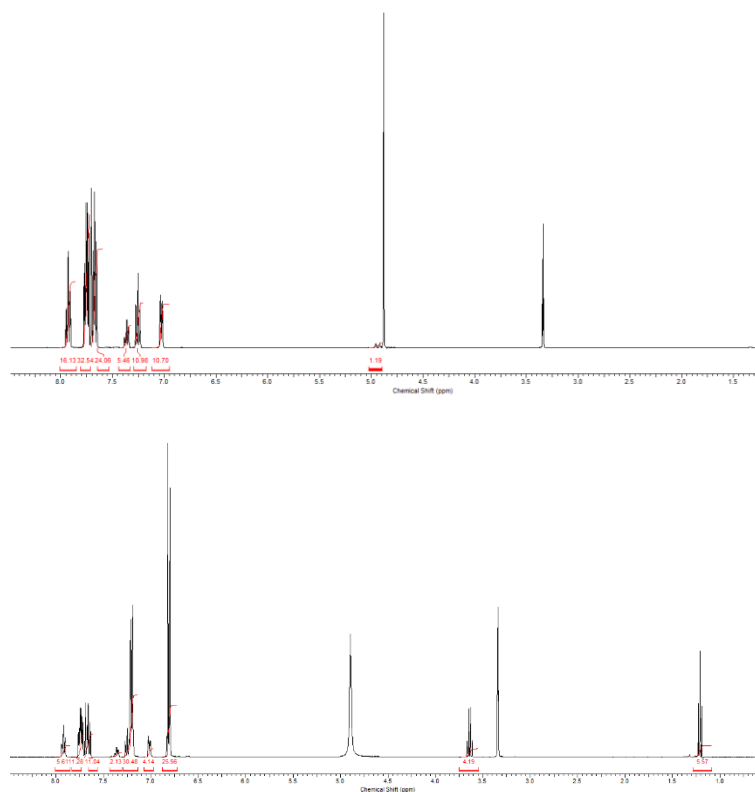


Figure 95.  $^1\text{H}$ -NMR spectra of benzyltriphenylphosphonium chloride (top) and crosslinking system 1 (bottom).

The aliphatic regions of the two spectra are simple: the only evident signal is located at 4.9 ppm and is relative to the  $-\text{CH}_2-$  of the benzyl group. In the aromatic region, there are two groups of signals, each of them composed of three multiplets: the signal relative to the *para* proton of the three phenyl groups can be found at 7.93 ppm; the multiplet of the two protons in the *meta* position of the three phenyl groups can be observed at 7.76 ppm; lastly, the signal of the *ortho* protons of the three phenyl groups is found at 7.67 ppm. The signals relative to the benzyl group are distributed as follows: the multiplet of the *para* proton at 7.37 ppm; the signal relative to the two protons in the *ortho* position at 7.25 ppm while the signal of the two *meta* protons at 7.03 ppm.

In the spectrum of the crosslinking system 1 (Fig. 95, down) the same signals can be found, with the addition of the two relative to the bisphenol AF.

Figure 96 shows the spectra of the tetrabutylphosphonium bromide (salt 2, top) and the crosslinking system 2 obtained with this salt (bottom).

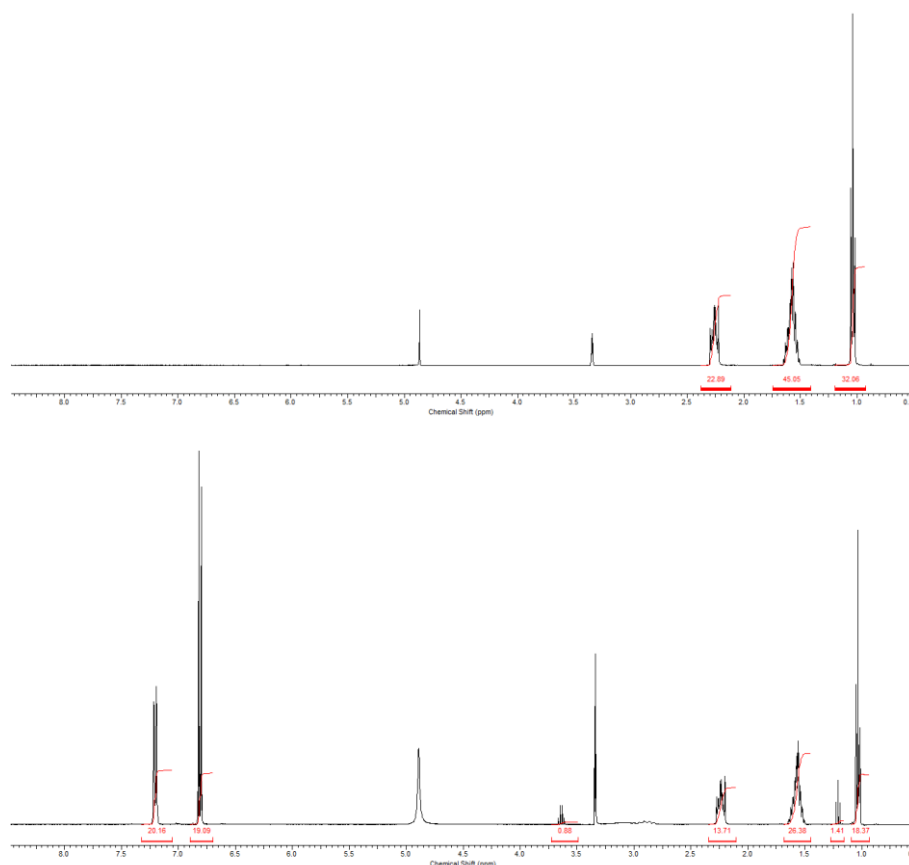


Figure 96.  $^1\text{H}$ -NMR spectra of tetrabutylphosphonium bromide (top) and crosslinking system 2 (bottom).

In this case, the aromatic region of the spectrum of the salt is devoid of any evident signal, while the three signals found are in the aliphatic region: that relative to the  $\alpha$   $-\text{CH}_2-$  to the P at 2.25 ppm, the

multiplet ascribable to two central  $-\text{CH}_2-$  of the chain at 1.51 ppm and the signal of the terminal  $-\text{CH}_3$  at 1.02 ppm.

The same signals can be found in the spectrum of the crosslinking system 2 (Fig. 96, bottom), with the addition of the two relative to the bisphenol AF, which are the only signal present in the aromatic region.

Figure 97 shows the spectra of the butyltriphenylphosphonium bromide (salt 3, top) and the crosslinking system 3 obtained with this salt (bottom).

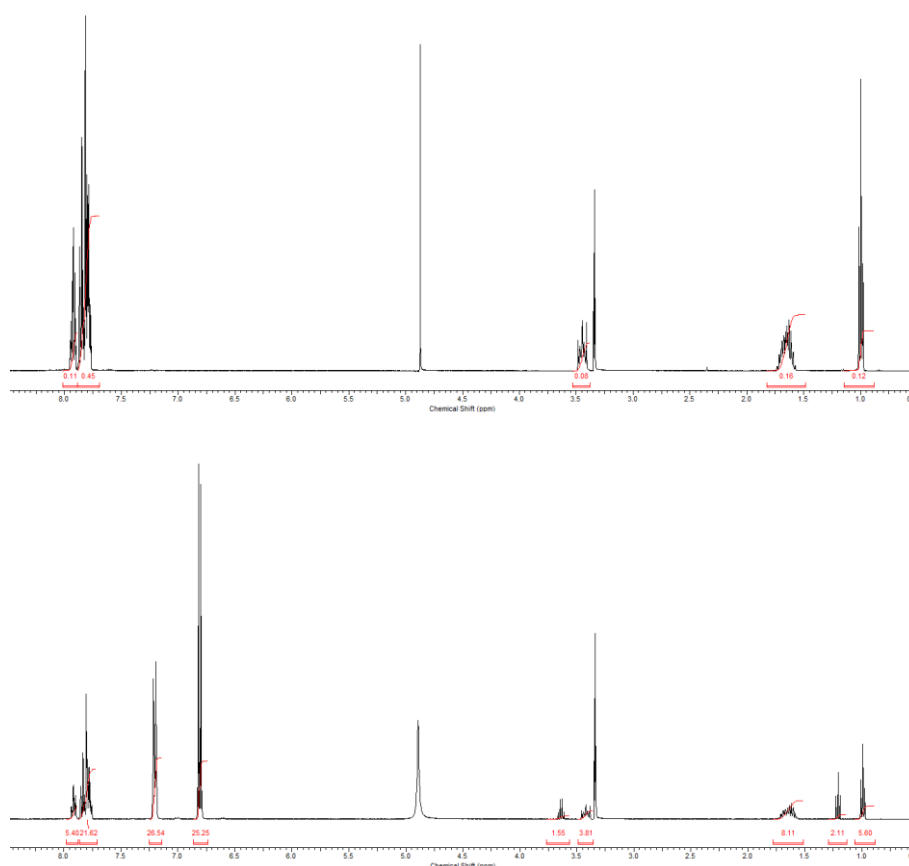


Figure 97.  $^1\text{H}$ -NMR spectra of butyltriphenylphosphonium bromide (top) and crosslinking system 3 (bottom).

The spectrum of butyltriphenylphosphonium bromide shows signals in both aromatic and aliphatic regions: the signal relative to the *para* proton of the phenyl rings at 7.92 ppm and the signals of the remaining protons of the phenyl rings in the area between 7.75 and 7.86 ppm. In the aliphatic region, the signal of the  $-\text{CH}_2-$   $\alpha$  to the P of the butyl chain is found at 3.50 ppm; the signals of the two central methylenic groups of the chain at 1.62 ppm and the triplet relative to the terminal  $-\text{CH}_3$  at 1.02 ppm.

The same signals can be found in the spectrum of the crosslinking system 3 (Fig. 97, bottom), with the addition of the two signals relative to the bisphenol AF, located at 7.85 and 7.24 ppm.

Figure 98 shows the spectra of the tetrabutylphosphonium hexafluorophosphate (salt 4, top) and the crosslinking system 4 obtained with this salt (bottom).

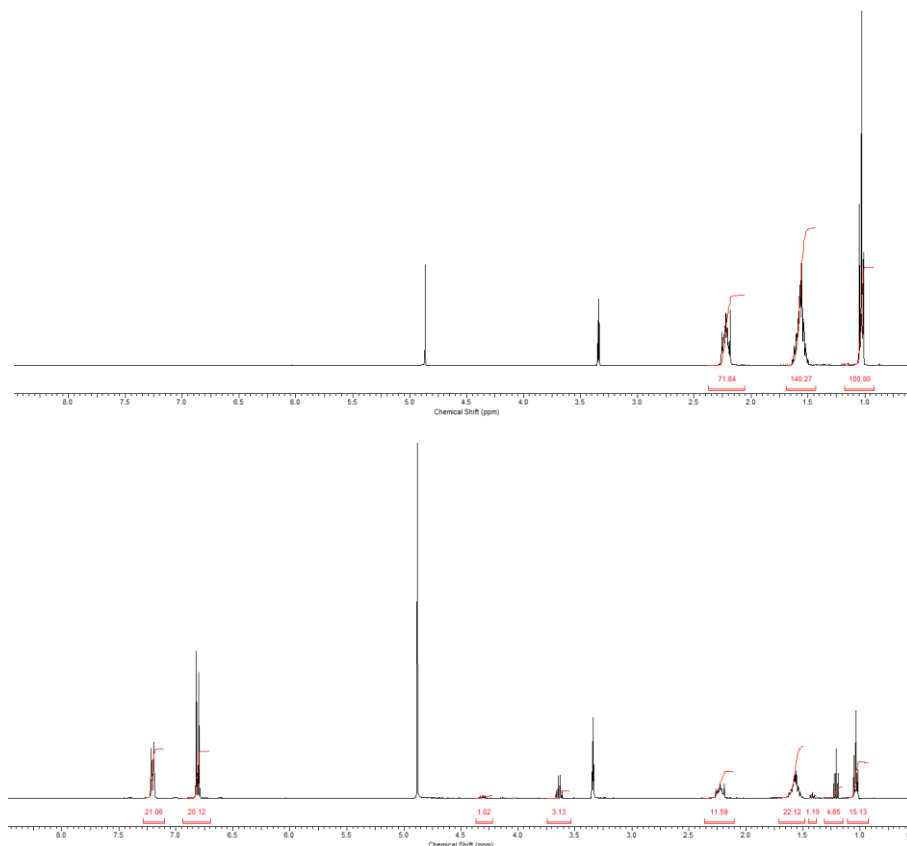


Figure 98.  $^1\text{H}$ -NMR spectra of tetrabutylphosphonium hexafluorophosphate (top) and crosslinking system 4 (bottom).

As it was for salt 2, in this case there are no signal in the aromatic region: the signal relative to the methylene group  $\alpha$  to the P can be found at 2.55 ppm; the signal attributable to the central methylenic groups of the chains at 1.52 ppm and the signal relative to the terminal methyl group of the chains at 1.02 ppm.

The same signals evidenced for salt 4 have been found in the spectrum of the crosslinking system 4 with the addition of the signals relative to the bisphenol AF in the aromatic region.

It should be noticed that, although the anion is different from salt 2, the chemical shifts of the butylic chains are not affected by this difference.

## 2.4 ODR ANALYSIS

ODR analysis were performed on rubber compounds, using the different crosslinking systems. The obtained curves for the analysis are reported in figure 99.



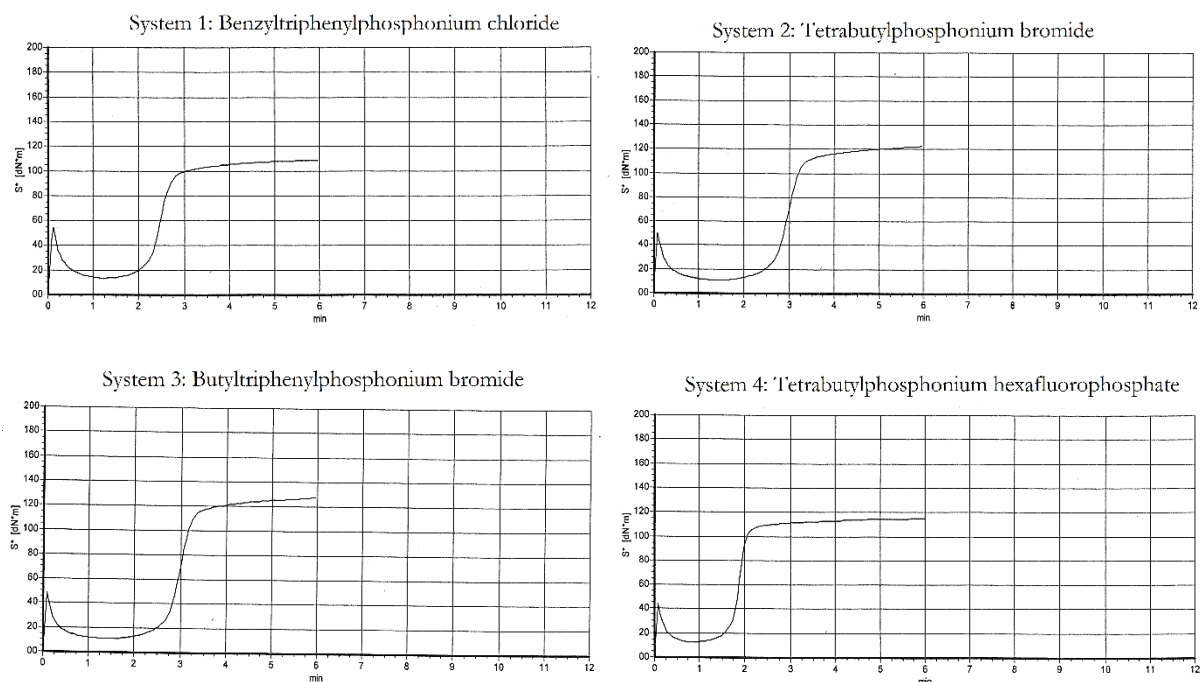


Figure 99. ODR curves for the four examined crosslinking systems.

In a typical ODR analysis, the viscosity of the system is measured as the torque made by the oscillating disk and it is the main indicator of the crosslinking progress. At the very beginning, the torque increases as the disk get in the compound; than the measured value decreases, due to the heating of the gum, until a minimum value of torque ( $M_L$ ) is reached; when the required temperature is achieved, the system begin to crosslink, increasing the value of the torque; after a certain time, a plateau value is reached ( $M_H$ ). Other interesting parameters are  $ts_1$ ,  $ts_2$  and  $t_{90}$  which are the time required to reach a value of torque higher of 1 point, 2 point and 90% of  $M_H$ , respectively.

The values obtained for the four crosslinking systems are reported in table 25.

Table 25. ODR values for the four examined crosslinking systems.

Compound	$M_L$ (dN*m)	$Ts_1$ (min.sec)	$Ts_2$ (min.sec)	$T_{90}$ (min.sec)	$M_H$ (dN*m)
1	13.50	1.33	1.42	2.59	108.63
2	10.95	1.49	1.58	3.26	122.21
3	10.98	1.49	1.59	3.25	127.24
4	12.60	1.09	1.17	2.06	114.88

All the four systems produce an effective crosslinking, but with slight difference between each other. The first system, shows typical values for this kind of materials, where the 90% of crosslinking occur in about 3 minutes from the beginning, reaching about 90 dN\*m of cure entity (calculated as  $M_H - M_L$ ). the second and the third systems are quite similar: both show  $M_L$  lower than the first one, suggesting that the crosslinking begins slightly later; this is confirmed by the other values: in fact, the compounds need about further 30 seconds to achieve the T90 time. Particularly interesting is the  $M_H$  values reached which are higher than the first compound; this determines a more rigid final material.

The last compound possesses the quickest times for curing, gaining almost 30 seconds when compared with the others, reaching anyway a good  $M_H$  value. This rapidity for curing may not be advantageous for industrial applications, because the compound can begin to crosslink during the injection phase into the mold, which is obviously not desirable.

## 2.5 STRESS-STRAIN CURVES

Traction curves were obtained using a bone-shaped sample cut from a tile of cured rubber which was post cured at 230°C for 24h that is pulled until break occurs. Then, the modulus (force/surface) versus percentage of elongation is reported.

The obtained curves for the analysis are reported in figure 100.

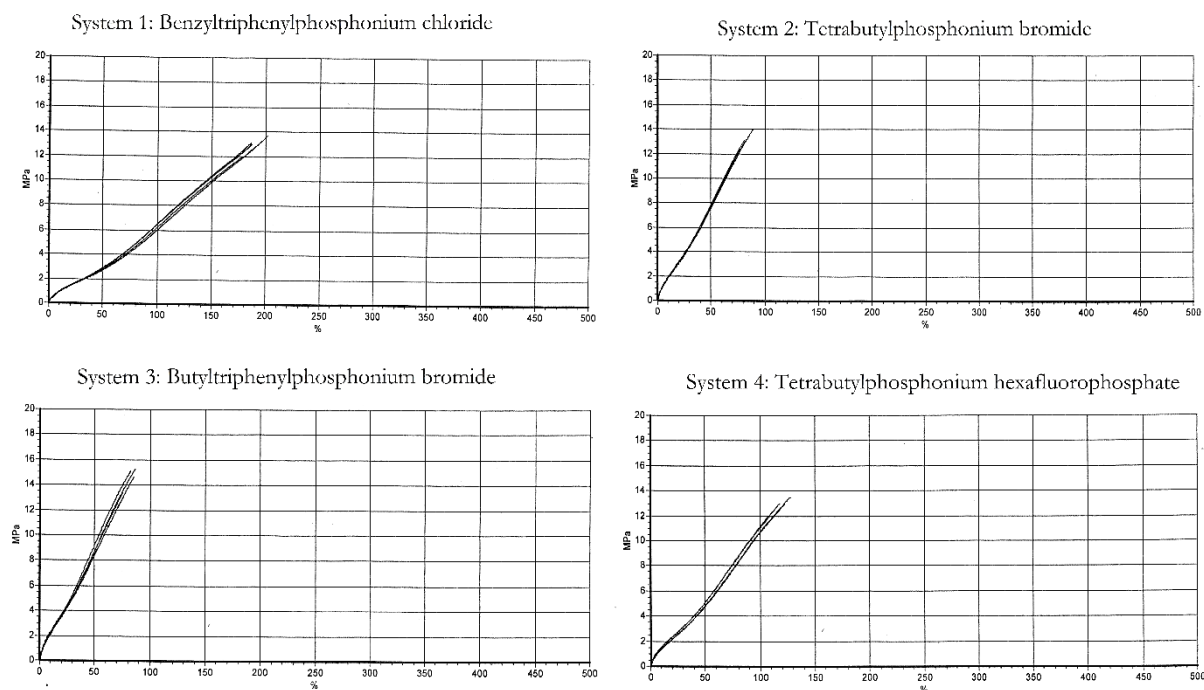


Figure 100. Stress-strain curves for the four crosslinking systems in exam.

Stress-strain curves report the tension (stress) as a function of the percentage of deformation (strain) and they are characteristic of every material. In particular, for an elastomer the elongation is particularly higher than a thermoplastic polymer, due to the crosslinking process which allows the elastomer to behave differently. Two parameters are important: the modulus at breaking point (TS) and the elongation percentage (Eb) at breaking point. These two parameters show if the rubber is hard or soft and give an idea of the curing entity; in fact, a more cured rubber, gives lower values of elongation at break because the material isn't elastic enough.

The values for the four examined crosslinking systems are reported in table 26.

*Table 26. Modulus and elongation at break for the four examined crosslinking systems.*

Compound	TS (N/mm <sup>2</sup> )	Eb (%)
1	12.96	189.53
2	12.92	80.97
3	14.35	81.49
4	12.84	119.27

The results agree with that previously said for the vulcanization curves: the first compound has the highest elongation at break which confirms the effectiveness of this crosslinking system; the second and the third systems show the lowest elongation due to the higher  $M_H$  values reached during the curing process, making the final rubber harder and less elastic; lastly, the fourth compound has a slightly higher elongation at break but still not even close to the first crosslinking system.

## 2.6 CONCLUSIONS

Four crosslinking systems have been prepared and they were tested as the curing system in rubber compound. The entity of the crosslinking was different from one system to another, which was confirmed both by ODR analysis and stress-strain curves. The most effective phosphonium salt is the benzyltriphenylphosphonium chloride which is, at the state of the art, the most common salt employed in this kind of materials. However, the study on different salts is crucial to better understand which is the exact mechanism of the curing process, in order to achieve better performances both for the curing itself and for the mechanical properties of the final material.

## CHAPTER 3: DEHYDROFLUORURATION OF VDF/HFP COPOLYMER

### *3.1 INTRODUCTION*

The most common crosslinking agent is the bisphenol system which is easy and affordable but has some disadvantages; however, the peroxide crosslinking allows to avoid these inconveniences but is more expensive due to the different starting polymer. In fact, a third monomer together with VDF and HFP is needed for a peroxide curable rubber; this monomer bears an Iodine or a Bromine atom, where the peroxide can bond during the crosslinking process.

This work is aimed to research a flexible polymer that can be used both for ionic (bisphenol) and peroxide curing in order to reduce cost and at the same time obtain a more flexible polymer starting from the same raw material.

The involved reaction is a dehydrofluoruration induced by a base in order to create unsaturations in the polymer backbone which can be employed to crosslink both with bisphenol and peroxide by exploiting the reactivity of the double bond.

### *3.2 EXPERIMENTAL*

#### *3.2.1 Instruments*

NMR spectra are recorded on a Varian Mercury Plus VX 400 spectrometer using 3-5% solution in THF- $d_8$ . Chemical shifts are expressed in ppm using  $CFCl_3$  as reference.

UV-Vis spectra are recorded on a Perkin Elmer Lambda 19 spectrophotometer on quartz slides from THF solution or using quartz cells.

FT-IR spectra are carried out on a Perkin Elmer Spectrum One spectrometer on Ge disk.

#### *3.2.2 Biphasic dehydrofluoruration reaction*

In a flask kept at a constant temperature 50 ml of NaOH aqueous solution and 0.1 g of tetrabutylammonium bromide are introduced. Then a solution of 10 g of copolymer (C20) in 100 ml of MTBE is added. The biphasic mixture is heated at temperature and times indicated in table 27. At the

end of the reaction, the mixture is poured into a separating funnel and 2% HCl is added until two phases are formed. The organic phase is collected and dried with  $\text{MgSO}_4$ . After filtration the solvent is removed under reduced pressure.

$^{19}\text{F}$ -NMR ( $d_4$ -THF, ppm):  $\delta$  -54.91; -60.23; -68.80; -73.21; -73.48; -73.67; -74.07; 89.22; -89.84; -90.68; -93.51; -101.61; -106.96; -108.54; -110.79; -111.81; -113.40; 114.11; -116.27; -116.79; -179.90; -181.85; -182.18.

Table 27. Conditions of biphasic dehydrofluoruration.

Products	Copolymer	NaOH (w/w)	Temperature	Time	Yield <sup>a</sup>	% molar of double bonds formed <sup>b</sup>
01	C20	23%	50°C	2 h	69,4%	1,1%
04	C20	46%	50°C	2 h	87,0%	0,6%

<sup>a</sup> (g products / g copolymer) · 100

<sup>b</sup> Determined by  $^{19}\text{F}$ -NMR

### 3.2.3 Homogeneous phase dehydrofluoruration

In a flask 5 g of polymer are dissolved in 100 ml of methanol and poured in a thermostatically controlled flask, then 30 ml of a solution of NaOH in methanol is added. Times, temperatures and NaOH concentrations employed are reported in table 28. At the end of the reaction, the mixture is poured in 100 ml of 5% HCl in methanol. The precipitated polymer is then filtered, washed several times with methanol and water and lastly dried in oven overnight.

Table 28. Conditions of homogeneous phase dehydrofluoruration.

Product	Copolymer	NaOH	Temperature	Time	Yield <sup>a</sup>	% molar of double bonds formed <sup>b</sup>
05	C20	0,6 g	50°C	2 h	94,6%	4,0%
06	C20	1,2 g	50°C	2 h	94,0%	9,5%
07	C20	0,6 g	50°C	4 h	94,5%	4,4%
08	C20	1,2 g	25°C	24 h	96,9%	9,4%

<sup>a</sup> (g products / g copolymer) · 100

<sup>b</sup> Determined by  $^{19}\text{F}$ -NMR

$^{19}\text{F}$ -NMR ( $\text{d}_4$ -THF, ppm): -54.24; -57.76; -58.09; -71.57; -74.22; -74.63; -75.43; 75.98; -91.97; -92.27; -104.41; -111.32; -112.13; -112.46; 113.55; -114.61; -116.91; 119.61; -182.70; -184.63; -184.88.

FT-IR (Ge Disk,  $\text{cm}^{-1}$ ): 2960; 2859; 1722; 1686; 1637; 1398; 1306; 1198; 1134; 1111; 1074; 884; 834.

### 3.2.4 Photocrosslink samples preparation

Two samples are prepared:

1. 1 g dehydrofluorinated polymer 06 + 2% w/w triethyleneglycol dimethacrylate + 1.5% w/w 1-hydroxycyclohexyl-phenylketone dissolved in 5 ml of THF
2. 1 g dehydrofluorinated polymer 06 + 4% w/w triethyleneglycol dimethacrylate + 3% w/w 1-hydroxycyclohexyl-phenylketone dissolved in 5 ml of THF

The obtained samples were used to cast thin films on quartz slides for UV-Vis analysis and on Ge disk for FT-IR analysis; the samples were then exposed to an UV Philips PL 11 W lamp and spectra were recorded after different times of exposure: 0 min, 30 min, 1h, 3h, 6h, 12h and 24 h.

Other samples were prepared in the same way in order to evaluate the photocrosslinking under sunlight illumination; for this samples, spectra were recorded after 18 and 32 days.

### 3.2.5 Compound preparation for thermal crosslinking

50 g of dehydrofluorinated polymer 06 are dissolved in 250 ml of THF then 15 g of carbon black, 1.25 g of TAIC (triallyl isocyanurate) and 0.6 g of Luperox (t-butyl peroxide) are added. The solvent is then removed and the polymer is dried in oven at  $60^\circ\text{C}$ .

## 3.3 RESULTS AND DISCUSSION

In order to obtain double bonds on a macromolecular chain composed of vinylidene fluoride ( $\text{CH}_2\text{CF}_2$ ) and hexafluoropropene ( $\text{CFCF}_3\text{CF}_2$ ) a dehydrofluoruration reaction is needed. This kind of reaction involves the elimination of HF from the macromolecular backbone by means of a base. The reaction is possible only in zones where at least one hydrogen is present that, in the case of the copolymer in exam, is characteristic only of the vinylidene fluoride units (Fig. 101).

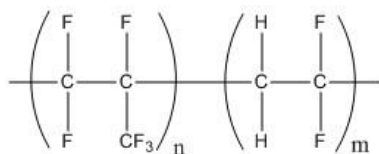
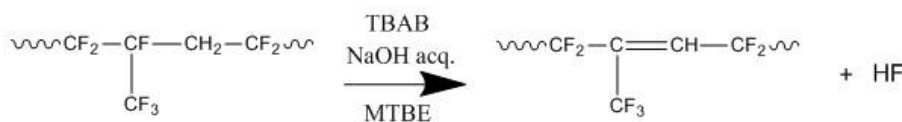


Figure 101. Schematic structure of VDF/HFP copolymer.

The starting point was the dehydrofluoruration using a biphasic system: the polymer is dissolved in an organic solvent, in our case MTBE, while the base (NaOH) is dissolved in water. The reaction takes place thanks to a phase transfer catalyst (tetrabutylammonium bromide, TBAB) that allows the transfer of the base from the aqueous phase to the organic one. The reaction mixture is then heated and the reaction starts as reported in scheme 23.



*Scheme 23. Biphasic dehydrofluoruration reaction.*

The adding of the NaOH leads to the immediate formation of a dark precipitate and the solution turns dark; this behavior can be ascribed to the formation of double bonds and to the consequent formation of crosslinked areas, also due to the presence of the phase transfer catalyst that could act as crosslinking accelerant. Furthermore, if the number of unsaturation is high, aromatic cycles, polyconjugated systems or double bonds oxidations can be formed, explaining the dark color of the mixture.

At the end of the reaction, the presence of TBAB prevents the separation of the two phases at a neutral pH. Only the addition of HCl allows the breaking of the emulsion and the recovery of the polymer but with low relatively yield (69-87%), as reported in the experimental section.

The biphasic reaction led to dark rubbery materials as shown in figure 102.

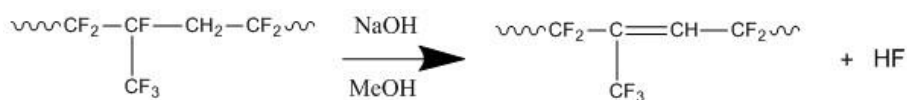


*Figure 102. Typical product for the biphasic dehydrofluoruration.*

The products have been characterized by  $^{19}\text{F}$ -NMR to determine the amount of the formed double bonds.

The main disadvantages of this procedure are the difficulty to recover the treated polymer and the low yields obtained.

To avoid these problems, a homogeneous phase reaction has been employed in order to avoid the formation of emulsions and simplify the contact between the polymer and the base. The chosen solvent was methanol because it is capable of solubilize both the polymer and the base. The new procedure, that follows the reaction in Scheme 24, provides for the solubilization of the polymer in methanol and the subsequent addition of a solution of NaOH in methanol. After the time required for the reaction, the polymer is recovered by acidification with HCl in methanol in order to precipitate the polymer



*Scheme 24. Homogeneous phase dehydrofluoruration reaction.*

By mean of this optimized reaction, the obtained polymer is less colored, with an orange appearance (Fig. 103)



*Figure 103. Typical product for homogeneous phase dehydrofluoruration.*

As reported in the experimental section, different conditions have been employed. In all cases good yields (94-96%) were obtained; this suggest that the temperature, the time and the amount of NaOH don't influence the stage of the recovery of the polymer.



### 3.3.1<sup>19</sup>F-NMR

In figure 104 are reported the spectrum of the copolymer (up) employed for the dehydrofluoruration and an expansion of this spectrum (down) in the region of the CF<sub>2</sub> and CF<sub>3</sub> groups. A typical <sup>19</sup>F-NMR spectrum of a FKM copolymer presents three different regions:

- the signals relative to the CF<sub>3</sub> groups are located in the -50 to -75 ppm range, belonging only to HFP unities;
- the signals relative to the CF<sub>2</sub> groups are located in the -80 to -120 ppm range, belonging both to HFP and VDF unities;
- the signals relative to the CF groups are located in the -120 to -180 ppm range, belonging only to HFP unities.

The attributions of all signals of a typical spectrum of a copolymer are reported in table 29.

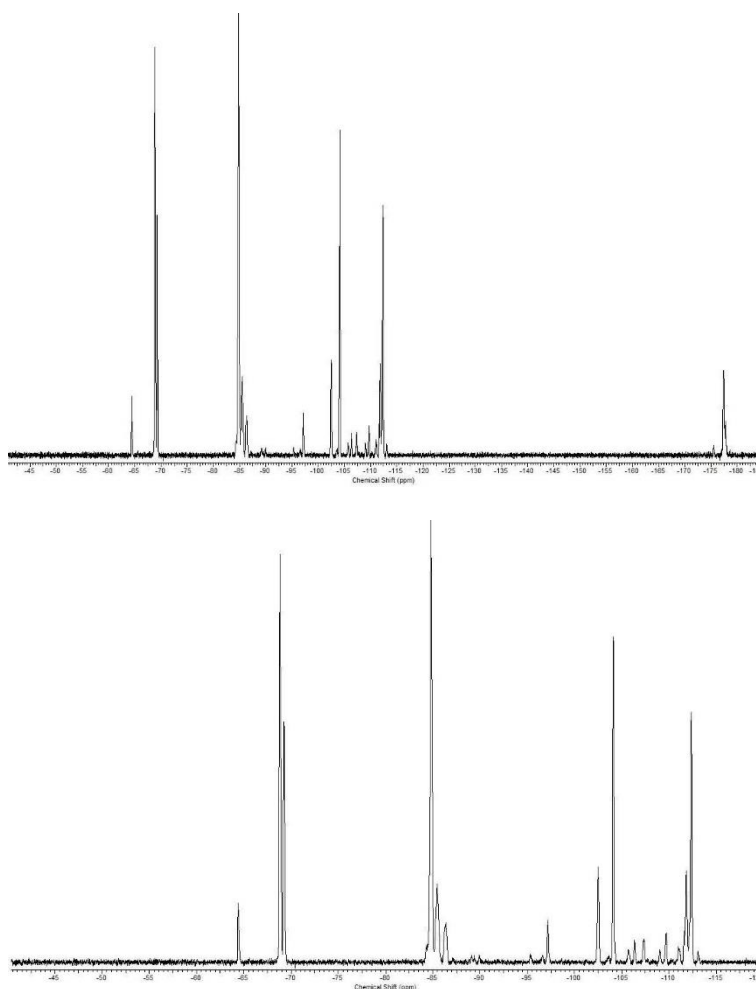


Figure 104. Typical <sup>19</sup>F-NMR spectrum (up) and expansion (down) of a FKM copolymer.

Table 29.  $^{19}\text{F}$ -NMR signals attribution for a typical VDF/HFP copolymer.

Chemical shift (ppm)	Attribution <sup>a</sup>
-64,5	-CH <sub>2</sub> CF <sub>2</sub> CF( <u>CF<sub>3</sub></u> )CF <sub>2</sub> CH <sub>2</sub> - -CH <sub>2</sub> CF <sub>2</sub> CF( <u>CF<sub>3</sub></u> )CF <sub>2</sub> CF <sub>2</sub> -
-69	-CH <sub>2</sub> CF <sub>2</sub> CF( <u>CF<sub>3</sub></u> )CH <sub>2</sub> CF <sub>2</sub> -
-69,5	-CF <sub>2</sub> CF <sub>2</sub> CF( <u>CF<sub>3</sub></u> )CH <sub>2</sub> CF <sub>2</sub> -
-84,5	-CH <sub>2</sub> CF <sub>2</sub> CH <sub>2</sub> <u>CF<sub>2</sub></u> CH <sub>2</sub> CF <sub>2</sub> -
-85	-CFCF <sub>2</sub> CH <sub>2</sub> <u>CF<sub>2</sub></u> CH <sub>2</sub> CF <sub>2</sub> -
-86,5	-CFCH <sub>2</sub> <u>CF<sub>2</sub></u> CH <sub>2</sub> CF <sub>2</sub> -
-89	-CH <sub>2</sub> CH <sub>2</sub> <u>CF<sub>2</sub></u> CH <sub>2</sub> CF <sub>2</sub> -
-90	-CH <sub>2</sub> CH <sub>2</sub> <u>CF<sub>2</sub></u> CH <sub>2</sub> CF <sub>2</sub> -
-95,5	-CFCH <sub>2</sub> <u>CF<sub>2</sub></u> CFCF <sub>2</sub> -
-96,5	-CF <sub>2</sub> CF <u>CF<sub>2</sub></u> CH <sub>2</sub> CF <sub>2</sub> -
-97	-CF <sub>2</sub> CH <sub>2</sub> <u>CF<sub>2</sub></u> CFCF <sub>2</sub> -
-102,5	-CFCH <sub>2</sub> <u>CF<sub>2</sub></u> CF <sub>2</sub> CF-
-103,5	-CF <sub>2</sub> CH <sub>2</sub> <u>CF<sub>2</sub></u> CF <sub>2</sub> CF-
-104	-CF <sub>2</sub> CH <sub>2</sub> <u>CF<sub>2</sub></u> CF <sub>2</sub> CF-
-106	-CH <sub>2</sub> CH <sub>2</sub> <u>CF<sub>2</sub></u> CF <sub>2</sub> CF-
-106,5	-CFCH <sub>2</sub> <u>CF<sub>2</sub></u> CF <sub>2</sub> CH <sub>2</sub> -
-107,5	-CF <sub>2</sub> CH <sub>2</sub> <u>CF<sub>2</sub></u> CF <sub>2</sub> CH <sub>2</sub> -
-109	-CH <sub>2</sub> CF <sub>2</sub> <u>CF<sub>2</sub></u> CH <sub>2</sub> CF <sub>2</sub> -
-109,5	-CH <sub>2</sub> CF <sub>2</sub> <u>CF<sub>2</sub></u> CH <sub>2</sub> CH <sub>2</sub> -
-112	-CH <sub>2</sub> CF <sub>2</sub> <u>CF<sub>2</sub></u> CFCH <sub>2</sub> -
-112,5	-CH <sub>2</sub> CF <sub>2</sub> <u>CF<sub>2</sub></u> CFCH <sub>2</sub> -
-175,5	-CH <sub>2</sub> CF <sub>2</sub> <u>CF</u> CF <sub>2</sub> CH <sub>2</sub> -
-177,5	-CF <sub>2</sub> CF <sub>2</sub> <u>CF</u> CH <sub>2</sub> CF <sub>2</sub> -

<sup>a</sup> the underlined unity contains the fluorine atom relative to the signal reported.

From the  $^{19}\text{F}$ -NMR spectrum it is possible to calculate the composition of the copolymer using the formula:

$$\%HFP = \frac{3(\sum CF_3)}{2(\sum CF_2)} * 100$$

$$\%VDF = 100 - \%HFP$$

In this formula  $\sum CF_3$  and  $\sum CF_2$  represent the sum of all the integrals from  $CF_3$  region and all the integrals from  $CF_2$  region, respectively. The examined copolymer is composed by 22.7% HFP and 77.3% of VDF.

In figure 105 is reported the expansion of the spectrum of a typical dehydrofluorinated polymer. All the obtained products have similar spectra; the only differences are in the values of the integrals that changes from product to product.

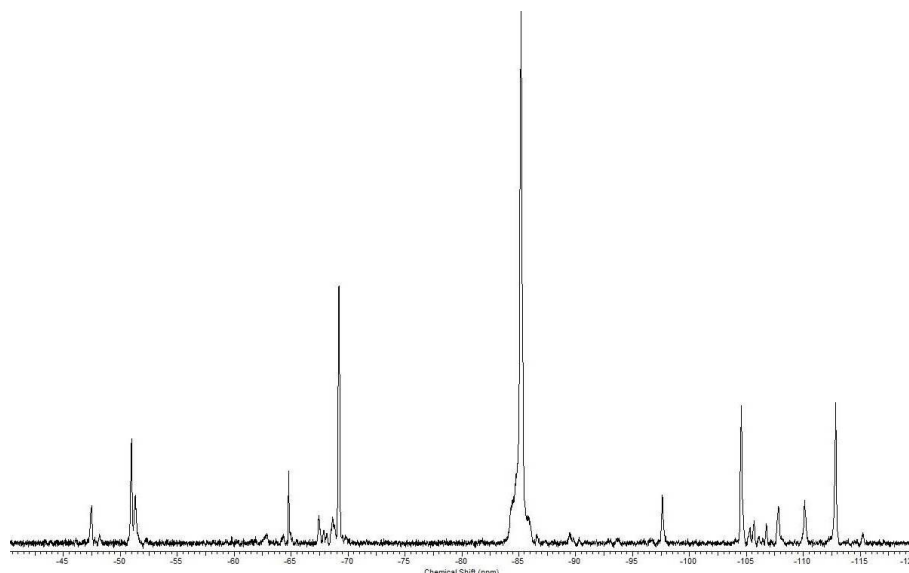
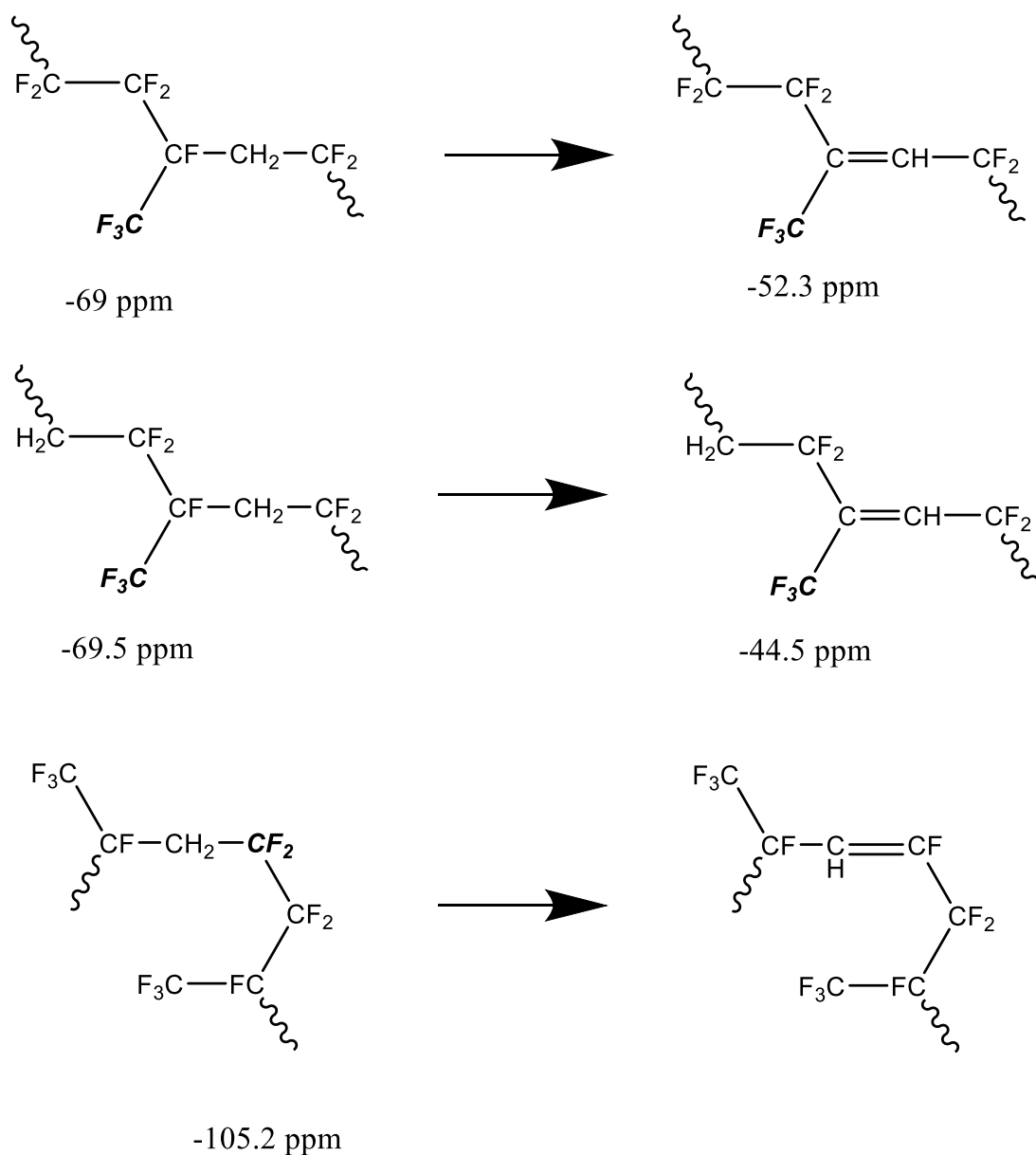


Figure 105.  $CF_3$  and  $CF_2$  region expansion of a typical spectrum of dehydrofluorinated polymer.

The main difference with the spectrum of the pristine polymer is the appearance of two new signals in the  $CF_3$  region at -44.5 and -52.3 ppm, that were not present at all in the pristine spectrum. Other differences include the decrease of some  $CF_2$  signals, in particular the ones at -69 and -102.5 ppm and the latter even disappears.

The dehydrofluoruration takes place in sites where a hydrogen atom is present, that is only on a VDF unity that can be bonded to a  $-CF(CF_3)$  or  $-CF_2$  unity. According to where the fluorine atom is extracted, a new double bond near a  $CF_3$  or a  $CF_2$  group can be formed, as shown in scheme 25.



Scheme 25. Possible mechanisms for FKM dehydrofluoruration.

In addition to the differences found in the spectra of the dehydrofluorinated polymers, a quantitative analysis can be made by means of the integrals of the signals.

The percentage of formed double bonds can be easily obtained by the following formula:

$$\%double\ bonds = \frac{\sum CF_3new}{\sum CF_3tot} * \%HFP$$

where  $\sum CF_3new$  represents the sum of the integrals of the new signals in the  $CF_3$  region, while  $\sum CF_3tot$  represents the sum of all the integrals from the  $CF_3$  region; by multiplying this results with the percentage of HFP, the double bonds content expressed in function of the composition of the copolymer can be obtained.

A summary of the values obtained is reported in table 30 together with the adopted procedure and the reaction conditions.

Table 30. Summary of the values obtained.

Product	Procedure	NaOH <sup>a</sup>	Temperature	Time	Yield	% molar of double bonds formed <sup>b</sup>
01	Biphasic	12%	50°C	2h	69,4%	1,1%
04	Biphasic	24%	50°C	2h	87,0%	0,6%
05	Homogeneous	12%	50°C	2h	94,6%	4,0%
06	Homogeneous	24%	50°C	2h	94,0%	8,5%
07	Homogeneous	12%	50°C	4h	94,5%	4,4%
08	Homogeneous	24%	25°C	24h	96,9%	9,4%

<sup>a</sup> w/w respect to the polymer

<sup>b</sup> Determined by <sup>19</sup>F-NMR

It is evident that the homogeneous phase dehydrofluoruration leads to products with higher percentage of double bonds formed together with higher yields, making this procedure more suitable for industrial application.

Moreover, the concentration of NaOH directly influences the amount of formed double bonds but the temperature seems not affecting this value at all. Furthermore, it seems that results are not affected by the reaction time, suggesting that the reaction takes place very quickly and arrives at a plateau value after a short time.

To confirm this hypothesis, a new reaction has been made and portions of the reaction mixtures have been removed at different times and analyzed. Following the same method as described above, it was possible to obtain a chart of the percentage of double bonds formed as a function of reaction time (Fig. 106)

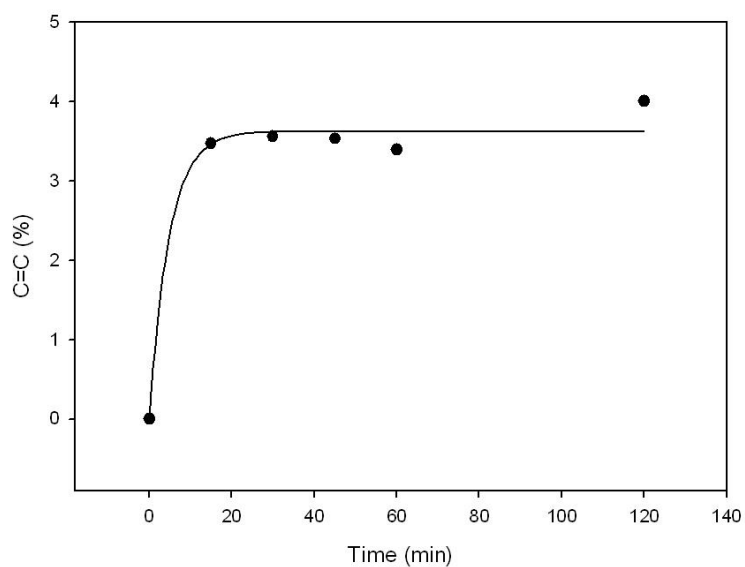


Figure 106. Percentage of double bonds formed as a function of reaction time.

It is clear that the dehydrofluoruration reaction is very quick and the time slightly affects the final value.

### 3.3.2 FT-IR analysis

FT-IR analysis was performed (Figure 107) both on pristine (left) and treated (right) polymer. These spectra confirm the obtainment of double bonds since the presence of new bands relative to double bonds stretching can be found.

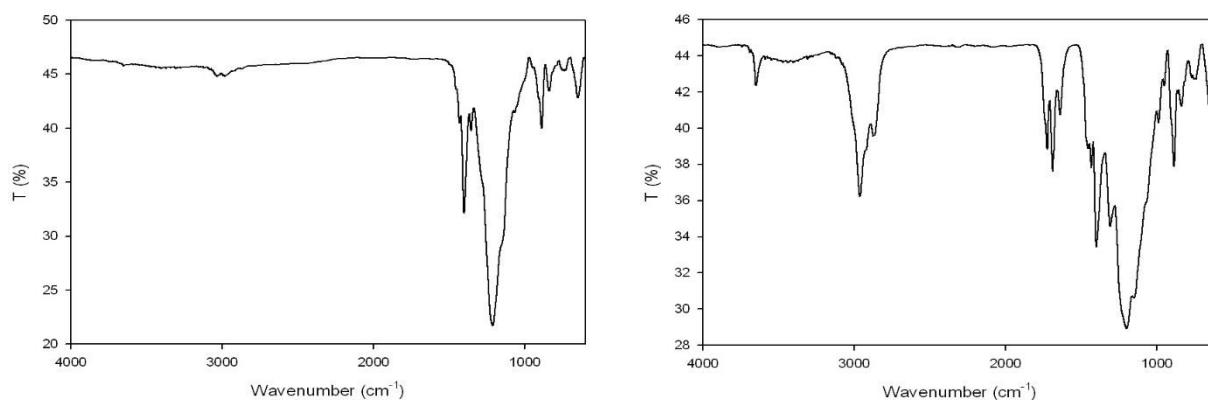


Figure 107. FT-IR spectra of the pristine (left) and treated (right) polymer in exam.

The complete attribution of the bands for a dehydrofluorinated product is reported in table 31.

Table 31. Attribution of FT-IR bands for a dehydrofluorinated product.

Frequency (cm <sup>-1</sup> )	Attribution
2960, 2859	$\nu$ C-H
1722, 1686, 1637	$\nu$ C=C
1398, 1074	$\nu$ C-F
1306, 1198, 1134, 1111	$\nu$ C-F <sub>2</sub>
884, 834	$\nu$ C-F <sub>3</sub>

The appearance of the bands at 1722 1686 and 1637 cm<sup>-1</sup> confirms the formation of double bonds on the polymeric backbone.

### 3.3.3 Photocrosslinking

The dehydrofluorinated polymers can be susceptible to peroxide crosslinking due to the reactivity of the double bonds. The first attempt was made by a photo induced crosslinking. For this purpose, two samples have been prepared using the sample with the higher percentage of double bonds; they were added by different amounts of a radical initiator (1-hydroxycyclohexylphenyl ketone) and of a crosslinking agent (triethyleneglycol dimethacrylate). In particular, sample 1 had 2% w/w of initiator and 1.5% w/w of crosslinking agent, while sample 2 had double amounts.

The polymer was dissolved in THF, then the required quantities of the crosslinking system was added and the solution was deposited on quartz and germanium slides and illuminated with an UV lamp for 24h. The crosslinking was monitored by UV-Vis and FT-IR spectroscopies.

The crosslinking take place easily also for the sample with the lower amount of crosslinking system, making the sample insoluble in organic solvents.

The FT-IR spectra (Fig. 108) show the decrease of the band relative to the double bonds stretching ( $\nu$  C=C); the ratio between the intensities of this band (located at 1637 cm<sup>-1</sup>) and of a constant band, for example that at 883 cm<sup>-1</sup> and relative to the  $\nu$  of C-F<sub>3</sub>, allows to obtain a graphical representation of the crosslinking progression, as shown in Figure 109.

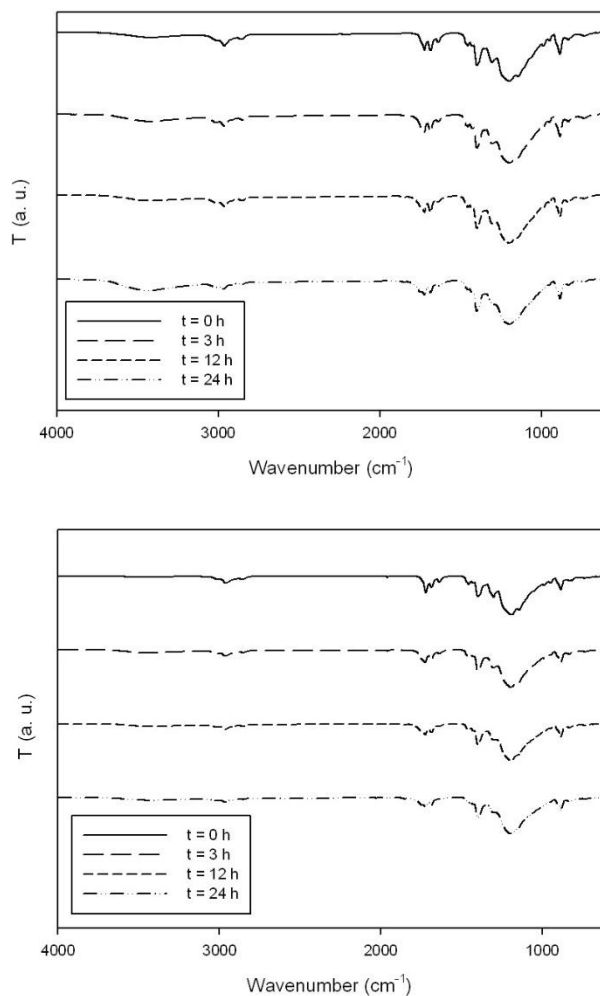


Figure 108. FT-IR spectra relative to sample 1 (up) and sample 2 (down) under UV radiation at different times

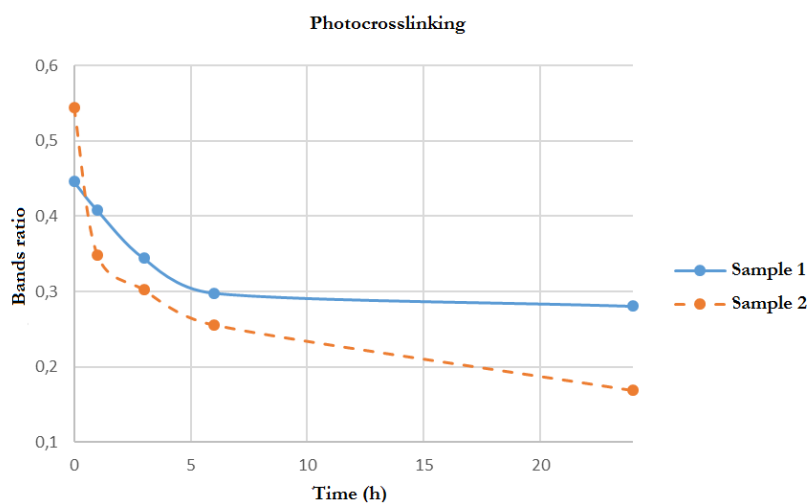


Figure 109. Bands ratio as a function of crosslinking time.

The UV-Vis spectra in film of sample 1 (up) and sample 2 (down) at different times after UV exposure are reported in figure 110.



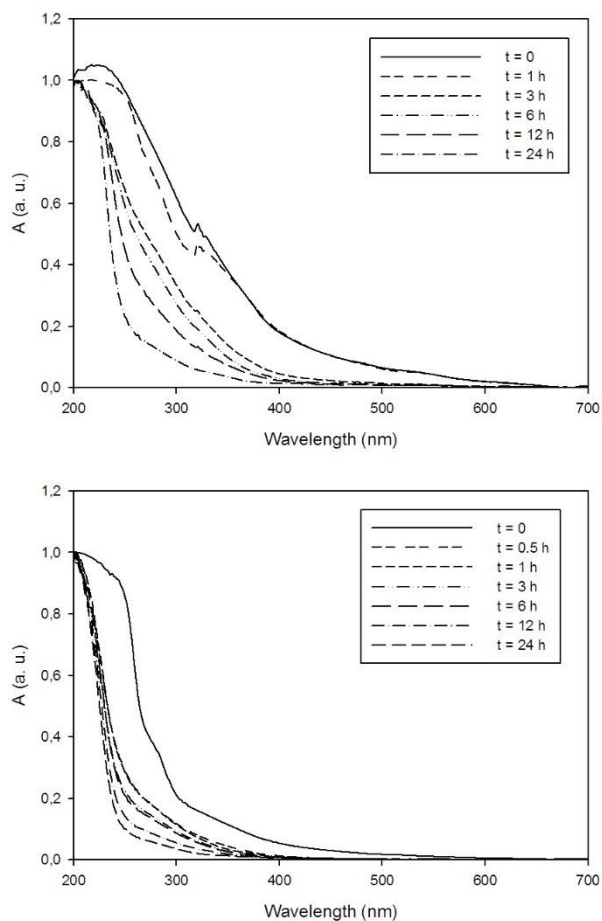


Figure 110. UV-Vis spectra in film relative to sample 1 (up) and sample 2 (down) at different times after UV exposure.

From the spectra, the decrease of the band located between 200 and 300 nm, attributable to the C=C double bonds is evident, indicating the progression of the photocrosslinking.

Lastly, another sample was prepared similarly to sample 1, but this time it was exposed to sunlight for 1 month. The FT-IR spectrum of this sample at different times is reported in figure 111.

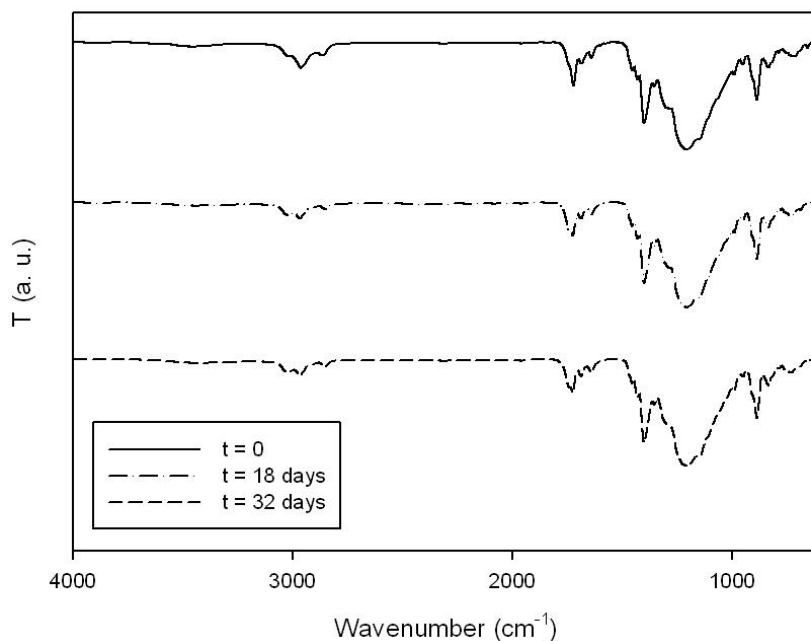


Figure 111. FT-IR spectra of a sample exposed to sunlight at different times.

In this case it is evident that the crosslinking took place after 18 days of exposure because after 32 days the spectrum is virtually unchanged.

It is clear that, also with the smallest quantities of crosslinking system, the polymer can easily undergo to a crosslinking reaction by means of a peroxide.

### 3.3.4 Thermal crosslinking

The dehydrofluorinated polymer has been employed in a peroxide-curable compound as used in normal industrial applications.

The polymer is dissolved in THF then 1.5% by weight of t-butyl peroxide, 2.5% by weight of triallylisocyanurate and 30% by weight of carbon black are added. After complete mixing and evaporation of the solvent, the compound was analyzed by ODR (Oscillating Disc Rheometer) at 180°C during the curing process. The relative curve is reported in figure 112.

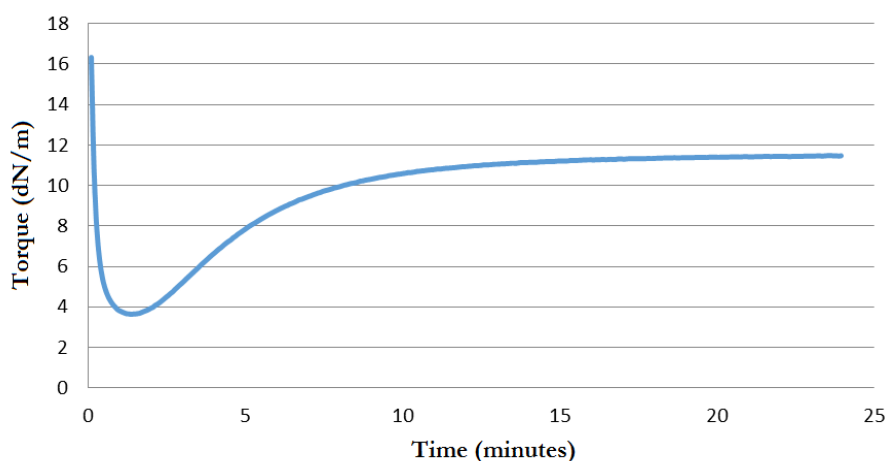


Figure 112. ODR curve for a peroxide-curable compound.

In the ODR analysis, the torque developed by a rotor submerged in the compound to maintain an oscillation of 3°C as a function of time is recorded at a temperature of 180°C. The starting torque decreases because of the heating of the compound, then the viscosity decreases together with the torque until a minimum value  $M_L$ . Subsequently, the torque increases as the crosslinking proceeds. When the curing is finished the torque stabilizes at a maximum value of  $M_H$ . Usually the values that characterize the compound together with  $M_H$ ,  $M_L$ , are  $T_{s1}$ ,  $T_{s2}$  which are the times from the beginning to obtain an increase of 1 and 2 unities more than  $M_L$  respectively and  $T'_{90}$ , that is the time required for the compound to reach the 90% of  $M_H - M_L$  value.

Data for the examined compound are reported in table 32.

Table 32. ODR data for a peroxide-curable compound.

ML (dN/m)	MH (dN/m)	Ts1 (min:sec)	Ts2 (min:sec)	T'90 (min:sec)
3,64	11,46	3:00	3:18	4:25

The obtained values confirm that the polymer used, normally cured by bisphenol crosslinking system, can be cured by a peroxide system after the dehydrofluorination process.

This result is particularly interesting since it is possible to obtain two different polymers by varying the kind of curing system starting from the same raw material.

### 3.4 CONCLUSIONS

The possibility of dehydrofluoruration for a VDF/HFP copolymer by means of a base has been studied. Two different techniques have been developed, using a biphasic or a homogeneous phase reaction; the latter was the most effective to obtain double bonds on the polymer backbone.

The double bonds formed in this way were exploited to cure a rubber compound *via* peroxide a method which is usually not suitable for this kind of material, owing to the need of having a third monomer in the starting raw polymer.

The obtained compound was cured both with UV and heat showing that in both cases the crosslinking takes place easily and quickly.

These results are particularly encouraging to obtain a flexible material whose properties can be tuned, depending on the need, changing the curing system.

The obtainment of double bonds on the polymeric backbone allows for the insertion of specific functional groups with particular properties for specific applications, opening the way toward polymer post functionalization.